Update Migration Study

Twenthe-Rijn – Phase 1-Part A+B
Reconstruction of cavern development, slurry filling and migration

Report Part 3 – Validation of the BJP-Algorithm by assessment of historical migration behaviour of selected TWR caverns and determination of the likelihood of migration.

Client: Nobian Industrial Chemicals BV
Boortorenweg 27
7554 RS Hengelo (O)
The Netherlands

Consultant: Reinvent GmbH
Heinrich-Heine-Straße 21
99706 Sondershausen
Thuringia, Germany

Processing team: 5.1.2.e 5.1.2.e

Date: 30/12/2024

FINAL Version V1

Contents

Executive Summary and Report Structure

Structure of the study

The historic development of the Nobian cavern fields within the Twenthe-Rijn mining permit (incl. extensions) has been divided into five phases ("Fases" 1 through 5), see the Figure below.

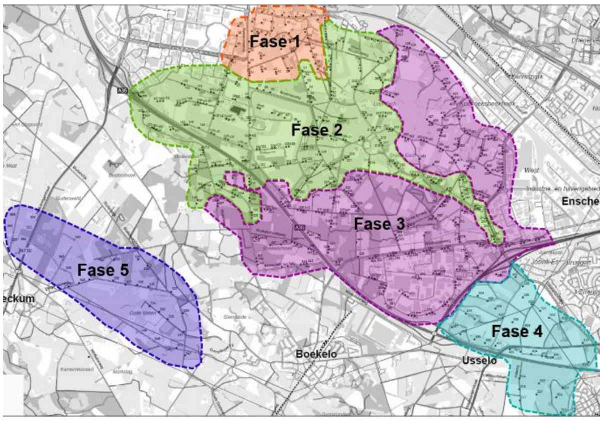

Historical development of TWR-area ("Fase" 1, 2, 3, 4, and 5)

For the caverns within the areas denoted "Fase 1" and "Fase 2", an update of the existing cavern migration assessments, prepared and continuously updated by the (late) Roland Bekendam, was sought by Nobian. REinvent GmbH (REinvent) and K-UTEC AG Salt Technologies (K-UTEC) were (sub-)contracted by Nobian to perform the study. Based on the assessment of ten (10) well-documented historical cavern migration cases, a subsidence prognosis algorithm has been developed, which will be validated in this report: "Report 3: "Validation of the input parameters by the assessment of migration behaviour of migrated caverns and determination of the likelihood of migration". The actual subsidence prognosis for relevant caverns that have not migrated to date will be included in Report 4, to be delivered in conjunction with this report.

The overall Update Migration Study Twenthe-Rijn (UMS-TWR) has been divided into three phases, i.e. Phase I, II and III:

- Phase I: Reconstruction of well documented cavern migration cases.
- Phase II: Update Subsidence Prognosis.
- Phase III: Subsidence assessment Fase 1 caverns
  (A study for Nobian internal documentation purposes).

The workload for each phase has been performed in three largely consecutive parts (A, B and C).

The reporting covering both the UMS-TWR Phases I and II is divided into four (4) parts, namely:

- Report 1: "Fundamental principles concerning cavern migration in the TWR brinefield".
- Report 2: "Description of the updated algorithm to predict subsidence caused by migration".
- Report 3: "Validation of the input parameters by the assessment of migration behavior of migrated caverns and determination of the likelihood of migration" (this report).
- Report 4: "Subsidence predictions for potential future migration and recommendations on mitigative action by means of backfilling".

Report 1 has been delivered in December 2023, describing the fundamental principles related to cavern development, backfilling, migration and subsidence. Report 2 describes the developed prognosis algorithm in detail and has been delivered in November 2024. Report 3 (this report) provides the validation of the developed prognosis algorithm. Validation is achieved by demonstrating that the derived relationships and parameters are applicable to the 10 well-documented migration cases and thereby for the entire TWR area. Report 4 delivers the actual updated subsidence prognoses for relevant caverns in the "Fase 2" and "Fase 3" areas and will be delivered in conjunction with this Report 3 before the end of 2024. Reporting on the future Phase III of the study will be covered by a Report 5 to be delivered to Nobian in 2025.

Prognosis algorithm development workflow

The UMS-TWR performed the following workflow steps to develop a new subsidence prognosis algorithm:

1. Reconstruction of cavern volume for ten (10) well-documented cavern migration cases.
2. Reconstruction of cavern backfilling for seven (7) of the 10 well-documented migration cases.
3. Reconstruction of the cavern migration of these caverns.
4. Assessment of the measured subsidence and comparison with the reconstructed migration.
5. Deduction of a set of relationships that describe potential cavern migration and consequent subsidence while considering cavern geometry, eventual backfilling and the geological conditions per cavern.

The set of relationships derived from the described workflow constitute the newly developed subsidence prognosis algorithm, further known as the Bekendam-Jakob-Pinkse (BJP)-Algorithm. The BJP-Algorithm is fundamentally based on the historically used Bekendam-method. The newly developed algorithm enables the calculation of subsidence due to cavern migration based on a set of general and cavern-specific input parameters. The following features were newly implemented in the BJP-Algorithm to enable a more realistic approximation of the cavern migration process:

- Three (3) basic cavern shapes: cylinder, cone, cylinder + cone.
- Three (3) basic migration column shapes: cylinder, cone, cylinder + cone.
- Migration column radius reduction mechanism for cone shaped caverns.
- Differentiation of five (5) subsidence stages of which the last 4 are relevant to the study:
    - Stage 1: due to the convergence of the cavern by salt creep (not relevant)
    - Stage 2: due to deformation of cavern and migration column volumes
    - Stage 3: due to deflection of the residual cavern roof pillar near the Top Rock
    - Stage 4: due to (plug) failure of the residual cavern roof pillar near Top Rock
    - Stage 5: due to the consolidation of bulked overburden and backfill in the cavern under the load of the Tertiary soils overlying the Top Rock.
- Stage 3 subsidence is introduced to enable a smooth transition between Stage 2 subsidence (i.e. Phase II in the Bekendam method) and the formation of Stage 4 subsidence, i.e. a trough or sinkhole. To achieve this smooth transition, the deflection of the residual cavern roof pillar, as the migration approaches the Top Rock, is approximated dependent on the residual cavern diameter.
- Introduction of a smooth transition between “Stage 4 Trough” and “Stage 4 Sinkhole” in the algorithm to eliminate a “stepped” output of the subsidence prognosis.
- Superposition of multiple subsidence stages and/or multiple subsidence sources.

The BJP-Algorithm produces the following outputs:

- Subsidence, Tilt, Strain, Curvature and Relative Rotation maximum values and contours.
- Output as a summary Excel file and geo-referenced contours in “.DXF”-format, thereby elimination elaborate post-processing and contour drafting stages.
- Output of minimum required cavern volume reduction to avoid Stage 4+5 subsidence.
- Output of minimum required cavern volume reduction to avoid Stage 3 subsidence with a Safety Factor (SF) of two (2), i.e. a very conservative estimate of the volume of backfill required to limit potential subsidence due to cavern migration to Stage 2 subsidence only.

Validation of the BJP-algorithm

The validation of the developed prognosis algorithm is achieved by demonstrating that the derived relationships and selected input parameters are applicable to 9 out of the 10 well-documented migration cases. Initial validation of the algorithm is achieved based on the reconstruction of 5 cavern migration cases. The validation is strengthened by the reconstruction of 4 complex migration cases. The applicability to poorly documented migration cases is demonstrated by operating the algorithm in reverse for 2 caverns to reconstruct the migration column and the likely original cavern shape. The validation shows that the algorithm is applicable to the entire TWR area. This validation of applicability focuses on the four main input parameters:

1. Effect of cavern shape on migration column shape.
2. Bulking Factor of insolubles, intermediate claystone benches and overburden.
3. Backfill volume balance: actual insitu backfill versus pumped slurry.
4. Backfill behaviour under load: consolidation by self-weight and under load of bulked overburden.

The studied migration cases and their role in the validation process are presented in the table below.

Cavern (-system)	Backfill applied?	Used for initial validation	Used to strengthen validation	Used in reverse operation	Not used for validation
C15	Yes	✓			
C30-31	No			✓	
C33-34-35-36	No			✓	
C37	No	✓			
C49*	Yes	✓			
C50*	Yes	✓			
C63-64-65	Yes		✓		
C69-70-71	Yes		✓		
C72-75-76-77	Yes		✓		
C86-87	No	✓			
C104-105-106-107	Yes		✓		
C167-168-169	Yes				✓

* Caverns C49 and C50 are further discussed as the cavern system C49-50 in relation to the reconstruction.

The reverse operation of the BJP-algorithm will be a critical workflow for Phase III of the UMS-TWR which aims at the reconstruction of migration columns and cavern development for the "Fase 1" area caverns (roughly caverns C1 to C50) for which no sonar images are available.

Cavern C167-168-169 has a very complex development history which was challenging to reconstruct. A plausible reconstruction was eventually achieved but proved of little value for the validation process due to the uncertainties in relation to the position of cavern volume and the influence of faults in the overburden. The performed reconstruction work on this cavern will be delivered in an addendum to this Report: i.e. ADDENDUM I, to be delivered in Q1-2025.

Likelihood of Migration

The likelihood of migration was historically not well understood nor was it considered in the previously used Bekendam method. Although several reports by Bekendam discuss the possible reasons for cavern migration and investigate the migration rate, a unified approach to cavern migration likelihood has not been proposed before the present UMS-TWR study.

The reconstruction work performed to develop and validate the BJP-Algorithm has also enabled the development of a migration likelihood scoring system based on criteria such as:

- the potential migration column diameter,
- the thickness of competent and intact strata in the cavern roof below the Röt-Claystone,
- historical exposure of the Anhydrite-E member to water during cavern development.

The processes which lead to deterioration and subsequent failure of an exposed Anhydrite cavern roof are now better understood. Furthermore, a site-specific relationship between the size and shape of a potential migration column and the likelihood of actual migration has been established by assessment of the so-called “Hydraulic Radius” as proposed by recently published research on cave propagation for underground mining (Block Caving Method) [1].

The developed scoring system has been used to estimate the likelihood of migration of both migrated and non-migrated caverns. The result of the assessment is that the likelihood of migration for known migration cases is very high without exception, whilst caverns that have not migrated generally score much lower on the likelihood scale. The likelihood of migration thus confidently explains why some caverns migrated while other similar caverns retain a stable cavern roof up to today.

The establishment of a unified cavern migration likelihood scoring system has now enabled Nobian to systematically determine the appropriate “Frequency (F)-class” for each studied cavern in their TWR cavern risk matrix. An impact assessment based on the output of the subsidence prognoses produced by the BJP-Algorithm, establishes the “Severity (S)-class” for each cavern. With both a F and S classification, the position of each cavern in the TWR cavern risk matrix is determined and appropriate mitigative measures (such as backfilling) can be planned by Nobian.

Structure of Report 3

After the just presented executive summary, Report 3, titled *“Validation of the BJP-Algorithm by assessment of historical migration behaviour of selected TWR caverns and determination of the likelihood of migration”*, continues with an Introduction in Chapter 1. The introduction describes the background of the UMS-TWR, the related scope of work performed and the overall reporting structure for the combined Phases I and II of the study. Chapter 2 discusses the methodology and input data used for the reconstruction of cavern development, backfilling and cavern migration. The actual validation of the BJP-Algorithm is provided by the reconstructions of well-documented cavern migration cases in Chapter 3. The initial validation based on the reconstructions for relatively straightforward cavern migration cases is presented in this chapter. To aid the readability and illustrate the work processes performed during the study, a high level of detail in the description for cavern 15 is provided. The descriptions of further reconstructions in this report will be more limited assuming a general understanding of the reconstruction processes. Chapter 4 continues with descriptions of the reconstructions made for the relatively complex cavern migration cases. To conclude the description of the validation process, the reverse operation of the algorithm is discussed in Chapter 5. The likely causes of migration for the caverns discussed in Chapter 3 and 4 will be discussed in Chapter 6. This chapter also presents the developed migration likelihood scoring system. The conclusions and recommendations with regards to the validation of the BJP-Algorithm will be presented in Chapter 7. References are listed in Chapter 8 and the APPENDIX II has been included in this report. APPENDIX I to Report 3 is delivered as a separate document to ease parallel reading of the report and this appendix.

5.1.2.e

Sondershausen, 29 December 2024

1. Introduction

1.1. Background

The historic development of the Nobian cavern fields within the Twenthe-Rijn mining permit (incl. extensions) has been divided into five phases (“Fase” 1 -5) as shown in Figure 1 below.

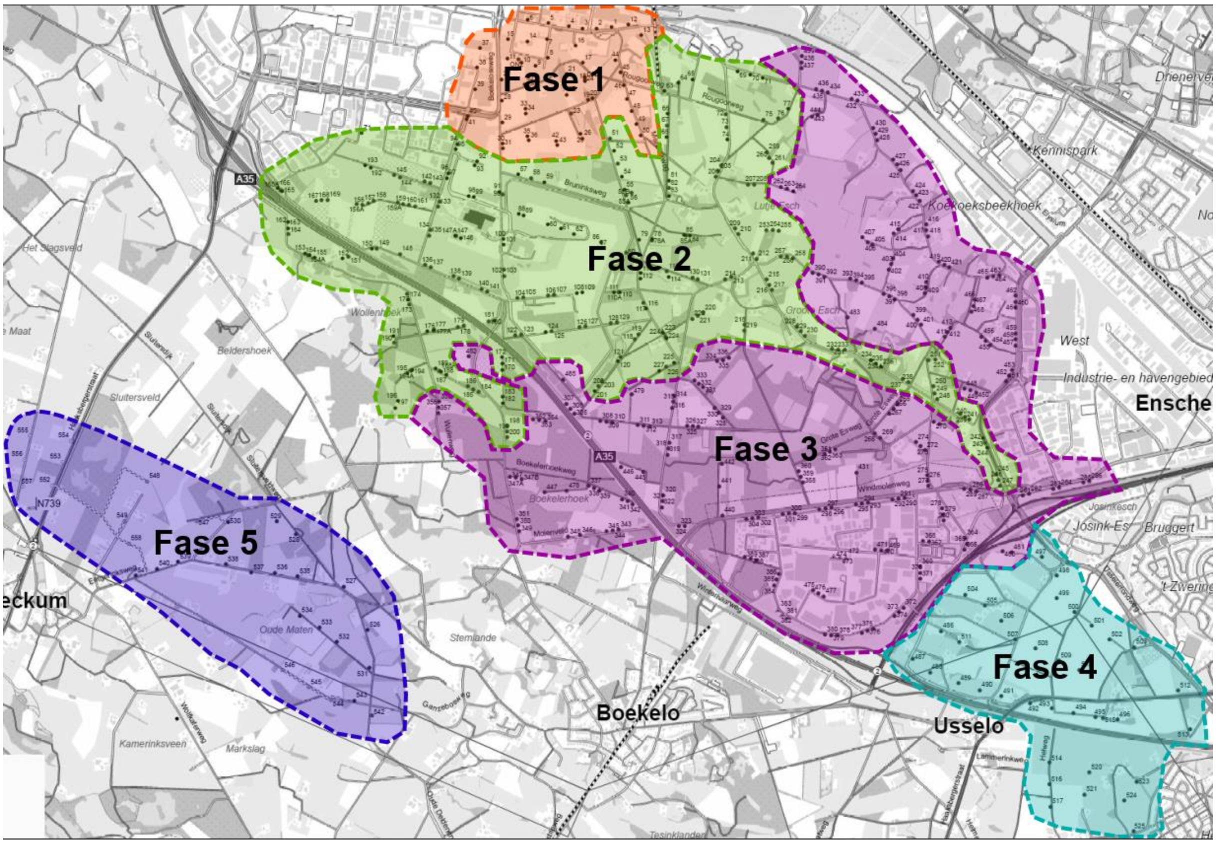

Figure 1: Historic development of Nobian cavern fields in the TWR permitting area, Twente, The Netherlands (Nobian, 20220919 – Opvolging werk Bekendam vs2.ppt)

For the caverns within the areas depicted “Fase 1” and “Fase 2” an update of the existing cavern migration assessments prepared by (late) Roland Bekendam was sought by Nobian. REinvent GmbH (Reinvent) and K-UTEC AG Salt Technologies (K-UTEC) were (sub-)contracted by Nobian to perform the study. Work was initiated in January 2023 and continues as this third report covering the overall study results is delivered.

The offered scope has been structured as proposed by Nobian and comprises three phases, each consisting of several parts, see paragraph 1.2 for details on the overall Scope of Work for the study.

1.2. Scope of work

The Update Migration Study Twenthe-Rijn (UMS-TWR) has been structured in three phases (I, II and III) with each up to three parts (A, B and C). The study phases and related parts are described in the following:

Phase I: Reconstruction of well documented cavern migration cases

The scope of work for Phase I, reconstruction of well documented cavern migration cases, was distributed over three parts:

Part A: Reconstruction cavern development.

Part B: Reconstruction of cavern migration process.

Part C: Effects at surface related to cavern migration.

The studied migration cases and their role in the validation process are presented Table 1 below. For details on the roles, see paragraph 3.1.

Table 1: Studied TWR cavern migration cases and their role in the BJP-Algorithm validation process

Cavern (-system)	Backfill applied?	Used for initial validation	Used to strengthen validation	Used in reverse operation	Not used for validation
C15	Yes	✓			
C30-31	No			✓	
C33-34-35-36	No			✓	
C37	No	✓			
C49*	Yes	✓			
C50*	Yes	✓			
C63-64-65	Yes		✓		
C69-70-71	Yes		✓		
C72-75-76-77	Yes		✓		
C86-87	No	✓			
C104-105-106-107	Yes		✓		
C167-168-169	Yes				✓

* Caverns C49 and C50 are further discussed as the cavern system C49-50 in relation to the reconstruction.

The last cavern studied as part of the BJP-algorithm development was cavern C167-168-169. The cavern development and migration processes for this cavern are fairly well documented but cannot be described by the BJP-algorithm. The reason is the presence of extensively fractured overburden strata, directly over the cavern, resulting in a laterally propagating migration column rather than the vertical propagation observed for all other studied cavern migration cases. As such, cavern C167 is not presented as a validation example of the BJP-algorithm input parameters. The reconstruction work performed will be delivered in an addendum to this Report (ADDENDUM I).

The scope of work for Phase I - Part A was defined as:

> The historic cavern development of ten (10) caverns, of which 7 are (partly) backfilled, will be reconstructed based on the available historic data and information. The aim of Part A is to construct reliable cavern geometries for the 10 selected caverns as a basis for the activities in Part B of the study. The reliability of the reconstructed geometries is limited by the quality of

the input data. No guarantee for the accuracy of reconstructed geometries can be provided due to the absence of validation opportunity (the caverns have already been migrated).

The scope of work for Phase I - Part B was defined as:

Based on the reconstructed cavern geometries from Part A, the historic slurry filling (where relevant) and cavern migration processes for the 10 selected caverns will be reconstructed in Part B, incorporating further historical data and information where available.

The scope of work for Phase I – Part C was defined as:

Combining the outputs from Part A and Part B, the effects at surface caused by the cavern migration of the 10 studied caverns will be investigated in Part C. The main task of this part is to match the actual, measured, subsidence development to the reconstructed cavern geometries and migration processes stemming from Parts A and B with the aim of establishing one (or more) formula(s) that can describe the subsidence effect at surface from cavern migration of the 10 selected caverns. This formula should be applicable to other caverns in the TWR region. The support from a geotechnical/ geo-mechanical specialist was required for Part C and Christian Jakob (K-UTEC) has taken this role.

Phase II: Update Subsidence Prognosis

The scope of work for Phase II, Update Subsidence Prognosis, was distributed over three parts:

Part A:	Classification of caverns and refining prognosis algorithm.
Part B:	Selection of input parameters and initial subsidence prognosis.
Part C:	Finalisation of subsidence prognoses for relevant “Fase 2 and 3” caverns and superposition.

Phase III: Subsidence assessment Fase 1 caverns

(A study for Nobian internal documentation purposes)

The scope of work for Phase III aims to reconstruct the cavern development, migration and consequential subsidence for the caverns in the “Fase 1” area and comprises three parts:

Part A:	Reconstruction cavern development
Part B:	Reconstruction of cavern migration process
Part C:	Effects at surface related to cavern migration

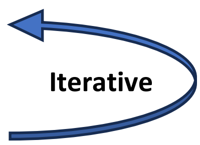

The work during Phase III of the overall study will rely heavily on operating the established BJP-algorithm in “reverse”, meaning that during Part C the known subsidence values from the “Fase 1” area will be used to validate the initially reconstructed migration history (Part B) and cavern geometry (Part A). Experience with such a reverse workflow has been acquired during Phase II of the study.

1.3. Reporting structure

Report 1 [2] covering the initial insights gained during Phase I of the study and was delivered in December 2023. It describes the fundamental principles used during the reconstruction of cavern development by leaching and subsequent migration development of the 10 caverns included in the study. The aim of this report was to explain the fundamental principles related to the reconstruction of cavern development, slurry filling, migration, as well as the consequential link to subsidence. This to support the reader in the understanding of the further parts of the overall reporting. Please note that some of the parameters first presented in Report 1 have been updated in later stages of the UMS-TWR. Where relevant, this will be noted in the following chapters.

Report 2 [3] describes the Bekendam-Jakob-Pinkse (BJP) subsidence prognosis algorithm for migrating salt caverns in a bedded stratigraphy as developed through performance of Phase I and II of the study. Report 2 was delivered in November 2024. The BJP algorithm has been developed based on the historically used "Bekendam-Method" for subsidence prognosis in addition to several new insights from Phase I and II of the UMS-TWR.

Report 3 (this report) presents detailed descriptions of the reconstructions and validates the assumptions made in the BJP algorithm such as values for Bulking Factor (BF) and migration column shape, see Report 2 and the remainder of this report for details. Report 3 can be considered the completion of Phase I of the UMS-TWR.

The Bekendam-Jakob-Pinkse (BJP) prognosis algorithm has been successfully validated using actual subsidence data for the studied caverns during Phase I of the UMS. The cavern-specific input parameters have been selected based on a unified workflow considering the cavern roof position in the stratigraphy, the actual cavern volume and shape, the potential migration column radius, and the likely cavern filling grade by bulked overburden for irregular shaped caverns. The selected input parameters transform an irregularly shaped cavern into a corresponding basic cavern shape (cylinder- and/or cone-shaped) which can be used as input for the BJP algorithm.

Intermediate reporting on the selection of input parameters and validations has been delivered in the form of two presentation slide-decks [4], [5]. A detailed description of these validations is included in this Report 3.

The final report, Report 4, discusses the cavern specific selection of input parameters following the unified workflow, as well as the outcome of the BJP-Algorithm for relevant caverns in the TWR area. Report 4 is titled "Subsidence predictions for potential future migration and recommendations on mitigative action by means of backfilling". It is expected to be delivered in conjunction with this Report 3. Report 4 can be considered the completion of Phase II of the UMS-TWR.

2. Methodology and input data

The fundamental principles for the reconstruction of cavern volume, slurry filling, migration and consequent subsidence have been described in Report 1. Further to this description, this chapter aims to detail the methodology and input data used during the algorithm development process by describing the several workflows applied:

1. For cavern volume reconstruction
2. For slurry backfilling reconstruction
3. For migration reconstruction
4. For the linking of subsidence to migration.

2.1. General workflow for the reconstruction and algorithm development process

The workflow for Part A was divided into the following steps:

- Transfer of data from Nobian to REinvent and review on completeness.
- General review and organisation of data.
- Extracting information from the provided data and populating Masterfile Phase I+II+III.
- Reconstruction of sump development of Reference Caverns
- Reconstruction of cavern development Phase I-Part A Caverns

It became clear, during the performance of Phase I – Part A, that a purely sequential performance of the consecutive parts of Phase I was not leading to the expected results. The leaching history of several caverns was not sufficiently understood at this stage to finalise the reconstruction of the 10 studied caverns. As a result, it was decided to initiate work on Part B (and Part C shortly after) to enable a more iterative approach to the Phase I Scope of Work. In the iterative approach, the following steps were added for Part B to the workflow list above:

- Extracting information from the provided data on slurry-filling and migration history of the caverns and populating the Masterfile Backfilling.
- Reconstruction of slurry-filling process for relevant caverns aimed at finding the slurry to backfill ratio, i.e. how much insitu unconsolidated backfill remains from a certain slurry volume.
- Reconstruction of consolidation behaviour of backfill under self-weight and under the load of bulked overburden.
- Reconstruction of the migration column development based on available information, such as sonar measurements and Gamma Ray (GR) logs.
- Iteration with Part A, cavern reconstruction to derive generalised cavern shapes and consequential migration column shapes, with and without backfill.
- Update of Part B backfill and migration column reconstructions after iteration with Part A, cavern reconstruction.
- Deriving an updated value for the Bulking Factor from the reconstructed migration columns.
- Deriving updated values for the consolidation behaviour of the insitu backfill by self-weight consolidation (SWC) and under the load of bulked overburden.

To enable iteration between Parts B and C the following steps were added to the workflow covering the Part C scope:

- Extracting information from the provided data on historical subsidence above the studied caverns and populating the Phase I-Part C Master-File.
- Deriving simplified cavern shapes and corresponding migration column shapes.
- Applying the outcomes of Part B (e.g. Bulking Factor for overburden, consolidation behaviour of backfill) to the simplified cavern and migration column shapes.
- Iteration with Part B, cavern backfilling and migration reconstruction to fit the calculated subsidence to the actual, measured subsidence above the 10 migrated caverns studied in Phase I of the study.
- Deduction of a subsidence prognosis algorithm that can be applied to the total population of caverns for which a subsidence prognosis based on a potential cavern migration is sought by Nobian.
- Validation of the algorithm, including the parameter selection by demonstrating that the algorithm can explain (nearly) all studied migration cases, with and without backfill, and including the well-known cases such as the cavern 69-70-71 sinkhole and the cavern 33-34-35-36 trough.

2.2. Software used during the study

The digital "Master-files" recording all information extracted from the numerous historical records provided by Nobian, were prepared using Microsoft Excel-workbooks. PowerPoint was used to capture graphical information such as subsidence graphs. The Excel-based Master-files are linked to each other to enable automatic updating of calculations with revised input values without manual labour, thus ensuring data consistency throughout the study Phases.

The reconstruction of caverns, cavern backfilling and cavern migration has been primarily performed using AutoDesk's AutoCAD 2023/2024 3D CAD modelling software. Caverns were modelled and referenced in 3 dimensions by representing produced salt in tons as cavern volume in cubic metres. Care was taken to place the cavern reconstructions in the correct position in relation to each other and at the correct depth. When sonar images where obviously rotated or translated (based on cavern wall geometry for instance) corrections of sonar image position where applied. Reasons for such errors in the sonar image position are the unquantified deviation of wells and erroneous processing of raw sonar images whereby a rotation of the image around the well-axis was introduced. Where relevant, such corrections are mentioned in this report and in Report 4.

During the performance of the workflow described in paragraph 2.1, the need for Boolean operations on sonar images arose. The actual cavern volume is not always represented by a single image and overlapping sonar images share a part of their volume but are measured from different viewpoint, i.e. wells. The ability to perform Boolean operators on sonar images has been a long-standing challenge for which an automated workflow was not available. Manual CAD-based combination of sonar images by SOCON Sonar Control Kavernenvermessung GmbH was the only known method and deemed too cumbersome for application in the TWR area.

By applying a set sequence of file conversions, a digital workflow was created which enables the application of Boolean operators on 3D sonar images of caverns. The main software package used for the manipulation of sonar images to derive an actual cavern volume from multiple, partly overlapping,

REINVENT

sonar images, is AutoDesk's Fusion360. This new workflow now also allows for sonar images of caverns to be accurately 3D printed at for example a convenient scale of 1:1000 for research and/or communication purposes. The developed file conversion and Boolean operator workflow is proprietary knowledge of REinvent GmbH and is as such not further detailed or published.

The developed subsidence prognosis algorithm is described in Report 2. To enable an automated workflow, the subsidence prognosis algorithm was coded into a Python script that automates input data processing, calculation of subsidence prognoses and generation of output data as well as output graphics. This Python script is proprietary knowledge of K-UTEC AG Salt Technologies and is as such not further detailed or published.

The reporting and dissemination of the study's outcomes is performed using Microsoft's Word and PowerPoint software packages. All graphics used in the reporting are produced by the authors using the drawing function of the Microsoft Office suite.

2.3. Cavern reconstruction process details

As detailed in Report 1, for each one (1) ton salt produced from a cavern, as per the historic production records, 0,562 m³ of cavern volume is created. Using this conversion factor, the historic records containing the annual production figures were converted to the corresponding cavern volume creation. By further using the geology, the well configuration information regarding casing shoe and string depths and any sonar data available, the spatial distribution of the created volume has been reconstructed. The reconstruction process comprises the following general steps:

1. Plot well configuration(s).
2. Establish circular or non-circular contour(s) that cover the extent of the cavern at subsequent development stages.
3. Determine duration of sump phase based on any (or all) notes in the drilling diaries, connection to adjacent wells, changes in well configuration and/or reaching of the maximum diameter/contour.
4. Reconstruct the sump phase as an inverted cone with a 15° cone angle (from horizontal). This value was chosen based on the reconstruction of reference caverns during the initiation of Phase I-Part A of the study.
5. Reconstruct vertical cavern extension based on the maximum diameter/contour in (multi-) yearly slices until the maximum volume has been fully represented.
6. Apply an eventual offset in the Z-direction to shift the cavern roof to the known roof depth based on sonar. The Z-shift shift is often necessary for caverns which were developed without a blanket medium to force a deep sump which caused the sump to have a much steeper cone angle and thus a much larger sump height. The principle of Z-shift is explained by Figure 2 on the next page.

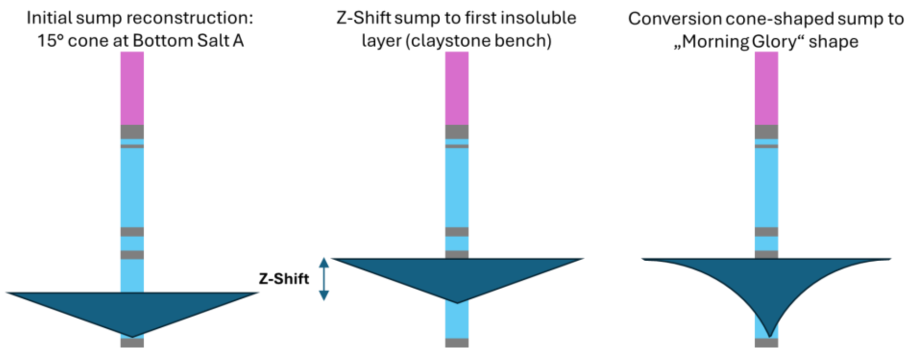

Figure 2: Z-Shift principle of sump used during reconstruction for caverns which were developed without a blanket-medium

As stated in paragraph 2.1, the cavern reconstruction work was performed iteratively with the backfill and migration reconstruction work in Phase I, Part B. The iterative process also involved the actual, measured subsidence collated as part of the Phase I, Part C performances.

The geological information used during the reconstruction was taken from the Nobian database to represent the most recent insight in the position of the geological strata in the subsurface. The stratigraphy has been represented in the reconstruction models as colour-coded columns, see paragraph 2.6 for details.

The reconstruction process of the sump-phase, as presented in Figure 2, was initially applied to all 10 caverns studied during Phase I. However, at some caverns the wells were hydraulically connected directly after drilling by so-called forced leaching[1]. The reconstruction of these cavern was unsuccessful using the process presented in Figure 2. Caverns for which forced leaching was applied during the sump development show highly asymmetric development, which is hard to capture using simple cylindric slices. The reconstruction of these caverns is therefore based on a complex contour construction based on the actual cavern geometries derived from the sonar data. The confidence in the reconstruction of such caverns is lower when compared to caverns which were not developed using forced leaching.

The forced leaching establishes a laterally extended sump contour with very little height. A sump contour developed by forced leaching is further named “forced leaching corridor” (FLC). During the forced leaching operation, the FLC seems to propagate preferably underneath an intermediate claystone bench. The insoluble material in the bench acts as a barrier for upward leaching. The depth at which the FLC intersects the wells is largely unknown. The notes in the well diaries regarding forced leaching operations are limited as service providers were apparently responsible for the execution. Despite the limited information available, it has been possible to reconstruct the forced leaching history and its outcome for all relevant caverns in this report.

After reconstruction of the total cavern volume, the reconstructed cavern is ‘filled’ with the volume of insoluble material inclusions in the salt and, where relevant, with the volume of claystone benches that intersect the reconstructed cavern. Each of these fill sources has a bulking factor that should be applied as the material collects on the cavern bottom (sump). Report 1 states bulking factors for these

[1] „Forced leaching“ is a process whereby two or more drilled and completed wells are pressurised with water to force a leached path between wells which can be used as a cavern sump for further cavern development. See Chapter 4 for details and examples.

sources based on the reconstruction of caverns in Phase I-Part A. During the performance of Phase II, the previously stated values were adapted to the values in Table 2.

Table 2: Bulking factors used during validation of the BJP-Algorithm compared to values presented in Report 1

Material source	Bulking Factor for validation (this report)	Bulking Factor Report 1
Insoluble material from salt	1,1	1,3
Intermediate claystone benches (AB & BC)	1,0	1,1
Claystone CD bench	1,15	--
Overburden	1,2	1,2

These values have been updated to introduce conservatism and are now based on the following:

- Insoluble material from salt has been extracted and studied as part of a M.Sc. Thesis project performed at Nobian in 2012[2]. Oedometer testing of insoluble material extracted from salt cores have shown that the initial porosity of settled insoluble material is approximately 33%. After applying a load of 120 kPa in an oedometer test representing self-weight consolidation, the porosity is reduced to 28%. A porosity of 25% equals a bulking factor of 1,3 and a bulking factor of only 1,1 is therefore selected as a very conservative value.
- The mechanics with which intermediate claystone benches collapse after being liberated by leaching (usually from the bottom side) are difficult to generalise as they will depend on several factors such as: the presence of soluble salt within the intermediate claystone benches, presence of fractures and block size of fragments, drop-height, drop path and location in the cavern, turbiditation and debris flow, etc. Literature values for the bulking of claystone vary between 1,2 and 1,5. The selected bulking factor of 1,0 assumes large fragments (slabs) of claystone settle within a matrix of insolubles settled in the sump without adding any porosity. A value of 1,0 and can consequently be considered a very conservative value. Where the volume of collapsed intermediate claystone benches could not be reconstructed with confidence, their volume was completely ignored to error on the safe side in terms of cavern filling by intermediate claystone bench material.
- The bulking factor used for the Claystone CD bench is 1,15. This value is based on a bulking factor for the overburden of 1,2 which will be validated in this report. The overburden BF=1,2 has been reduced to represent some of the collapsed Claystone CD bench material being (partly) buried in either insolubles material and/or backfill material present in a cavern at the time of collapse. Compared to literature values, see the previous item in this list, a bulking factor of 1,15 is deemed conservative.

2.4. Cavern backfilling and migration reconstruction process details

Caverns in the TWR area have been backfilled using a slurry comprising brine purification residues (BPR), i.e. mainly gypsum and calcium carbonate precipitation products. The BPR have been pumped to caverns from which brine production through leaching was suspended. BPR particles settle in the cavern while the brine used as their carrier fluid is returned to the salt plant. The settled particles can be considered as backfill material after self-weight-consolidation (SWC) has taken place.

[2] http://resolver.tudelft.nl/uuid:dda45cb7-e64d-4e23-b616-90457d01997a

It has always been assumed that the BPR particles lead to a reduction in potential migration height of caverns as the overall cavern volume is reduced by the presence of BPR solids. In the Bekendam-method the presence of backfill material directly reduced the migration height, as the cavern height was reduced by the backfill. Bekendam generally used a factor of five (5) to convert from cubic metres of slurry to cubic meters of backfill in the cavern, e.g. 1000 m³ slurry = 200 m³ backfill in the cavern. In this manner, any backfill applied was considered to effectively have properties similar to the original insitu rock salt as no further consolidation of the backfill in the cavern was considered. The SWC and subsequent consolidation under the load of bulked overburden, in case of migration, are both considered in the BJP-Algorithm.

The slurry/backfill (S/F) factor has been maintained at five (5) in the present study. Refer to Report 2 for more details on the consolidation behaviour of slurry based backfill. The assumed S/F = 5 and the consolidation behaviour described in Report 2 will be validated in Chapter 3 of this Report 3.

The historical volumes of BPR slurry pumped to each cavern have been deduced from both internal memos and a recent analysis of production figures (brine volume production) from caverns being filled with the BPR slurry. The precise solids content of the slurry is not recorded, nor is it expected to have been constant throughout the decades of operation of the brinefield. As a result, it has not been possible to exactly determine how much solid material has been pumped to caverns historically, nor is that exactly known in the current operation.

Notwithstanding the absence of an exact solids content value for the BPR-slurry, a repeatable well-fitting volume balance was derived from the assessment of historically and recently backfilled caverns, considering both the total BPR slurry volume pumped to a cavern and before-and-after sonar images of a cavern. The slurry/backfill reconstruction process thus comprises the following general steps:

1. Establish the total BPR slurry volume pumped to a cavern, preferably using specific operational details (e.g. cavern system configurations, injection/production wells) trough time.
2. Correlate the pumped slurry volume to cavern volume reduction as shown by sonar images and/or reconstructed cavern volumes:
   - Apply a Boolean combination of multiple sonar images and/or reconstructed cavern volumes where relevant to establish the most accurate possible total cavern volumes.
   - Perform a comparison of the reconstructed cavern volume and/or the volume determined by Boolean combination of sonar images with the production data to align cavern volume to total salt production.
   - Perform a volume analysis of pumped slurry volume, fresh backfill volume, backfill volume after SWC and backfill volume after loading with bulked overburden.
3. Establish remaining cavern volume after backfilling as a basis for the reconstruction of cavern migration.
4. Check if the cavern volume may have been enlarged due to NaCl-undersaturation of the pumped slurry, by comparing (combined) sonar volumes with production figures and operational regime of cavern systems. Where appropriate, a cavern volume increase has been applied to compensate for undersaturated slurry.

Once the cavern volume and the (net backfill volume, i.e. after SWC) backfill volume have been established, the reconstruction of the migration column can be initiated. The migration reconstruction process comprises the following steps:

5. Select most likely migration contour based on the intersection of cavern volume with the Claystone CD, Salt D and Anhydrite-E members.
6. Select the appropriate migration column shape (cylinder, cone or cylinder + cone) based on the (reconstructed) cavern shape.
7. Reconstruct the migration column using the established cavern volume, shape and (net) backfill volume.
8. Compare the reconstructed migration column to any historical evidence of migration as indicated by for example sonar images, Gamma Ray (GR) logs and observations noted in well diaries.

The cavern backfilling and migration reconstruction process for the 10 studied cavern migration cases during Phase I of the study was performed iteratively to achieve a set of reliable input parameters for the BJP-algorithm that are applicable to the majority of the studied caverns.

2.5. Establishing the link between cavern migration and subsidence

The actual subsidence over the well-documented cavern migration cases has been measured and recorded during the regular levelling campaigns performed by Nobian and its legal predecessors. The available subsidence data for the studied caverns was collated from the report "Meetreeksen boringen Twenthe-Rijn" by Oranjewoud [6]. The processed input data (in Excel file format) used to prepare this report was also made available which eased data processing, and the production of the graphical representation used in the remainder of this Report 3.

The subsidence over older caverns in the TWR area was originally measured using dedicated levelling points at short distance from the wells. This practice was later abandoned in favour of the current practice using a wider chain of levelling points at a larger distance from the caverns to establish a more reliable levelling result. For the purpose of establishing the actual subsidence development for the studied caverns however, the original levelling points near the wells, provided an accurate resource to establish the maximum depth of a subsidence bowl caused by the migration of most studied caverns, albeit only up to 2005.

Assessing the development of the maximum depth of each subsidence bowl allowed for the fitting of reconstructed migration columns based on the fundamental principles explained in Report 1 and the relationships between migration and subsidence described in Report 2. Initial fitment of reconstructed migration to actual measured subsidence was done "manually" using volume balancing in Microsoft Excel. This allowed for initial migration reconstructions for C15, C49 and C50.

However, as explained in paragraph 2.1, an iterative approach to the three parts of Phase I allowed for a more efficient performance of the study. As a result, the development of the updated prognosis BJP-Algorithm was achieved before the reconstruction of the remaining well-documented cavern migration cases was completed. This enabled the use of the newly developed algorithm to perform the reconstruction of the remaining caverns, thus creating a more efficient workflow as the processing of input data was done by a Python script rather than manually in Excel. The link between cavern migration and actual measured subsidence for the studied caverns is detailed in Chapter 3 where appropriate.

2.6. Stratigraphy representation (Recap Report 1)

The representation of the overburden stratigraphy used in the cavern reconstruction process is presented in Figure 3. A detail representation of the salt bearing strata is included in this figure. The position of the strata interfaces has been based on the most recent data available in the Nobian geological database.

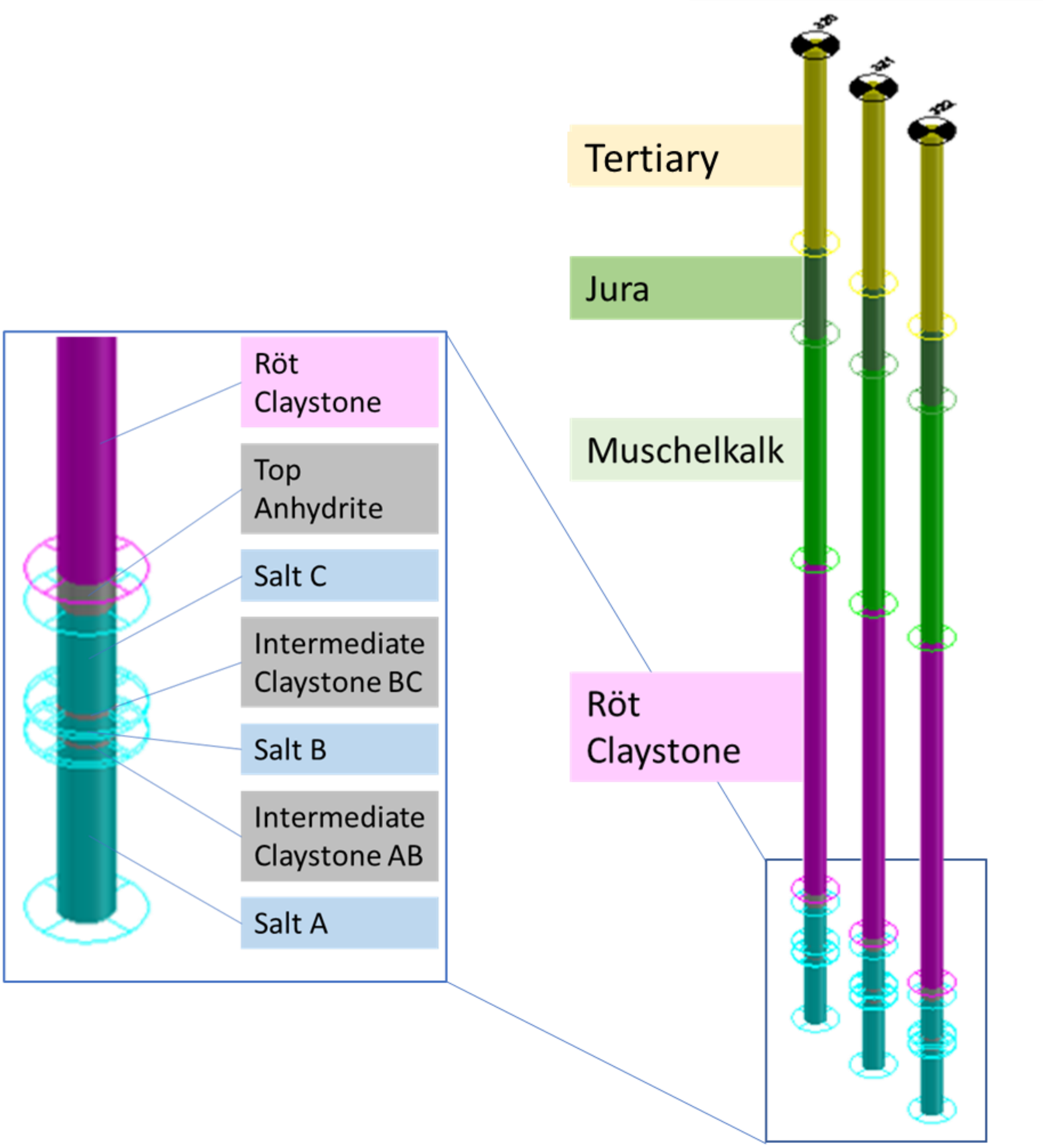

Figure 3: Stratigraphy of the overburden and salt-bearing strata at the brinefield. The Top Anhydrite comprises the Claystone CD, Salt D and Anhydrite-E members.

The defining characteristics of each stratum in the stratigraphy shown in Figure 3 are summarized in Table 3.

Table 3: Defining characteristics of geological strata found in the study area (source: well logs, available at NLOG.nl).

Stratum	Defining properties for the reconstruction of cavern development and migration
Tertiary	Comprises mostly unconsolidated sand and clay. Tertiary sediments are not capable of spanning a large roof span. Consequently, when a cavern of sufficient diameter and height migrates upwards and reaches the bottom of the Tertiary, failure of the Tertiary sediments may occur leading to significant subsidence.
Jura	Rarely present in the study area (only at cavern 167). Comprises marl interbedded with limestone and contains gypsum nodules and shell fragments. Rocks of Jurassic age in the study area are assumed to have geo-mechanical properties similar to the underlying Muschelkalk and thus (temporarily) support a cavern roof span.
Muschelkalk	Comprises mostly marl with some limestone and gypsum nodules. Logs also mention sandstone and claystone layers as part of this stratum. Does not occur at all wells in the study area.
Röt Claystone	Forms the main overburden member overlying the saline strata. The Röt-Claystone comprises carbonate-rich mud- and claystones, as well as sandy claystones, with and without gypsum nodules. For most migrated caverns in the study area, the Röt-Claystone is the main stratum through which cavern migration has propagated.
Top Anhydrite	Comprises claystones and anhydrite, sometimes with rock salt interbeds ("Salt D"). It has been observed that the Top-Anhydrite can maintain a stable cavern roof span for considerable time (decades). Deterioration and/or collapse of the Top-Anhydrite is unpredictable considering the observations in the brinefield. In some cases, the Top Anhydrite collapsed during production, while in other cases, the Top Anhydrite has been stable for several decades after production has stopped. The collapse of the Top Anhydrite in some cases may have been triggered by the presence of faults in the overburden as established in some areas of the brinefield, e.g. around cavern 69-70-71 where a sinkhole was formed in 1991 after migration of the cavern. Collapse may also be initiated by water or weak brine being present directly underneath and enabling the formation of gypsum and consequential "scaling" of bedded layers of Anhydrite, claystone and salt. As Anhydrite has a very low and temperature independent solubility, it has acted as a natural "blanket medium" for cavern development, i.e. acting as the maximum depth underneath which leaching takes place, see also Chapter 3 for examples.
Salt C	Upper main salt production member for the caverns in the study area. Comprises rock salt with a low percentage of insolubles (assumed 5 m.-%).
Salt B	Minor salt production member, sometimes very thin (< 5 m). Rock salt from this member may have fallen to the bottom of the cavern in combination with collapsing intermediate rock benches after which dissolution of the salt is slowed by the relative high salinity of brine near the bottom of a cavern.
Salt A	Lower main salt production member for the TWR caverns. For the caverns in the study area, leaching of the Salt A member is often limited by the absence of a controlled (oil) blanket, forcing the leaching upwards and into the Salt B and C members.
Intermediate Claystone benches	Salt members are separated by intermediate rock benches comprising claystone, anhydrite and dolomite. Once sufficiently exposed, these benches collapse and the (insoluble) material sinks to the bottom of the cavern. During cavern development, the material from the intermediate rock benches, combined with the insolubles from the rock salt, will (partly) fill the initial sump volume of the cavern.
Bottom Anhydrite	Lowest member of the saline strata comprising mainly Anhydrite. Due to the low solubility of the anhydrite in this member, it can be assumed that cavern development has always taken place above this stratum.

2.7. Subsidence stages (Recap Report 2)

Within the Update Migration Study TWR, potential surface subsidence, that can develop as a result of the presence of a cavern in the underground, is differentiated into five (5) possible stages. These stages are illustrated in Figure 4 below.

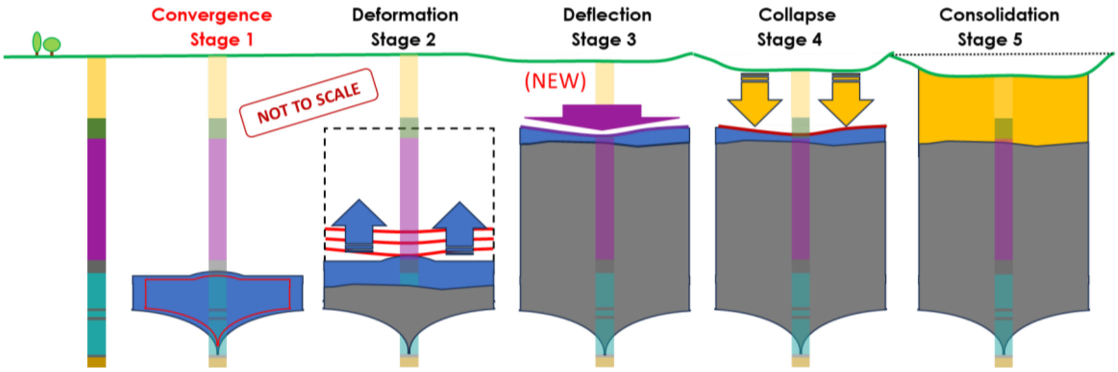

Figure 4: Possible subsidence stages for the studied caverns

The first stage of subsidence shown in Figure 4 is caused by cavern convergence due to salt creep. This type of subsidence is present for all caverns in the TWR area. Subsidence by convergence is not relevant for the UMS-TWR and therefore not further considered. Subsidence stages that are considered are all result from the migration of a cavern. Not all subsidence stages are always relevant, migration can stop due to cavern geometry well before all subsidence stages have developed. Short descriptions of each subsidence stage considered by the BJP-algorithm are provided by the following:

Stage 2 Subsidence caused by the deformation of the cavern and migration column as it propagates upwards through the stratigraphy, i.e. mainly by deformation of the Röt Claystone and the overlying Muschelkalk formations.

Stage 3 Subsidence caused by the deflection of the last remaining beam of competent rock over a migrated cavern below the unconsolidated Tertiary soils before the cavern migration reaches the critical depth d_crit.

Stage 4 Subsidence caused by the collapse of the last remaining beam over competent rock and subsequent “plug-failure” of the Tertiary soils into the remaining cavern volume.

Stage 5 Subsidence caused by the consolidation of the bulked overburden under the load of the Tertiary soils.

The implementation of each of these subsidence stages in the BJP-algorithm is detailed in Chapter 3 of Report 2 [3].

2.8. Basic denotations and indexes (Recap Report 2)

Table 4 gives an overview of the most important denotations and indexes for the BJP subsidence prognosis algorithm. Indexes are frequently used several times for one denotation. In these cases, the indexes are separated by commas (e.g. $d_{(Tcav,act)}$ means depth of the actual cavern top in meters below ground level).

Table 4: Basic denotations and indexes in the BJP-Algorithm

Symbol	Unit	Description
Denotations		
d	mbGL	Depth (always given in meters below ground level, i.e. increasing with depth)
H	m	Height (vertical distance)
R	m	Radius
V	m^3	Volume
η	m	Surface subsidence
$fconsol$	%	Consolidation factor for backfill
Indexes		
X_{TR}	-	Index for top of overburden rock (top rock)
X_{cav}	-	Index for cavern
X_{Tcav}	-	Index for cavern top
X_{Bcav}	-	Index for cavern bottom
X_{cyl}	-	Index for cylindrical part of the cavern
X_{cone}	-	Index for conical part of the cavern
X_{ini}	-	Index for initial state of the cavern
X_{act}	-	Index for actual state or starting state for calculation algorithm
X_{mig}	-	Index for migration volume
X_{crit}	-	Index for critical depth (below top rock)
X_Y	-	Index for stage Y subsidence for Y in {2, 3, 4, 5}
X_{hmb}	-	Index for half-height of the migration body
X_{final}	-	Index for final stage of cavern migration
$X_{(no\ backfill)}$	-	Index indicating the absence of backfill
X_{solids}	-	Index for unconsolidated backfill solids

3. Validation of BJP-Algorithm by well-documented migration cases

3.1. Introduction – what and how to validate?

The BJP subsidence prognosis algorithm was developed using the work processes described in the previous chapter. To ensure that the developed algorithm is applicable to the largest possible population of caverns for which future migration cannot be ruled out, it was validated using the insights gained from the reconstruction of well-documented cavern migration cases.

The validation of the developed prognosis algorithm is achieved by demonstrating that the derived relationships and selected input parameters are applicable to the well-documented migration cases and thereby for the entire TWR area while remaining conservative in the selection of parameters. This demonstration of applicability focuses on the four main input parameters:

1. Effect of cavern shape on migration column shape.
2. Bulking Factor of insolubles, intermediate claystone benches and overburden materials.
3. Backfill volume balance: actual insitu backfill versus pumped slurry.
4. Backfill behaviour under load: consolidation by self-weight and under load of bulked overburden.

The validation of the developed BJP-Algorithm is initially demonstrated by the reconstruction of cavern development, backfilling and subsequent migration for five (5) caverns with either a relatively simple geometry / migration history or which are very well documented in this Chapter 3. These caverns are C15, C37, C49-50 and C86-87. The relatively extensive amount of available information on these caverns has enabled the reconstruction processes and allowed confident fitting of the input parameters to match the actual observed migration and the actual measured subsidence.

The validation of the BJP-Algorithm is subsequently strengthened by the reconstruction of more complex cavern migration cases in terms of cavern geometry, backfilling history and/or migration history in Chapter 4. These caverns are C64-65, C69-70-71 (location of the 1991 sinkhole formation) and C106-107, which are all well-documented. The reconstruction process for these caverns demonstrates that the initially selected input parameters can also be confidently applied to more complex cavern migration cases.

The cavern development and subsequent migration history of caverns C30, C33 and C35 are not sufficiently documented to allow the reconstruction process applied to the caverns described prior. Nonetheless, these caverns were reconstructed using the BJP-algorithm by operating it in “reverse”. In other words, using the actual measured subsidence and the production history as the input parameters to, iteratively, determine the most likely migration column shape and extend. The reverse operation of the algorithm enabled the reconstruction of the original cavern volumes with confidence, see Table 1 for an overview, and is discussed in Chapter 5.

3.2. Reconstruction C15

3.2.1. Cavern development by leaching

Cavern 15 (C15) is a single completion cavern (SCC) developed from well TWR-015 drilled in 1948. The key data for C15 are included in Table 5 below and additional information can be found in APPENDIX I.

Table 5: Key data Cavern 15

Wells	X (WGS84)	Y (WGS84)	Z (mNAP)	Final depth (mbgl)	Final depth (mNAP)	Well ready	Start production	End production	Cemented
15	250764,6	473847,1	19,62	406,95	-387,33	14-10-1948	14-10-1948	7-2-1968	20-10-2000

The sump phase of the C15 has been reconstructed based on the maximum contour as derived from a sonar image from 25-09-1967. The reconstruction of the sump with an initial cone angle of 15° has been applied for the first three years of production, i.e. 1948 until 1950. The sump cone dimensions until 1950 are as presented in Table 6 and fit well to the maximum contour derived from the 1967 sonar image in terms of overall diameter.

Table 6: Reconstruction SCC Sump 15

Cavern (SCC)	Year	Production (t)	Sump volume (m³)	Cone radius (m)	Cone height (m)
15	1950	64.450	36.755	50,8	13,61

The reconstructed sump phase of cavern 15 is presented in Figure 5 where the mentioned sonar image from 1967 is also shown for comparison of the maximum contour. Please note that the sump has been positioned 15,1 m above the bottom of Salt A at this stage because of a Z-shift discussed later in this paragraph.

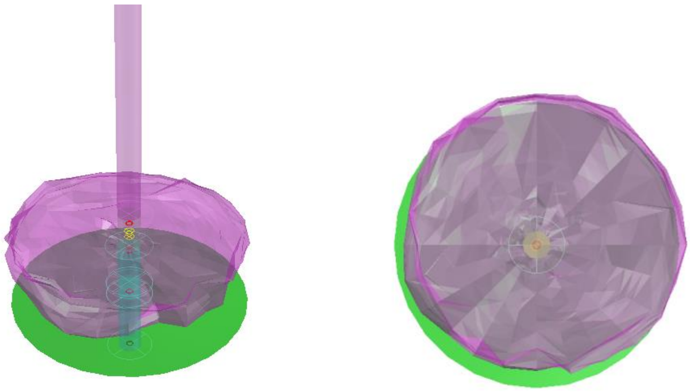

Figure 5: Isometric (left) and top (right) view of the reconstructed sump SCC 15 (green)and sonar image from 1967 (magenta)

After the development of a sump with a radius of 50,8 m, the cavern was further reconstructed by extending the maximum contour upwards to account for the tonnage of salt produced according to the historical salt production records. As can be seen in Figure 5, the assumed upward development is confirmed by the row of production string shoes at decreasing depth that are drawn in as small red and yellow circles, i.e. the leaching depth in the cavern was reduced several times to promote vertical expansion of the sump. The depth values of the production string shoe were taken from the well diaries.

The yearly slices of cavern volume added between 1951 and 1961 by leaching, and the resulting reconstructed cavern is presented in Figure 6. The total volume of the cavern is 232.572 m³ at this stage. In 1961 brine production by leaching is stopped as the top of Salt C has been reached and the cavern is prepared for slurry filling.

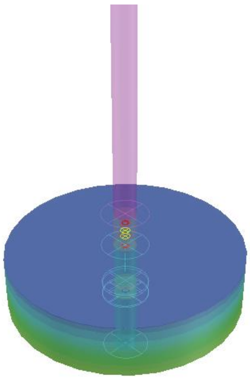

Figure 6: Isometric view of the reconstructed SCC 15 in yearly slices until 1961 (end of production by leaching)

The reconstructed cavern intersects two intermediate claystone benches over the full span of the cavern. The volume of the broken material from the benches on the bottom of the cavern is derived using a bulking factor of 1,0 as explained in paragraph 2.3. No bulking is attributed to the intermediate claystone benches to emulate the situation in which claystone bench material will be buried in a matrix of insolubles liberated from the salt. Omitting bulking of this material is deemed a conservative approach.

Once the top of the reconstructed cavern is established by adding the volume of the fallen benches (red in Figure 7), a shift of the total reconstructed volume by 15,1 m in positive vertical direction (Z-shift) and stretching of the sump was applied to align the top of the total reconstructed volume with the top of Salt C and create a "Morning glory" sump shape. The resulting reconstructed cavern and the corresponding sonar image from 1967 are shown in Figure 7.

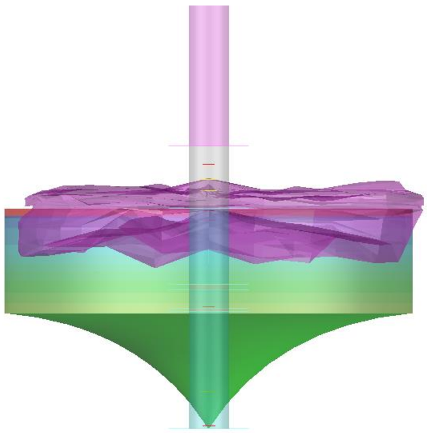

Figure 7: Side view of the reconstructed C15 until 1961 with adjusted sump shape ("Morning glory") and volume induced by falling rock benches visible in red. Infill with claystone bench material not visible at this stage.

With the reconstructed cavern volume based on production complete and positioned correctly, the filling of the sump with insoluble material from the rock salt and the intermediate claystone benches can be subtracted from the reconstructed cavern volume. The derived fill volumes based on volume of the intersected rock benches and the total cavern volume until 1961 are presented in Table 7.

Table 7: C15 – Intermediate claystone benches and insoluble material fill until 1961 (end of production by leaching)

Rock bench fill		
Rock bench BC	10.377	m³
Rock bench AB	5.675	m³
Total	16.052	m³
Bulking factor	1	
Bench fill volume	16.052	m³
Insoluble fill		
1961 cavern volume	232.572	m³
Bulking factor	1,1	
Insoluble fill volume	13.499	m³
Total fill volume	**29.551**	

The total volume of (bulked) material as calculated in Table 7 is sufficient to mostly fill up the sump. The final shape of the reconstructed cavern after application of the infill as described in Table 7, is shown in Figure 8.

The total volume of the final 1961 reconstructed cavern is 219.074 m³.

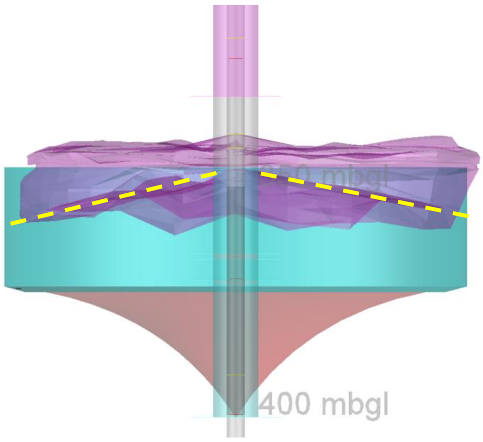

Figure 8: Reconstructed cavern (blue) until 1961 and sonar image (magenta) from 25-09-1967. Yellow dashed lines indicate slurry backfill applied between approx. Oct. 1961 and the sonar date. Insolubles and intermediate claystone benches fill in the sump indicated by red.

The well diary of C15 records in October 1961 that the cavern is prepared and ready for slurry filling. Figure 8 clearly shows the slurry fill in the cavern, after being pumped to the cavern between October 1961 and September 1967, as a cone with an angle of repose of 15-25° from horizontal (yellow dashed lines).

The sonar image of 1967 also shows that the actual cavern has extended vertically into the strata overlying Salt C, as can be seen from Figure 8, where the magenta sonar extents above the blue top of Salt C. The roof position of C15 in 1967 is caused by the (gradual or sudden) collapse of the claystone bench CD over Salt C. Salt-D is not present according to the drilling log. This roof position is most likely linked to the presence of a (semi-)competent Anhydrite-E layer which halted further collapse.

To accommodate for the collapse of the claystone bench CD in the reconstruction, the cavern volume as shown in Figure 8 was updated with this event. The calculation for the cavern volume reduction due to this event is presented in Table 8. The applied bulking factor is taken from Table 2.

Table 8: Cavern 15 - Claystone bench CD roof collapse and bulked material fill until 1967 (sonar image)

1961-67 Claystone bench CD collapse		
1961 Reconstructed volume	219.074	m³
Top Anhydrite breakout	35.320	m³
Bulking factor	1,15	
Top Anhydrite fill	40.618	m³
Remaining cavern	213.776	m³

A visual representation of the roof collapse of claystone bench CD is shown in Figure 9. Please note that the bulked material from this claystone bench will not necessarily have fallen onto the bottom of the cavern, as the cavern was being backfilled at the time of the collapse. The exact timing of the collapse relative to slurry filling is not known. Figure 9 thus only illustrates reconstruction of the cavern volume as guided by Table 8, not the actual spatial distribution of cavern volume in 1967.

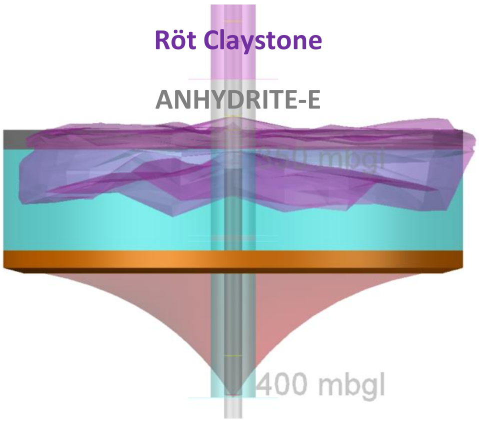

Figure 9: Reconstructed cavern (blue) until 1967 and sonar image (magenta) from 25-09-1967. Collapsed claystone bench CD indicated by grey and its bulked overburden as orange. Insolubles and intermediate claystone benches fill in the sump indicated by red.

Notwithstanding the possible presence of a (semi-)competent Anhydrite-E layer above the collapsed claystone bench CD in 1967, migration is observed for this cavern after 1967 according to sonar images from later years and several well diary recordings up to the year 2000. The slurry filling and subsequent migration of C15 will be discussed in the next two paragraphs.

3.2.2. Slurry filling of C15

The slurry filling of C15 has been exceptionally well-documented as the exact slurry volumes pumped to the cavern per month between October 1961 and November 1968 have been recorded in a memo retrieved from the Nobian archives. The digitized values from this memo are presented in Table 9 indicating a total pumped slurry volume of 654.982 m³. As the pumped slurry volumes are available per month for this cavern (this level of detail is not available for any other well-documented cavern migration case), an exact pumped slurry volume at the time of the sonar in 1967 can be established. Using this volume, a conversion factor between the pumped slurry volume and the actual insitu backfill volume remaining after settlement of the solid particles in the slurry can be derived. The sonar image was taken in September 1967 and the pumped slurry until that date is 529.078 m³.

Table 9: Slurry pumped to cavern 15 in m³ per month (1961-1968)

m³ Slurry pumped to cavern 15 (Memo: "TWR-015 - productie en slurryberging", 21-12-1968)									
	1961	**1962**	**1963**	**1964**	**1965**	**1966**	**1967**	**1968**	
jan		5.525	5.110	7.580	8.680	15.582	11.105	3.180	
feb		4.640	8.282	10.200	5.400	8.895	9.979	5.975	
mar		4.035	7.540	8.685	1.780	7.584	11.405	9.605	
apr		4.810	8.785	5.730	4.390	6.955	10.215	8.240	
may		3.240	5.585	5.670	3.675	10.857	10.365	9.435	
jun		3.060	2.980	4.180	8.805	9.720	12.630	8.925	
jul		955	5.630	7.410	8.480	10.503	12.990	10.883	
aug		6.985	5.400	4.160	4.450	11.273	12.040	10.924	
sep		6.345	7.220	8.170	3.105	11.060	7.795	10.490	
oct	365	6.580	8.635	4.800	7.285	2.720	11.130	10.949	
nov	2.845	6.660	5.615	6.160	9.520	11.690	9.843	10.705	
dec	5.059	7.685	7.835	5.080	21.847	11.067	5.620		
total/y	**8.269**	**60.520**	**78.617**	**77.825**	**87.417**	**117.906**	**125.117**	**99.311**	Total m³
av./month	*2.756*	*5.043*	*6.551*	*6.485*	*7.285*	*9.826*	*10.426*	*9.028*	**654.982**

Using the reconstructed cavern volume as shown in Figure 9, the insitu volume of the backfill can be determined by reconstructing the backfill using the sonar image bottom as the top of the backfill heap (as per the yellow dashed lines in Figure 8). The reconstructed insitu backfill is shown in Figure 10 below, in green. The volume of the reconstructed insitu backfill is 122.264 m³. This value now establishes an initial conversion factor for pumped slurry volume to insitu backfill volume of:

654.982 m³/ 122.264 m³ = 4,33.

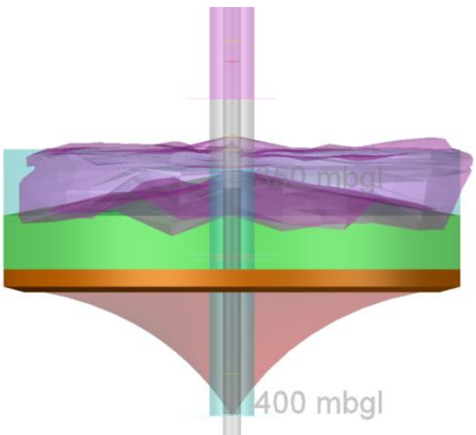

Figure 10: Reconstructed cavern (blue) until 1967 and sonar image (magenta) from 25-09-1967. Insitu backfill heap indicated by green, bulked material of the collapsed claystone bench CD indicated by orange. Insolubles and intermediate claystone benches fill in the sump indicated by red.

The reconstructed insitu backfill volume as shown in Figure 10 has undergone consolidation under its own weight, i.e. by self-weight consolidation (SWC). Applying the historically used value of 5 for the conversion for the pumped slurry volume to insitu backfill volume, see paragraph 2.4, the SWC is estimated at:

(1 - 4,33 / 5) = 13 %.

As the insitu backfill in C15 at the time of the sonar image in 1967 is very fresh, SWC will not have been fully developed. A conservative value of 15% SWC is therefore selected for the remainder of the reconstructions in the study. This value will be further validated by the reconstructions performed for C49-50, see paragraph 3.4.

3.2.3. C15 migration

The migration history of C15 is very well documented by consecutive sonar measurements, Gamma Ray (GR) logs and observations recorded in the well diary. This allowed for a detailed reconstruction of the migration process following the several sonar images available between 1967 and 1971 as shown in Figure 11 below. The cavern bottom profile of the sonar images between 1967 (left in Figure 11) and 1971 (right in Figure 11) propagate from a positive (z-direction) cone-shape, via a flat bottom to a negative cone-shape. This visible transition confirms the expected consolidation of the backfill under the load of bulked overburden. Reconstruction of the backfill consolidation volume, as indicated by the orange diamond-shape in Figure 11, was now possible and will be discussed later in this paragraph.

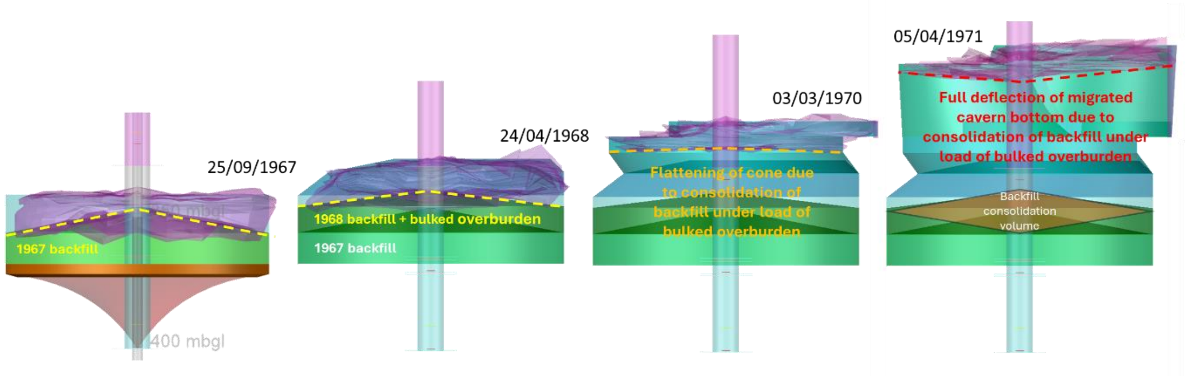

Figure 11: Migration of C15 captured by consecutive sonars between 1967 and 1971. Reconstructed migration column in shades of blues, original sonar images in shades of magenta. The flattening and subsequent deflection of the original upward directed backfill cone in the cavern due to consolidation of the backfill is clearly visible. The derived backfill consolidation volume due to the load of bulked overburden is indicated by the orange diamond-shape.

The detailed migration reconstruction of C15 in four steps between 1967 and 1971 allows for an estimation of the overburden bulking factor. This estimation has also been performed historically for this cavern leading to the well-known bulking factor value of 1,11. It has been established during the performance of the UMS-TWR, that this estimate was made without properly considering the consolidation of the backfill present in this cavern under the load of bulked overburden. In the current study the historical estimation was revised to account for this consolidation which led to an estimated bulking factor of approximately 1,2. The effect of accounting for consolidation of backfill during cavern migration is explained by Figure 12.

In the top picture of this figure, a model representation of the sonar images from 1968 and 1970 at C15 is shown in the left picture. The 1968 sonar in blue with the backfilled portion of the cavern in brown. The consecutive sonar capturing the migration process from 1970 is shown in lilac. The distance between the cavern roofs of the consecutive sonar is shown in the middle picture. Please note that the shown dimensions are not necessarily reflecting the actual situation at C15, rather are chosen to ease this exemplary estimation.

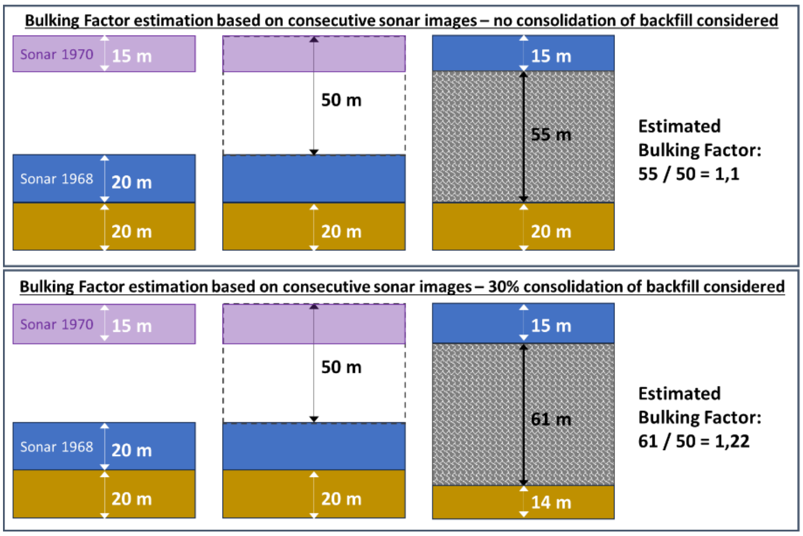

Figure 12: *C15: Estimation of bulking factor from consecutive sonar images during migration. Top picture – not considering backfill consolidation; Bottom picture: considering 30% consolidation*

When the bulking factor is estimated from the just described model representation, i.e. without considering consolidation of the backfill in the cavern, the situation in the right picture is leading, i.e. the backfill height remains 20 m as shown. The bulking factor is therefore estimated at:

BF = Bulked overburden height (55 m) / Intact overburden height (50 m) = 1,1

In the bottom box of Figure 12, the same model representation of the sonar images from 1968 and 1970 is shown, however now considering consolidation of the backfill in the cavern. The original backfill height of 20 m is thus reduced with 30% to 14 m due to the load of the bulked overburden. As can be seen, the estimated bulking factor is now higher and is estimated at:

BF = Bulked overburden height (61 m) / Intact overburden height (50 m) = 1,22

This principle is a fundamental difference between the Bekendam method and the BJP approach and significantly influences the manner in which migration is calculated. Consequently, this principle also influences the amount of subsidence that can develop due to cavern migration.

When accounting for consolidation of the backfill in C15 between 1967 and 1971 an average bulking factor of 1,2 is found to best suit the volume reconstruction. This fitment is based on the inclusion of 30% additional consolidation of the backfill under the load of the bulked overburden, i.e. in addition to the 15% SWC. The value of 1,2 is thus applied for this cavern and is further validated by the reconstruction of the caverns C37, C49-50 and C86 later in this chapter.

Sonar images that could document the further migration of cavern 15 after 1971 are not available. However, a number of other observations, mainly GR logs and notes on obstructions in the well diary, did enable a qualitative initial reconstruction of the migration column after 1971. This reconstruction also allowed for a direct comparison with the Bekendam method. The observations from sonar images and notes from the well diary are graphically organized in Figure 13.

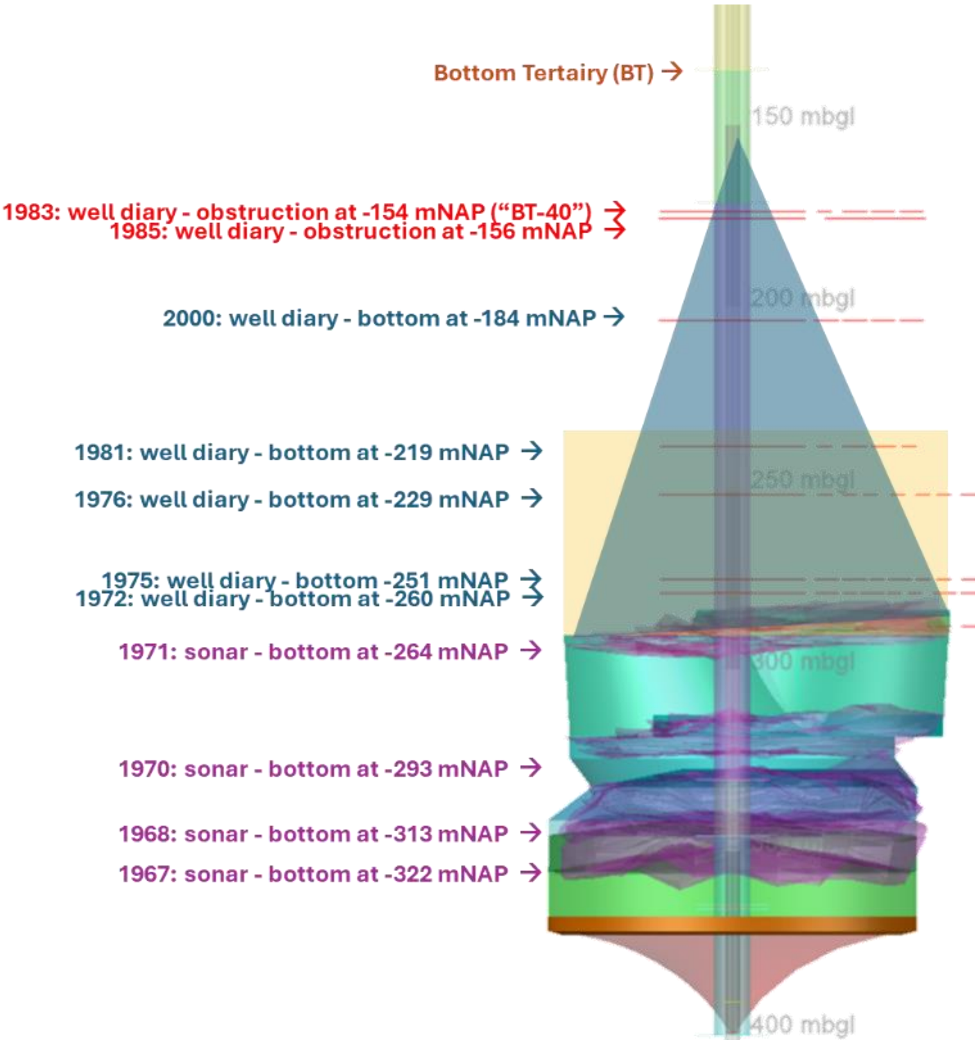

Figure 13: *Migration column development at cavern 15 between 1967 and 2000. The decreasing depth of the cavern bottom is indicated based on sonar (purple), well diary notes (blue) and obstruction observations due to most likely pulled-apart casing pipes (red). The favoured migration column development after 1971, with a reducing column diameter (cone-shaped) is indicated by the blue triangle. The alternative cylindrical migration column after 1971 is indicated by the yellow rectangle.*

The recorded observations in the well diary allow for two possible overall migration scenarios:

1. A cylindrical migration column after 1971 using a bulking factor of approximately 1,2 thus reaching a depth of approximately 240 mbgl, shown as the light-yellow cylinder in Figure 13.
2. A cone-shaped migration column after 1971, using a bulking factor of approximately 1,2 reaching a depth of approximately 150 mbgl, shown as the dark blue cone in Figure 13.

The cone-shaped migration fits best with the well diary notes recorded between 1971 and 2000 as the cylinder does not reach the depth of the residual cavern recorded in 2000. The cone shaped migration on the other hand exceeds the depth of the recorded bottom in 2000 at approximately 204 mbgl. This is in line with the expected transition between collapsed, bulked overburden in the "mobilized zone" and delaminated overburden, which has not collapsed just deflected, in the "yielded zone". An "air gap" separates these two zones. A detailed explanation of the several zones in a migration column is provided in Figure 14.

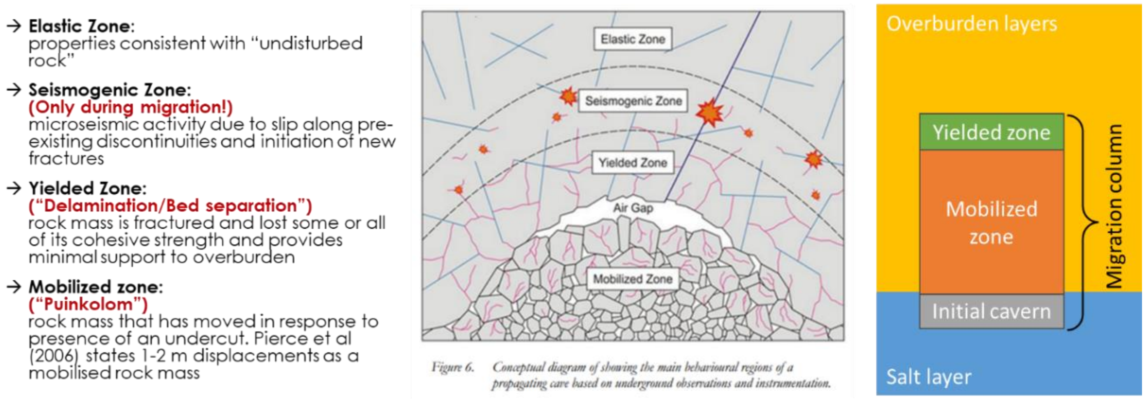

Figure 14: Subdivision of migration column in zones: (from top to bottom) elastic, seismogenic, yielded and mobilized (adapted from [1]).

The just described qualitative migration history of cavern 15 using a cone-shaped migration column after 1971, rather than the continuation of the prior cylindrical migration is validated using the BJP - algorithm in paragraph 3.2.5. This validation is partly based on the depth of the transition between the mobilized and yielded zones as confirmed by the available GR logs.

Continuing the description of the migration history, the well diary recordings between 1983 and 1996 require elaboration as these all relate to obstruction in the well before the (final) bottom of the cavern was observed in the year 2000. This can be explained by the following:

> As the migration column propagated upward between 1967 and 1983, an increasing tension on the cemented casing string was exerted by the bulked overburden in the migration column thus pulling on the casing. The build-up in tension over the years likely caused a casing screw connection failure at approximately 174 mbgl. This consequently led to an obstruction in the well as the bottom part of the casing string likely shifted slightly in a lateral direction. The repeated recording of this obstruction in the well diary led to the historic assumption that the migration of cavern 15 reached 174 mbgl and was thus the origin for the so-called "Basis Tertiary minus 40 m criterion" (BT-40m). This criterion was independent of cavern diameter and has now been replaced by the principle of a "bending" final Top Rock roof beam (pillar) for which the deflection is dependent on the (residual) cavern diameter at the relevant depth. This principle is explained in Report 2, paragraph 2.7 [3]).

In the year 2000 the earlier obstructions were overcome and access to the well was established to a depth of approximately 200 mbgl by using a 3-1/2 -inch drill string to push through the obstruction, rather than the sonar/GR dummy tool used in previous years. At this depth a very small cavern, most likely representing the mentioned "air gap", was encountered and recorded in the well diary.

With regards to the earlier mentioned estimation of the consolidation volume of the backfill due to loading with bulked overburden (see Figure 11) the following:

> Comparing the sonar image from 1967 (top of backfill heap) with the image from 1971 (cavern bottom), the transformation of a positive cone-shaped cavern bottom, i.e. the backfill heap, to a negative cone-shaped bottom can be clearly seen. The backfill consolidation volume in case of C15 is estimated at approximately 35.000 m³.

Comparing this 35.000 m³ to the backfill volume after SWC (approx. 130.000 m³), a consolidation of 23% by loading of the backfill with bulked overburden can be determined for the situation in 1971.

This consolidation by bulked overburden is on top of the SWC. Considering that the migration of C15 continued after 1971, see Figure 13, the total consolidation of the backfill by bulked overburden will have been higher. For the BJP-Algorithm a conservative value of 30% on top of 15% SWC has been selected as a result of this reconstruction. These consolidation values are further validated by the reconstruction of C49-50 and C86-87.

In conclusion, the cavern development and migration reconstruction of C15 clearly points towards a combined cylindrical and cone-shaped migration column, eventually reaching approximately 150 mbgl. The slurry filling of the cavern is well-documented enabling a detailed volume reconstruction of the backfill material and its consolidation under load. The link between the reconstructed migration and the resulting subsidence at the ground level is presented in the next paragraph.

3.2.4. Link migration to subsidence

The measured subsidence around cavern 15 was correlated with the reconstructed migration. The subsidence around the well location of C15, i.e. at the deepest point of the subsidence bowl, is presented in Figure 15. See paragraph 2.5 for details on the source of this figure and paragraph 2.7 for an explanation of the subsidence stages relevant for cavern migration cases. The subsidence contours shown in Figure 15 are taken from [7] and represent the cumulative subsidence in this area until 2005.

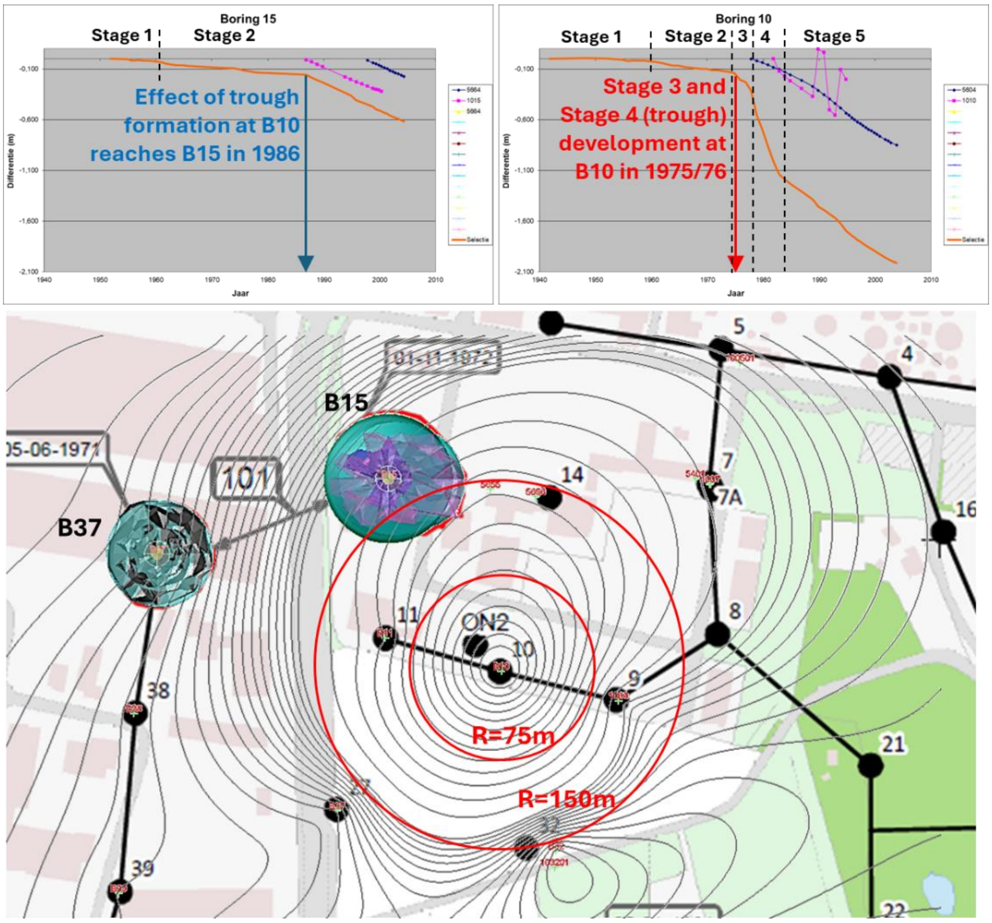

Figure 15: Subsidence development around wells TWR-015 (top l.) and TWR-010 (top r.) [6], plan view with locations of B15 and adjacent caverns (bottom). Contours in grey indicate cumulative subsidence caused by the migration of caverns in this area up to 2005 [7]. Scale can be derived from the two red circles with indicated radii and their centre at TWR-010.

The main source for subsidence in the wider area of C15 is the migration of the cavern system developed from wells TWR-9, -10 and -11 as can be seen in Figure 15. The cumulative subsidence until 2006 at well TWR-010 was approx. 2 m. All the subsidence stages have been developed due to the migration of the TWR-9, -10 and -11 cavern system, as is indicated in the top right graph in this figure. For C15 only Stage 2 subsidence has developed between 1960 and 1986 as can be seen from the top left graph. The sudden subsidence rate increase at TWR-015 in 1986 is thus not related to the migration of C15, but to the migration of caverns developed from wells TWR-9, -10 and -11.

In conclusion, the migration of C15 does not seem to have caused Stage 3 and 4 subsidence. Only Stage 2 subsidence developed due to the deformation of the rock mass around the migration column shown in Figure 13. The application of the BJP-Algorithm on the just described reconstructions for C15 are described in the next paragraph.

3.2.5. C15 BJP-Algorithm application to reconstructed migration

The application of the BJP-Algorithm to the reconstructed migration of C15 has been performed using the subsidence prognosis work process described in Report 2 [3] and elaborated in [5]. The first step in this work process is the selection of input parameters for the algorithm.

The first of the input parameters, the potential migration column radius, was selected by determination of the exact surface area of the maximum cavern contour and expressing this area into a radius. The determination of this area was achieved by construction of an intersection plane between the cavern volume, as represented by the 1967 sonar image, and the Top of Salt C, as per the stratigraphy description for this cavern, see APPENDIX I.

The construction of this intersection is shown in Figure 16 and indicated by the red contour.

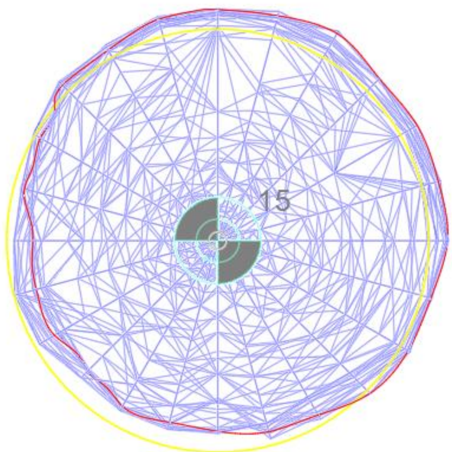

Figure 16 Intersection of Top Salt C with cavern 15 volume based on the 1967 sonar image, actual intersection in red, simplified cavern contour (BJP input parameter) in yellow

The surface area of the red contour is approx. 7.500 m². The selected input parameter R_{cav} is therefore:

7.500 m² = π * R_{cav} ² → R_{cav} = 49,0 m

The selected radius is subsequently used as the basis for the construction of a so-called "representative cavern volume". This volume is based on the just selected radius and the salt production figures, after application of the salt tonnage to cavern volume conversion described in paragraph 2.3.

In the case of C15, the representative cavern volume is constructed combining a cone to represent the original sump and a cylinder to represent the later cavern development. The sonar image from 1967 is taken as guidance for the selection of the cylindrical cavern wall height. The resulting construction of the representative volume is shown in Figure 17.

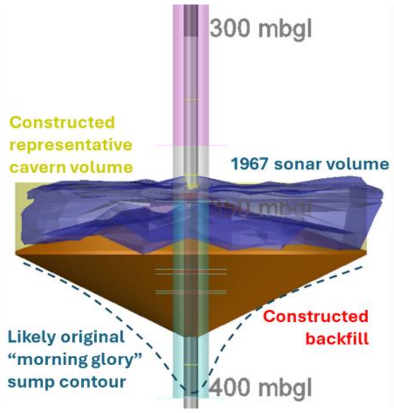

Figure 17: Cavern 15: Reconstruction of „Representative volume" (yellow) and constructed backfill volume in 1967 (red). Original sonar volume is shown in blue.

Based on the reconstruction of all relevant geometries as shown in this figure, a set of input parameters for the BJP-Algorithm were derived. All cavern-specific input parameters for C15 are presented in Table 10 on the next page.

This table is split into four main areas:

- The top of the table contains all the input parameters pertaining to the location of the well and the depth of the cavern and the relevant geological interfaces. The total height of the cavern is calculated from the input parameters in the lower part of the table.
- The "Volume fitting" part of the table is used to compare the cavern volume derived from the salt production with the observed/reconstructed cavern volume. In the case of C15, this comparison is mainly based on reconstructed volumes as no sonar images of the entire cavern are available. For other caverns this comparison can be made between salt production volume and (combined) sonar volumes.
  The volume fitting for C15 shows that only 8% of the total production volume is not accounted for by the reconstructed cavern volume. This is a low percentage compared to other studied caverns and can be considered a conservative approach. The 8% is corresponding to the volume of insolubles and collapsed intermediate claystone benches as discussed in paragraph 3.2.1.
- The "Cavern geometry conversion" part of the table contains all input parameters pertaining to the conversion of the actual cavern volume to the "representative volume" used by the BJP-Algorithm. In the case of C15, this representative volume comprises a cone with 49 m radius and 26 m height plus a cylinder with the same diameter and a height of 20 m. The representative volume is 93% of the salt production volume, thus conservatively overshooting the reconstructed cavern volume which equals 92% of the salt production volume.

REINVENT
SOLUTIONS

- The “Cavern geometry conversion” part of the table contains all input parameters pertaining to the conversion of the actual cavern volume to the “representative volume” used by the BJP-Algorithm. In the case of C15, this representative volume comprises a cone with 49 m radius and 26 m height plus a cylinder with the same diameter and a height of 20 m. The representative volume is 93% of the salt production volume which is deemed a conservative value.

Table 10: C15 cavern specific input parameters

Cavern	**15**
Relevant borehole	15
X coordinate	250764,6
Y coordinate	473847,1
Z coordinate GL (mNAP)	19,6
Depth of top rock [mbGL]	134,8
Depth of top salt [mbGL]	345,8
Base of actual cavern [mbGL]	386,6
Base of initial cavern [mbGL]	400,6
Top of actual cavern [mbGL]	340,6
Height of cavern (m)	46,0
X coordinate migration centre	250764,6
Y coordinate migration centre	473847,1
Volume fitting	
Maximum BPB Prod.(t)	413919
Cavern vol based on BPB (m³)	**232622**
Actual volume (recon./sonar)(m³)	215852
Insolubles (bulked) (m³)	12274
Part of BPB prod. Vol. not acc. (m³)	16770
Part of BPB prod. Vol. not acc. (%)	**7%**
Cavern geometry conversion	
Migration column Surface area (m²)	7500
Constructed cavern radius [m]	49,0
Hydraulic Radius constructed cav. [m]	24,5
Const. cavern height (cylindrical) [m]	20,0
Const. cavern height (conical) [m]	26,0
Constructed volume (cylindrical) [m³]	150859
Constructed volume (conical) [m³]	65372
Constructed volume total [m³]	216232
Part of BPB prod. Vol. not acc. (m³)	16391
Part of BPB prod. Vol. not acc. (%)	7%
Height correction backfill insitu [m]	2
Backfill insitu unconsolidated (m³)	111347
Backfill consolidation (%)	30%

At the bottom of Table 10, the input parameters pertaining to the backfill volume in the cavern are included. The height correction (2 m) represents the layer of backfill to which no load bearing capacity can be attributed, see Report 2, paragraph 2.3 [3]. The backfill volume stated is the volume derived from the slurry volume, reduced with 15% SWC. The 30% consolidation input parameter represents the total consolidation of the stated backfill volume under the load of bulked overburden during migration.

Using the stated input parameters, the BJP-Algorithm produced the output presented in Figure 18. This figure compares the available sonar images (left picture) with a graphical representation of the algorithm output (right picture).

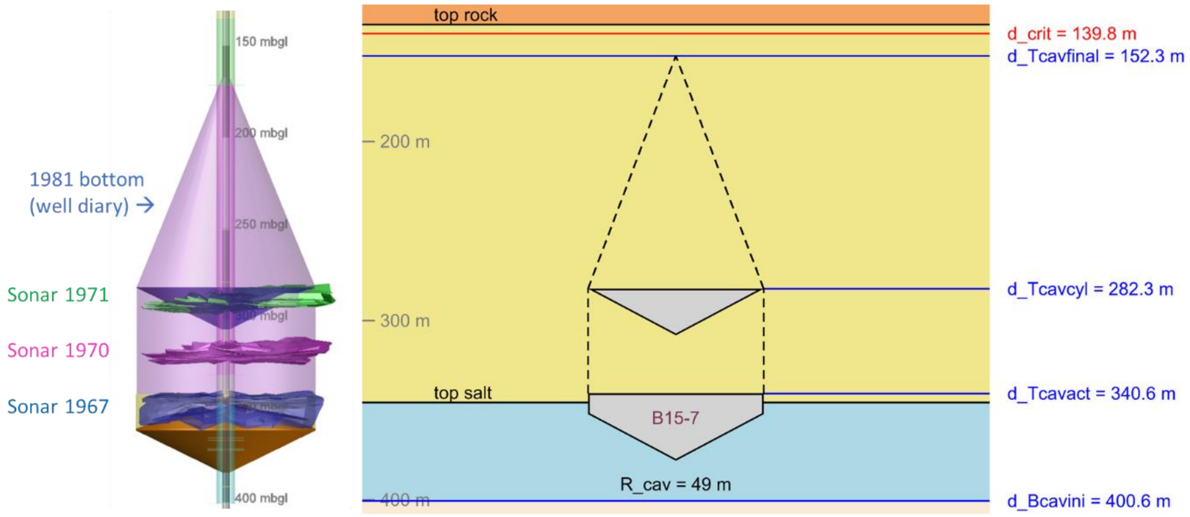

Figure 18: *Comparison of the observed migration of cavern 15 from sonar images (l) and the calculated output of the BJP-Algorithm (r).*

As can be seen from Figure 18, the BJP-Algorithm has determined that the migration process of C15 includes both a cylindrical and a conical part as also derived from the sonar and well diary observations discussed in paragraph 3.2.3. The migration of C15, accounting for the backfill, reaches 152,3 mbgl, staying well away from the critical depth of 139,8 mbgl. As a result, only Stage 2 (and a negligible amount of Stage 3 subsidence) is developed by migration of C15, in line with the observed subsidence as discussed in the previous paragraph. Stage 4 (trough/sinkhole) formation and subsequent Stage 5 subsidence do not occur, again in line with the observed subsidence.

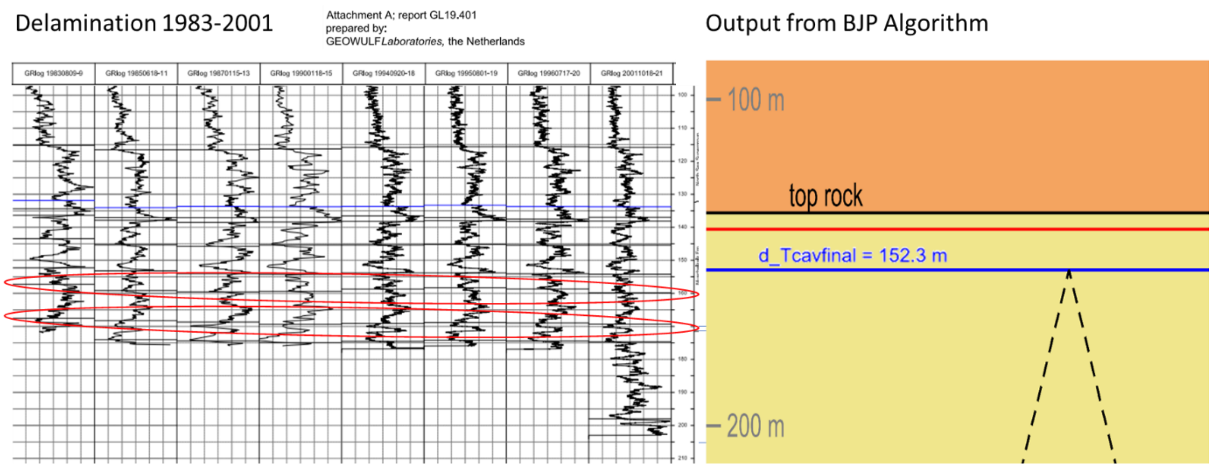

Figure 19: *Cavern 15 migration: deflection of strata near top of the migration column as observed from GR logs 1983-2001, adapted from Attachment A to [8].*

The conical top of the migration column contains transition between the bulked overburden (the mobilized zone) and deflected overburden strata (yielded zone) near the top of the migration cone. The actual position of this transition (air gap) is most likely around 200 mbgl, where the cavern bottom was observed in 2000. The deflection of the strata above the final cavern bottom can be observed from the available Gamma Ray logs (GR-logs) as is shown in Figure 19. The blue marker near the top rock does not move at all between 1983 and 2001, whilst the markers within the red ellipses show a slight but gradual deflection over this same time period. This gradual deflection represents the formation of the yielded zone above the mobilized zone as the migration approached its final depth.

The estimated and consequently used bulking factor of 1,2 thus includes both the mobilized zone and the yielded zone in addition to any air gap that is left behind after the migration of a cavern is completed. As such a bulking factor of 1,2 can be considered an average value for the migration column, not a maximum value.

The output of the BJP-Algorithm also comprises graphical representations of the subsidence contours and all its derivatives. The calculated subsidence contour for C15 is shown in Figure 20 below. The measured subsidence at C15 is also shown in this figure for comparison.

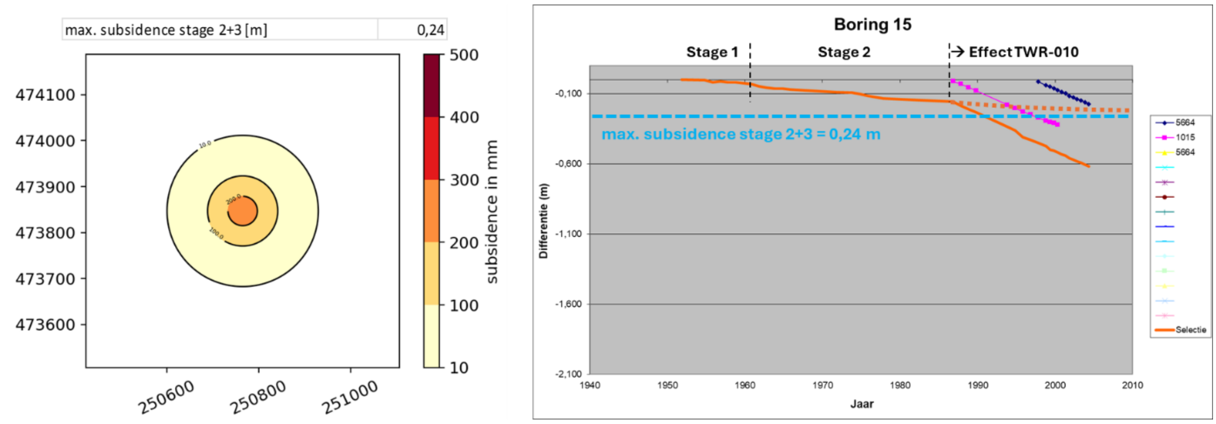

Figure 20: Cavern 15: subsidence contours as calculated by the BJP-Algorithm (l) and actual measured subsidence (r).

As can be seen from this figure, the calculated subsidence fits well to the actual measured subsidence considering the influence of the subsidence bowl caused by migration at well TWR-010 after 1986. It must be noted that the calculated subsidence is independent of time as it is simply the total subsidence calculated by the algorithm base on the input parameters. The actual subsidence will slow down over time as the migration approaches its final depth thus not showing the maximum value in the measured subsidence.

In conclusion, the application of the BJP-Algorithm to the cavern migration and subsequent subsidence development for C15 shows the applicability of the chosen methods and parameters and thus supports the validation process.

3.3. Reconstruction C37

The validation of the algorithm is continued with the reconstruction of cavern development, migration and subsequent subsidence development of Cavern 37 (C37). This cavern is similar to C15 in terms of shape, but no backfill has been applied thus simplifying the reconstruction process. As the description of the reconstruction processes for C15 have been elaborate, the level of detail in the descriptions of further caverns will be reduced to streamline this report.

C37 is a single completion cavern from well TWR-037 drilled in 1955. The key data for C37 are included in Table 11 below and additional information can be found in APPENDIX I.

Table 11: Key data Cavern 37

Wells	X (WGS84)	Y (WGS84)	Z (mNAP)	Final depth (mbgl)	Final depth (mNAP)	Well ready	Start production	End production	Cemented
37	250582,8	473788,1	19,45	419,6	-400,15	4-7-1955	16-7-1955	1-8-1979	Yes*
* Cemented in 1979, reopened in 2003 and finally cemented in 2010.									

There is no indication that C37 was ever backfilled. The adjacent (and connected) caverns C38 and C39 were backfilled. If the slurry pumped to these caverns was undersaturated, any volume increase would have likely occurred near the slurry injection, i.e. at C38 and C39 respectively. It is unlikely that any additional was created at C37 as the cavern volume based on the production is very accurately represented by the sonar image as will be discussed later in this paragraph.

The sump phase of SCC37 has been reconstructed based on maximum contours as derived from a sonar image from 05-06-1971. The initial reconstruction of the sump with a cone angle of 15° has been initially applied for the first three years of production, i.e. 1955 until 1957. The sump cone dimensions until 1957 are presented in Table 12.

Table 12: Reconstruction SCC Sump 37

Cavern (SCC)	**Year**	**Production (t)**	**Sump volume (m³)**	**Cone radius (m)**	**Cone height (m)**
37	1957	16.399	9.214	32,02	8,58

The cone-shaped cavern is subsequently stretched into a "Morning Glory" sump which fits well to the minimum contour derived from the 1971 sonar image in terms of diameter of the lower part of the cavern. The reconstructed sump phase of C37 is presented in Figure 21 where the mentioned sonar image from 1971 is also shown for comparison of the mentioned contours.

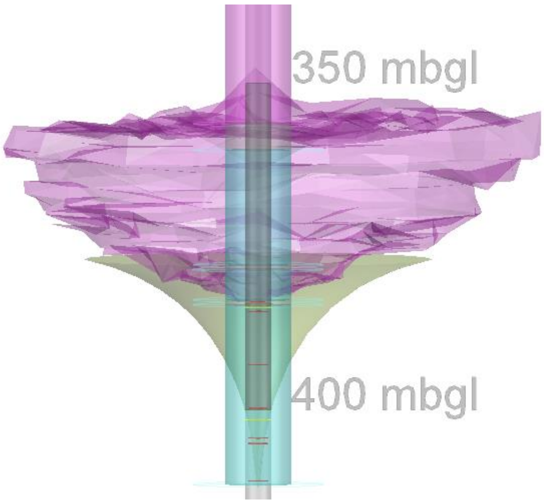

Figure 21: Side view of the reconstructed sump SCC 37 until 1957 (green) and sonar image from 1971 (magenta).

After the development of a sump, the cavern was further reconstructed by extending and widening this contour upwards for the years 1958 and 1959. The slices of cavern volume added in 1958 and 1959 as well as the resulting reconstructed cavern in 1967 are presented in Figure 22. The cavern development between 1960 and 1967 has been reconstructed as a further widening vase-shape to improve the correlation to the 1971 sonar image. The level of the injection and production strings as recorded from the well diaries support this assumption. The top of the 1960-1967 has been aligned with the top of Salt C.

As the cavern development in these years intersect both intermediate claystone benches, the volume of these benches has been added to the slices. The resulting bulked infill of this material is not shown in this figure as it will be discussed in combination with insoluble material fill. The total volume of the reconstructed cavern is 52,866 m³ at the end of 1959 and 80.545 m³ in 1967.

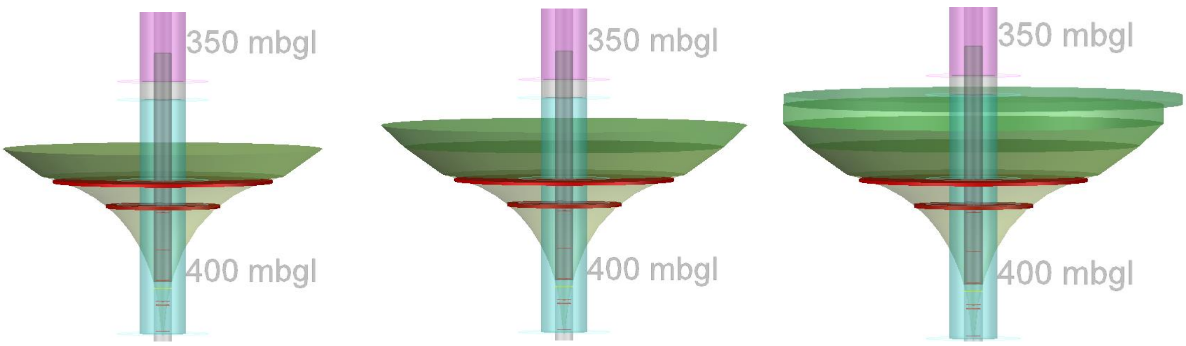

Figure 22: Side view of the reconstructed cavern SCC 37 in 1958 (l) and 1959 (m) and 1967 (r), volume induced by falling rock benches is visible in red. Bench fill material not shown in this figure.

A hydraulic connection was established with the adjacent MCC 38-39-40-41 on 29-06-1967 according to the production records. From the so-called “Slurryberging- & Stromingstabel” (showing the in- and outgoing streams of each well) it is known that well TWR-037 was used as a brine production well from at least 1975 onwards until the entire series was taken out of production in 1979. From the hydraulic connection in 1967 until 1974 there are no records showing if well TWR-037 was used for water injection or brine production. Considering the sonar volume of 1971, it is unlikely that well TWR-037 was ever used as a water injection well after 1967 as this would have led to a much larger cavern volume. Consequently, all the production from the MCC 37-38-39-40-41, between establishment of hydraulic connection in 1967 and 1974, has been excluded from the reconstruction of C37.

With the reconstructed cavern volume based on production complete and positioned with the top aligning with the top of Salt C, the filling of the sump with insoluble material and the intermediate claystone bench material can be subtracted from the reconstructed cavern volume. The derived fill volumes based on volume of the intersected rock benches and the total cavern volume until 1967 are presented in Table 13.

Table 13: Cavern 37 -Claystone bench and insoluble material fill until 1967 (end of production by leaching)

Rock bench fill		
Rock bench BC	1212	m³
Rock bench AB	368	m³
Total	1580	m³
Bulking	1	
Bench fill volume	1.580	m³
Insoluble fill		
1967 cavern volume	80.545	m³
Bulking	1,1	
Insoluble fill volume	3.956	m³
Total fill volume	**5.536**	

The total volume of (bulked) material is sufficient to partly fill the sump. The final shape of reconstructed cavern is shown in Figure 23.

The total volume of the final reconstructed cavern is 75.010 m³.

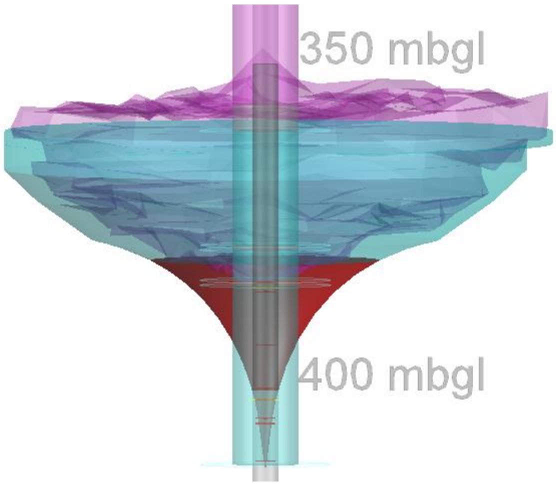

Figure 23: C37: final reconstructed cavern (blue) until 1967 and sonar image (magenta) from 1971. Bench and insolubles fill visible in red.

The sonar image of 1971 shows that the actual cavern has extended vertically into the overburden layers. This position could be caused by either gradual disintegration or sudden collapse of the claystone bench CD layer. Salt-D is not present according to the drilling log, see APPENDIX I. The higher cavern bottom in the sonar image compared to the reconstruction, indicates that this could be the bulked claystone bench CD.

To accommodate for the collapse of the claystone bench CD in the reconstruction, the cavern volume as shown in Figure 23 was updated with this event. The calculation for the cavern volume reduction due to this event is presented in Table 14. The applied bulking factor is taken from Table 2.

Table 14: Cavern 37 - Claystone bench CD roof collapse and bulked material fill until 1971 (sonar image)

1967-1971 Claystone bench CD collapse		
1967 Reconstructed volume	75.010	m³
Top Anhydrite breakout	22.227	m³
Bulking factor	1,15	
Top Anhydrite fill	25.561	m³
Remaining cavern	71.676	m³

A visual representation of the roof collapse of claystone bench CD is shown in Figure 24. The collapsed claystone bench CD at the top of the cavern is indicated by light grey, whilst the bulked material on the bottom of the cavern is indicated by orange.

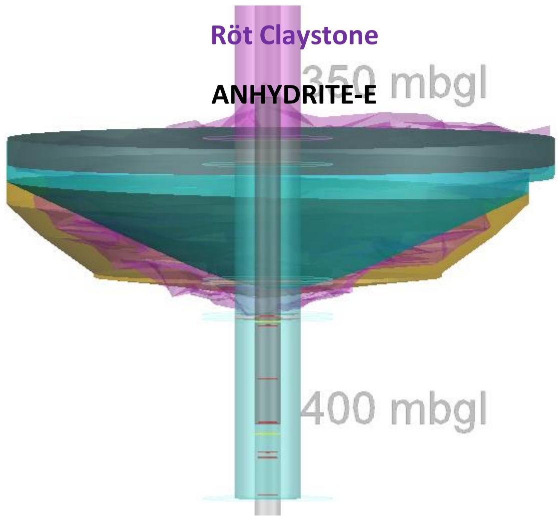

Figure 24: Reconstructed cavern (blue) until 1971 and sonar image (magenta) from 1971. Collapsed claystone bench CD indicated by grey and its bulked overburden as orange.

The volume of the 1971 sonar image is 71.800 m³ which is a near perfect correlation to the reconstructed volume in 1971 (71.676 m³) as stated in Table 14.

The presence of Anhydrite-E is not noted on the drilling log and GR logs for this depth interval are not available. Nonetheless, it is likely that Anhydrite-E was present at this cavern since nearby wells show its presence. Notwithstanding a (semi-)competent Anhydrite-E layer above the collapsed claystone bench CD in 1971, migration is observed for this cavern after 1967 according to well diary recordings ("bend pipes") and GR logs from later years

Ahead of the use of the BJP-Algorithm to reconstruct cavern migration, the migration of C37 was first manually reconstructed in AutoCAD, see Figure 25. This reconstruction uses a bulking factor of 1,2 and the radius reduction mechanism for the migration column. The manual reconstruction was supported by the availability of a GR log from 1979 in which a residual cavern above the original cavern can be observed.

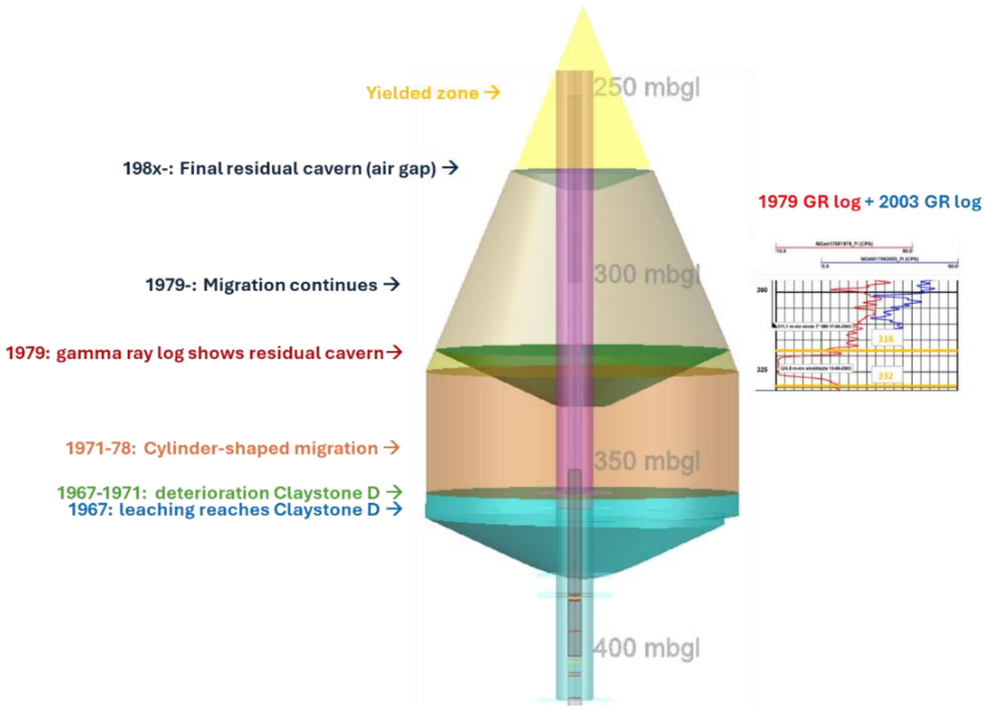

Figure 25: Cavern 37: manual migration reconstruction (l) aided by available GR log from 1979 (r).

The manual migration reconstruction for C37 confirms the radius reduction mechanism introduced in during the migration reconstruction of C15. Moreover, as C37 is not backfilled, the effect of a cone-shaped sump on the migration column shape can be reliably validated using this cavern. The likely final residual cavern (air gap) is most likely situated at approximately 270 mbgl as shown in Figure 25. This depth corresponds to a remark in the "B37 Eindrapport" (final well report) from 2003 [9]:

- De vergelijking van de gammametingen 1979 en 2003 laat zien dat tot op een diepte van 270 m –mv beide curves parallel lopen. Vanaf 270,0 m –mv vertoont de curve uit 2003 een verzet naar beneden ten opzichte van de curve uit 1979.

"The comparison of GR logs from 1979 and 2003 shows that up to a depth of 270 mbgl both curves run parallel. From 270 mbgl down, the 2003 curve shows a downward offset compared to the 1979 curve."

It must be noted that this air gap is not necessarily a discrete residual cavern as shown in Figure 25, it can also be a series of stacked delaminated and deflected strata collectively amounting to the volume of the residual cavern volume shown in this figure. This would explain how the GR log does not show a residual cavern as in 1979 below 318 mbgl. In addition, the situation in 2003 may have not been the final position of the residual cavern. A slow progression of the migration process after 2003 may have occurred. After the manual migration reconstruction for C37, the BJP-Algorithm was used to calculate the subsidence due to migration at this cavern. The selected input parameters are presented in Table 15 and depicted in Figure 26.

Table 15: C37 cavern specific input parameters

Cavern	37
Relevant borehole	37
X coordinate	250582,8
Y coordinate	473788,1
Z coordinate GL (mNAP)	19,5
Depth of top rock [mbGL]	136,1
Depth of top salt [mbGL]	360,2
Base of actual cavern [mbGL]	384,5
Base of initial cavern [mbGL]	411,4
Top of actual cavern [mbGL]	359,5
Height of cavern (m)	25,0
X coordinate migration centre	250582,8
Y coordinate migration centre	473788,1
Volume fitting	
Maximum BPB Prod.(t)	142570
Cavern vol based on BPB (m³)	**80124**
Actual volume (recon./sonar)(m³)	75010
Insolubles (bulked) (m³)	4228
Part of BPB prod. Vol. not acc. (m³)	5115
Part of BPB prod. Vol. not acc. (%)	**6%**
Cavern geometry conversion	
Migration column Surface area (m²)	5000
Constructed cavern radius [m]	40,0
Hydraulic Radius constructed cav. [m]	20,0
Const. cavern height (cylindrical) [m]	10,0
Const. cavern height (conical) [m]	15,0
Constructed volume (cylindrical) [m³]	50265
Constructed volume (conical) [m³]	25133
Constructed volume total [m³]	75398
Part of BPB prod. Vol. not acc. (m³)	4726
Part of BPB prod. Vol. not acc. (%)	**6%**
Height correction backfill insitu [m]	0
Backfill insitu unconsolidated (m³)	0
Backfill consolidation (%)	0

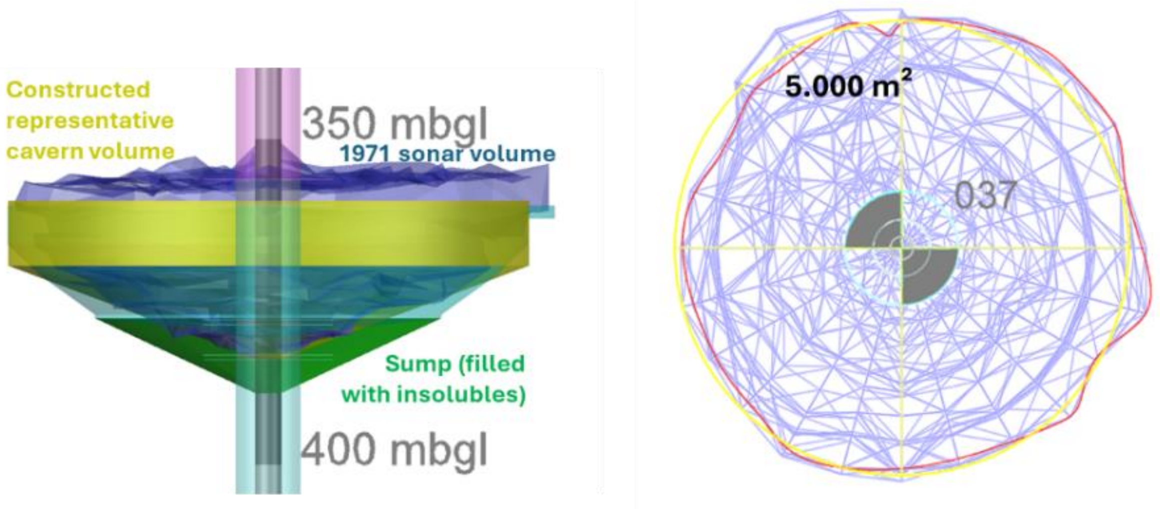

Figure 26 Cavern 37: Reconstruction of „Representative volume" (yellow) and constructed insoluble fill volume in 1967 (green). Original sonar volume is shown in blue.

As the reconstructed cavern volume was near identical to the sonar volume it was taken as the representative volume. The representative volume comprises a cone-shaped sump with a 40 m radius and 15 m height and a cylinder with 40 m radius and 10 m height. No backfill has been applied. A comparison of the results of the subsidence calculations by the BJP-Algorithm and the observations from GR logs are shown in Figure 27. This figure shows the full GR logs from 1979 and 2003 at the correct depth in relation to the graphical representations of the migration column (by AutoCAD and by algorithm) as well as the likely position of the transition between the mobilized zone and the yielded zone at ~270 mbgl near the top of the cone-shaped migration column.

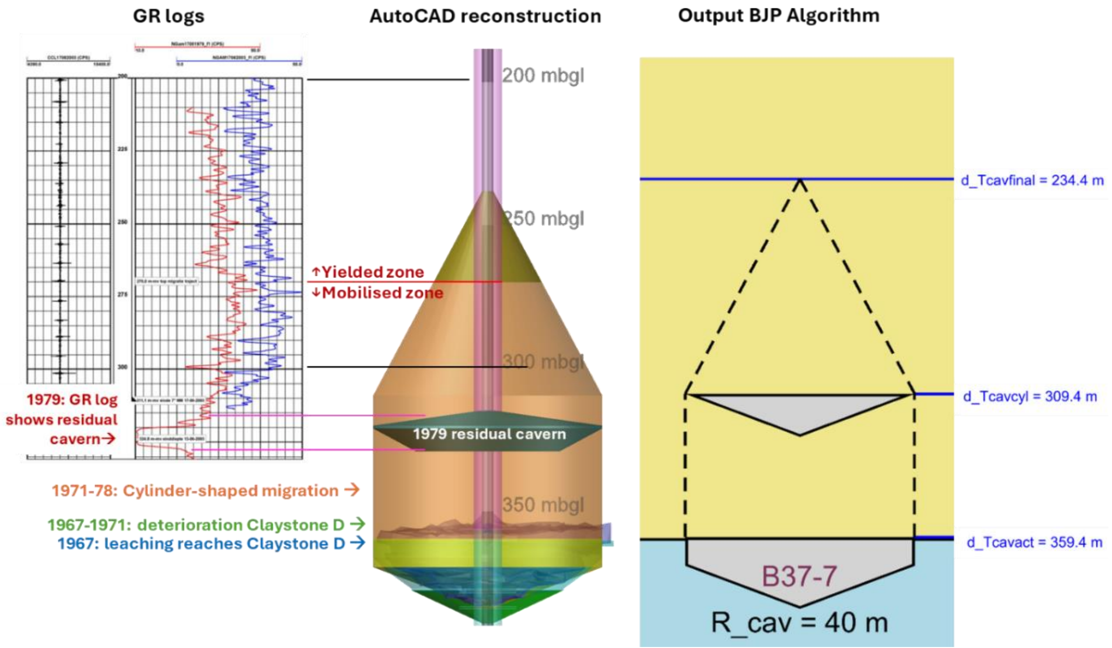

Figure 27: C37 Comparison BJP-Algorithm output and observations from GR logs, adapted from [9] Bijlage 5.

The output of the BJP-Algorithm also comprises graphical representations of the subsidence contours and all its derivatives. The calculated subsidence contours for cavern 37 are shown in Figure 28. The actual measured subsidence at C37 is also shown in this figure for comparison.

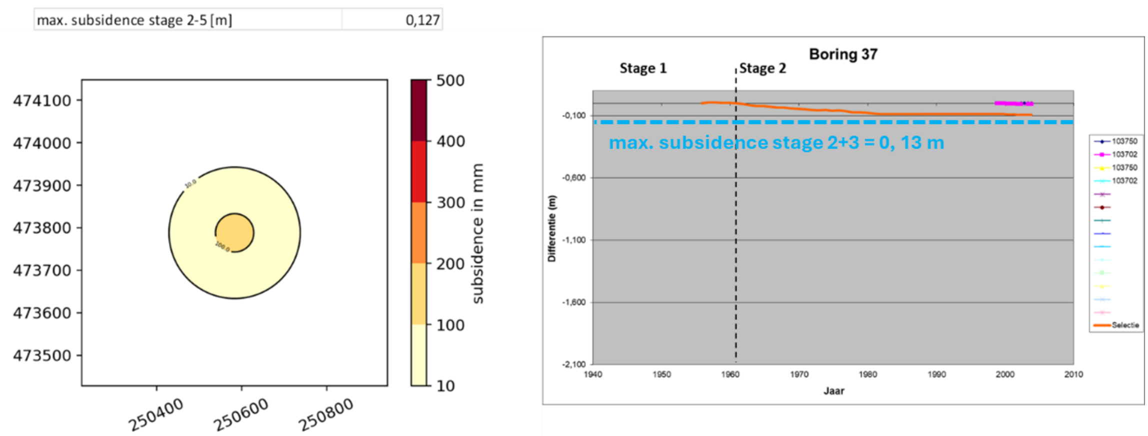

Figure 28: C37: subsidence contours as calculated by the BJP-Algorithm (l) and actual measured subsidence (r).

As can be seen from this figure, the calculated subsidence fits well to the actual measured subsidence. It must be noted that the calculated subsidence is independent of time as it is simply the total subsidence calculated by the algorithm base on the input parameters. The actual subsidence will slow down over time as the migration reaches its final depth and the migration column settles.

In conclusion, the application of the BJP-Algorithm to the cavern migration and subsequent subsidence development for C37 shows the applicability of the chosen methods and parameters for a cavern without backfill and thus supports the validation process.

3.4. Reconstruction C49 and C50 (C49-50)

The validation of the algorithm is continued with the reconstruction of cavern development, migration and subsequent subsidence development at caverns C49 and C50, i.e. cavern system C49-50. These caverns are similar to C15 in terms of shape, with backfill applied in both. C49 and C50 have been developed as independent SCCs but, at a late stage in their development, connected at top which has influenced the backfilling process, thus making the reconstruction process more complex.

Cavern 49-50 (C49-50) was mostly developed as two Single Completion Caverns (SCC) from 1958 until a hydraulic connection was established on 28-10-1965 according to the production records. The wells were operated as MCC 49-50 after the connection until 1967.

The key data for C49-50, comprising wells B49 and B50, are included in Table 16 below and additional information can be found in APPENDIX I.

Table 16: Key data C49-50

Wells	X (WGS84)	Y (WGS84)	Z (mNAP)	Final depth (mbgl)	Final depth (mNAP)	Well ready	Start production	End production	Cemented
49	251599,3	473295,7	21,29	394,35	-373,06	10-7-1958	1-8-1958	1-1-1973	20-8-1991
50	251628,0	473221,9	21,4	380,8	-359,41	29-9-1958	16-10-1958	1-1-1973	4-12-1975

The reconstruction of the sump of SCC 49, with a cone angle of 15°, has been applied for the first year of production, 1958, which results in a sump diameter of 26,2 m. The further lateral extension of the sump is limited in the following year to avoid early intersection of the reconstructed sumps of the two SCCs. As such, production from SCC49 in 1959 is reconstructed as a cylinder-shape after which production from 1960 is represented by an extending vase-shape. This development is in part derived from the sonar image taken on 25-11-1965.

The reconstruction of the sump of SCC 50 cannot be correlated to a sonar image as the only existing image from 11-03-1963 is of poor quality and unlikely to represent the real volume at the measurement date when compared to the production figures. This sonar image is thus ignored for the reconstruction of SCC 50. Instead, the fact that a hydraulic connection was established in 1965, will be used as a measure for the maximum contour. A suitable maximum contour can be reconstructed using the 15° cone after three years of production, i.e. 1958-1960.

The reconstructed sump phases for SCC 49 and SCC 50 until 1960 are dimensioned as presented in Table 17.

Table 17: Reconstruction SCC Sumps 49 and 50

Cavern (SCC)	Year	Production (t)	Slice volume (m³)	Radius (m)	Height (m)
49	1958	9.010	5.063	26,2	7,0 (cone)
49	1959	10.960	6.158	26,2	2,9 (cylinder)
49	1960	25.115	14.112	32 – 26,2	5,3 (vase)
Total for 49	*1960*	*45.085*	*25.332*	--	--
50	1958-60	44.075	24.765	44,5	11,9

The reconstructed sump phases of SCC 49 and SCC 50 are presented in Figure 29 where the mentioned sonar images from 1963 (SCC 50) and 1965 (SCC 49) are also shown for comparison of the constructed contours. Please note that the sump for SCC 49 has been positioned 5.6 m above the bottom of Salt A to align the reconstructed cavern with the Top of Salt C. The same applies to SCC 50 with a z-shift of

6.24 m. Figure 29 also shows why the 1963 sonar image from well TWR-050 cannot be considered realistic as the diameter and volume are too small to represent the salt production from this cavern until 1963.

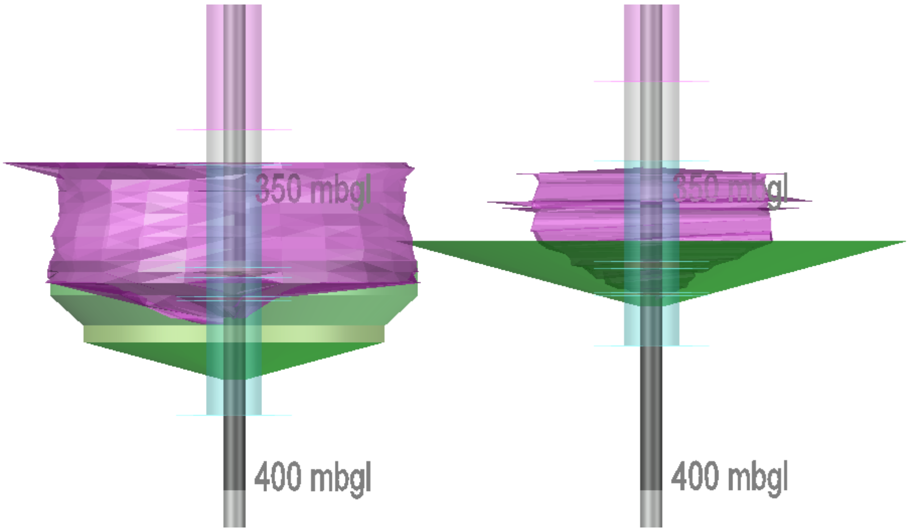

Figure 29: *Side view of the reconstructed sumps of SCC 49 (left) and SCC 50 until 1950 (green) and sonar images from 1965 (left) and 1963 (right) in magenta.*

After the development of the shown sumps, the caverns were further reconstructed by extending these contours upwards for the years 1961 until 1965 when hydraulic connection is established. The resulting reconstructed caverns are presented in Figure 30. As the cavern development in these years intersect both intermediate claystone benches, the volume of these benches has been added to the yearly slices. The resulting bulked infill of this material is not shown in this figure as it will be discussed in combination with insoluble material fill.

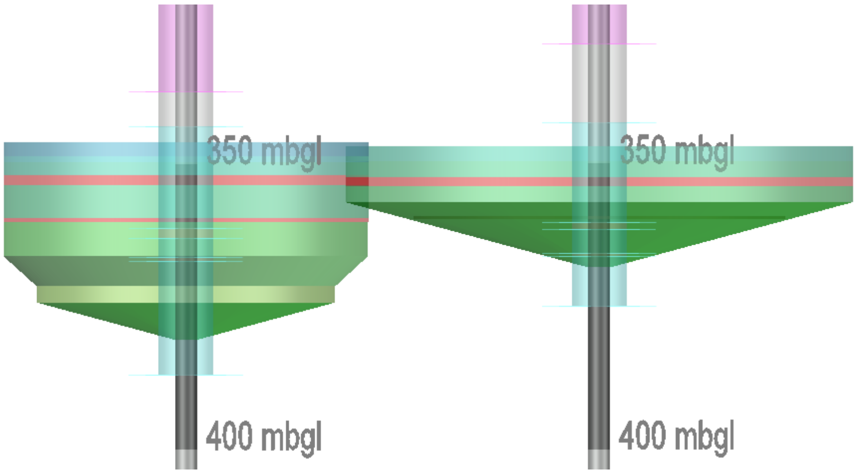

Figure 30: *Side view of the reconstructed SCC 49 (left) and SCC 50 until 1965.*

The production after 1965 is limited to the years 1966 and 1967 where it is conservatively assumed that well TWR-049 was used for water injection. This assumption is based on the establishment of a hydraulic connection between the two cavern parts from 1966 onwards for only the last year of production. This assumption is conservative as it increases the height of C49 which is the highest of the two caverns before 1966. Applying this assumption results in a reconstructed volume for those years centred around well TWR-049 while extending the maximum contour to further accentuate the hydraulic connection, see Figure 31.

With the reconstructed cavern volume based on production complete and positioned aligned with the top of Salt C, the filling of the sump with insoluble material from the rock salt and the intermediate claystone benches can be subtracted from the reconstructed cavern volume of C49-50. The derived fill volumes based on volume of the intersected rock benches and the total cavern volume until 1967 are presented in Table 18.

Table 18: C49-50 -Claystone bench and insoluble material fill until 1967 (end of production by leaching)

SCC 49 + MCC 49-50				SCC 50		
Rock bench fill				**Rock bench fill**		
Rock bench BC	5372	m³		Rock bench BC	7472	m³
Rock bench AB	2091	m³		Rock bench AB	1666	m³
Total	7463	m³		Total	9138	m³
Bulking	1			Bulking	1	
Bench fill volume	7.463	m³		Bench fill volume	9.138	m³
Insoluble fill				**Insoluble fill**		
1967 cavern volume	92.502	m³		1965 cavern volume	101.879	m³
Bulking	1,1			Bulking	1,1	
Insoluble fill volume	4.130	m³		Insoluble fill volume	4.549	m³
Total fill volume	**11.593**			**Total fill volume**	**13.687**	

The total volume of (bulked) material as calculated in Table 18 is sufficient to largely fill the sump at well TWR-049. At well TWR-050 the cone sump is also largely filled. A morning glory type cavern was not reconstructed as it does not change the shape of the final reconstruction significantly. The final shape of reconstructed cavern is shown in Figure 31.

The total volume of the final reconstructed cavern is 88.372 + 97.331 = 185.703 m³.

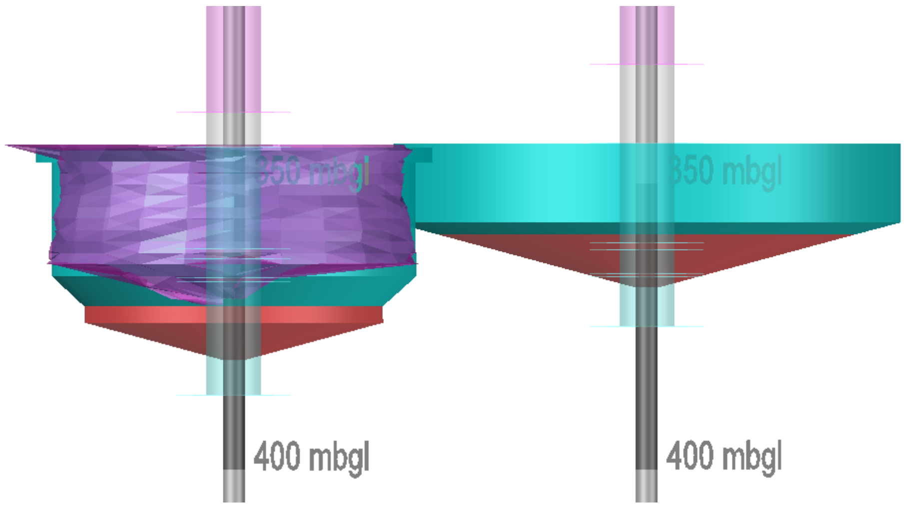

Figure 31: C49-50: Final reconstructed cavern (blue) until 1967 and sonar image (magenta) from 25-11-1965. Intermediate claystone bench and insolubles fill visible in red.

The sonar image of 1965 shows the actual cavern at the same vertical position as the reconstruction. Migration of the cavern roof has thus unlikely started at this stage as the Claystone CD seems to be intact. The bottom of the cavern is higher in the sonar image compared to the reconstruction. This is likely caused by the conservative values taken for the bulking factor of insolubles and intermediate claystone benches, see paragraph 2.4.

The production records and well diary state that a hydraulic connection has been established with the adjacent MCC 47-48 in May 1967. The well diary mentions that well TWR-049 is used as brine production well which means water injection was done through well TWR-047 and/or TWR-048. As such no significant volume development around wells TWR-049 and TWR-050 is expected. The additional recorded production between May 1967 and January of 1973 has thus not been considered in the reconstruction.

Evidence of backfilling at C49-50 has been found in the (handwritten) memo “Slurry hoeveelheden in caverns 1966-1991”, dated 25-2-1992 [10]. An extract from this memo is shown in Figure 32.

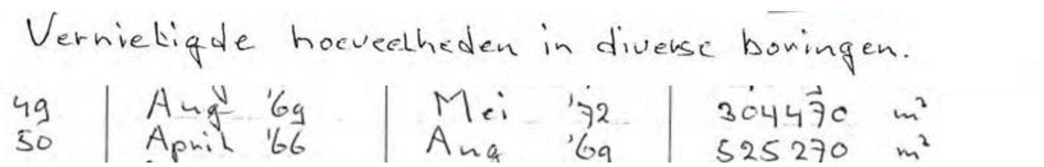
Vernietigde hoeveelheden in diverse boringen.

49	Aug '69	Mei '72	304470 m^3
50	April '66	Aug '69	525270 m^3

Figure 32: Slurry filling C49 and C50 according to memo dated 25-2-1992.

The total slurry volume injected in C49-50 from 1966 to 1972 is 829.740 m^3.

Using S/F = 5 the total volume of insitu backfill in the caverns before any consolidation is 165.948 m^3.

Assessing the volumes of slurry volumes per cavern in more detail, it is clear that part of the slurry pumped to well TWR-050 must have spilled over to C49. C50 is simply too small for the slurry volume attributed to this cavern in the 1992 memo, i.e. 97.331 m^3 cavern volume versus 105.054 m^3 insitu backfill.

The most likely scenario is that approximately 6% of the slurry pumped into well TWR-050 would have flowed to C49. An overview of the resulting insitu backfill volumes in each cavern, before and after application of 15% SWC is presented in Table 19.

Table 19: Slurry filling of C49 and C50, insitu backfill volume and filling grade before and after 15% SWC

	Well 49			**Well 50**	
1967 Reconstructed cavern volume water leaching	88.372	m^3		97.331	m^3
Slurry/Fill Ratio	**5,00**			**5,00**	
Initial Insitu Fill Volume	71.358	m^3		94.590	m^3
1972 remain. volume after slurry fill NO CONS.	17.015	m^3		2.740	m^3
Filling grade without consolidation	81%			97%	
Consolidation of slurry under self weight	15%			15%	
Insitu Fill Volume after SW CONS.	60.654	m^3		80.402	m^3
1972 remain. volume after slurry fill SW CONS.	27.718	m^3		16.929	m^3
Filling grade with self weight consolidation	69%			83%	

C49 and C50 thus contain 60.654 m^3 and 80.402 m^3 backfill respectively after application of 15% self-weight consolidation. This is the starting point for the BJP-Algorithm. A graphical representation of the backfill volumes before and after application of 15% SWC is presented in Figure 33 below.

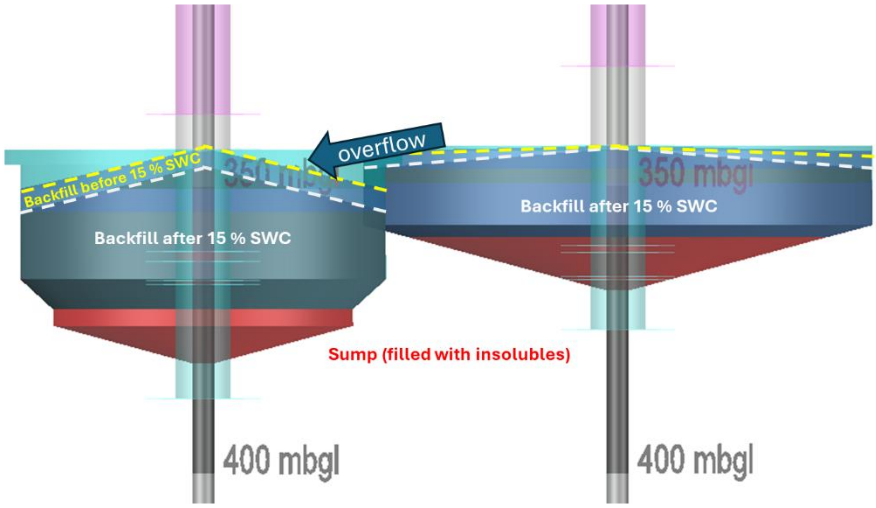

Figure 33: *C49-50: insitu backfill in the caverns before and after 15% SWC*

The possibility that undersaturated backfill slurry was pumped to wells TWR-049 and TWR-050 was tested, but did not lead to a better fitting to the observed information. Since additional volume would also mean a higher bulking factor to reach the same (observed) migration depth, it is deemed conservative to not consider cavern volume increased during slurry filling.

The drilling logs for wells TWR-049 and TWR-050 note the presence of Anhydrite-E. Notwithstanding the presence of a (semi-)competent Anhydrite-E layer above the C49-50 in 1965 (the year of the sonar image in C49), migration is observed for C49 after 1967 according to GR logs from later years. Deterioration of the Anhydrite-E was likely caused by exposure to water and, after connection to C50, a growing roof span. The combined effect causing eventual collapse of the Anhydrite layer.

An initial manual reconstruction of the migration for caverns C49 and C50 was prepared as for C15 and C37. As the initial manual reconstruction did not account for a cone-shaped sump, it was later superseded by the application of the BJP-Algorithm to the migration of these two caverns. As such, the initial manual reconstruction is not further discussed.

After some iterations, the BJP-Algorithm was used to calculate the subsidence due to migration at this cavern, accounting for the cone-shape sumps. The selected input parameters are presented in Table 20 and depicted in Figure 34 below.

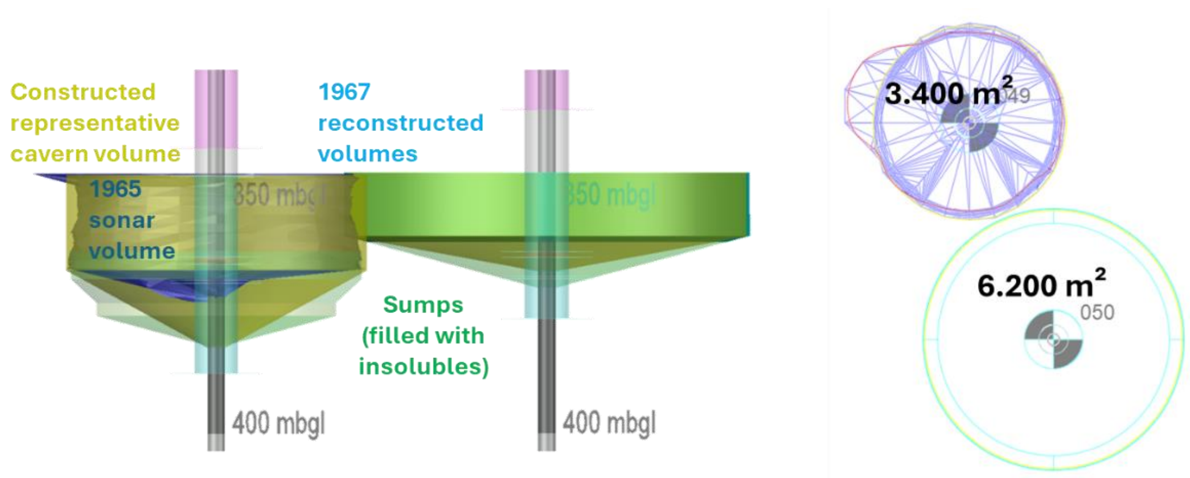

Figure 34: *C49-50: Reconstruction of „Representative volume" (yellow). Original sonar volume shown in blue.*

Table 20 C49-50 cavern specific input parameters

Cavern	49	50
Relevant borehole	49	50
X coordinate	251599,3	251628,0
Y coordinate	473295,7	473221,9
Z coordinate GL (mNAP)	21,3	21,4
Depth of top rock [mbGL]	127,3	125,6
Depth of top salt [mbGL]	343,5	342,9
Base of actual cavern [mbGL]	382,3	365,4
Base of initial cavern [mbGL]	386,9	374,9
Top of actual cavern [mbGL]	343,3	342,9
Height of cavern (m)	39,0	22,5
X coordinate migration centre	251599,3	251628,0
Y coordinate migration centre	473295,7	473221,9
Volume fitting		
Maximum BPB Prod.(t)	178728	204842
Cavern vol based on BPB (m³)	**100445**	**115121**
Actual volume (recon./sonar)(m³)	88372	97331
Insolubles (bulked) (m³)	5300	6074
Part of BPB prod. Vol. not acc. (m³)	12073	17790
Part of BPB prod. Vol. not acc. (%)	**12%**	**15%**
Cavern geometry conversion		
Migration column Surface area (m²)	3400	6200
Constructed cavern radius [m]	33,0	44,0
Hydraulic Radius constructed cav. [m]	16,5	22,0
Const. cavern height (cylindrical) [m]	21,0	14,0
Const. cavern height (conical) [m]	18,0	8,5
Constructed volume (cylindrical) [m³]	71845	85150
Constructed volume (conical) [m³]	20527	17233
Constructed volume total [m³]	92372	102382
Part of BPB prod. Vol. not acc. (m³)	8073	12739
Part of BPB prod. Vol. not acc. (%)	**8%**	**11%**
Height correction backfill insitu [m]	2	2
Backfill insitu unconsolidated (m³)	60654	80402
Backfill consolidation (%)	30%	30%

As the reconstructed cavern volume of C49 is relatively close to the sonar volume, the 12% unaccounted volume was only slightly reduced in the representative volume as can be seen in the table. This is considered a conservative approach.

The representative volume of C49 comprises a cone-shaped sump with a 33 m radius and 18 m height and a cylinder with 33 m radius and 21 m height. A total of 60.654 m³ backfill has been applied in this cavern. The representative volume of C50 comprises a cone-shaped sump with a 44 m radius and 8,5 m height and a cylinder with 44 m radius and 14 m height. A total of 80.402 m³ backfill has been applied in this cavern.

Using the input parameters stated in Table 20, the BJP-Algorithm produced the output for C49 as presented in Figure 35. A comparison of the results of the subsidence calculations by the BJP-Algorithm for C49 and the observations from GR logs are shown in this figure. The GR logs from 1975 and 1991 are plotted at the correct depth in relation to the graphical representations of the calculated migration.

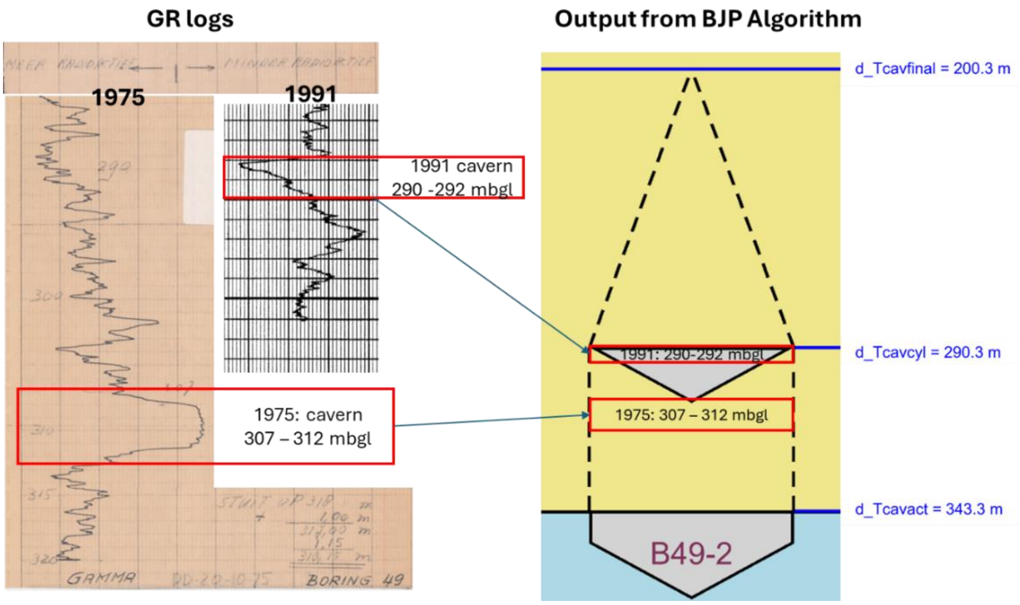

Figure 35: *C49: Comparison BJP-Algorithm output and migration observations from GR logs 1975 and 1991*

The BJP-Algorithm output for C50 is presented in Figure 36 below.

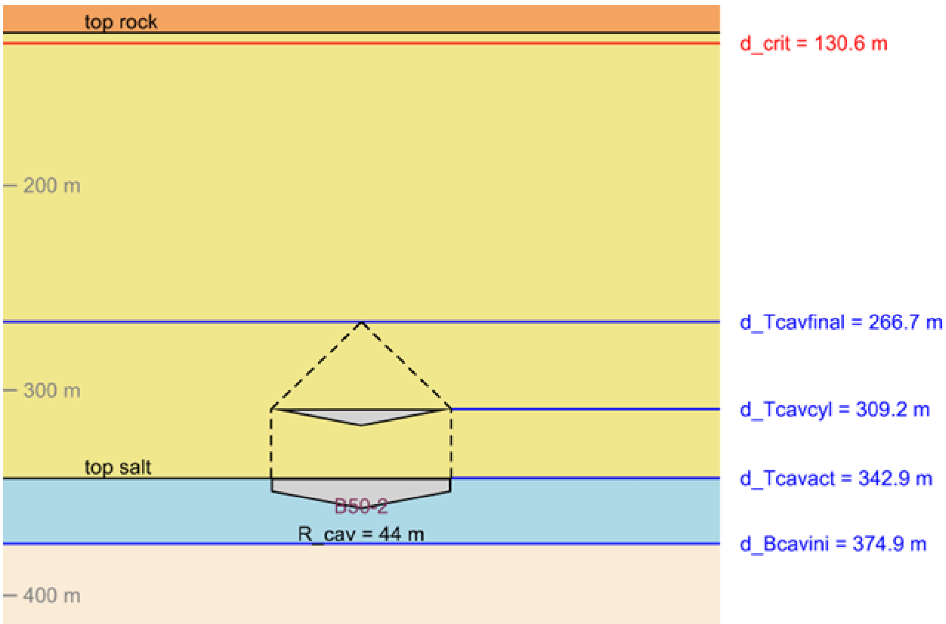

Figure 36: *C50 BJP-Algorithm output summaries (l & m) and section view of the migration process (r)*

The calculated subsidence contours for C49 are shown in Figure 37. The actual measured subsidence at C49 and C50 is also shown in this figure for comparison.

max. subsidence stage 2+3 [m]	0.113

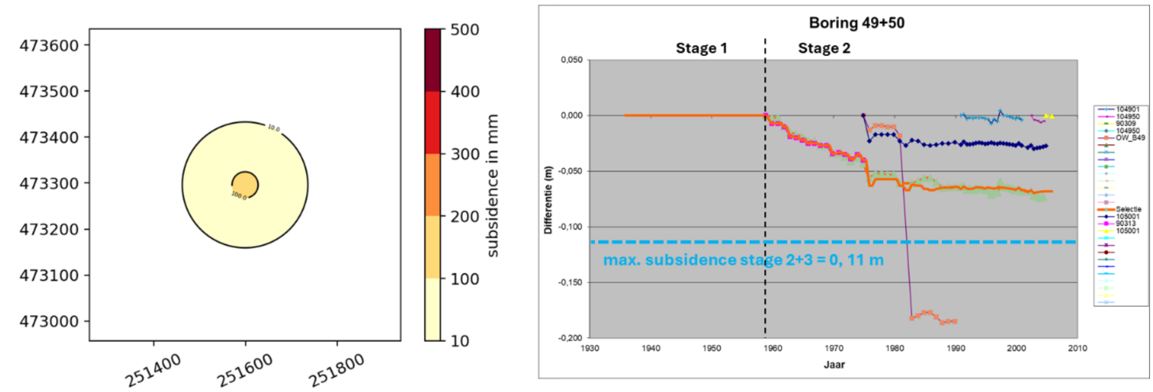

Figure 37: C49: subsidence contours as calculated by the BJP-Algorithm (l) and actual measured subsidence (r).

As can be seen from this figure, the calculated subsidence fits well to the actual measured subsidence. The slight overestimation by the algorithm (11 cm versus 8 cm measured) can be attributed to the several conservative approaches discussed in previous paragraphs. It must also be noted that the calculated subsidence as shown in Figure 37 only includes the contribution by the migration of C49.

There is some evidence of migration at C50 noted in the well diary. During plugging of well TWR-050 in 1975, access to the well was only possible down to approximately 312-314 mbgl. This is approximately 30 meters above the top of Salt C and coincides with the residual cavern shown in Figure 36. The migration of C50 was thus limited by the backfill and may not have reached the calculated depth of 267 mbgl shown in Figure 36 due to the conservative selection of input parameters.

In conclusion, the application of the BJP-Algorithm to the cavern migration and subsequent subsidence development for cavern C49-50 further demonstrate the applicability of the chosen methods and parameters for caverns with backfill and thus supports the validation of the BJP-Algorithm.

REINVENT

3.5. Reconstruction C86-87

The validation is continued with the reconstruction of cavern development, migration and subsequent subsidence development at Cavern 86-87 (C86-87). Relative to caverns discussed prior, this cavern has a complex development history and an irregular cavern shape. C86-87 has not been backfilled, making it comparable to C37. The complex development history and irregular shape have however resulted in a cavern migration process which is distinctly different than as observed at C37.

C86-87 was initially developed as two Single Completion Caverns (SCC) between 1964 and 1968 until a hydraulic connection was established on 19-03-1968. The date of connection was established from the well diary and confirmed by the production records. According to the well diary, the pair of caverns was used to post-saturate the unsaturated brine from each other during the SCC development until 1966. As a result, the development of the caverns was quite slow up to that point. From 1966 to 1968 the SCCs were operated in bottom injection mode, causing a heightening of the cavern rather that a widening. This was further accentuated by the use of diesel oil as a blanket medium during sump development. An oil blanket was not used during the development of the previously discussed caverns. After making connection between the two SCCs 86 and 87, the wells were operated as MCC 86-87 until 1973.

The key data for C86-87, comprising wells TWR-086 and TWR-087, are included in Table 21 below and additional information can be found in APPENDIX I.

Table 21: Key data Cavern 86

Wells	X (WGS84)	Y (WGS84)	Z (mNAP)	Final depth (mbgl)	Final depth (mNAP)	Well ready	Start production	End production	Cemented
86	251371,3	472527,7	21,85	441,6	-419,75	19-2-1964	5-3-1964	1-12-1978	29-6-1983
87	251350,3	472490,8	22,0	441,7	-419,75	24-3-1964	12-4-1964	1-12-1978	9-1-1980

The further cavern development by leaching was characterised by an irregular leaching operation leading to cavern development at multiple depth levels. As such, a full manual reconstruction of the cavern development process in AutoCAD for C86-87 proved unsuccessful. Alternatively, a careful assessment of the available information in the well diaries and from sonar images was performed to establish the most likely cavern development history and a plausible spatial distribution of the resulting cavern volume.

The first step in deciphering the cavern development history was the correction of several sonar images as they clearly did not line up as expected. Several sonar images taken from wells B86 and B87 appear to be shifted or rotated as can be seen from Figure 38 (left picture) where the sonar outer contours are not aligned with each other.

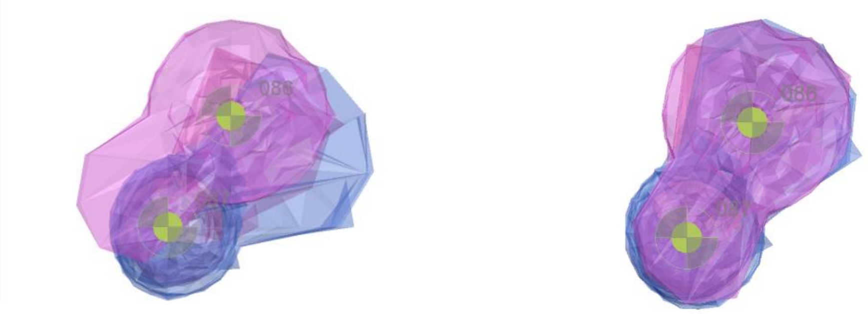

Figure 38: *Top view of C86-87 sonar images from 04-04-1972 at well TWR-086 (right/top) and 02-04-1969 & 27-03-1972 at well TWR-087 (left/bottom). Position of images as provided (l) and corrected (r) by rotation around z-axis of 25° and 15° CCW respectively.*

This misalignment can be caused by an unknown deviation of the two wells which would shift the images over to a better fit. Alternatively, a rotational error could have been made during measurement or processing of the sonar data. When a correction of counterclockwise 25° rotation around well TWR-086 is applied and a 15° (1969 sonar) and 25° (1972 sonar) around well TWR-087 are applied, the sonar images are fitting very well as can be seen in Figure 38 (right picture). Although no evidence can be found that supports the application of either correction, the sonar images speak for themselves, and a correction is thus considered justified. The corrected sonar position has been subsequently used for the cavern volume assessment process.

The volume assessment was performed based on the available production information, sonar measurements and observations on the leaching process recorded in the well diaries. The first "snapshot in time" that can be reliably visualised is the situation in 1969. A comparison of the cavern volume according to the production records and the sonar volumes in 1969 is presented in Table 22 below. The net cavern volume has been calculated from the salt production records and the corresponding insolubles volume.

Table 22: *C86-87: 1969 cavern volume according to production records compared to sonar volumes*

Volume according to production			Sonar volumes	Unaccounted Volume	Remarks
	86	87			
1967 sump (m³)	15.140	11.745	-	-	No sonar avail.
1969 BPB (m³)	53.463				
1969 insol. (m³)	2.387				Sonar "shadow"
1969 net vol. (m³)	51.076		24.420	52%	in B87 image

A graphical representation of the situation in 1969 is provided in Figure 39. The shown position of the salt strata and the overlying Claystone-D, Salt-D and Anhydrite-E have been interpreted from the original drilling logs and the available GR logs, see APPENDIX I for details. In 1969, only one sonar image is available from well TWR-087. This causes a "sonar shadow" that cannot capture part of the cavern volume developed around well TWR-086. In Figure 39 the possible volume in this shadow is marked with a blue dashed line.

In 1969, C86-87 is positioned below the intermediate claystone benches and Salt-B. The roof position at TWR-087 is confirmed by the sonar. At TWR-086 the roof position is inferred from notes in the well diary. The effect of the discussed operational conditions, i.e. post-saturation, bottom injection and blanket medium, is visible in this figure as the early cavern development is not as laterally extended as the previously discussed caverns, but rather vertically. The initial sump cones are not visible in the sonar image. This can be due to filling with insolubles and/or due to sonar shadow. The likely sump cones for SCC 86 and SCC 87 are shown in green in the figure.

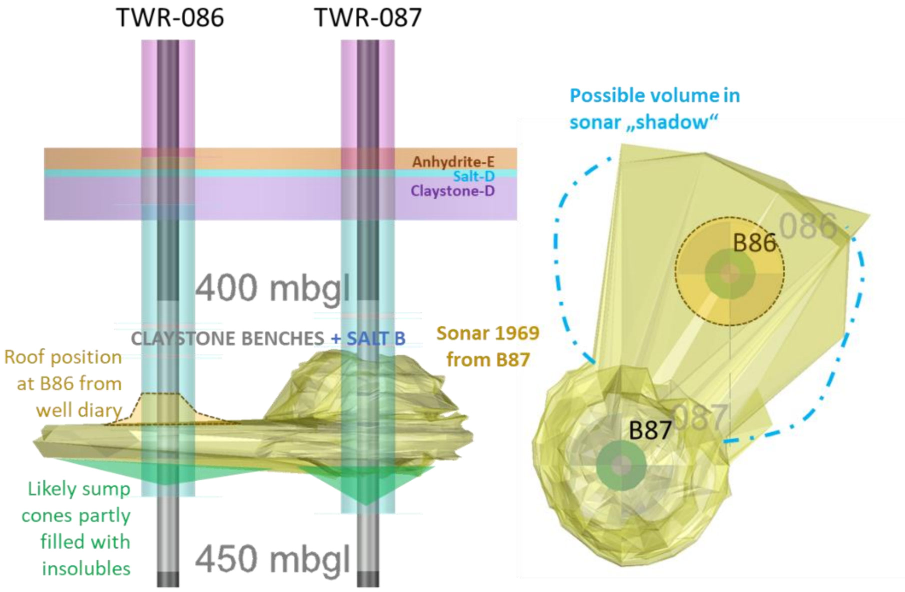

Figure 39: C86-87: 1969 sonar volume and geology in side view (l) and plan view (r)

The unaccounted volume in 1969 is 52%, as noted in Table 22, and comprises both the possible volume in the sonar shadow around TWR-086 and the sump cones at both wells.

The next snapshot in the development of C86-87 is the situation in 1972. Sonars from both wells TWR-086 and TWR-087 are available from this year and a Boolean union of these two sonar images established an accurate sonar volume at this time. A comparison of the cavern volume according to the production records and the sonar volumes in 1972 is presented in Table 23. The net cavern volume has been calculated from the salt production records, the corresponding insolubles volume and the collapse of intermediate claystone benches and Salt B, as well as part of the Claystone-D.

Table 23: C86-87: 1972 cavern volume according to production records compared to sonar volumes

Volume according to production			Sonar volumes	Unaccounted Volume	Remarks
	86	87			
1967 sump (m³)	15.140	11.745	-	-	No sonar avail.
1969 BPB (m³)	53.463				
1969 insol. (m³)	2.387				Sonar "shadow" in B87 image
1969 net vol. (m³)	51.076		24.420	52%	
1972 BPB (m³)	106.115				
1972 insol. (m³)	4.738				Boolean union of sonars 1969+1972 volumes in Fusion360
1972 clayst. (m³)	2.931				
1972 net vol. (m³)	98.447		77.371	21%	

A graphical representation of the situation in 1972 is provided in Figure 40. The cavern development between 1969 and 1972 has mainly taken place around well TWR-087. The upward development of the cavern at this well was likely caused by the collapse of the intermediate claystone benches and the subsequent upward leaching around well TWR-087. The roof positions in 1972 are confirmed by notes in the well diary.

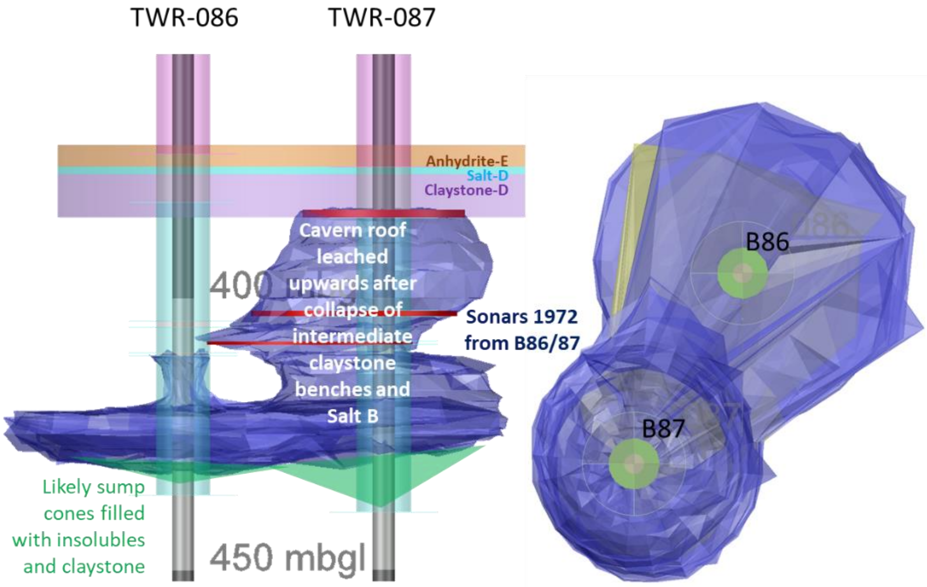

Figure 40: C86-87: 1972 combined sonar volumes and geology in side view (l) and plan view (r). collapsed claystone benches shown in red.

The unaccounted volume in 1972 is 21%, see Table 23, which is in line with the expected value based on the assessment of all caverns in the TWR-UMS. This means that the situation shown in Figure 40 can be considered as an accurate representation without significant volume in shaded areas. All unaccounted volume is thereby caused by the sumps filled with insolubles and material from claystone benches.

Between 1972 and early 1973 a collapse event is recorded in the well diary of TWR-087. A sonar image taken in 1973 from this well shows that the bottom of the cavern has risen significantly. Furthermore, a direct line-of-sight from well TWR-087 towards the cavern volume around well TWR-086 is no longer available. The comparison of the cavern volume according to the production records and the sonar volumes in 1973 is presented in Table 24 below. The effect of the collapse is that the unaccounted volume has risen to 56% in 1973. This is likely caused by potential residual volume around well TWR-086 not visible from well TWR-087 and the bulking of collapsed claystone material.

Table 24: C86-87: 1973 cavern volume according to production records compared to sonar volume

Volume according to production			Sonar volumes	Unaccounted Volume	Remarks
	86	87			
1967 sump (m³)	15.140	11.745	-	-	No sonar avail.
1969 BPB (m³)	53.463				
1969 insol. (m³)	2.387				Sonar "shadow"
1969 net vol. (m³)	51.076		24.420	52%	in B87 image
1972 BPB (m³)	106.115				
1972 insol. (m³)	4.738				Boolean union of
1972 clayst. (m³)	2.931				sonars 1969+1972
1972 net vol. (m³)	98.447		77.371	21%	volumes in Fusion360
1973 BPB (m³)	116.585				
1973 insol. (m³)	5.205				
1973 clayst. (m³)	1.561				Collapse of Salt B
1973 net vol. (m³)	109.819		48.560	56%	and rock benches?

The situation in 1973 is presented in Figure 41. The well diary notes the bottom of the cavern at B86 at 383,5 mbgl, which is in the Claystone CD according to the interpreted geology. This means a "secondary" cavern development in Salt D towards B86 has been initiated between 1972 and 1973. This volume was only connected to the residual cavern volume positioned lower in Salt A by the original borehole. Further development of the cavern around well TWR-086 has taken this second leaching level in Salt D as basis as will be discussed later.

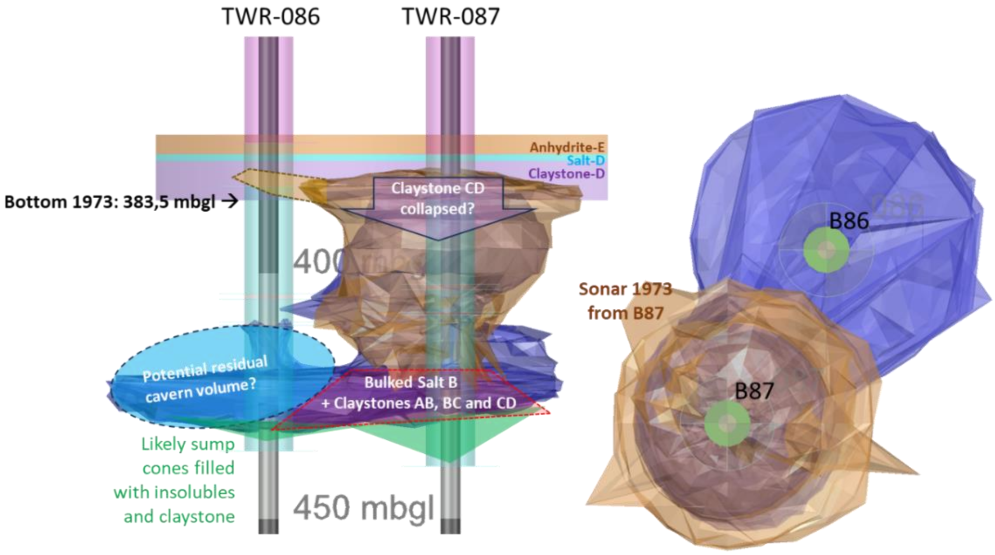

Figure 41: *C86-87: 1973 sonar (brown) and combined 1972 sonar volumes (blue) in side view (l) and plan view (r). possible collapsed intermediate claystone benches shown in orange, possible collapsed Claystone CD shown in purple. Indicated bottom 1973 at 383,5 mbgl in well TWR-086 is taken from the well diary.*

The sonar image from 1973 clearly shows a heap of bulked material on the bottom of the cavern around well TWR-087. This has been visualised by the red trapezoid in Figure 41. This heap has likely closed off the access to cavern volume around well TWR-086 in Salt A (and possibly also Salt B and/or Salt C). The unaccounted volume stated in Table 24 thus comprises insolubles, bulked claystone material and residual cavern volume not visible from well TWR-087, both at the top of the cavern in Claystone CD / Salt D and in Salt A/B/C.

The next snapshot in the development of C86-87 is from 1977. A digital copy of a sonar measurement performed in this year is not available. However, a 2-dimensional sketch of the section across the two wells was found in the well diary showing the likely extend of the cavern in 1977. This sketch has been superimposed over the sonar images shown prior and a likely roof contour has been established based on an evolution of the secondary cavern initiated between 1972 and 1973, see Figure 41. As no digital sonar image is available, a comparison of the cavern volume according to the production records and the sonar volumes in 1977 is not possible. The unaccounted volume in 1977 is thus unknown. The net production volume of the cavern in 1977 is presented in Table 25 below.

Table 25: C86-87: 1977 cavern volume according to production records, no comparison to sonar volume possible

Volume according to production			Sonar volumes	Unaccounted Volume	Remarks
	86	87			
1967 sump (m^3)	15.140	11.745	-	-	No sonar avail.
1969 BPB (m^3)	53.463				
1969 insol. (m^3)	2.387				Sonar "shadow"
1969 net vol. (m^3)	51.076		24.420	52%	in B87 image
1972 BPB (m^3)	106.115				
1972 insol. (m^3)	4.738				Boolean union of
1972 clayst. (m^3)	2.931				sonars 1969+1972
1972 net vol. (m^3)	98.447		77.371	21%	volumes in Fusion360
1973 BPB (m^3)	116.585				
1973 insol. (m^3)	5.205				
1973 clayst. (m^3)	1.561				Collapse of Salt B
1973 net vol. (m^3)	109.819		48.560	56%	and rock benches?
1977 BPB (m^3)	172.424				No digital sonar avail.
1977 insol. (m^3)	7.698				- only skecth in
1977 net vol. (m^3)	164.726		-	-	well diary

The described superimposed 1977 sonar sketch from the well diary is presented in Figure 42.

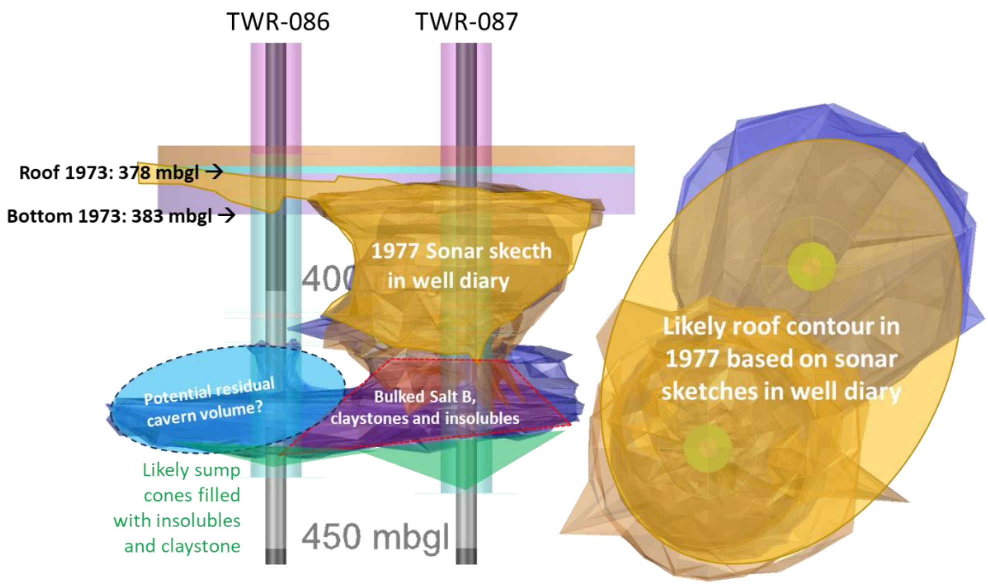

Figure 42: C86-87: 1977 sonar sketch (yellow) superimposed over prior sonar volumes (l). Likely roof contour shown in top view (r). Indicated 1977 cavern roof (378 mbgl) and cavern bottom (383) in well TWR-086 are taken from the well diary.

As this figure shows, the volume development by leaching between 1973 and 1977 has most likely taken place in Salt D. Leaching has laterally extended the roof contour, thus exposing an increasing surface area of the Anhydrite-E to water. This water exposure may have promoted deterioration and subsequent collapse of the Anhydrite-E member in later years.

The final snapshot in the development by leaching of C86-87 is 1979, the final year of production. No sonar images are available that show the final cavern, only an indicative reconstruction was therefore possible. A direct comparison of the cavern volume according to the production records and the sonar volumes in 1979 is also not possible. The net production volume of the cavern in 1979 is presented in Table 26 below. The final net production volume of C86-87 is 173.939 m³ after subtraction of the insolubles volume.

Table 26: C86-87: 1979 cavern volume according to production records, no comparison to sonar volume possible

Volume according to production			Sonar volumes	Unaccounted Volume	Remarks
	86	87			
1967 sump (m³)	15.140	11.745	-	-	No sonar avail.
1969 BPB (m³)	53.463				
1969 insol. (m³)	2.387				Sonar "shadow"
1969 net vol. (m³)	51.076		24.420	52%	in B87 image
1972 BPB (m³)	106.115				
1972 insol. (m³)	4.738				Boolean union of
1972 clayst. (m³)	2.931				sonars 1969+1972
1972 net vol. (m³)	98.447		77.371	21%	volumes in Fusion360
1973 BPB (m³)	116.585				
1973 insol. (m³)	5.205				
1973 clayst. (m³)	1.561				Collapse of Salt B
1973 net vol. (m³)	109.819		48.560	56%	and rock benches?
1977 BPB (m³)	172.424				No digital sonar avail.
1977 insol. (m³)	7.698				- only skecth in
1977 net vol. (m³)	164.726		-	-	well diary
1979 BPB (m³)	184.656				
1979 insol. (m³)	10.718				No digital sonar avail.
1979 net vol. (m³)	173.939		-	-	- only sketch shown

The likely extend of the final cavern in 1979 is presented in Figure 43. The possible position of cavern development by leaching between 1977 and 1979 is shown in the side view as a dashed blue ellipse (left in figure). An indicative final roof contour is shown in the plan view (right in figure). The Anhydrite-E is fully exposed over the area indicated in this figure and as such can be used as the migration contour.

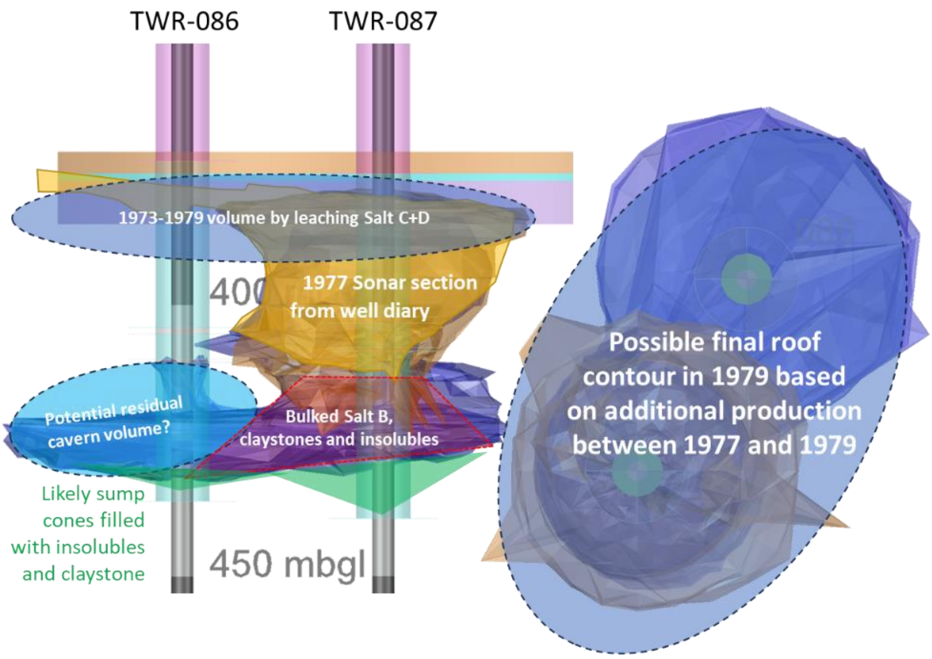

Figure 43: C86-87: 1979 possible position of cavern development by leaching 1977-1979 shown in side view as a dashed blue elips (l). Likely final roof contour shown in plan view (r), Anhydrite-E is fully exposed.

Although a direct comparison of the final cavern volume based on production and sonar images is not possible, an estimate of the cavern volume available for bulked overburden in case of migration can be derived from the information in Table 26 and Figure 43. The estimate assumes that all cavern volume development between 1973 and 1979 has taken place above the intermediate claystone benches. Under this assumption, no cavern volume was developed in the residual cavern positioned in Salt A around well TWR-086. The volume of the cavern above the intermediate claystone benches can thus be derived using the following calculation:

$\mathbf{V_{available\ for\ bulked\ overburden} = V_{sonar}\ 1973 + (V_{production}\ 1979 - V_{production}\ 1973\ ) = 112.680\ m^3}$

This leads to a final unaccounted volume of 39% of the final production volume and 35% after subtracting the insolubles volume. This percentage is higher than what can be expected for the TWR area but is easily explained in this case by the extensive collapses of the claystone benches and the likely presence of a residual cavern in Salt A around well TWR-086. The possible position of the calculated cavern volume available for bulked overburden in case of migration (112.680 m^3) is shown in Figure 44 as a red dashed shape (left in figure) and roof contour (right in figure). The roof contour of C86-87 in 1979 as shown in this figure is approximately 6.000 m^2.

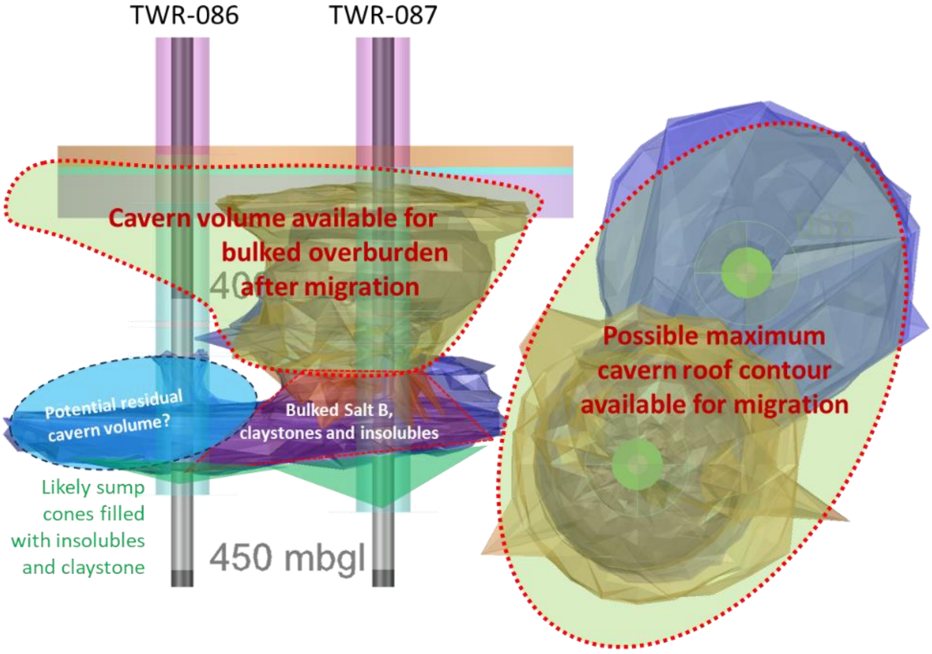

Figure 44: C86-87: 1979 possible position of cavern volume available for bulked overburden in case of migration. Shown in side view as a dashed red shape (l) and a red dashed contour in top view (r).

As a first step in the migration reconstruction, the ellipse-shaped roof contour shown in Figure 43 has been converted to a circle with a radius of 44 m and a centre point between wells TWR-086 and TWR-087. This is illustrated by Figure 45 (right picture in figure). Based on the volume available for bulked overburden this circle has been extruded to a cylinder to construct the representative volume of cavern C86-87 in 1979. The representative volume is indicated by the orange cylinder (left picture in figure).

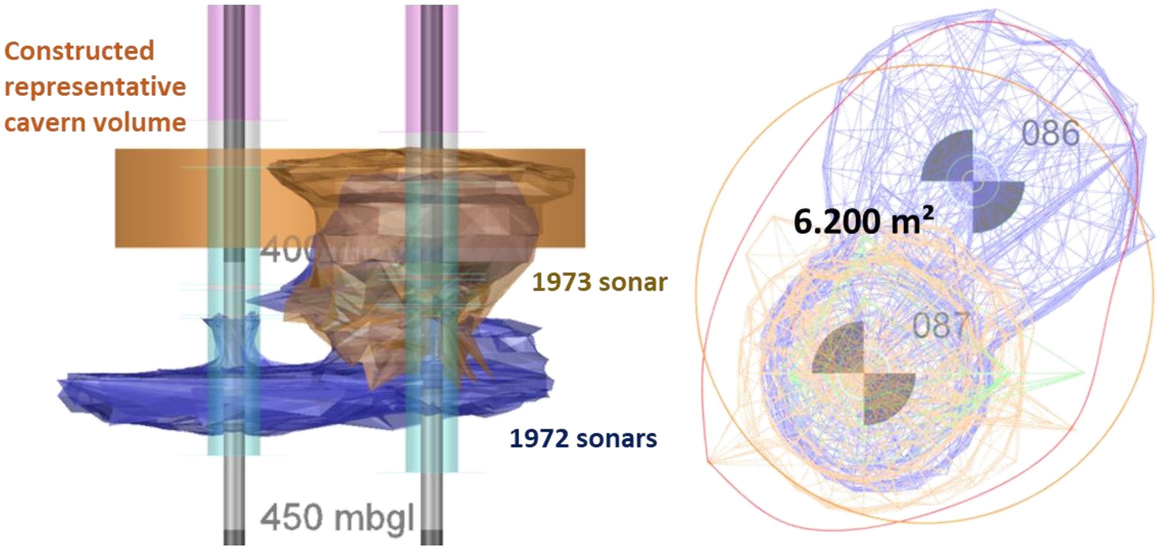

Figure 45: *C86-87: Reconstruction of „Representative volume" (orange). Original sonar volume shown in blue (1972) and brown (1973).*

The selected input parameters for the BJP-Algorithm as derived from the geometries shown in Figure 45 are presented in Table 27.

Table 27 *C86-87 cavern specific input parameters*

Cavern	86
Relevant borehole	87
X coordinate	251350.3
Y coordinate	472490.8
Z coordinate GL (mNAP)	22.0
Depth of top rock [mbGL]	120.2
Depth of top salt [mbGL]	385.3
Base of actual cavern [mbGL]	397.5
Base of initial cavern [mbGL]	439.4
Top of actual cavern [mbGL]	379.0
Height of cavern (m)	18.5
X coordinate migration centre	251350.3
Y coordinate migration centre	472490.8
Volume fitting	
Maximum BPB Prod.(t)	328641
Cavern vol based on BPB (m³)	**184696**
Actual volume (recon./sonar)(m³)	112680
Insolubles (bulked) (m³)	9745
Part of BPB prod. Vol. not acc. (m³)	72016
Part of BPB prod. Vol. not acc. (%)	**39%**
Cavern geometry conversion	
Migration column Surface area (m²)	6000
Constructed cavern radius [m]	44.0
Hydraulic Radius constructed cav. [m]	22.0
Const. cavern height (cylindrical) [m]	18.5
Const. cavern height (conical) [m]	0.0
Constructed volume (cylindrical) [m³]	112519
Constructed volume (conical) [m³]	0
Constructed volume total [m³]	112519
Part of BPB prod. Vol. not acc. (m³)	72177
Part of BPB prod. Vol. not acc. (%)	39%
Height correction backfill insitu [m]	2
Backfill insitu unconsolidated (m³)	0
Backfill consolidation (%)	30

The cavern volume available for bulked overburden considers 39% overall unaccounted volume and 35% net unaccounted volume as explained prior. To maintain a conservative approach the 39% value was used to establish the representative volume as can be seen in the table. The representative volume of the C86-87 cavern volume available for bulked overburden comprises a cylinder with 44 m radius and 18,5 m height. No backfill has been applied in this cavern. Using the input parameters stated in Table 27, the BJP-Algorithm produced the output presented in Figure 46.

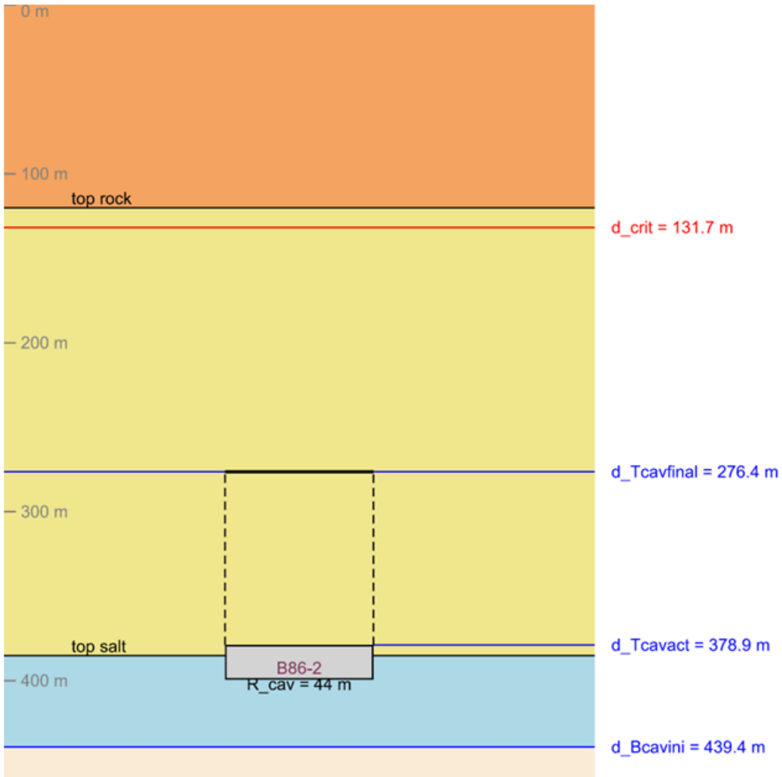

Figure 46: C86-87 BJP-Algorithm output: section view of the calculated migration column

The migration of C86-87 has been extensively studied since this cavern is located underneath the landfill of Twence B.V. in Hengelo [11]. The wells TWR-086 and TWR-087 were initially plugged and abandoned in the early 1980's, see Table 21. Access to this cavern was regained by drilling a borehole with a large outstep in 2022 (TWR-087A). The well path was designed to enter the cavern for a sonar measurement and be a suitable backfill location. Upon hitting the migration column, it was decided to continue drilling towards the original cavern bottom. The output from the BJP algorithm has been superimposed on the well path in Figure 47. The TWR-087A well path enters the calculated migration column in the yielded zone near the top corner as can be seen in this figure. The start of drilling fluid loss was observed at 305 mbgl which coincides well with the likely transition between the yielded and mobilized zones in the migration column.

REINVENT

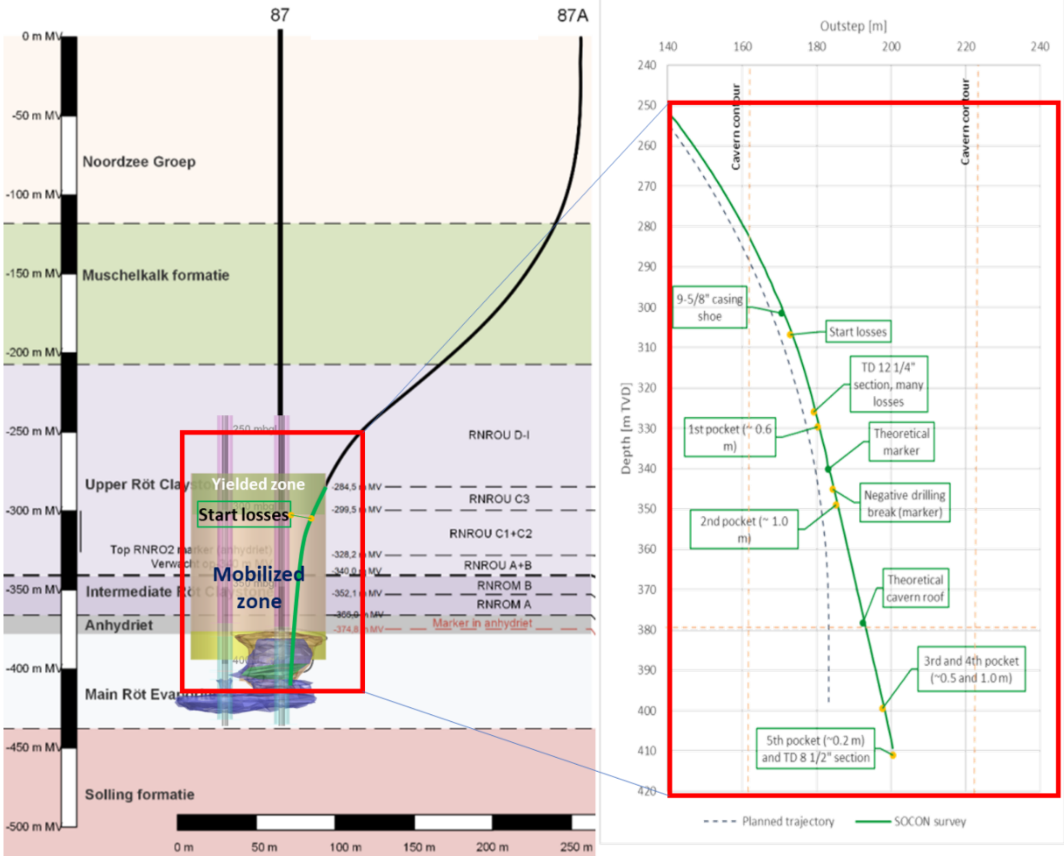

Figure 47: *C86-87: algorithm output superimposed on 2022 well path (l) and observations during drilling (r)*

The TWR-087A well reaches 410 mbgl, which is the bottom of the reconstructed cavern volume available for bulked overburden as shown in Figure 44. In conclusion, the calculated migration column fits very well to the observations in the TWR-087A well and thereby support validation of the algorithm.

The calculated subsidence contours for C86-87 are shown in Figure 48. The actual measured subsidence at C86-87 is also shown in this figure for comparison.

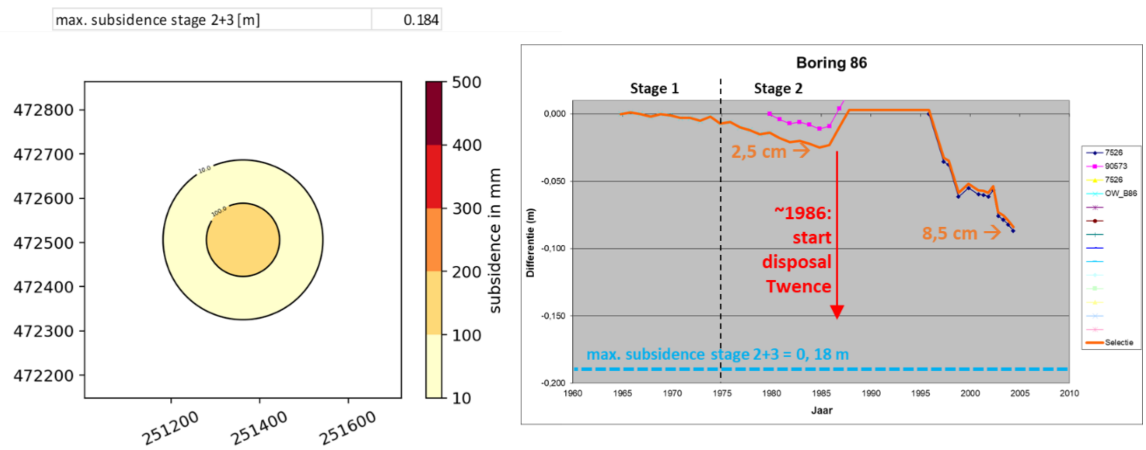

Figure 48: *C86-87: subsidence contours as calculated by the BJP-Algorithm (l) and actual measured subsidence (r).*

As can be seen from this figure, the calculated subsidence of 18 cm does not fit well to the actual measured subsidence of 8,5 cm at first glance. However, the measured subsidence is very likely influenced by the start of disposal in the landfill around 1986. It is unclear whether the measurement point was moved to a different location or directly influenced by the landfill. A new measurement point was erected around 1996, see the blue series 7526 in the subsidence graph. The new point does seem to capture further subsidence in this area. How much of that is related to the gradual build-up of the landfill or to the migration of C86-87 is not clear.

A reconstruction of the likely subsidence in this area can be derived from Figure 48:

- Total subsidence in 1985 (before landfill) = ~2,5 cm
- Subsidence 1996 to 2005 (new point) = ~8,5 cm

Total subsidence in 2005 = ~11 cm

The subsidence rate in 2005 is still high according to the measurements between 2002 and 2005, a total calculated subsidence of ~18 cm is thus in reach considering the conservative selection of input parameters. The comparison between calculated and measured subsidence is thus plausible for C86-87, despite the possible influence of the landfill.

3.6. Input parameter sensitivity based on C15, C37 C49-50 and C86-87

To illustrate the sensitivity of three of the algorithm's main input parameters, i.e. cavern shape, bulking factor and backfill consolidation under the load of bulked overburden, this paragraph provides several examples which strengthen the validation process. The examples presented are all based on the reconstruction of the caverns discussed previously in this chapter.

3.6.1. Effect cavern shape on migration column shape

The effect of the cavern shape on the migration column development is first illustrated with a comparison of C37 and C86-87. Both these caverns lack backfill which eliminates this variable. Cavern C37 has been reconstructed as a cylinder with a cone-shaped sump. The sumps of C86-87 are flatter because a blanket was used. The subsequent complex development history of C86-87 also did not yield a cone-shaped cavern bottom shape at any time. Although the 1973 sonar image from TWR-087 seems to have a cone shaped bottom in Figure 45, the application of a cone-shaped bottom is not deemed applicable for the following reasons:

- Careful observation of the sonar image in 3-dimensional space shows the presence of a heap of material (bulked claystones and Salt B) in the centreline of the well TWR-087, and thus not a cone-shaped bottom.
- The somewhat sloped sides of the bottom half of the 1973 sonar volume are considered too steep to allow for the radius reduction mechanism to work as material will not accumulate on these sloped cavern walls as it would on a sloped cavern bottom.

Therefore, the reconstructed volume is a cylinder without a cone-shaped cavern bottom.

The importance of the migration column radius reduction mechanism included in the algorithm is first underlined by two scenarios presented for C37 in Figure 49.

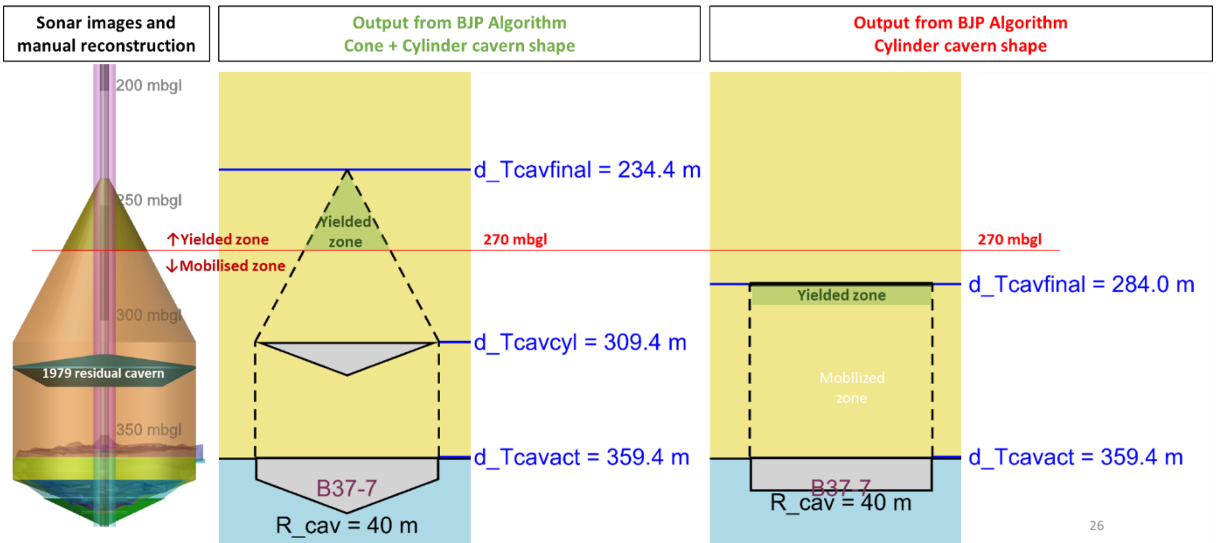

Figure 49: Comparison migration column shapes for C37: realistic cone + cylinder (l) and unlikely cylinder (r)

The first scenario (left in figure) is the output from the BJP-Algorithm as shown in Figure 27 in paragraph 3.3, i.e. with a representative cavern shape based on a cone-shaped sump and a cylinder. This outcome fits to the observed migration and measured subsidence. The second presented scenario is (B37-3, right in figure) shows the migration column of a cylindrical cavern with the same volume and position in the stratigraphy. The observed transition between the yielded zone and the mobilized zone at approximately 270 mbgl is marked with a red line.

As can be seen from Figure 49, a cylindrical migration column does not reach the observed transition and is thus unlikely to represent the actually occurred situation. As such, this example validates the use of a cone-shaped bottom for relevant caverns in the TWR area.

The second example which underlines the importance of making a distinction between cone-shaped sumps or (near) flat-shaped sumps is presented in Figure 50.

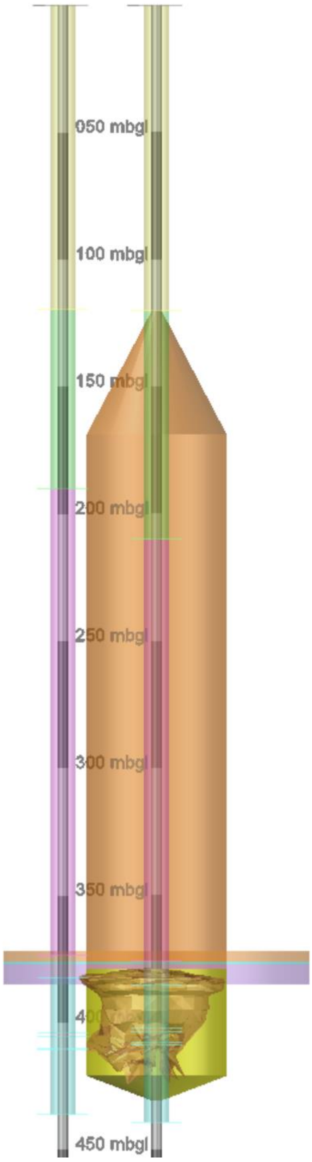

Figure 50: C86-87: alternative scenario leading to Stage 4 subsidence which did not occur.

This figure shows an alternative scenario for the migration of C86-87 in which the representative cavern volume comprises a cone-shaped cavern bottom and a cylindrical vertical extension. In this scenario, the 1973 sonar is taken as the basis for further volume development by leaching between 1973 and 1979. The volume of the shown (yellow) cavern is thus equal to the cavern volume available for bulked overburden used in the previously discussed reconstruction of this cavern, i.e. 112.680 m³.

As can be seen from Figure 50, the calculated migration column for this alternative representative cavern just reaches the Tertiary and therefore would have caused Stage 4 subsidence (trough or sinkhole). The bulking factor used for this scenario is 1,2.

This scenario clearly does not reflect the observations from the TWR-087A well track nor the measured subsidence. As such this scenario is deemed unrealistic and it is unlikely to represent the actual situation.

The presented alternative scenario for C86-87 shown in Figure 50 demonstrates that the choice of cavern shape is critical during the selection of input parameters. Careful assessment of the available sonar information, the unaccounted volume and the development history of the cavern is required to arrive at plausible subsidence prognoses for caverns with migration potential in the TWR area. This will be elaborated in Report 4.

The effect of the cavern shape on the migration column development for backfilled caverns has been evaluated by comparing two scenarios for C15 as presented in Figure 51. The migration column reconstruction for a cone-cylinder combination (left in figure) is compared to the migration column that would develop based on a purely cylindrical shaped cavern (right in figure). The cylindrical migration column only reaches 255 mbgl, whereas the cavern bottom in 1981 is observed at 238,5 mbgl according to the well diary. A cylindrical migration at C15 is not corresponding the observations and is therefore rejected as a possibility.

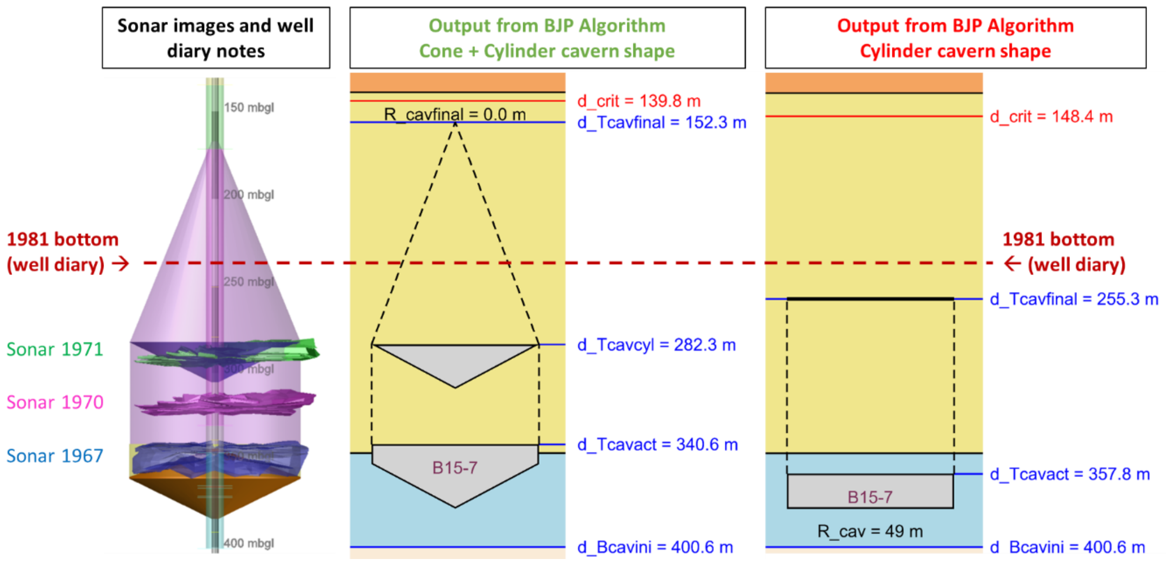

Figure 51: C15: effect of cavern shape on migration column shape – cone+cylinder (l) and cylinder only (r)

This example shows that also for a backfilled cavern it is important to consider the original shape of a cavern rather than the cavern shape after backfilling.

3.6.2. Bulking factor overburden

The sensitivity of the selected bulking factor for the overburden is tested with three examples based on the reconstructions of C37 and C86-87 to eliminate the influence of backfill on migration, as well as C15 which is backfilled. In all examples the bulking factor is varied between 1,11 (as historically used), 1,2 (as currently used) and 1,29 (to equalise the offset between scenarios tested).

The first example shows the calculated migration column and resulting subsidence for these three bulking factor values for C37 in Figure 52. As can be seen in the left picture in this figure, the selection of a bulking factor of 1,11 would have led to Stage 4 subsidence according to the BJP-Algorithm output, albeit with very little impact due the limited maximum subsidence (13,5 cm). This scenario does not correspond to the observed migration in GR logs. As such this scenario is not plausible and a bulking factor of 1,11 is not applicable.

The middle picture in this figure shows the base case with a bulking factor of 1,20 and is identical to Figure 27. As discussed, the subsidence (12,7 cm) and the observations with regards to the migration column are well aligned with the calculated migration column.

The selection of a bulking factor of 1,29, shown in the right picture in Figure 52, leads again to a plausible subsidence value (12,7 cm), thus identical to the subsidence for the base case. However, the final migration column depth is underestimated in relation to the GR logs and well observations from 2003 which show the transition between the mobilized and yielded zones at 270 mbgl [9], see the red line in this Figure. The migration column for a bulking factor 1,29 stops below this depth and is this value is thus too optimistic. As such, a bulking factor of 1,29 is also not plausible and thereby not applicable to the TWR area.

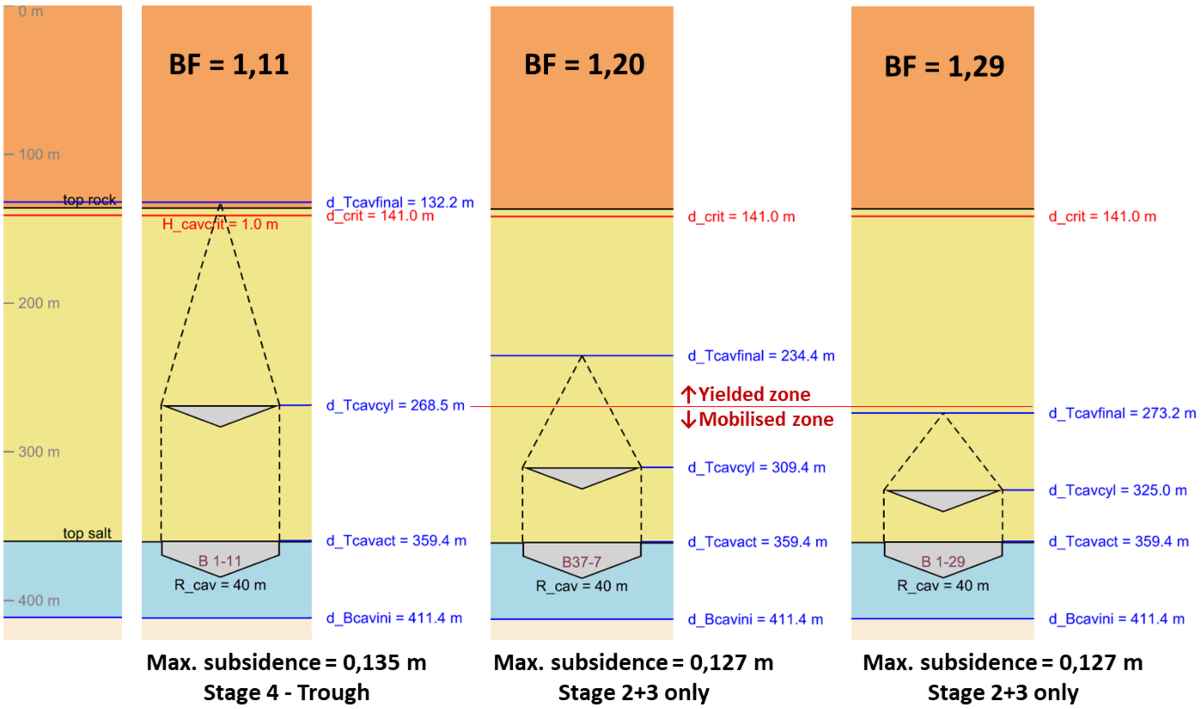

Figure 52: *C37: comparison of bulking factors 1,11 (l), 1,20 (m) and 1,29 (r). The observed transition between mobilized zone (bulked overburden) and yielded zone (delamination) is shown by a red line.*

To confirm the test performed for C37, a similar test was performed for C86-87 which is presented in Figure 53 below. The respective migration columns for a bulking factor of 1,11 (red), 1,2 (green) and 1,29 (yellow) are shown in the right picture in this figure together with the TWR-087A well path.

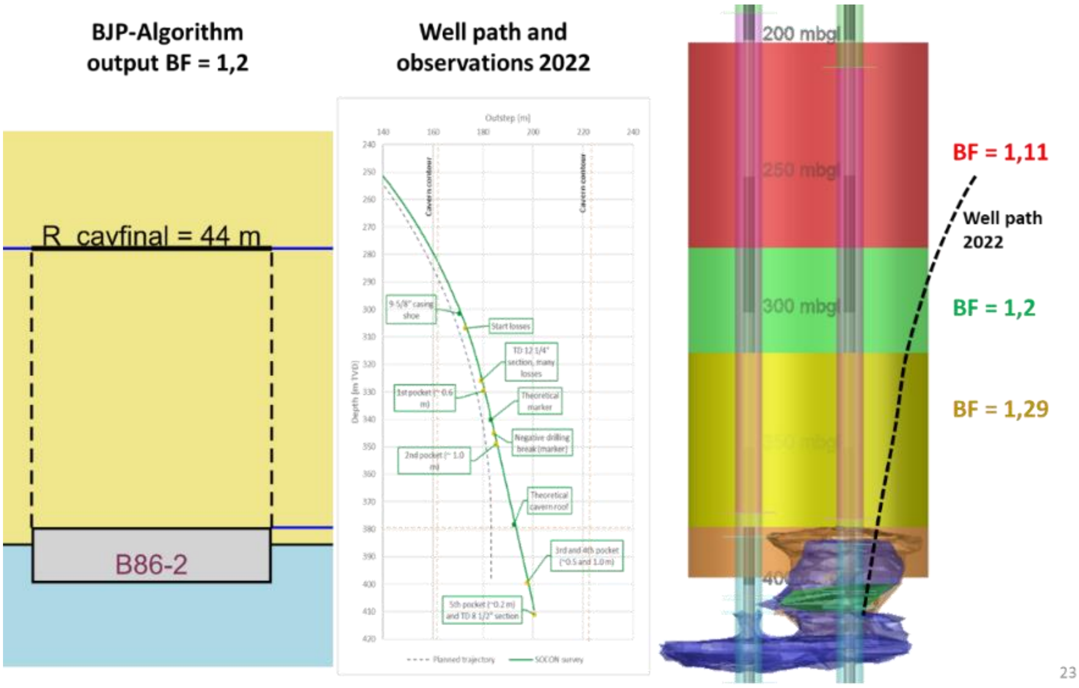

Figure 53: *C86-87: calculated migration column for BF=1,2 (l), well path and observations from 2022 borehole (m) and comparison of bulking factors 1,11, 1,2 and 1,29 (r).*

The migration column for the scenario with BF=1,11 reaches the Muschelkalk. This outcome is not supported by the observations in the TWR-087 and TWR-087A wells. A bulking factor of 1,29 significantly underestimates the observed migration column. Both scenarios are thus not plausible and support the application of a bulking factor of 1,2 for the TWR area.

A third example shows the calculated migration column and resulting subsidence for three bulking factor values for C15 in Figure 54. This cavern is backfilled, and this example thus shows the influence of bulking factor variation on the migration of a backfilled cavern.

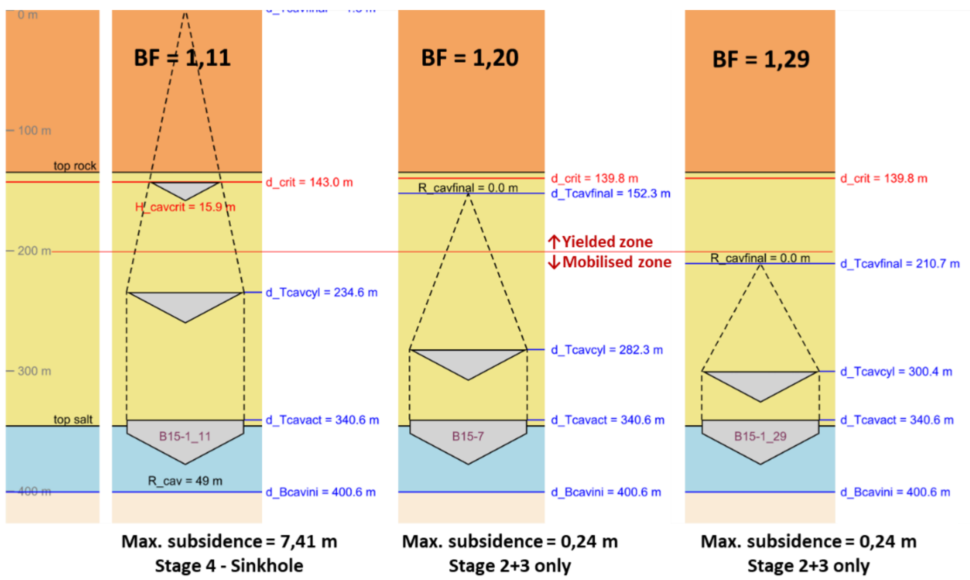

Figure 54: *C15: comparison of bulking factors 1,11 (l), 1,2 (m) and 1,29 (r).*

As can be seen in the left picture in this figure, the selection of a bulking factor of 1,11 would have led to Stage 4 Sinkhole subsidence despite backfill. The maximum subsidence according to the BJP-Algorithm output is 7,41. This does not correspond to the observed subsidence at that location. Furthermore, the observed migration from GR logs and well observations, see Figure 18, do not align with this scenario.

3.6.3. Backfill behaviour

Variation of the backfill consolidation under the load of bulked overburden has been tested for C15 as presented in Figure 55. The subsidence seems less sensitive to the backfill consolidation under the load of bulked overburden than the bulking factor when comparing this figure to Figure 54. As such, 30% consolidation is deemed a conservative but realistic value which can be applied to the BPR-Slurry from the Hengelo salt plant.

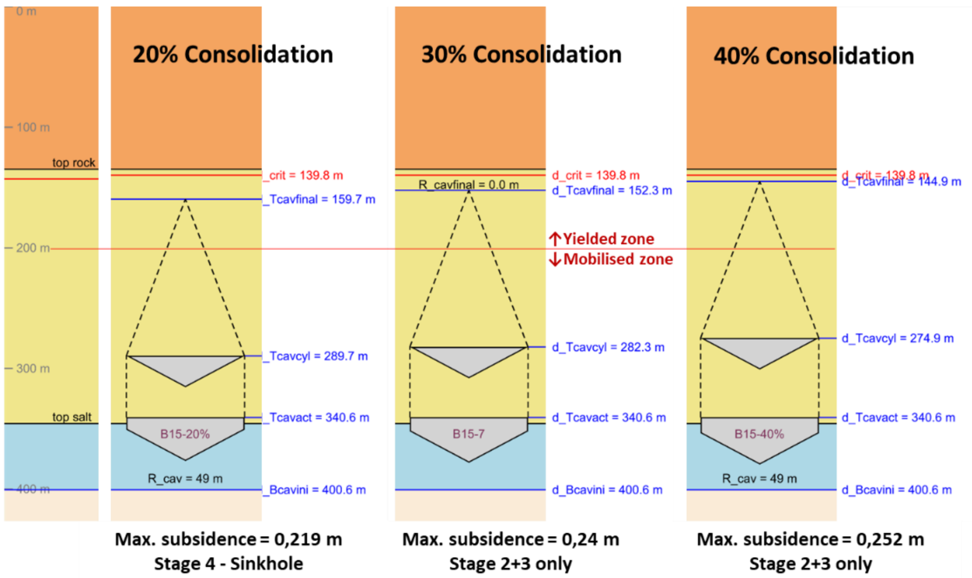

Figure 55: C15: comparison of backfill consolidation under load of bulked overburden 20% (l), 30% (m) and 40% (r).

The height correction (2 m) for which the slurry does not have any load baring capacity is directly proportional to the final depth reached by migration (see Report 2, paragraph 2.3 [3]). In other words, a height correction of 4 m would lead to a final depth which is 2 m shallower than for a height correction of 2m. As the 2 m is the maximum observed during field tests and it fits well with the observed migration in Figure 55, this value this value is deemed a conservative but realistic value which can be applied to the BPR-Slurry produced by the Hengelo salt plant.

4. Reconstruction of complex cavern migration cases

The reconstruction of complex cavern migration cases strengthens the validation of the BJP-Algorithm as presented in the previous paragraphs of this chapter. The complexity of the cavern migration cases presented in this paragraph relates to the application of forced leaching (see paragraph 2.3), the cavern geometry, the backfilling history and/or the migration history. The complex cavern migration cases discussed in this paragraph are C63-64-65, C69-70-71 (location of the 1991 sinkhole formation) and C106-107. All these migration cases are all well-documented. The reconstruction process for these caverns demonstrates that the selected input parameters can also be confidently applied to complex cavern migration cases.

4.1. Reconstruction C63-64-65

Cavern 63-64-65 (C63-64-65) is a multi-completion cavern (MCC) comprising wells TWR-063, TWR-064 and
TWR-065. The key data for this are included in Table 28 below and additional information can be found in APPENDIX I.

Table 28: Key data C63-64-65

Wells*	X (WGS84)	Y (WGS84)	Z (mNAP)	Final depth (mbgl)	Final depth (mNAP)	Well ready	Start production	End production	Cemented
63	251781,9	473511,7	21,12	372,1	-350,98	2-11-1960	1-6-1961	1-6-1978	23-6-1978
64	251872,9	473563,3	21,66	367,68	-346,02	31-3-1961	1-6-1961	1-6-1978	15-9-1976
65	251965,0	473586,6	21,1	363,3	-342,25	9-5-1961	1-6-1961	1-6-1978	8-8-1978

* forced hydraulic connection in May 1961 according to well diaries

The development of C63-64-65 was initiated by forced leaching, see paragraph 2.3. An FLC developed by water injection during an unknown period between the completion of the wells in May 1961 and the end of 1961. The further development of this cavern has not been detailed in the well diaries for the years 1961-1967. The first available sonar images of C63-64-65 date from 1967 and are shown in Figure 56 below.

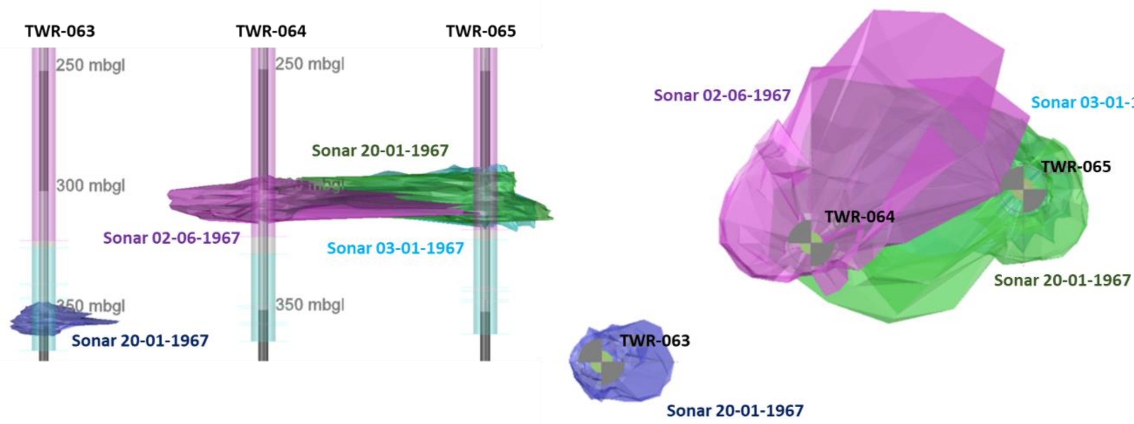

Figure 56: C63-64-65 available sonar images from 1967. Side view (l) and Top view (r).

As can be seen from this figure, the position of cavern volume around wells TWR-064 and TWR-065 is located above Salt C in the Röt Claystone. This indicates that the cavern had already migrated in 1967, thus after only five years of production. As no sonar or other information is available which can directly guide the reconstruction of the sump phase and the cavern development until 1967, a cavern volume assessment based on the production figures was performed as an approximation.

As a first step in the approximation, the total volume of the migrated C64-65 has been estimated using a Boolean combination of the available three sonar images. The volume of the migrated cavern is approximately 145.000 m³. The second step is the estimation of the surface area of the migration column, i.e. the area of the maximum contour formed by these sonar images. This area is approximately 14.200 m2. The distance between the roof of the residual cavern in 1967 and the likely roof of the cavern before migration, i.e. Top Salt C, is approximately 23 m.

Using these values, the volume development of C63-64-65 has been reconstructed starting with the residual cavern volume of C64-65 in 1967 and working backwards. In other words, the residual cavern volume is taken as the starting point, and the original C64-65 volume is derived from the migration column volume, via the bulking factor. Once the volume of C64-65 is known, the volume of C63 is estimated by subtracting the C64-65 volume from the total salt production volume. Insoluble and claystone material have been considered analogue to the previously discussed caverns.

The thus reconstructed cavern volume development is presented in Table 29 which also states the assumed operation, i.e. in which well(s) water was injected or brine was produced.

Table 29: Cavern volume approximation based on combined 1967 sonar volume of C64-65

	Approximate volumes [m³]			**Assumed operation**		
	C63	**C64-65**	**Remarks to source**	**TWR-063**	**TWR-064**	**TWR-065**
1961 Vol. By Forced leaching		15.089	from prod. data	X	Water	X
1962 Vol. By Leaching (m³)		61.442	from prod. data	Water	Brine	Water
1966 Vol. By Leaching (m³)	50.000	222.686	from prod. data	Water	Brine	Water
1966 insolubles vol. (m³)	2.902	12.925	insol. + claystone			
1966 net vol. (m³)	47.098	209.761	calculated			
1966 Migration height (m)		23	from section			
1966 Migration contour (m²)		14.200	from top view			
1966 Migration column vol. (m³)		322.340	calculated			
BF		1,2	assumed			
1967 Bulked overburden		386.808	calculated			
1967 Total void vol. (m³)		532.101	calculated			
1967 Residual cavern vol. (m³)		**145.293**	from sonar images			
1967-1969 Vol. By leaching (m³)	22.623		from prod. data	Water	Brine	
1967-1969 insolubles vol. (m³)	1.313		insol. + claystone			
Final net vol. by prod. (m³)	**68.408**	**209.761**	**calculated**			

To check the plausibility of these volumes, a geometrical reconstruction using AutoCAD was subsequently prepared. The reconstructed cavern geometries are shown in Figure 57 below.

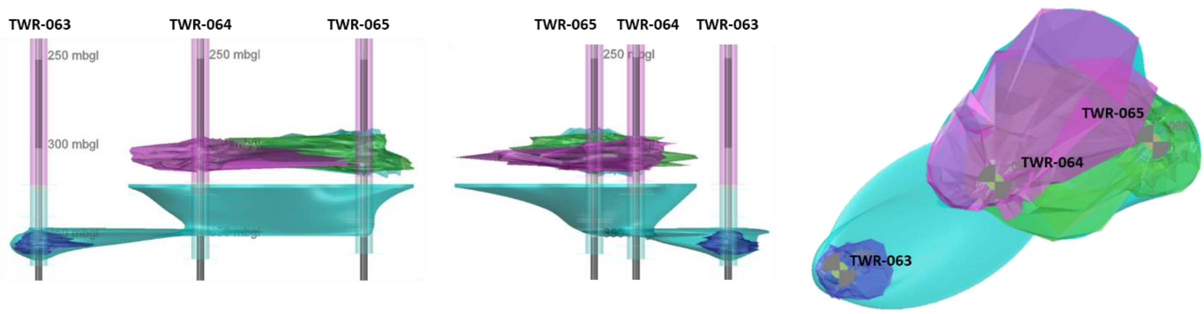

Figure 57: C63-64-65 Approximation of cavern geometries: viewing North (l), viewing West (m) and Top view (r).

REINVENT
SOLUTIONS

In the reconstruction of the approximate cavern geometry, care was taken to represent the volumes as stated in Table 29 as close as possible. The shape of the caverns assumed that much of the water injected in well TWR-063 between 1961 and 1967 was utilized to leach Salt C at C64-65. This can be explained by the position of C63 directly underneath the intermediate claystone benches and the fact that the sump development of this cavern system was initiated by forced leaching. The reconstruction shows that the FLC developed underneath the intermediate claystone benches towards TWR-063, but above these benches towards TWR-065. As a result, water injected at TWR-063 quickly leached upward towards C64-65 without significantly leaching Salt A in C63. This also explains the small sonar volume at TWR-063 in 1967.

The drilling logs show that Anhydrite-E is present at the location of this cavern. No GR logs to confirm the drilling logs are available. The quick upward development of the cavern likely exposed the Anhydrite-E to water at an early stage in the cavern development. The rapidly expanding roof contour in combination with the water exposure most likely caused the migration of C64-65 at some point in 1965-1966. The migration is confirmed by the 1967 sonar images from wells TWR-064 and TWR-065.

Salt production from this cavern system continued between 1967 and 1969 by operation of TWR-063 as a SCC. As such it is assumed that no volume in C64-65 was developed through water injection at TWR-063. The reconstructed shape of C63 as shown in Figure 57 is based on a 2-D sketch of a sonar measurement performed in 1976. No digital version of this sonar measurement is available.

In 1969 salt production by water injection was suspended at this cavern prepare for backfilling according to the TWR-063 well diary. It was planned to use this well as the brine production well during slurry injection in C64-65, but it is unclear if this was actually operated as noted in the diary.

In April of 1969 backfilling of C64-65 was initiated with slurry injection at TWR-065 according to [10]. Between 1969 and 1977 a total of 921.415 m³ slurry was pumped to C64-65 via both wells TWR-064 and TWR-065 according to this source. Using the Slurry/Backfill ratio of 5, this amounts to 184.283 m³ of insitu backfill before SWC. It is not clear in what exact configuration (slurry in / brine out) the wells were operated during the backfilling period 1969-1977 but is likely that slurry input was alternated between wells.

Considering the geometry of the cavern system after 1969 comprising C63 at its original position and C64-69 migrated well into the Röt Claystone, it seems unlikely that TWR-063 was used as a brine production well during backfilling of C64-65. As such it is assumed that no further volume development in C63 took place during backfilling, even in case the slurry was undersaturated. In the latter case, salt in the original C64-65 contour would have been leached as this was located at the shortest distance from the slurry injection point. The volume of C63 in 1969 as noted in Table 29 is thus the final volume.

Taking into account that the residual cavern volume of C64-65 in 1967 is only ~145.000 m³, some of the backfill must have flowed into the pore space of the bulked overburden on the bottom of the original cavern and perhaps even towards C63. Even when applying 15% SWC to the 184.283 m³ of insitu backfill, 156.641 m³ remains and this volume still does not fit in the 1967 residual cavern. The distribution of backfill between residual cavern space and pore space of the bulked overburden is unknown.

To alleviate the unknown distribution, the BJP-Algorithm was applied to the C64-65 reconstructed cavern geometry before migration as presented in Figure 57. This geometry was converted into a representative volume based on the approximated area of the maximum contour and the volume distribution presented in Table 29. The selected input parameters for the algorithm are presented in Table 30 and depicted in Figure 58.

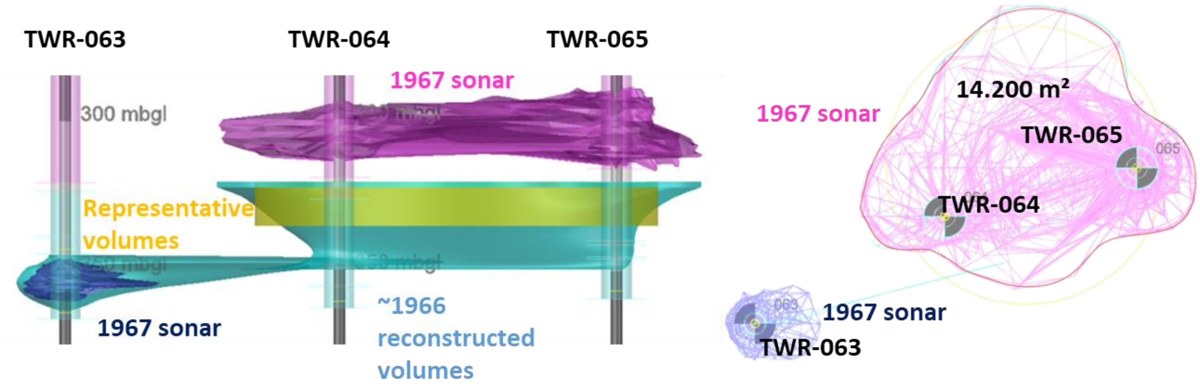

Figure 58: C64-65: Reconstruction of „Representative volume" (yellow), sonar volumes shown in blue/magenta.

As only a reconstructed cavern volume of C64-65 is available, the 6% unaccounted volume was only slightly reduced to 5% in the representative volumes as can be seen in the table. This 5% unaccounted volume is considered very conservative.

Table 30: C64-65 cavern specific input parameters

Cavern	64
Relevant borehole	64
X coordinate	251872,9
Y coordinate	473563,3
Z coordinate GL (mNAP)	21,7
Depth of top rock [mbGL]	124,2
Depth of top salt [mbGL]	326,7
Base of actual cavern [mNAP]	-314,0
Base of actual cavern [mbGL]	335,7
Base of initial cavern [mbGL]	362,9
Top of actual cavern [mbGL]	320,7
Height of cavern (m)	15,0
X coordinate migration centre	251910,0
Y coordinate migration centre	473595,0
Volume fitting	
Maximum BPB Prod.(t)	396.324
Cavern vol based on BPB (m³)	**222686**
Actual volume (recon./sonar)(m³)	209761
Part of BPB prod. Vol. not acc. (m³)	12925
Part of BPB prod. Vol. not acc. (%)	6%
Cavern geometry conversion	
Migration column Surface area (m²)	14200
Constructed cavern radius [m]	67,0
Hydraulic Radius constructed cav. [m]	33,5
Const. cavern height (cylindrical) [m]	15,0
Const. cavern height (conical) [m]	0,0
Constructed volume (cylindrical) [m³]	211539
Constructed volume (conical) [m³]	0
Constructed volume total [m³]	211539
Part of BPB prod. Vol. not acc. (m³)	11147
Part of BPB prod. Vol. not acc. (%)	5%
Height correction backfill insitu [m]	2
Backfill insitu unconsolidated (m³)	156641
Backfill consolidation (%)	30%

The representative volume of C64-65 comprises a cylinder with 67 m radius and 15 m height. A total of 156.641 m³ backfill has been applied in this cavern.

Using the input parameters stated in Table 30, the BJP-Algorithm produced the output for these caverns as presented in Figure 59. A comparison of the results of the subsidence calculations and sonar information from 1967 is shown in this figure at the correct depth. No GR logs are available which have captured any further migration of this cavern.

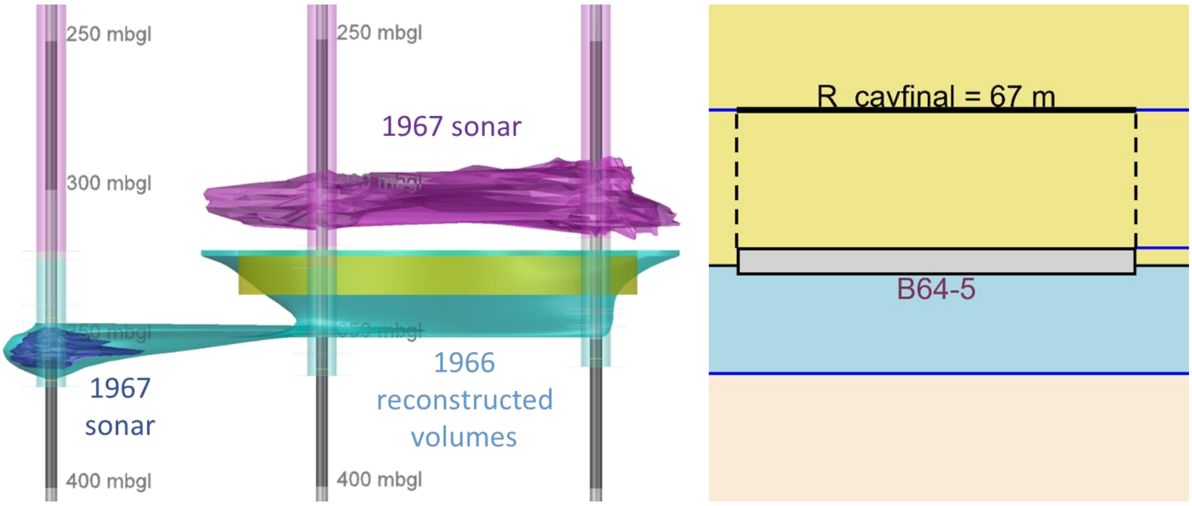

Figure 59 C64-65: Comparison BJP-Algorithm output and migration observations from sonar 1967

The well diary of TWR-064 states that in 1976 the bottom of the well (not the cavern!) was positioned at 290,3 mbgl. This corresponds to the roof of the 1967 cavern and provides an indication that migration did propagate after 1967. The well diary of TWR-065 describes several operations in 1970 and 1971 to regain access to the cavern by milling the casing several times each time at a shallower depth. This also indicates migration of the cavern. The last milling depth was at 276 mbgl in 1971. This corresponds to the top of the calculated migration column. In 1976 access to well TWR-065 was only possible to a depth of 241 mbgl due to the casing being obstructed with backfill material. This would indicate that the backfill pumped into the cavern has fully filled up any residual volume and was forced into the well by deformation of the migration column.

In conclusion, the observations from the well diary correspond very well to the calculated migration column position in the stratigraphy and the algorithm thus provides a plausible reconstruction of the actual migration process at C64-65. The calculated subsidence contours for C64-65 are shown in Figure 60. The actual measured subsidence at C64-65 is also shown in this figure for comparison.

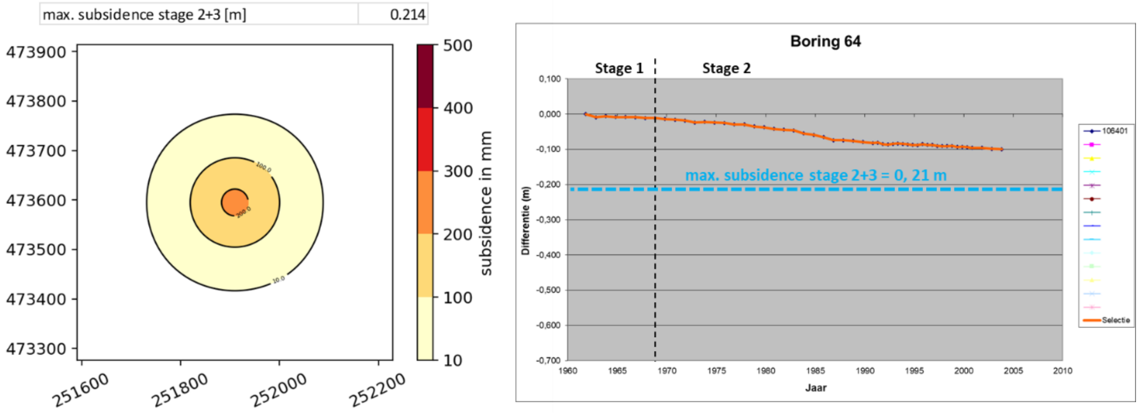

Figure 60: C64-65: subsidence contours as calculated by the BJP-Algorithm (l) and actual measured subsidence (r).

As can be seen from this figure, the measured subsidence does not reach the calculated subsidence until 2005. The apparent overestimation of the subsidence by the algorithm can be partly attributed to the selection of conservative parameters as with the other discussed caverns in this report. However, the difference between calculated and measured subsidence for this cavern is likely also caused by backfilling the residual cavern during an advanced stage of the migration instead of before. This may have influenced the consolidation behaviour of the backfill as the loading situation differed from the cases discussed prior. The SWC may not have had time to develop and loading the backfill with bulked overburden happened instantly rather than gradual.

This alternative loading case may have reduced overall consolidation of the backfill, effectively making the backfill function more efficient and thus reducing subsidence. As this effect cannot be quantified, the application of the algorithm in this case represents a conservative approach. Despite this apparent increase in backfill efficiency, it not recommended to wait with a backfilling operation until cavern migration has commenced due to the operational risks involved. These risks are mostly related to the integrity of the well during migration, as was discussed for C15 in paragraph 3.2.3, and which have also been noted in the well diaries for C64-65.

In conclusion, the application of the BJP-Algorithm for C64-65, despite overestimating subsidence, has demonstrated the applicability of the algorithm for a cavern which has already started migration before backfilling has been completed.

4.2. Reconstruction C69-70-71

Cavern 69-70-71 (C69-70-71) is a multi-completion cavern (MCC) comprising wells TWR-069, TWR-070 and TWR-071. The key data for this cavern are included in Table 31 below and additional information can be found in APPENDIX I.

Table 31: Key data C69-70-71

Wells*	X (WGS84)	Y (WGS84)	Z (mNAP)	Final depth (mbgl)	Final depth (mNAP)	Well ready	Start production	End production	Cemented
69	252258,0	473638,2	22,00	348,5	-326,50	16-11-1961	29-6-1962	1-12-1977	6-12-1977
70	252340,1	473615,6	22,24	347,5	-325,26	15-12-1961	29-6-1962	1-12-1977	26-1-1978
71	252420,9	473593,2	22,23	345,75	-323,52	31-1-1962	29-6-1962	1-12-1977	23-1-1978

* forced hydraulic connection from 3-5-1962 to 19-6-1962 according to well diaries

Like C63-64-65, the development of C69-70-71 cannot be reconstructed using the generalised workflow for sump reconstruction due to the performance of forced leaching between at least wells TWR-070 and TWR-071 in April of 1962. The well diary records a failed forced leaching attempt between these wells but according to the production records, the connection between TWR-070 and TWR-071 was made before any brine production had taken place. The connection between well TWR-069 and then MCC 70-71 followed shortly after, perhaps within a few weeks, further indicating the presence of a FLC reaching from TWR-070 to (nearly) well TWR-069 in April 1962. Operation of the MCC 70-71 extended the initial FLC volume until a connection was made with TWR-069 after which the cavern was operated as the MCC 69-70-71.

As the exact position of the FLC is unknown, the reconstruction of this cavern was based on a careful assessment of the available sonar images, production data and information from well diaries. The first step in this assessment is the correction of the available sonar images as shown in Figure 61 below. For scale, the distance between the wells in this figure is approx. 85 m.

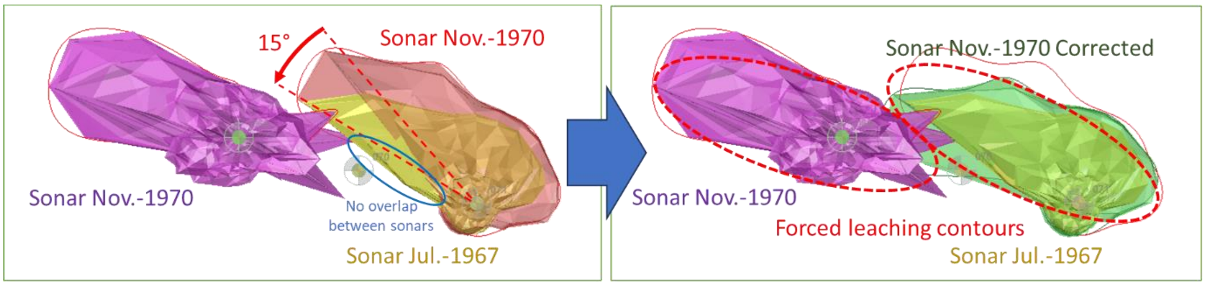

Figure 61: Left: Sonar images from 11-03-1970 at well TWR-069 (magenta), 25-07-1967 (yellow) and 11-02-1970 (red) at well TWR-071. Right: Corrected sonar image at well TWR-071 and likely forced leaching contour.

As can be seen in the right picture in Figure 61, the overlap between the sonar measurements taken in November 1970 from wells TWR-069 and TWR-071 are not overlapping with each other nor with well TWR-070. This seems unlikely as the cavern was operated as a MCC between 1962 and 1970. To allow for more overlap, the TWR-071 sonar image was rotated 15° counter clockwise as shown by the red arrow in this picture. The corrected position of all the sonar images is shown in the right picture in Figure 61. The most likely position of the forced leaching contours is shown as ellipses.

A second correction relates to the sonar volume of the 1970 sonar image from well TWR-069. A side view of this sonar image is presented in Figure 62 in the top picture. The addition of the two sonar volumes shown in this figure results in 373.740 m³, whereas the production volume up to that point only amounts to 333.827 m³. This made it clear that the digital file of the 1970 TWR-069 sonar does not represent the actual cavern measured at that time. This was confirmed by a sketch from the original Prakla sonar report from 1970 which included a primary and a secondary reflection.

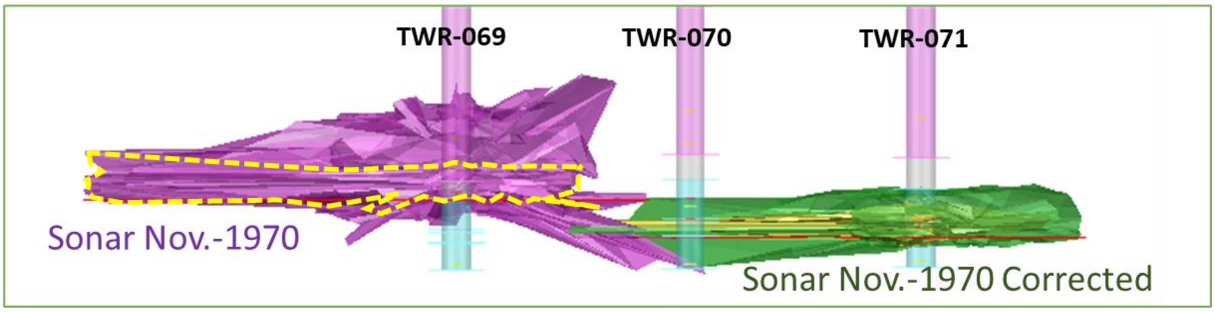

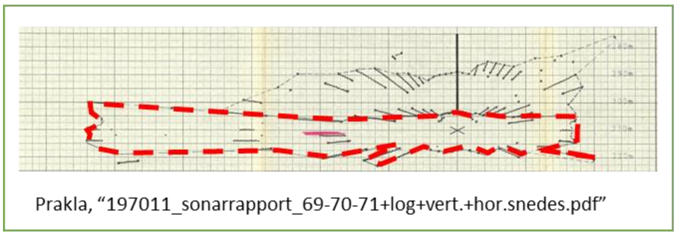

Volume acc. to production (m³)	Sonar Volume TWR-069 (m³)	Sonar Volume TWR-071 (m³)	Total Sonar Volume (m³)
333.827	213.710	160.030	373.740

Figure 62: Volume correction of 1970 sonar image at TWR-069: digital version shown in top picture (magenta), 2D sketch from original Prakla sonar report shown in bottom picture (red) and projected in top picture (yellow).

The primary reflection is shown as dashed contours in Figure 62. As demonstrated by the 2D sketch, the digital sonar file captured the second reflection and thus significantly overestimated the sonar volume by a minimum of 40.000 m³. The actual sonar volume cannot be directly derived from the 2D sketch, but an approximate geometry was prepared in AutoCAD which enabled reconstruction of the cavern system development.

The reconstruction of the cavern system starts in 1962 after a connection between all three wells was established by forced leaching and subsequent leaching. Between 1962 and 1967 a total cavern volume of 256.135 m³ is developed according to the production records. After subtraction of approximately 15.000 m³ insolubles and claystone material, the net cavern volume in 1967 is ~241.000 m³. The available sonar from 1967 in TWR-071, a 1967 sonar sketch in TWR-070 and the corrected sonar contour of 1970 in TWR-069 were used as guides for the reconstruction of the cavern geometry. The resulting cavern geometry is presented in Figure 63.

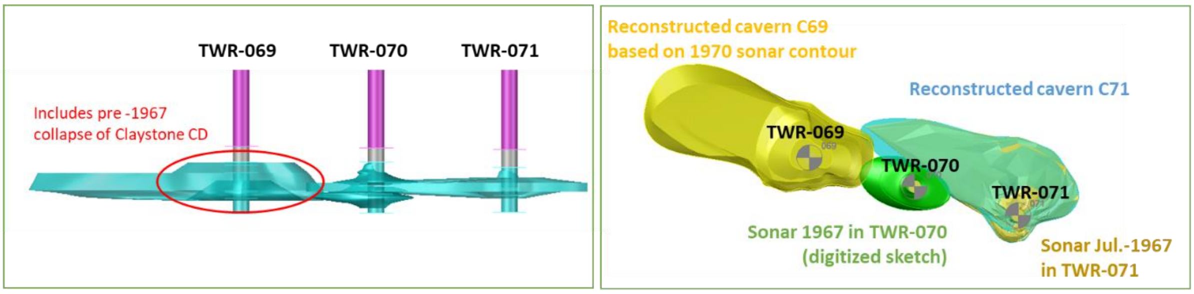

Figure 63: C69-70-71 Cavern volume development 1962 – 1967: side view (left) with collapsed Claystone CD, top view (right) with available sonar images projected.

A collapse of part of the Claystone CD prior to 1967 has been considered in the reconstruction of C69. The presence of Claystone CD and Salt D was confirmed by a GR log in TWR-069, see APPENDIX I. The Anhydrite-E was thus exposed to water around well TWR-069 from at least 1967 onwards. The water exposure of the Anhydrite-E around well TWR-069 was one of the likely causes of cavern migration starting after 1967 in C69. Another possible cause was the presence of faults as shown in Figure 5 of

[12]. In this memo by SodM, an interpretation of two faults intersecting C69-70-71 is provided. This interpretation has been projected onto the reconstructed cavern in Figure 64 below.

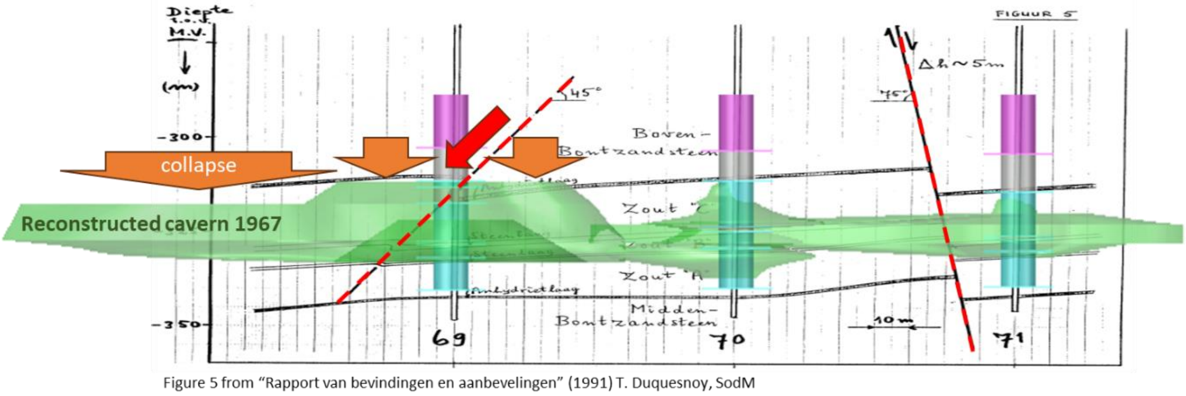

Figure 64: C69-70-71 possible position of faults intersecting the cavern and (partly) causing start of migration (red dashed lines) and subsequent roof collapse (orange arrows).

The water exposure and fault(s) at C69 caused the collapse indicated in Figure 64 by orange arrows in December of 1967 according to the well diary. This led to the situation as measured by the 1970 sonar (primary reflection) from well TWR-069 and presented in Figure 65.

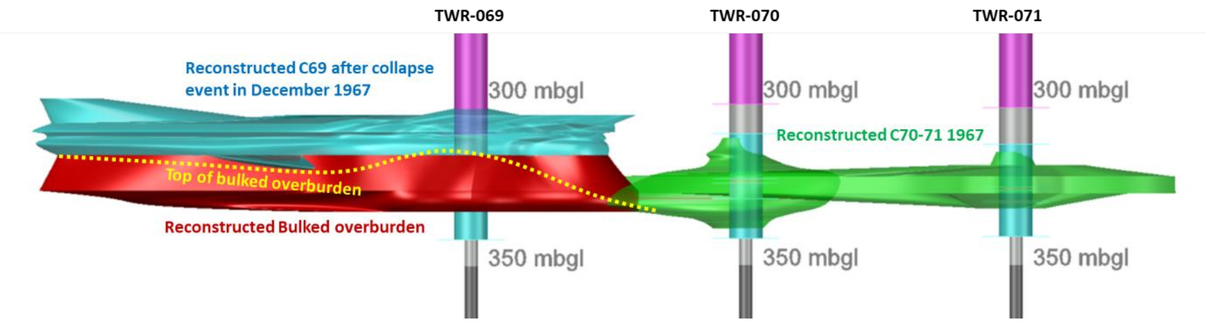

Figure 65: C69-70-71 Situation after 1st collapse event in December 1967.

The C69 part of the C69-70-71 cavern system has a volume of approximately 144.000 m³ before collapse in December 1967. Reconstruction of the 1970 sonar volume (primary reflection) shows that C69 has a volume of approximately 122.000 m³ after the collapse. The calculated bulking factor based on the reconstructed volumes and their position in the stratigraphy is approximately 1,25.

Production from the cavern system is continued after the collapse event in C69 by leaching Salt C in C70-71 between 1967 and 1970. In 1970 a total of 333.827 m³ cavern volume was developed, i.e. the "production volume". This resulted in a net cavern volume of approximately 310.000 m³ after subtraction of insolubles and claystone bench material in the cavern sump. It is assumed that all volume development between 1967 and 1970 was from Salt C in C70-71 as C69 was positioned in the Röt Claystone in that period. The situation in 1970 is presented in Figure 66 below.

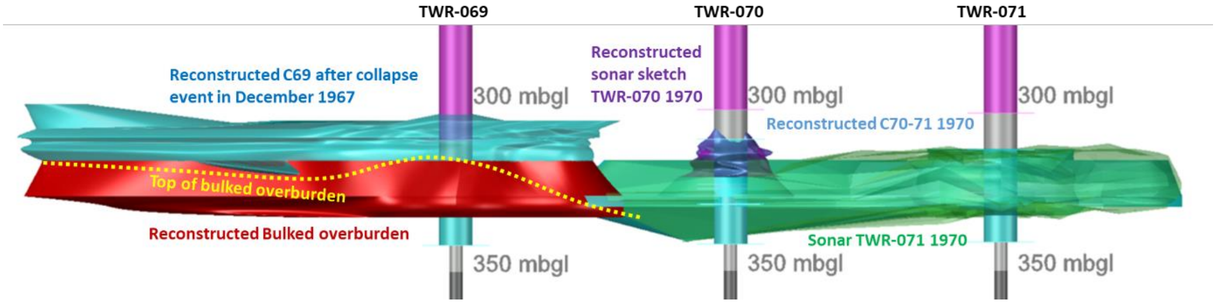

Figure 66: C69-70-71 Situation after leaching between 1967 and 1970: all additional volume by leaching in C70-71.

During the next year (1970) the water injection well was most likely TWR-070, as the roof of TWR-071 was located at the top of Salt C or above. According to the production records 18.678 m³ cavern volume developed in this period bringing the total production volume to 352.505 m³ by the end of 1970.

In February of 1972 backfilling of the migrating C69 was initiated with slurry injection at TWR-069 according to [10]. Between 1972 and 1976 a total of 717.465 m³ slurry was pumped to C69. Using the Slurry/Backfill ratio of 5, this amounts to 143.493 m³ of insitu backfill before SWC.

The residual cavern volume of C69, before backfilling, is ~122.000 m³. As such, it can be assumed that part of the backfill has flowed into the pore space of the bulked overburden, similar to C64-65 in the previous paragraph. The amount of backfill that flowed into the pore space is unknown and consequently only an approximation of the residual cavern space at C69 after backfilling can be established.

Considering the geometry of C69, i.e. migrated into the Röt Claystone, it seems unlikely that further volume development in C69 took place during backfilling in case the slurry was undersaturated. The production data does record salt production indicating that the slurry was indeed slightly undersaturated. A total of 15.876 m³ cavern volume developed in this period bringing the total production volume to 368.381 m³ by the end of 1976. The additional volume is assumed to be developed around well TWR-070 as this was the brine production well and Salt C and Salt D were present here. The approximate situation at the end of the backfilling period is presented in Figure 67.

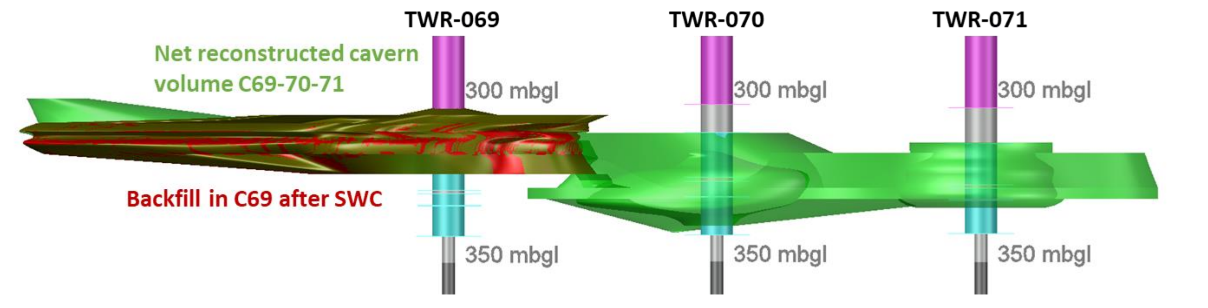

Figure 67: C69-70-71: Approximate situation after leaching between 1970 and 1971 and backfilling of C69 between 1972 and 1976: all additional volume by leaching around well TWR-070.

The roof of the reconstructed cavern volume around well TWR-070 in 1976 as shown in this figure is positioned at the top of Salt C. This position cannot be confirmed, and the actual roof position may have been higher in the stratigraphy, for example just underneath the Anhydrite-E.

The situation in 1977 is documented by a partial sonar image of a (residual) cavern at well TWR-070 positioned in the Röt Claystone thus indicating (further) migration of the cavern. The sonar measurement was only performed in four directions through which the digital representation only captures parts of the actual cavern in 1977. An approximation of the actual cavern volume around well TWR-070 in 1977 was therefore prepared in AutoCAD. The estimated volume of the residual cavern is approximately 45.000 m³ based on this reconstruction. The 1977 situation is presented in Figure 68.

The information on the actual volume and contour area of the residual cavern at TWR-070 in 1977 is deemed too limited for use in the reconstruction of the migration column. The reconstructed volume shown in Figure 68 is unlikely to represent the actual residual cavern during migration of C70-71. As such, it will not be used in the cavern migration reconstruction of C70-71.

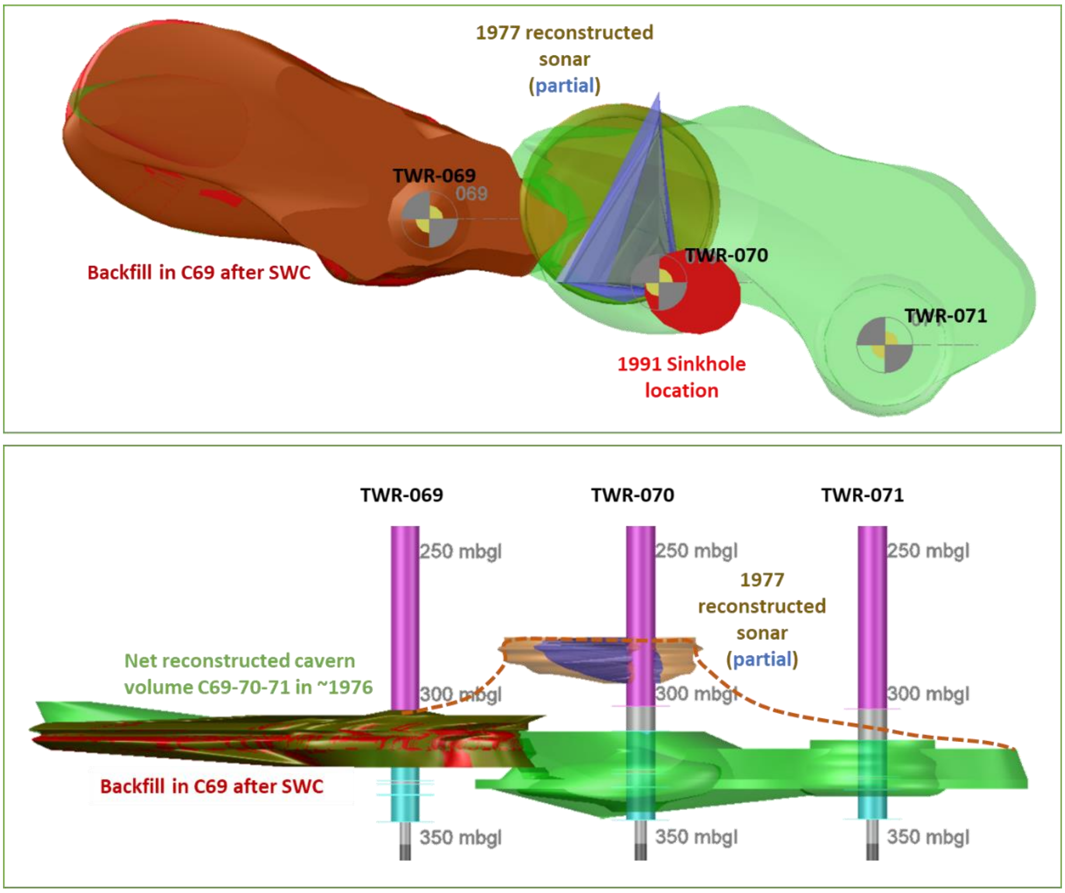

Figure 68 *C69-70-71 Cavern migration 1976-1977: side view (bottom picture) with available sonar image 1977 projected, top view (top picture) with location of 1991 sinkhole projected (red).*

The BJP-Algorithm was used to reconstruct the migration of C69-70-71. The starting point for the algorithm was derived by construction of an approximate intersection of the 1976 cavern with the bottom of the Anhydrite-E member. This intersection represents the cavern roof before migration started and has a surface area of approximately 11.400 m². This contour is shown in Figure 69 as a red line. The representative volume of the cavern was constructed using the 11.400 m² area as a measure for the migration column diameter. This area corresponds to a circle with a radius of 60 m. The representative volume was subsequently aligned with the centre of the 1991 sinkhole as shown in Figure 69.

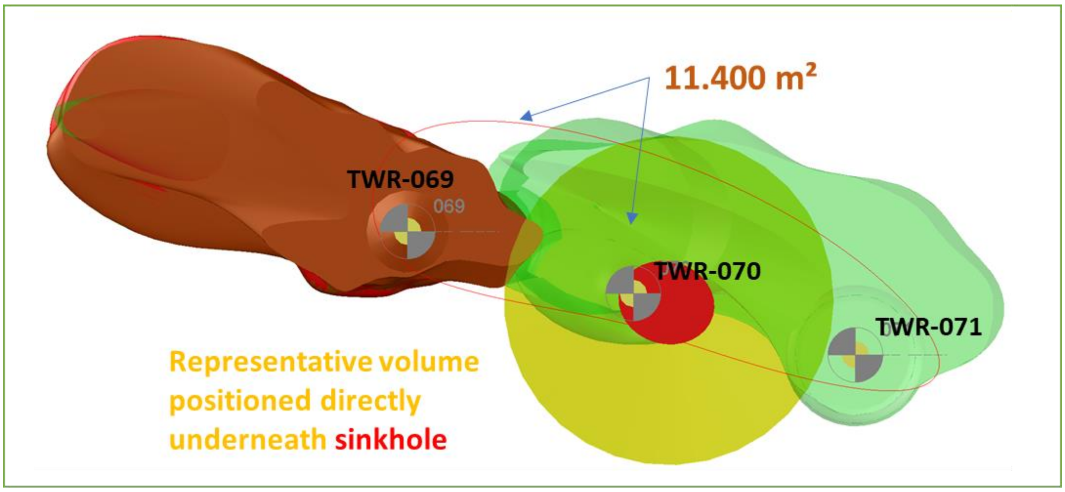

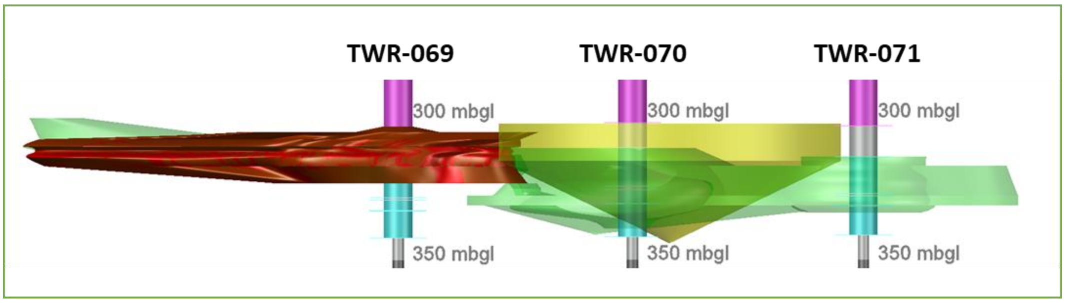

Figure 69: C69-70-71: Reconstruction of „Representative volume" (yellow), reconstructed cavern volumes shown in green. Intersection with Anhydrite-E marked as a red ellipse. Backfill in C69 shown as red shading.

As the subsidence resulting from the migration of C69-70-71 is known, the BJP-Algorithm was used to iteratively find the best fitting shape of the representative volume using 69% of the production volume. This volume has been established on the basis of the total production volume minus the insolubles (6%) and minus the backfill volume after SWC in C69 (25%). As the likely migration contour of C70-71 that caused the sinkhole did not load the backfill in C69 with bulked overburden, consolidation of this backfill is excluded in the calculation of the migration column.

The input parameters are presented in Table 32. The representative volume of C70-71 comprises a cone-shaped sump with a 60 m radius and 26 m height and a cylinder with 60 m radius and 14 m height. No backfill has been applied in this representative volume as discussed prior.

Table 32 *C69-70-71 cavern specific input parameters*

Cavern	69
Relevant borehole	70
Z coordinate GL (mNAP)	22,2
Depth of top rock [mbGL]	118,5
Depth of top salt [mbGL]	310,8
Base of actual cavern [mbGL]	342,2
Base of initial cavern [mbGL]	341,9
Top of actual cavern [mbGL]	302,2
Height of cavern (m)	40,0
X coordinate migration centre	252353,0
Y coordinate migration centre	473613,0
Volume fitting	
Maximum BPB Prod.(t)	658000
Cavern vol based on BPB (m³)	**369796**
Actual volume (recon./sonar)(m³)	346648
Insolubles (bulked) (m³)	19512
Part of BPB prod. Vol. not acc. (m³)	23148
Part of BPB prod. Vol. not acc. (%)	**6%**
Cavern geometry conversion	
Migration column Surface area (m²)	11400
Constructed cavern radius [m]	60,0
Hydraulic Radius constructed cav. [m]	30,0
Const. cavern height (cylindrical) [m]	14,0
Const. cavern height (conical) [m]	26,0
Constructed volume (cylindrical) [m³]	158336
Constructed volume (conical) [m³]	98018
Constructed volume total [m³]	256354
Part of BPB prod. Vol. not acc. (m³)	113442
Part of BPB prod. Vol. not acc. (%)	**31%**
Height correction backfill insitu [m]	0
Backfill insitu unconsolidated (m³)	0
Backfill consolidation (%)	0

The output of the algorithm for these input parameters is shown in Figure 70 below. The calculated migration column reached the Tertiary and thus causes Stage 4 – Sinkhole subsidence.

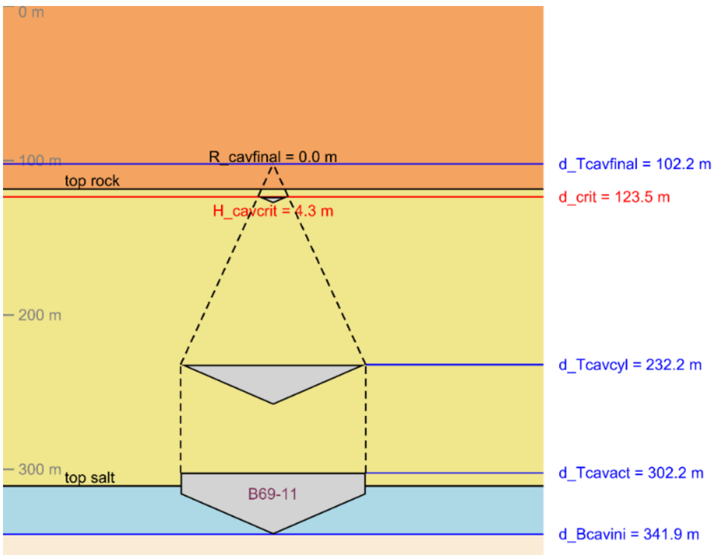

Figure 70: *C70-71: calculated migration column best fitting to the measured subsidence (Stage 4 – Sinkhole)*

To illustrate the fitting of the calculated subsidence with the actual subsidence, first a comparison of calculated and measured Stage 2 and Stage 3 subsidence development is presented in Figure 71. A detailed view of the Stage 2 development is included in the right picture in this figure. The detailed view shows that the Stage 2 subsidence development went in several "steps" between 1975 and 1990.

These steps are likely caused by the migration being temporarily halted by more relatively competent overburden layers in the stratigraphy.

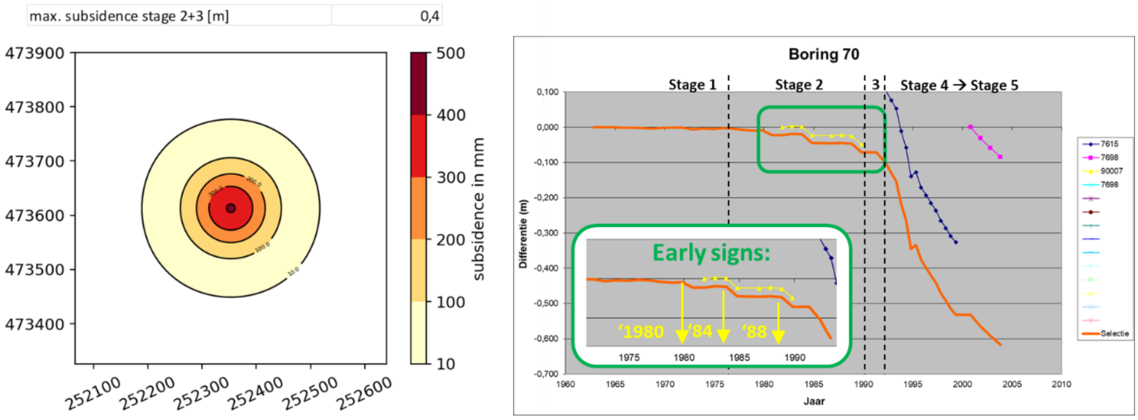

Figure 71 *C70-71: Stage 2+3 subsidence contours as calculated by the BJP-Algorithm (l) and measured subsidence (r). A detail of the Stage 2 subsidence is shown in the green box titled "Early signs" (for Stage 4 subsidence).*

The calculated Stage 2+3 subsidence is 40 cm as shown in the left picture in Figure 71. This value is not reached in the measured values during the Stage 2 period (1975-1990). This can be explained by considering that the measured subsidence is based on yearly measurements and thus not captured the contours shown in the left picture of Figure 71. The levelling measurement point used to measure subsidence near well TWR-070 was most likely destroyed by the sinkhole and a new point (presumably at some distance from the sinkhole) was erected to continue subsidence monitoring, this is illustrated by the blue series (7815) in the right picture of Figure 71.

A comparison of the calculated and observed Stage 4 subsidence is shown in Figure 72 below. As can be seen in this figure, both the depth of the observed sinkhole, approximately 3,5 m and its diameter, approximately 25 m, were accurately matched by the calculated Stage 4 subsidence contours.

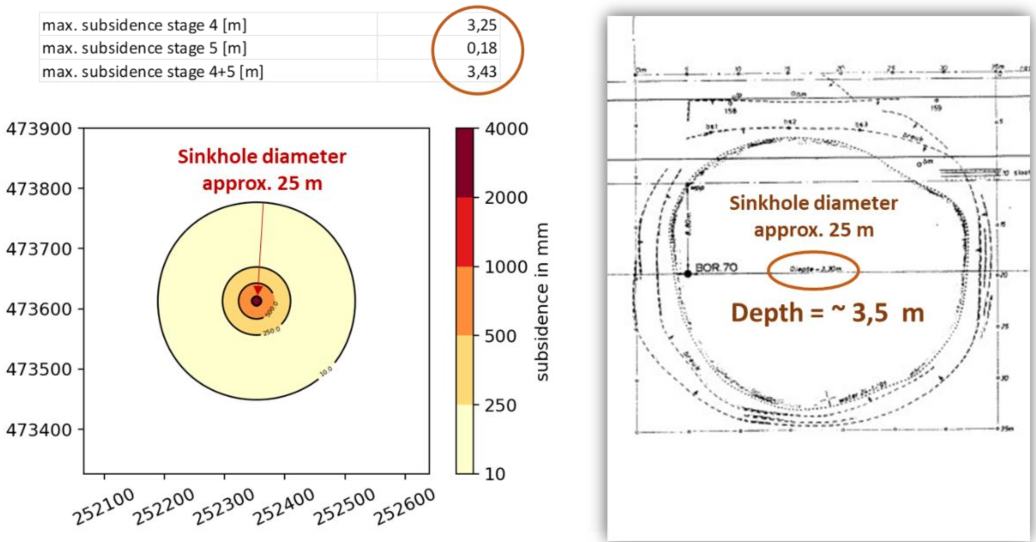

Figure 72: *C70-71: Stage 4 – Sinkhole subsidence contours as calculated by the BJP-Algorithm (l) and observed sinkhole dimensions (r) as included in BIJLAGE I of [12].*

More than ten (10) scenarios with varying cavern shapes and dimensions were tested during the reconstruction workflow for C69-70-71. Alternative scenarios using only a cylinder-shaped cavern could not explain the formation of Stage 4 subsidence as the migration column in this scenario does not reach the critical depth causing Stage 4 subsidence. As such this scenario was rejected. Even when applying a lower bulking factor, such as the historically used value of 1,11, a cylinder-shaped cavern representation of C69-70-71 will not lead to the observed sinkhole formation.

This exercise shows that the presented representative cavern shape is the singular geometry that can lead to the observed subsidence. As such, this confirms that the applied “shape simplification”, from an irregular shaped cavern (based on sonar images) to a representative volume comprising a cylinder and cone, is justified and can be applied in the algorithm for the TWR area.

In conclusion, a plausible reconstruction of the C69-70-71 migration case has been enabled by the application of the BJP-Algorithm. The chosen bulking factor of 1,2 and a combined cone-cylinder-shaped cavern geometry can emulate the observed migration case with confidence. This example thus further underlines the importance of considering a cone-shaped cavern bottom where relevant.

4.3. Reconstruction C72-75-76-77

Cavern 72-75-76-77 (C72-75-76-77) is a multi-completion cavern (MCC) comprising wells TWR-072, TWR-075, TWR-076 and TWR-077. The key data for this cavern are included in Table 33 below and additional information can be found in APPENDIX I.

Table 33: Key data C72-75-76-77

Wells*	X (WGS84)	Y (WGS84)	Z (mNAP)	Final depth (mbgl)	Final depth (mNAP)	Well ready	Start production	End production	Cemented
72	252180,8	473360,8	21,48	360,85	-339,37	17-8-1962	21-12-1962	2-1-2002	
75	252426,2	473324,0	22,2	350	-327,83	2-5-1962	5-8-1962	2-1-2002	
76	252522,1	473331,7	22,2	353	-330,79	5-8-1962	5-8-1962	2-1-2002	
77	252586,1	473395,8	23,0	351,03	-328,03	5-7-1962	5-8-1962	16-6-1982	2-5-1983
* forced hydraulic connections between January 1962 and March 1963 according to well diaries and production data									

As with C63-64-65 and C69-70-71, the development of C72-75-76-77 cannot be reconstructed using the generalised workflow for sump reconstruction due to the (attempted) performance of forced leaching. Several operations attempted a forced connection between wells TWR-072, TWR-073, TWR-074, TWR-075, TWR-076 and TWR-077 between January of 1962 and March of 1963. The well diaries allowed reconstruction of the following list of forced leaching operations and their outcome:

1. Jan. 1962 - Pump at TWR-072, connection to TWR-073 failed, continued pumping until connection to TWR-075 was established on 21 Dec. 1962. Salt production from MCC 72-75 was then initiated according to the production records[3].
2. 14 Feb. 1962 – Pump at TWR-073, connection to TWR-072 failed but connection to TWR-074 was established on 28 Feb. 1962. Salt production from MCC 73-74 was started in Mar. 1962.
3. Jan. 1963 - pump at TWR-076, connection to TWR-075 and TWR-077 in Mar. 1963. Salt production from MCC 72-75-76-77 commenced directly after.

[3] The production records state that wells TWR-072 and TWR-077 were connected on 21-12-1962. This is a likely error caused by a typo in the “klad” diary of well TWR-072. In this diary a connection from TWR-072 to TWR-077 is written, however a connection to TWR-075 is meant as deducted from the text.

A graphical representation of the outcome of these operations is projected on the cavern map in Figure 73.

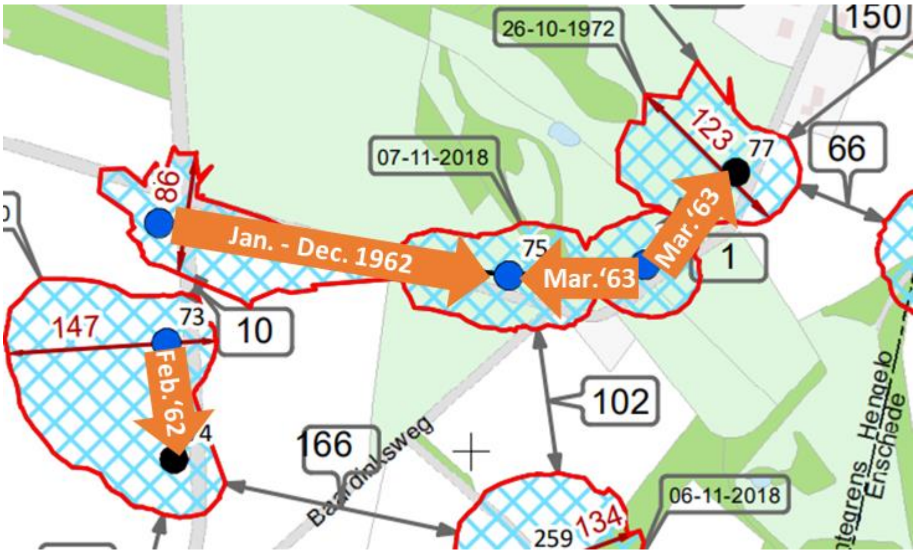

Figure 73: Forced leaching operation around C72-75-76-77 between Jan. 1962 and Mar. 1963

It becomes clear from this figure that the forced connection between wells TWR-072 and TWR-075 was unplanned. After failing to reach TWR-073, pumping at well TWR-072 was continued for nearly a year until in December a connection to TWR-075 was established. Considering the relative distance between these wells, the chain of events is remarkable. A possible explanation for the unplanned connection can be found considering the presence of offsets in the stratigraphy in the area. Figure 74 presents a cut-out of the Depth Map of the Top RNSO (Solingen Formation), i.e. the Bottom of the Salt A member, and shows the identified offsets as red lines.

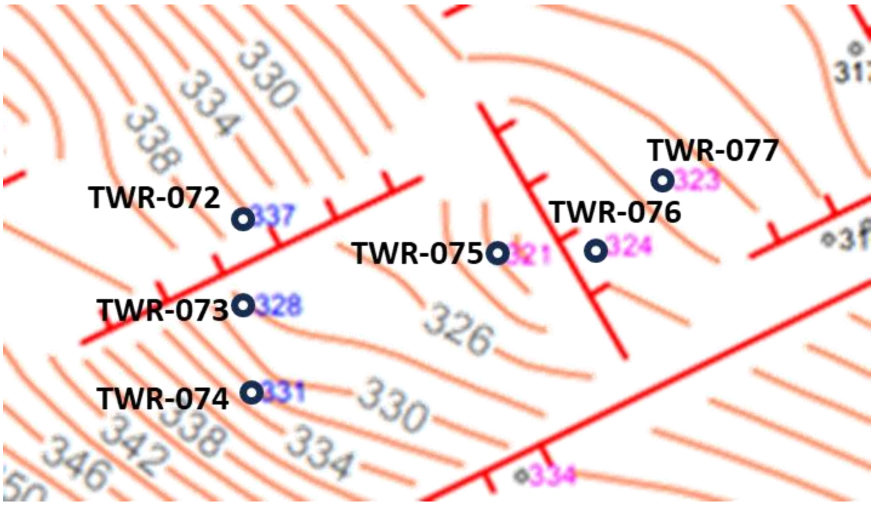

Figure 74: C72-75-76-77 area: Detailed view from Depth Top Solingen Formation Map with offsets indicated as red lines, adapted from Attachment C to [13]

These offsets can be interpreted as faults in the Solingen formation. These faults do not propagate through the salt members, but the offset in the base of the salt members will have cause salt flow (due to salt creep) on a geological time scale. The salt flow has either thinned-out or thickened salt layers thereby causing “misalignment” of the salt members and intermediate claystone benches. As can be seen from this figure, a 10 m offset has been identified between wells TWR-072 and TWR-073. Another smaller offset is present between wells TWR-075 and TWR-076.

The misalignment of the salt members between wells may have acted as a barrier for the development of a "forced leaching contour" (FLC) in some cases, which resulted in the described chain of events. This hypothesis is further supported by a sketch from a 1968 sonar report by Prakla as presented in Figure 75 below.

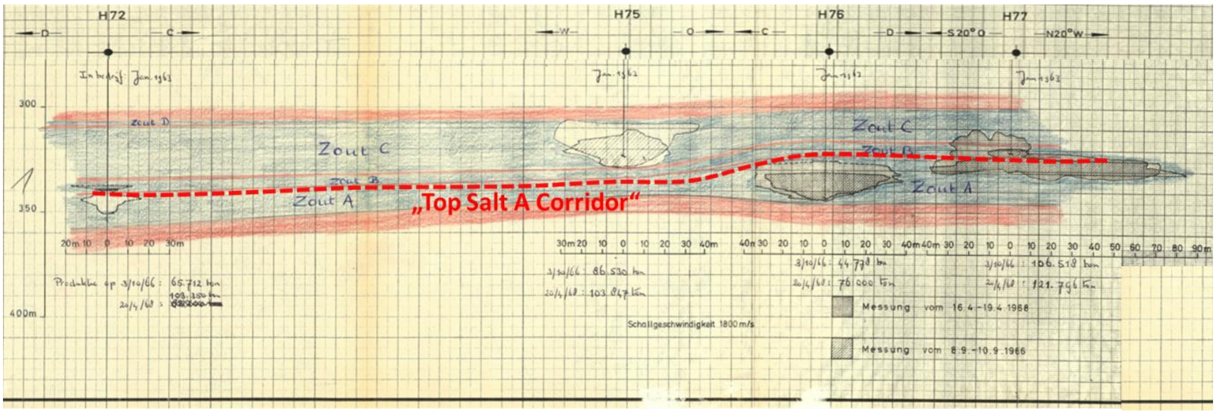

Figure 75: C72-75-76-77: Cross section from well TWR-72 to TWR-077 showing possible position of "Top Salt A Corridor" connecting the wells after forced leaching, adapted from Attachment to [14].

The sketch shows the 1966 and 1968 sonar images projected onto an interpretation of the salt member including intermediate claystone benches. The thickness of Salt A significantly increases from well TWR-075 towards TWR-076. This corresponds to the previously described offset between these wells. Not shown, but likely of similar appearance, would have been the situation between wells TWR-072 and TWR-073 thus possibly acting as a barrier for a FLC.

The chain of events and the later development of the cavern system C72-75-76-77 leads to the assumption that a FLC was present underneath the Claystone AB bench in the top of Salt A. This "Top Salt A Corridor" is shown in the figure as a red dashed line. The position of the Claystone AB dictated the relative depth at which the FLC intersected with the respective wells in the cavern system. Consequently, initial cavern volume was developed in either Salt A (C72, C76 and C77) or Salt C (C75) causing a very complex overall cavern system development.

The (expected) complexity of the cavern development was already recognised by the operator at the start of salt production from this cavern system as the monthly water volumes injected per well were recorded in the well diaries. This was not a standard practice for other multi-completion-caverns in the TWR area at that time. Apart from the recording of monthly volumes, the sketch shown in Figure 75 includes salt production figures per cavern in 1966 and 1968. These notes and the monthly volumes enabled reconstruction of the volume development and an approximate reconstruction of the spatial distribution of said cavern volume development for C72-75-76-77.

The reconstruction process of the cavern of C72-75-76-77 started with the reconstruction of sonar images for which only 2-D sketches were available, and the correction of some digital sonar images by rotation around the well as was explained in the previous paragraph. The performed reconstructions and corrections have not been detailed in this report to aid legibility, their outcome is applied in the relevant figures in this paragraph.

The first snapshot of the cavern development that could be reconstructed, is the situation in 1968 after performance of sonar measurements in all four wells of the system. This snapshot has been reconstructed on the basis of sonar images from 1966 and 1968. A comparison of the sonar volumes and the corresponding salt production figures noted in this figure is provided by Table 34 below.

Table 34: C72-75-76-77 Cavern volume development 1963-1968 based on production records and sonar images from 1966 and 1968.

	Well	72	75	76	77	Totals
3-10-1966	Production (t)	65.712	86.530	44.778	106.518	303.538
	Production. Vol. (m³)	36.922	48.619	25.160	59.850	170.552
	Sonar Volume (m³)	1.430	10.230	16.970	25.670	54.300
20-4-1968	Production (t)	103.350	103.847	76.000	121.796	404.993
	Production. Vol. (m³)	58.070	58.349	42.703	68.435	227.557
	Sonar Volume (m³)	--	27.220	33.900	61.040	122.160

The total sonar volume of the cavern systems in 1966 and 1968 is significantly less than the corresponding production volumes based on tonnage salt produced. The difference is:

227.557 – 122.160 = 105.397 m³

The difference is much larger than can be explained by the collection of insolubles and claystone bench material alone. As such, the difference points towards the presence of cavern volume which could not be captured by the sonar measurements performed. The most likely position of this unaccounted volume is along the "Top Salt A Corridor", first developed by forced leaching in 1962 and 1963. Water injected into well TWR-072 during these years preferably flowed "uphill" towards TWR-075 and TWR-076 leaching cavern volume along the corridor underneath the Claystone AB bench and was invisible for sonar.

The next snapshot captures the situation in 1972 and is illustrated in Figure 76 below.

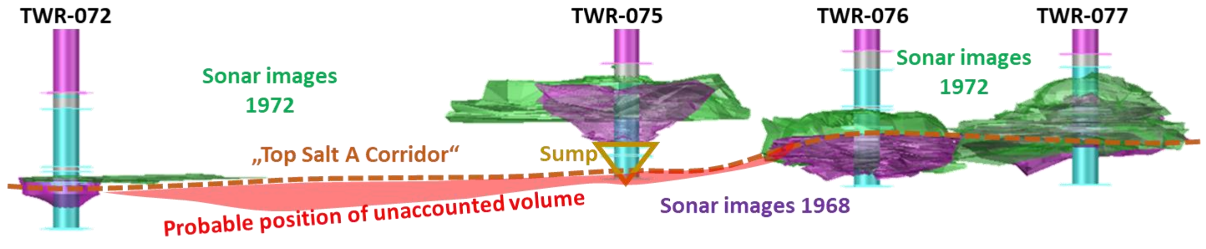

Figure 76: C72-75-76-77: side view of cavern system in 1972 showing possible position of "Top Salt A Corridor" and the probable position of unaccounted volume in Salt A between wells TWR-072 and TWR-076.

As can be seen from this figure, cavern volume development according to the 1972 sonar images is clearly visible at C75, C76 and C77. At well TWR-072 however the sonar image only comprises a very shallow slit pointed towards C75. This slit was likely the entrance to the Top Salt A Corridor cavern volume, indicated by the red shape in this figure. The cavern volumes of the situation shown in Figure 76 and compared to the corresponding production volumes are presented in Table 35.

Table 35: C72-75-76-77 Cavern volume development 1963-1972 based on production records and sonar images from 1966, 1968 and 1972.

	Well	72	75	76	77	Totals
31-10-1972	Production (t)	301.491	125.621	132.272	179.564	738.948
	Production. Vol. (m^3)	169.401	70.584	74.321	100.893	**415.199**
	sonar (m^3)	4410	63.200	66.470	90.480	**224.560**

The total sonar volume of the cavern system in 1972 is still significantly less than the corresponding production volume based on tonnage salt produced. The difference in 1972 is:

415.199 – 224.560 = 190.639 m^3

The difference is partly explained by the unaccounted volume along the “Top Salt A Corridor” and partly by a likely sonar shadow in the 1972 measurement at TWR-072. The 190.639 m^3 is thus not fully assigned to the Top Salt A Corridor volume as will be clear after the next snapshot.

The third snapshot in the development of C72-75-76-77 is the situation in 1976. Although sonar measurements were performed in this year, digital files of these measurements are not available. Fortunately, 2D sketches of these measurements in two directions (N-S and E-W) were recovered from the archives, which enabled their approximate reconstruction in AutoCAD. The reconstructed sonar images are presented in Figure 77. Cavern volume development between 1972 and 1976 was primarily in Salt C between wells TWR-072 and TWR-75 as can be seen from this figure. The upward development of C72 in Salt C is linked to (partial) collapse of the Claystone AB bench between 1972 and 1976.

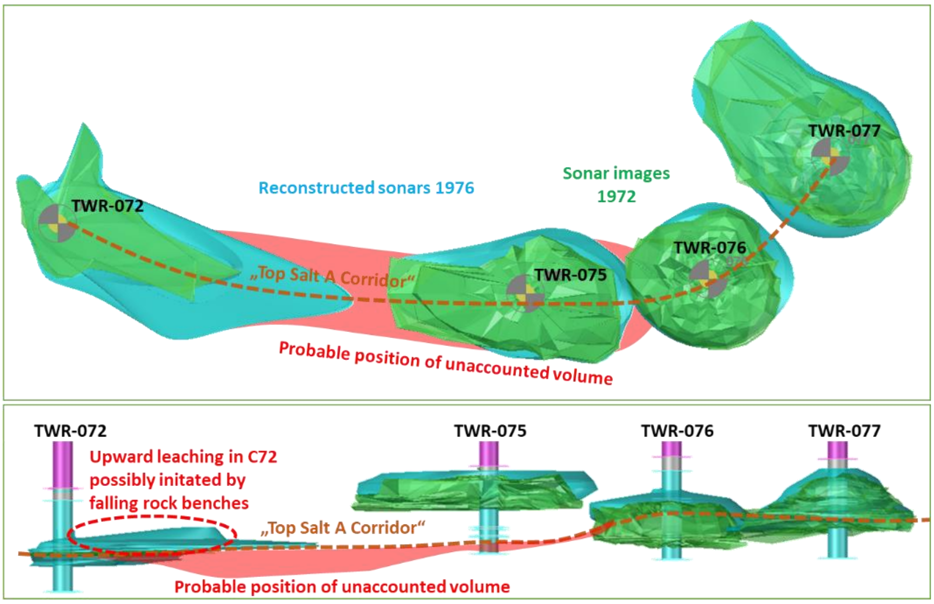

Figure 77: C72-75-76-77: situation in 1976, top view (top picture) and side view (bottom picture). 1976 reconstructed sonar volume in blue, probable position of unaccounted volume in red.

An estimate of the volume of the Top Salt A Corridor volume can be derived from the situation at C72 in 1976 as is presented in Table 36. The production volume for C72 in 1976 is 218.448 m^3. After subtracting insolubles and claystone bench material, 199.391 m^3 of net cavern volume remains. The reconstructed sonar has a volume of 63.439 m^3 which brings the unaccounted volume to 135.952 m^3, most of which is assumed to be located in the Top Salt A Corridor.

Table 36: C72-75-76-77 Cavern volume development 1963-1976 based on production records and sonar images from 1966, 1968 and 1972 as well as reconstructed sonar images from 1976.

	Well	72	75	76	77	Totals
1-10-1976	Production (t)	388.853	191.407	141.232	207.667	929.160
	Production. Vol. (m³)	218.488	107.548	79.355	116.684	522.075
	Isol. Vol. (m³)	19.097	9.400	6.936	10.199	45.632
	Net Vol. (m³)	199.391	98.147	72.419	106.485	476.443
	Reconstructed Sonar Vol. (m³)	63439	96.336	71.185	104.645	335.605
FLC Vol. 1976 = Tot. Prod. Vol. - Recon. Son. Vol. (m³)		135.952	Total Prod. Vol. 1976 (m³)			522.075

After the sonar measurements in the cavern system in 1976, backfilling was initiated. Two main sources are available which state the slurry volumes injected into C72-75-76-77 between 1976 and 2001. The first source is [10], the second source is an excel file prepared by Nobian based on the data in the production database [15]. To compile this file, the brine production data for the wells between 1991 and 2001 was used as a measure for the total slurry volume.

These sources only mention total slurry volumes per year, contain however no information on the actual wells used for injection of slurry and production of brine. This information was retrieved from a hand-drawn table titled "Slurryberging Stromingstabel" which recorded the in- and outgoing media for all operational wells in the TWR area between 1975 and 1998 [16]. This table allowed an approximate reconstruction of the backfilling operation at C72-75-76-77. The backfilling period 1976-2001 can be divided into four phases as shown in Figure 78.

	PHASE 1								PHASE 2						PHASE 3			PHASE 4								
	1976	1977	1978	1979	1980	1981	1982	1983	1984	1985	1986	1987	1988	1989	1990	1991	1992	1993	1994	1995	1996	1997	1998	1999	2000	2001
TWR-072	B	B	B	B	B	B	B	B	W	W	H	W	W	W	B	H	B	S	H	H	H	S	S	S	S	S
TWR-075	B	B	B	B	B	B	B	B	B	B	H	B	B	B	S	H	S	B	H	H	H	B	B	B	B	B
TWR-076	S	B	S	B	S	B	S	S	H	S	H	H	H	H	F	F	F	F	F	F	F	F	F	F	F	F
TWR-077	B	S	B	S	H	S	F	C	C	C	C	C	C	C	C	C	C	C	C	C	C	C	C	C	C	C

Legend	B Brine production	W Water injection	C Cemented
	S Slurry injection	H On Hold	F Fully backfilled

Figure 78: C72-75-76-77: Input-Output per well of the cavern system by year, adapted from [16].

The input and output media shown in this figure are summarized per year. This means that only the dominantly used medium per year was included which leaves out some detail. A more detailed version showing the input and output on a monthly basis is thus provided in APPENDIX II for reference.

The leaching by water input and slurry filling during Phase 2 was detailed in another handwritten memo with slurry and water volumes specified separately [17]. The information in this memo enabled the reconstruction of a fourth snapshot in the development of C72-75-76-77, capturing the situation in early 1990. A total of 145.428 m³ of additional cavern volume was leached in the cavern between 1976 and January 1990, i.e. 667.503 m³ production volume in Jan. 1990 (see Table 37) minus 522.075 m³ in 1976 (see Table 36). It is assumed that all volume by water leaching has developed at the top of C72 and not in the FLC. The volume of the FLC is noted separately from the caverns in Table 37 as the FLC is assumed not leached after 1976. An estimated volume of insolubles and claystone material was subtracted from the production volume to attain the net cavern volume available for backfill per well in the cavern system.

Table 37 C72-75-76-77: Cavern volume development 1976-Jan.1990 based on production records.

	Well	72	75	76	77	FLC	Totals
January 1990	Production (t)	382.543	191.407	141.232	207.667	265.135	1.187.984
	Production. Vol. (m³)	214.943	107.548	79.355	116.684	148.973	667.503
	Isol. Vol. (m³)	18.787	9.400	6.936	10.199	6.651	51.974
	Net Vol. (m³)	196.155	98.147	72.419	106.485	135.952	615.529

The slurry pumped to the cavern system was undersaturated as the recording of salt production after 1990, when only slurry was pumped to the cavern, continued. The saturation of the slurry was estimated by comparing the salt production between 1990 and 1998 with the total volume of slurry in this period. The estimated saturation of the slurry is 235 g/l NaCl, assuming a brine saturation of 312 g/l NaCl in the calculation of the slurry saturation. The 235 g/l slurry saturation was subsequently applied to the reconstruction of all backfilling operations at C72-75-76-77 to establish the additional cavern volume leached by slurry. The additional leached volumes and the resulting final cavern volumes are presented in Table 38.

Table 38: C72-75-76-77: Additional volume development due to undersaturated slurry (235 g/l NaCl)

Well	72	75	76	77	FLC	Totals
Production volume (m³)	214.943	107.548	79.355	116.684	148.973	**615.529**
Additional volume by undersaturated slurry (m³)	72.033	4.104	28.974	28.498	0	**133.609**
Final production volume (m³)	286.976	111.651	108.329	145.182	148.973	**652.138**
Estimated insol. Vol. (m³)	12.813	4.985	4.837	6.482	6.651	**29.116**
Final Net volume (m³)	274.163	106.667	103.493	138.700	135.952	**623.023**
Final production tonnage per cavern (t)	*382.543*	*191.407*	*141.232*	*207.667*	*265.135*	*1.187.984*

A comparison of the slurry volumes from [10], [15] and [17] shows that the relevant slurry volumes in all sources are in correspondence with each other. As such, careful combination of all available information on individual cavern volumes, the unaccounted volume in the Top Salt A corridor and the slurry volumes, enabled an approximate volume reconstruction of the total backfilling period. This reconstruction is summarized in the following per phase as shown in Figure 78.

Phase 1 1976-1983

Table 39 below summarizes the backfill operation at of C72-75-76-77 between 1976 and 1983.

Table 39: C72-75-76-77 Phase 1 backfilling between 1976 and 1983

		Well 72	Well 75	Well 76	Well 77	FLC	Totals	Dim.
	1976 Available cavern volume (Reconstructed - **NO FILL**)	63.439	96.336	71.185	104.645	135.952	335.605	m³
	1976 Cavern volume available for Fill	63.439	96.336	71.185	104.645	40.786	376.391	m³
						30%		
Filling Phase 1 1976-1983	Fill months until 1983	1	-	32	48		81	
	1976-1983 Add. Volume by slurry fill	594	-	18.999	28.498		48.090	m³
	1983 Reconstructed cavern volume	64.033	96.336	90.184	133.143	40.786	383.695	m³
	Fill/Slurry Ratio	**5,00**	**5,00**	**5,00**	**5,00**			
	1976-1983 Initial Insitu Fill Volume	3.100	-	58.427	148.818	40.786	210.345	m³
	1983 remain. cavern volume after slurry fill NO CONS.	60.932		72.543	- 15.675			
	1983 Filling grade without consolidation	0	-	1	1			
	Consolidation of slurry under self weight	15%	0%	15%	15%	15%		
	1983 Insitu Fill Volume after SW CONS.	2.635	-	49.663	126.496	34.668	178.794	m³
	1983 Remain. volume after slurry fill SW CONS.	**61.397**	**96.336**	**40.521**	**6.647**			m³
	1983 Filling grade with self weight consolidation applied	**4%**	**0%**	**45%**	**95%**			
	1983 Cavern volume available for Fill	61.397	96.336	40.521			198.254	m³

The cavern volume in 1976 available for backfill is noted at the top of Table 39, these values correspond to the net cavern volume as stated in Table 36. To establish the slurry volume per cavern, the total slurry volume of 1.255.655 m³ was divided by the total number of months (81) that slurry was pumped to C72-75-76-77 according to the "Slurryberging Stromingstabel". This established an average monthly slurry volume of 15.502 m³. Using this average value, the total volume of slurry was distributed over wells TWR-072, TWR-076 and TWR-077 as stated in the table.

It became clear during the reconstruction of the backfill operation that the slurry volume pumped to the cavern system was too large for the available cavern volume. This led to the following two-part hypothesis:

- Some of the backfill drained into the Top Salt A Corridor from both sides during the backfilling operation between 1976 and 2001. The total unaccounted volume is assumed to be backfilled.
- The slurry was undersaturated in relation to Sodium Chloride and thus caused additional cavern volume to develop by leaching (see Table 38).

The hypothesis was iteratively tested until a plausible scenario for backfill drainage to the Top Salt A Corridor was found. The plausible scenario is stated in Table 39: 30% of the corridor is backfilled from TWR-076. Based on the total slurry volume in Phase 1, a total of 48.090 m³ additional cavern volume was created during backfilling between 1976 and 1983. This additional volume formed most likely at the top of caverns C76 and C77. The described situation is illustrated by Figure 79 which also shows (reconstructed) sonar images from 1980 that confirm additional volume at C76 and C77 in the roof section.

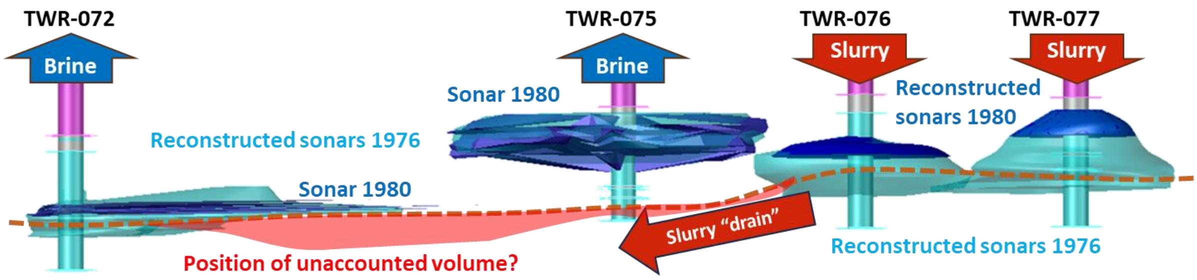

Figure 79: C72-75-76-77 Backfilling Phase 1 - 1976-1983.

After utilisation of 30% of the Top Salt A Corridor volume and application of 15% SWC, the final filling grade of C77 is 95% according to the backfill volume reconstruction presented in Table 39. C77 is thus completely filled up in 1982 and the well was abandoned in May 1983, see Table 33.

Phase 2 1984-Jan.1990

Table 40 below summarizes the backfill operation at of C72-75-76-77 between 1984 and January 1990.

Table 40: C72-75-76-77 Phase 2 backfilling between 1984 and Jan. 1990

		Well 72	Well 75	Well 76	Well 77	FLC	Totals	Dim.
	1983 Cavern volume available for Fill	61.397	96.336	40.521			198.254	m³
Filling Phase 2 1984-Jan.1990	1984-Jan.1990 Add. Volume by slurry fill	-	-	9.975			9.975	m³
	Jan.1990 Reconstructed cavern volume	61.397	96.336	50.496			208.230	m³
	1983-Jan.1990 Initial Insitu Fill Volume	-	-	52.090			52.090	m³
	Jan.1990 remain. cavern volume after slurry fill NO CONS.	61.397	96.336	- 1.594				m³
	Jan.1990 Filling grade without consolidation	0%	0%	103%				
	Consolidation of slurry under self weight	0%	0%	15%				
	Insitu Fill Volume after SW CONS.	-	-	44.277			44.277	m³
	Jan.1990 remain. volume after slurry fill SW CONS.	61.397	96.336	6.219				m³
	Filling grade with self weight consolidation	4%	0%	94%				
	1983-Jan.1990 Add. Volume by Water Leaching at B72	145.428						

Backfilling at TWR-076 continued in Phase 2 until it was “full” as confirmed by a sonar image from 17 January 1986. After application of 15% SWC, the final filling grade of C76 is 94% according to the backfill volume reconstruction presented in Table 40. Between the end of 1983 and January 1990, cavern volume developed in C72 due to water leaching at TWR-072 as previously mentioned and stated in Table 40. The situation at the end of Phase 2 is presented in Figure 80. Additional volume at C72 is confirmed by a sonar image from 1989 at well TWR-072.

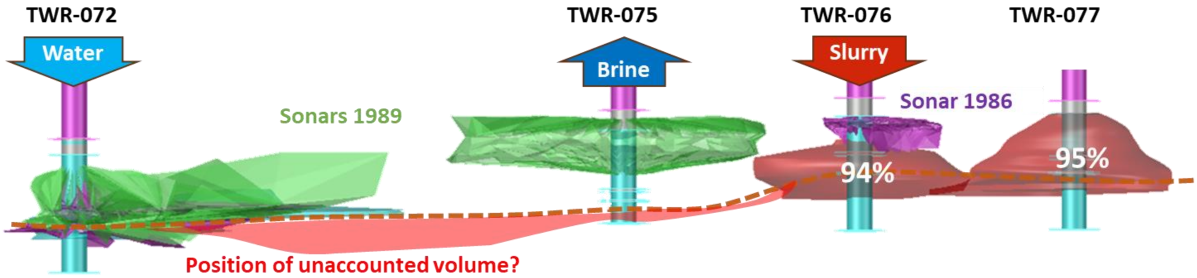

Figure 80: C72-75-76-77 Backfilling Phase 2 - 1984-Jan.1990.

Phase 3 1990-1992

Table 41 below summarizes the backfill operation at of C72-75-76-77 between 1990 and 1992.

Table 41: C72-75-76-77 Phase 3 backfilling between 1990 and 1992

		Well 72	Well 75	Well 76	Well 77	FLC	Totals	Dim.
	Jan.1990 Cavern volume available for Fill	206.825	96.336			13.595	303.161	m^3
						10%		
Filling Phase 3 1990-1992	1990-1992 Add. Volume by slurry fill	-	4.104				4.104	m^3
	1992 Reconstructed cavern volume	206.825	100.440			13.595	307.265	m^3
	1992 Initial Insitu Fill Volume		35.377			13.595	35.377	m^3
	1992 remain. Cavern volume after slurry fill NO CONS.		65.063					m^3
	1992 Filling grade without consolidation		65%					
	Consolidation of slurry under self weight		15%			15%		
	Insitu Fill Volume after SW CONS.	2.635	30.070			11.556	32.705	m^3
	1992 remain. volume after slurry fill SW CONS.	206.825	70.370					m^3
	Filling grade with self weight consolidation	1%	30%					
	1993 Cavern volume available for Fill	206.825	70.370			81.571	358.766	m^3
						60%		

In Phase 3 backfilling started at TWR-075 until it was halted in July 1992 as confirmed by [16]. No slurry has been pumped to TWR-075 since. The volume of the 2018 sonars (~69.000 m^3) was used as a "data anchor" to approximate the volume of slurry that drained to the Top Salt A Corridor. To fit the calculated residual volume to the sonar volume, 10% of the Top Salt A Corridor volume must have been filled by slurry injection at TWR-075. The 1992 remaining cavern volume after subtraction of backfill with 15% SWC is 70.370 m^3 as shown in the table. This value fits well to the sonar volumes. The backfill remaining in the cavern brings the filling grade of C75 to 30%. The situation at the end of Phase 3 is presented in Figure 81.

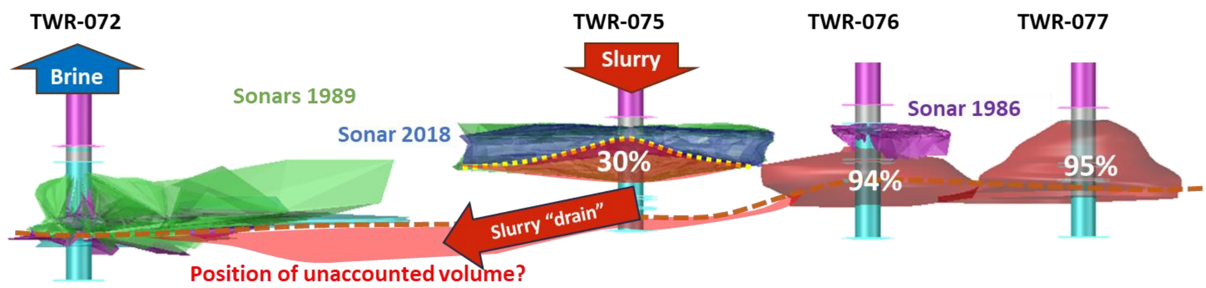

Figure 81: C72-75-76-77 Backfilling Phase 3 - 1991-1992.

Phase 4 1993-2001

Table 42 below summarizes the backfill operation at of C72-75-76-77 between 1993 and 2001.

Table 42: C72-75-76-77 Phase 4 backfilling between 1993 and 2001

		Well 72	Well 75	Well 76	Well 77	FLC	Totals	Dim.
	1993 Cavern volume available for Fill	206.825	70.370			81.571	358.766	m³
						60%		
Filling Phase 4 1993-2001	1993-2001 Add. Volume by slurry fill	71.440	-				71.440	m³
	2001 Reconstructed cavern volume	278.265	70.370			81.571	348.635	m³
	1993-2001 Initial Insitu Fill Volume	291.491	-			81.571	291.491	m³
	2001 remain. volume after slurry fill NO CONS.	- 13.226	70.370					m³
	2001 Filling grade without consolidation	105%						
	Consolidation of slurry under self weight	15%				15%		
	Insitu Fill Volume after SW CONS.	247.767				69.336	247.767	m³
	2001 remain. volume after slurry fill SW CONS.	30.497	70.370					m³
	Filling grade with self weight consolidation	89%	30%					
	2001 Cavern volume available for Fill		70.370				70.370	m³

Backfilling at TWR-072 was initiated in 1993. It is estimated that 71.440 m³ additional cavern volume was leached by the slurry in C72 between 1993 and 2001. In addition to the additional volume, it is also assumed that the remaining 60% of the Top Salt C Corridor was filled from TWR-072 as indicated in Table 42. After subsequent application of 15% SWC, the filling grade of C72 in 2001 is approximately 88% according to the backfill volume reconstruction presented in this table. The filling grade of the Top Salt A Corridor is equal to 1 – SWC = 85%. The situation at the end of Phase 4 is presented in Figure 82.

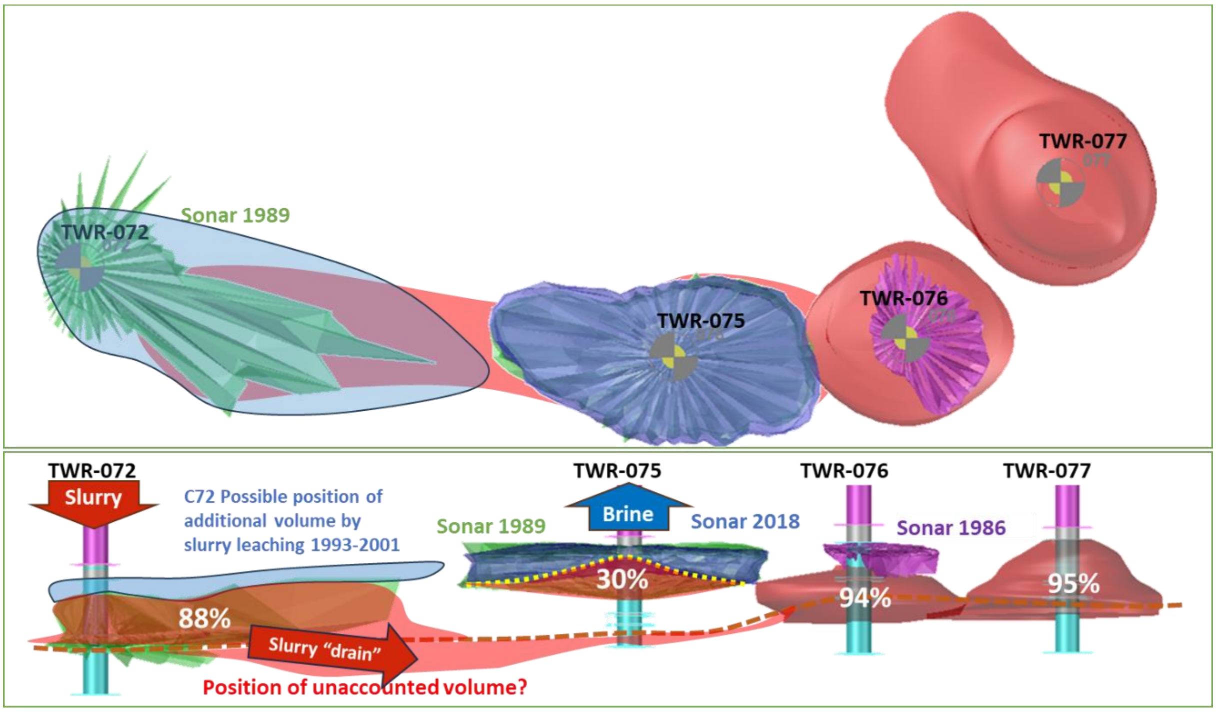

Figure 82: C72-75-76-77 Backfilling Phase 4 - 1993-2001, top view (top picture) and side view (bottom picture).

No sonar measurement of C72 after backfilling is available which can confirm the situation presented in Figure 82. The shown approximate roof contour of the residual cavern between wells TWR-072 and TWR-075 was based on the last available sonar image from 1989. The roof of the residual cavern was most likely positioned directly underneath the Claystone CD or underneath the Anhydrite-E. In the latter case, the undersaturated slurry may have deteriorated the Anhydrite-E which promoted the later migration of this part of the C72-75-76-77 cavern system.

In conclusion, the backfilling operation fully filled the Top Salt A Corridor (FLC), caverns C72, C76 and C77 and partly filled cavern C75. The FLC is both positioned in Salt A and fully backfilled and is assumed not to contribute to migration potential of the cavern system. The roof contour of C75 is positioned at the top of Salt C since 1989 without any indication of migration up to the most recent sonar measurement from November 2023. C76 also did not migrate as confirmed by a camera run in TWR-076 in 2024 which reached the 1986 cavern roof and showed the backfill. Migration of C77 cannot be established from the available information as this well was abandoned in May 1983, see Table 33. Due to the high filling grade and the relatively small roof contour area, C77 may not have migrated and very likely never will.

With the reconstruction of the backfilling operation at C72-75-76-77 completed, the BJP-Algorithm was used to reconstruct the (potential) migration of this cavern system. The starting point for the algorithm was derived by construction of approximate intersections of the individual caverns in the system with the top of Salt C. These intersections represent the cavern roof before migration is initiated and have surface areas as presented as red contours in the top picture of Figure 83.

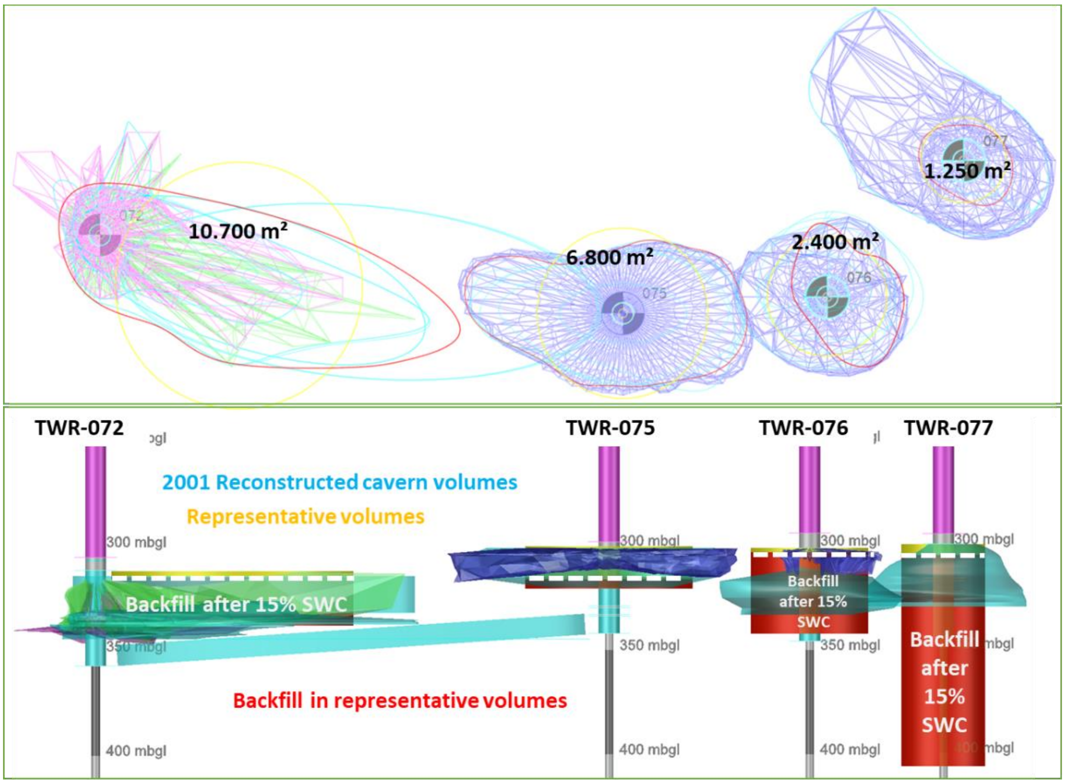

Figure 83: *C72-75-76-77: Reconstruction of „Representative volume" (yellow), reconstructed volumes shown in blue, sonar images in green. The FLC is not considered in the migration calculation.*

The representative volumes of the caverns were constructed using the established areas as a measure for the migration column diameter. Backfill was applied in the representative volumes as can be seen in this figure. The selected input parameters for the algorithm are presented in Table 43.

Table 43: C72-75-76-77 cavern specific input parameters

Cavern	72	72	72	72
Relevant borehole	72	75	76	77
X coordinate	252180,8	252426,2	252522,1	252586,1
Y coordinate	473360,8	473324,0	473331,7	473395,8
Z coordinate GL (mNAP)	21,5	22,2	22,2	22,7
Depth of top rock [mbGL]	121,5	117,3	117,0	113,9
Depth of top salt [mbGL]	311,2	305,8	301,2	299,7
Base of actual cavern [mbGL]	337,5	320,7	342,2	408,2
Base of initial cavern [mbGL]	357,1	342,1	345,7	344,7
Top of actual cavern [mbGL]	311,5	300,2	301,2	301,7
Height of cavern (m)	26,0	20,5	41,0	106,5
X coordinate migration centre	252246,0	252426,0	252522,0	252586,0
Y coordinate migration centre	473337,0	473324,0	473332,0	473396,0
Cavern geometry conversion				
Migration column Surface area (m²)	10700	6800	2400	1250
Constructed cavern radius [m]	58,0	40,0	28,0	20,0
Hydraulic Radius constructed cav. [m]	29,0	20,0	14,0	10,0
Const. cavern height (cylindrical) [m]	26,0	20,5	41,0	106,5
Const. cavern height (conical) [m]	0,0	0,0	0,0	0,0
Constructed volume (cylindrical) [m³]	274776	103044	100983	133832
Constructed volume (conical) [m³]	0	0	0	0
Constructed volume total [m³]	274776	103044	100983	133832
Height correction backfill insitu [m]	2	2	2	2
Backfill insitu unconsolidated (m³)	247767	30070	93939	126496
Backfill consolidation (%)	30	30	30	30

The cavern volume fitting part of the table is not shown as the representative volumes were derived in an alternative volume reconstruction process as summarized by Table 38. The volumes per cavern in this table are slightly reduced to derive the representative volumes to account for bulked claystone bench material in the caverns.

Using the input parameters stated in Table 43, the BJP-Algorithm produced the output presented in Figure 84 for C72. The calculated migration column for C72 is compared to GR logs from 1996 to 2022 in this figure. It can be concluded from this figure that the cavern collapsed between 1996 and 2003, and that migration was completed in 2022. This is also confirmed by observations from the well as detailed in [18]. The calculated migration height is likely overestimated due to the selection of conservative parameters to consider the uncertainties in the estimation of the initial migration contour surface area.

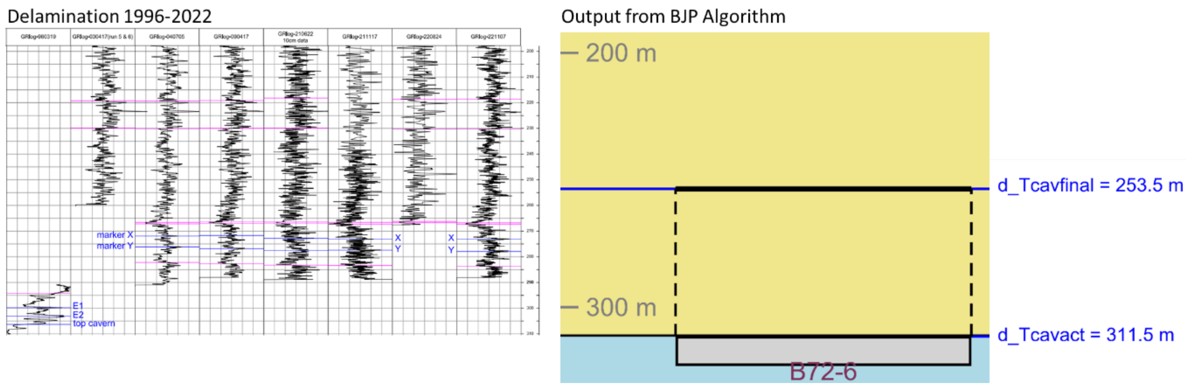

Figure 84: C72: Comparison BJP-Algorithm output and migration observations from GR logs 1996 to 2022 [19]

The calculated subsidence contours for C72 are shown in Figure 85. The actual measured subsidence is also shown in this figure for comparison.

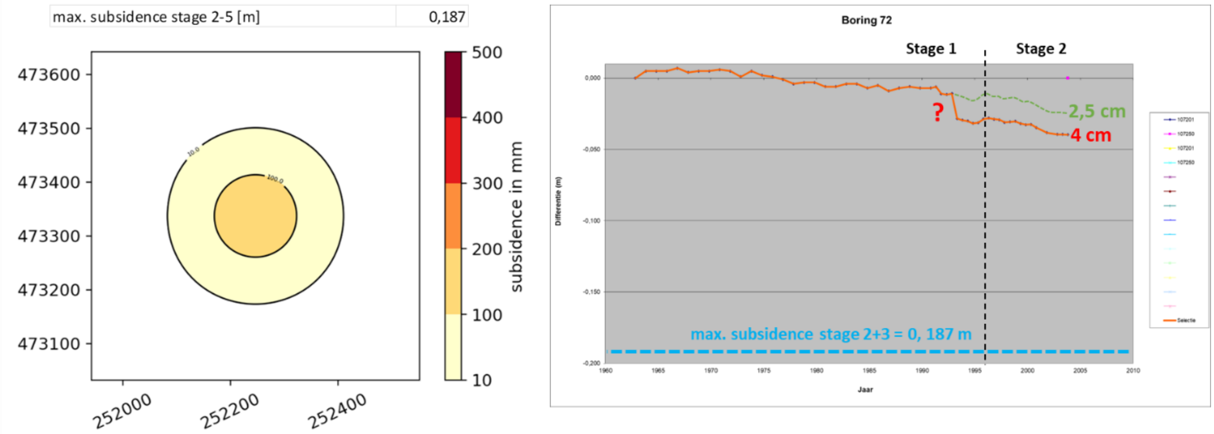

Figure 85 *C72: Stage 2+3 subsidence contours as calculated by the BJP-Algorithm (l) and measured subsidence (r). Stage 2 subsidence started in 1996 with the start of cavern migration. Measured subsidence in 2005 in red (4 cm), corrected subsidence in 2005 in green (2,5 cm)*

The shown comparison can only demonstrate that Stage 2 subsidence initiated in 1996 as can be derived from the slight increase in measured subsidence rate. As the subsidence data used in this figure stops at 2005, the full subsidence caused by migration of C72 is not captured. It is recommended that a future assessment of the measured subsidence from 2005 onwards is performed to complete the shown comparison.

4.4. Reconstruction C104-105-106-107

Cavern 104-105-106-107 (C104-105-106-107) is a multi-completion cavern (MCC) comprising wells TWR-104, TWR-105, TWR-106 and TWR-107. The cavern comprises two parts, C104-105 and C106-107, which are hydraulically connected through a forced leaching contour (FLC). Backfill has been applied in both caverns. The key data for this cavern are included in Table 44 and additional information can be found in APPENDIX I.

Table 44: Key data C104-105-106-107

Wells*	X (WGS84)	Y (WGS84)	Z (mNAP)	Final depth (mbgl)	Final depth (mNAP)	Well ready	Start production	End production	Cemented
104	250825,9	472166,6	21,6	491,5	-469,9	13-5-1965	28-2-1966	29-6-1999	
105	250865,3	472169,9	21,75	489,9	-468,15	2-6-1965	28-2-1966	29-6-1999	
106	251025,2	472183,9	22,35	482	-459,65	23-6-1965	14-8-1965	29-6-1999	
107	251064,5	472187,6	22,5	479	-456,55	14-7-1965	14-9-1965	29-6-1999	
* forced hydraulic connection in June/July 1965 according to well diaries and production data									

As with the previous complex migration cases discussed in this paragraph, the development of C104-105-106-107 cannot be reconstructed using the generalised workflow for sump reconstruction due to the (attempted) performance of forced leaching. Several operations attempted a forced connection between respectively wells TWR-104/TWR-105 and TWR-106/TWR-107 starting in June 1965. A complete overview of all connections and operations between 1965 (start operation) and 1999 (end of operation) is presented in Figure 86. Not all attempts were successful as can be seen in this figure.

	1965	1966	1967	1968	1969	1970	1971	1972	1973
TWR-104	FL SCC	SCC	SCC	SCC	SCC	SCC	FL SCC	SCC	HC MCC
TWR-105	FL SCC	SCC	SCC	FL SCC	HC MCC	MCC	MCC	MCC	HC
TWR-106	FL MCC	MCC	MCC	MCC	HC				HC
TWR-107	FL				HC				HC

	1974	1975	1976	1977	1978	1979	1980	1981	1982	1983	1984	1985	1986	1987	1988	1989	1990	1991	1992	1993	1994	1995	1996	1997	1998	1999
TWR-104	B	B	W	W	H	S	S	W	W	W	W	W	W	W	W	W	H	B	B	B	B	B	B	B	B	B
TWR-105	W	B	B	B	H	S	H	S	S	S	W	W	W	W	B	B	H	H	H	H	H	H	H	H	H	H
TWR-106	W	W	B	B	H	B	B	B	B	B	B	B	B	B	H	H	H	S	H	H	H	H	H	H	S	H
TWR-107	B	W	W	W	H	B	B	B	B	B	B	B	B	B	H	H	H	H	S	S	S	S	S	S	S	S

Legend				
	MCC	Multi completion cavern	W	MCC - Water in
	SCC	Single completion cavern	B	MCC- Brine out
	FL	Forced leaching successful	S	MCC - Slurry in
	FL	Forced leaching failed	H	MCC - On Hold
	HC	Hydraulic connection by leaching		

Figure 86: C104-105-106: Input-Output per well of the cavern system by year, adapted from [16].

The sump development for this cavern system was influenced by the presence of a Forced Leaching Corridor (FLC). The presence of a FLC is confirmed by the remarkable hydraulic connection history after the starting situation. For further reference, the distance between the wells is shown in an extract from the cavern map in Figure 87.

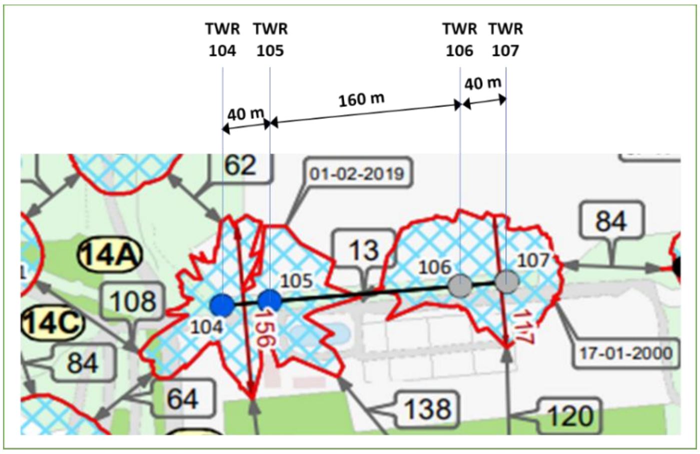

Figure 87: C104-105-106-107, distance between well spud-in positions, projected on cavern map [20]

After the initial start of brine production from SCC 104, SCC 105 and MCC 106-107 in 1965 and 1966 respectively, hydraulic connections were attempted or established as stated in Figure 86. Concerning the hydraulic connection between SCC 105 and MCC 106-107 in 1969 it must be noted that the distance between wells TWR-105 and TWR-106 (160 m) is much larger than the distance between wells TWR-104 and TWR-105 (40 m). The order of events can thus only be caused by the presence of an extensive FLC (nearly) connecting wells TWR-105 and TWR-106 after the forced leaching operation. As the exact position of the FLC is unknown, the reconstruction of this cavern system was based on a careful assessment of the available sonar images, production data and information from well diaries.

The much later established connection between SCC 104 and MCC 105-106-107 can be explained by the first snapshot in the cavern development presenting the situation in 1979 after performance of sonar measurements in all four wells of the system between October 1978 and May 1979. These sonar images are presented in Figure 88. C104-105-106-107 is operated as a MCC in 1979, all wells are thus connected at that time.

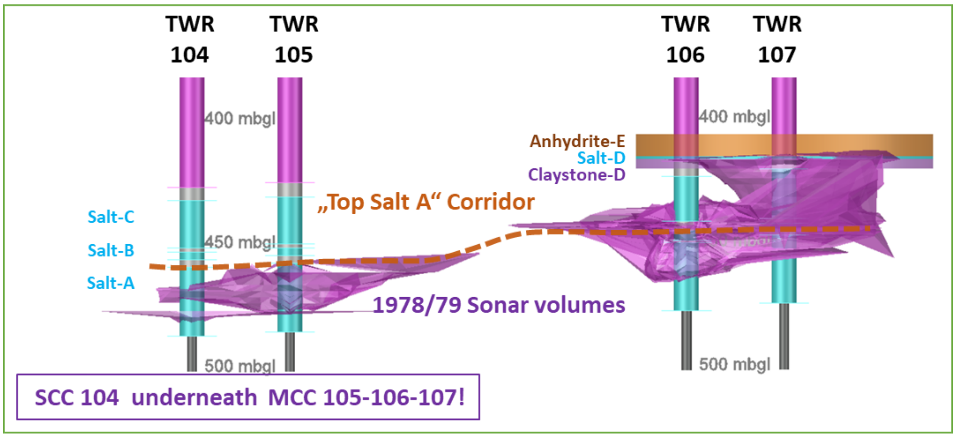

Figure 88: *C104-105-106-107: Side view of situation in 1979. Sonar volumes in magenta, probable position of FLC "Top Salt A Corridor" in tan. Top Anhydrite geology as TWR-107 based on GR logs.*

As can be seen from this figure, the C104 part of the cavern system is positioned in the lower half of Salt A, underneath the C105 part. This explains the repeated failed connection attempts between these parts of the cavern system. The earlier connections between wells TWR-105, TWR-106 and TWR-107 were established along a probable FLC at the top of Salt A. This FLC will be named "Top Salt A Corridor" as indicated in the figure. The salt production volume is approximately 371.000 m^3 at the end of 1978. As all production is recorded as a single yearly value, the spatial distribution of the total volume in the caverns system is unknown. An approximate estimate of this distribution will be discussed later in this paragraph.

The cavern roof at TWR-107 is positioned directly underneath the Anhydrite-E in 1979. As such, it was exposed to water during later years of production and deteriorated. This can be confirmed by the next snapshot describing the situation in 1987 as illustrated by Figure 89. The cavern roof at TWR-107 in 1987 is positioned slightly higher in the Anhydrite-E thus confirming its deterioration by water exposure between 1979 and 1987.

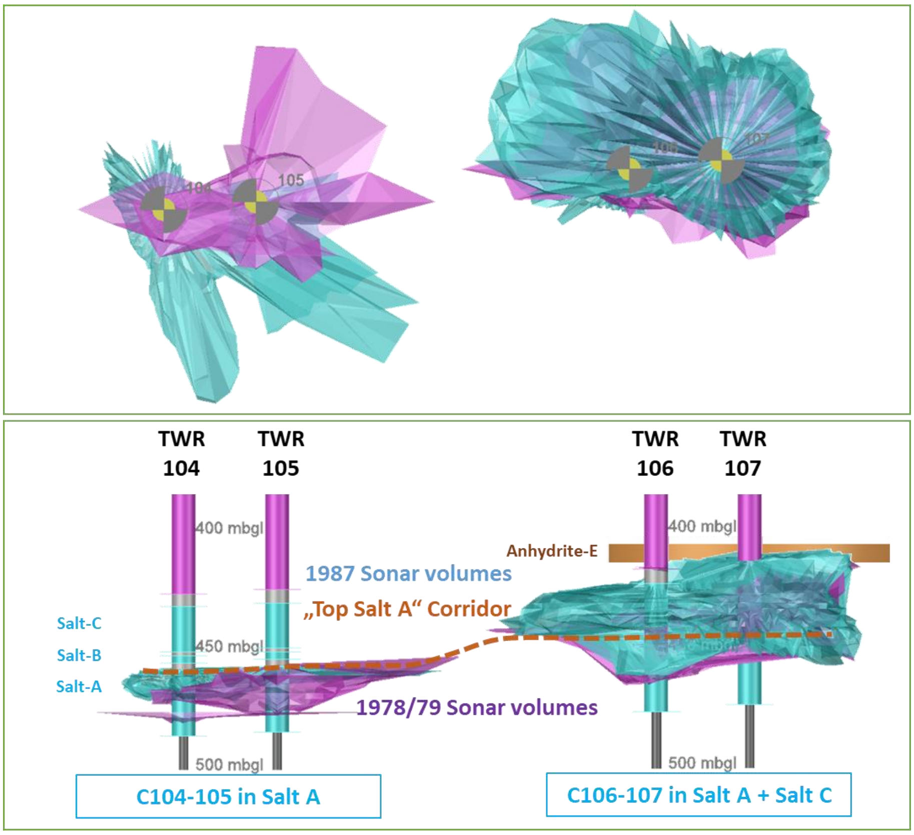

Figure 89: *C104-105-106-107: situation in 1987, top view (top picture) and side view (bottom picture). Sonar volumes 1979 in magenta, 1987 in light blue. Anhydrite-E at TWR-107 based on GR logs.*

In 1987 the C104-105 part of the cavern system is still fully positioned in Salt A as can be seen in this figure. The original C104 cavern is no longer visible and the bottom of C105 has significantly risen due to a backfilling operation at wells TWR-104 and TWR-105 between 1979 and 1981. Wells TWR-106 and TWR-107 are used for brine production during slurry pumping according to [16]. As slurry pumping is switched from TWR-104 to TWR-105 in 1981, water injection is restarted at TWR-104 to further develop this part of the cavern system. It is possible that the backfill was applied to promote an upwards leaching direction, i.e. into Salt C, rather than extend the contour in Salt A. This was not successful as C104-105 remains positioned in Salt A to present day.

The development of the C106-107 part of the cavern system between 1979 and 1987 covers both Salt A and Salt C. The bottom region of the 1987 sonar image in TWR-107 also shows the presence of backfill due to a backfilling operation at wells TWR-106 and TWR-107 in 1982 and 1983 respectively. The backfill material forms a visible heap. Apart from backfill, this heap most likely also comprised bulked material that originated from the collapse of intermediate claystone benches (AB, BC and CD) and possibly Salt B. The sonar images do not capture the connection between the C104-105 and C106-107 volumes.

The slurry volume pumped to the cavern system between 1979 and 1983 is retrieved from [15] and presented in Table 45.

Table 45: C104-105-106-107: Slurry volumes 1979-1983 and resulting insitu backfill volume before and after SWC

Well	Period	Volume (m³)	Total (m³)	S/B ratio	5	SWC	15%
TWR-104	1979	62145					
TWR-104	1980	141965					
TWR-105	1981	110575					
TWR-106	1982	76735					
TWR-107	1983	42080	433.500	**Backfill (m³)**	**86.700**	**After SWC**	**73.695**

After 1983, salt production from the cavern system continued by water injection into C104-105 and brine production from wells TWR-106 and TWR-107 until late 1987. Between 1987 and 1989, salt production continued by water injection into TWR-104 and brine production from TWR-105. The C106-107 part of the system was not used during this time. The total salt production volume from the cavern system, before further backfilling is initiated in late 1990, is approximately 565.000 m³.

The slurry volume pumped to the cavern system between 19991 and 1999 is retrieved from [15] and presented in Table 46.

Table 46: C106-107: Slurry volumes 1991-1999 and resulting insitu backfill volume before and after SWC

Well	Period	Volume (m³)		S/B ratio	5	SWC	15%
TWR-106	1991	147464					
TWR-107	1992	142534					
TWR-107	1993	171335					
TWR-107	1994	297850					
TWR-107	1995	365605					
TWR-107	1996	337736					
TWR-107	1997	370029					
107-106	1998	392537					
TWR-107	1999	207670	2.432.760	**Backfill (m³)**	**486.552**	**After SW**	**413.569**

The final snapshot in the development of C104-105-106-107 is the situation in 2000, i.e. after completion of the backfilling operation at this cavern. This situation is shown in Figure 90. Sonar measurements in 2000 were performed in wells TWR-104 and TWR-107. Respective sonar images show the residual caverns C104-105 and C106-107 after backfilling. A clear backfill heap is visible in the TWR-107 sonar image.

In the TWR-104 image this is less pronounced, but as only a shallow slit between the top of the backfill and the cavern roof was available for the tool, sonar shadows may have obscured part of the cavern volume. Obscured volume is likely present towards TWR-105, thus masking the backfill heap in the image. More recent (2019 and 2024) sonars at TWR-104 confirm the status of 2000. A camera-run (26-03-2024) in TWR-105 confirmed the top of the backfill heap at the Last Cemented Casing (LCC). From this observation it seems that C106-107 is indeed completely filled up.

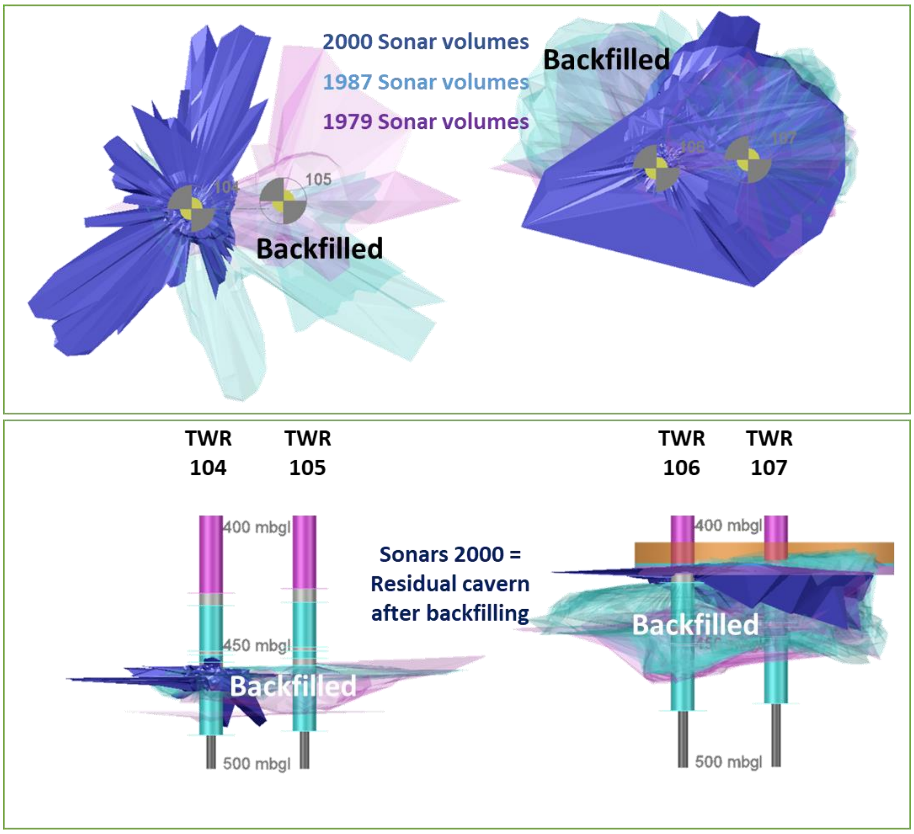

Figure 90: *C104-105-106-107: situation in 2000, top view (top picture) and side view (bottom picture). Sonar volumes 1979 in magenta, 1987 in light blue and 2000 in blue.*

The presented situation in 2000 also allows an approximate volume distribution reconstruction as shown in Table 47 by using the C106-107 residual cavern volume as a "data anchor" to which an approximate volume distribution can be fitted by trial-and-error.

Table 47: *C104-105-106-107: approximate volume distribution based on the residual cavern volume in 2000 and information from well diaries and [16] with regards to operational conditions*

	TWR-104	TWR-105	TWR-106	TWR-107	Total
1966 sump vol. (m³)	4.888	4.279	16.175		25.342
1968 production volume (m³)	18.385	20.864	55.585		94.834
1972 production volume (m³)	39.966	137.476			177.442
1972 probable distribution (m³)	39.966	51.378	86.098		177.442
1978 production volume (m³)	371.199				371.199
1978 probable distribution (m³)	107.781	119.192	144.225		371.199
1983 production volume (m³)	406.612				406.612
1983 probable distribution (m³)	116.634	128.046	161.932		406.612
1987 production volume (m³)	519.703				519.703
1987 probable distribution (m³)	139.253	150.664	229.786		519.703
1991 production volume (m³)	565.231				565.231
1991 probable distribution (m³)	139.253	150.664	275.314		565.231
1999 Final salt prod. (t)	*1.284.495*				
1999 production volume (m³)	721.730				721.730
1999 probable distribution (m³)	139.253	150.664	431.814		721.730
1999 volume per cavern (m³)	289.917		431.814		721.730
1999 Final insolubles vol. (m³)	16.827		25.063		41.890
1999 Final net cavern vol. (m³)	273.090		406.751		679.841
1999 Backfill vol. after SW Cons. (m³)	233.663		253.601		487.264
2000 Sonar volume TWR-107 = Residual Volume C106-107 after backfilling (m³)					153.150
2000 Calculated Residual Volume C104-105 after backfilling (m³)					39.426
2000 Sonar volume TWR-104 (m³)					*18.620*

The estimation of the volume distribution is firstly based on the salt production data for the total cavern system. The corresponding production volumes were calculated for a number of key dates in the cavern development as shown in the first column of Table 47. Information of the operational conditions, i.e. which wells were used for water injection and brine production, was taken from [16] and the well diaries. The hydraulic connection history as discussed at the start of this paragraph was also considered as a boundary condition. Lastly, available sonar images were used as guidance to check plausibility of the estimated distribution of volume across the cavern system.

The outcome of the estimation as presented in Table 47 shows that in 1999 the C106-107 net cavern volume was approximately 407.000 m³ without backfill. The insitu backfill in C106-107 after 15% SWC is approximately 254.000 m³ leaving the ~153.000 m³ residual cavern volume after backfilling shown by the 2000 sonar image in TWR-107. Based on this residual volume, the backfill volume in C104-105 could be determined by subtracting the C106-107 backfill volume from the total backfill volume after 15% SWC.

The outcome of the distribution estimate as presented in Table 47 also shows that in 1999 the C104-105 net cavern volume was approximately 273.000 m³ without backfill. The insitu backfill in C104-105 after 15% SWC is approximately 233.000 m³ leaving ~40.000 m³ residual cavern volume after backfilling. The 2000 sonar volume is 18.620 m³ thus undershooting the estimated residual cavern volume. This can be explained by the previously mentioned sonar shadows during measurement from TWR-104.

In conclusion, the volume distribution presented in this table is deemed plausible as demonstrated by the fitment to the discussed data anchor. As such, it was used as the starting point of the migration reconstruction by application of the BJP-Algorithm.

As C104-105 has not migrated to date due its position in Salt A, the reconstruction of potential migration is not discussed in this report as it does not contribute to the validation of the algorithm. The migration reconstruction for C106-107 was initiated by the construction of an approximate intersection of the cavern with the top of Salt C. This intersection represents the cavern roof before migration is initiated and has a surface area as presented in the right picture of Figure 91.

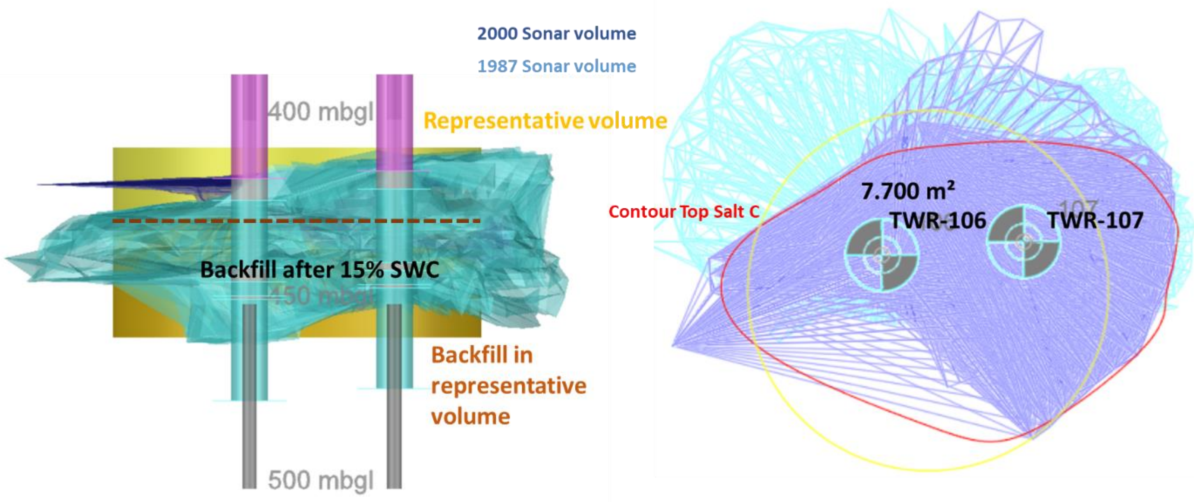

Figure 91: C106-107: Reconstruction of „Representative volume" (yellow), sonar images in blue and light blue. Cavern contour Top Salt C shown in red. Backfill in cavern is shown as orange within the representative volume.

The representative volume of the C106-107 was constructed using the established areas as a measure for the migration column diameter. The representative cavern volume is shown as a yellow cylinder in this figure. The applied backfill is shown as an orange fill of the representative volume and demarked by a tan dashed line. The selected input parameters for the algorithm are presented in Table 48.

Table 48: C106-107 cavern specific input parameters

Cavern	106
Relevant borehole	106
X coordinate	251025,2
Y coordinate	472183,9
Z coordinate GL (mNAP)	22,4
Depth of top rock [mbGL]	118,5
Depth of top salt [mbGL]	421,8
Base of actual cavern [mbGL]	459,4
Base of initial cavern [mbGL]	476,1
Top of actual cavern [mbGL]	407,4
Height of cavern (m)	52,0
X coordinate migration centre	251038,0
Y coordinate migration centre	472174,0
Volume fitting	
Maximum BPB Prod.(t)	768.518
Cavern vol based on BPB (m³)	**431907**
Actual volume (recon./sonar)(m³)	406751
Insolubles (bulked) (m³)	22789
Part of BPB prod. Vol. not acc. (m³)	25156
Part of BPB prod. Vol. not acc. (%)	**6%**
Cavern geometry conversion	
Migration column Surface area (m²)	7700
Constructed cavern radius [m]	50,0
Hydraulic Radius constructed cav. [m]	25,0
Const. cavern height (cylindrical) [m]	52,0
Const. cavern height (conical) [m]	0,0
Constructed volume (cylindrical) [m³]	408407
Constructed volume (conical) [m³]	0
Constructed volume total [m³]	408407
Part of BPB prod. Vol. not acc. (m³)	23500
Part of BPB prod. Vol. not acc. (%)	**5%**
Height correction backfill insitu [m]	2
Backfill insitu unconsolidated (m³)	257457
Backfill consolidation (%)	30

The cavern volume available for bulked overburden considers 5% of unaccounted volume in relation to the production volume as a conservative approach. The dimensions of the representative volume of C106-107 are stated in this table.

Using the input parameters stated in Table 48, the BJP-Algorithm produced the output presented in Figure 92 for C106-107. The calculated migration column for C106-107 is compared to GR logs from 1987 to 2011 in this figure [21]. It can be concluded from this figure that the cavern migration initiated between 2001 and 2005. A detailed description of the migration after 2005 is provided by [22]. Observations in this source extend to 2024 and conclude that the migration practically ended between 2022 and 2024, but that further deformation of the migration column may still occur. The depth that migration reached is estimated at approximately 270 mbgl according to the observations in this memo. The calculated migration height reaches 250 mbgl and is likely overestimated due to the selection of conservative parameters to consider the uncertainties in the estimation of the spatial cavern volume distribution.

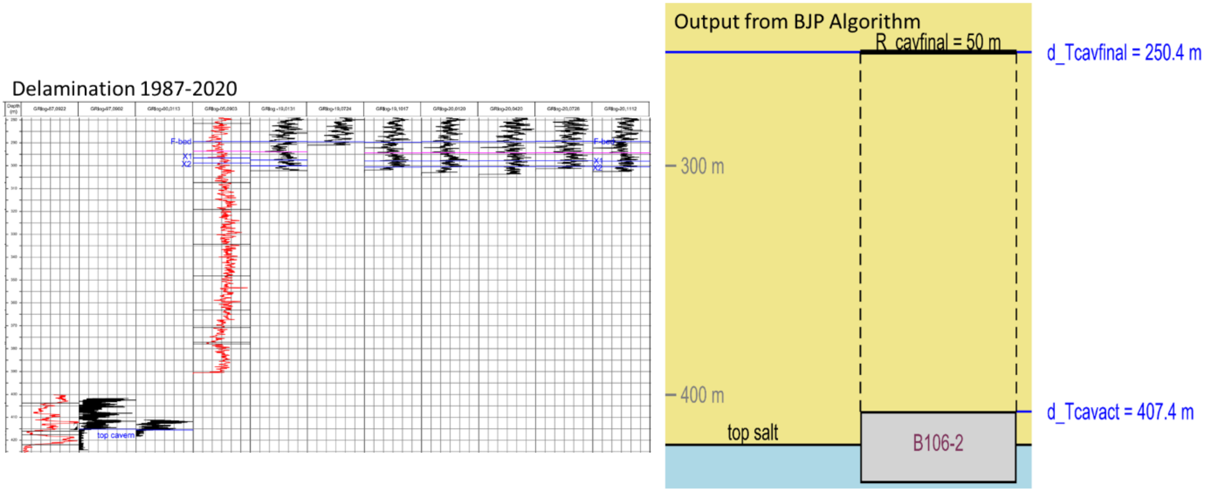

Figure 92: C106-107: Comparison BJP-Algorithm output and migration observations from GR logs 1987 to 2011 [21]

The calculated subsidence contours for C106-107 are shown in Figure 93. The actual measured subsidence is also shown in this figure.

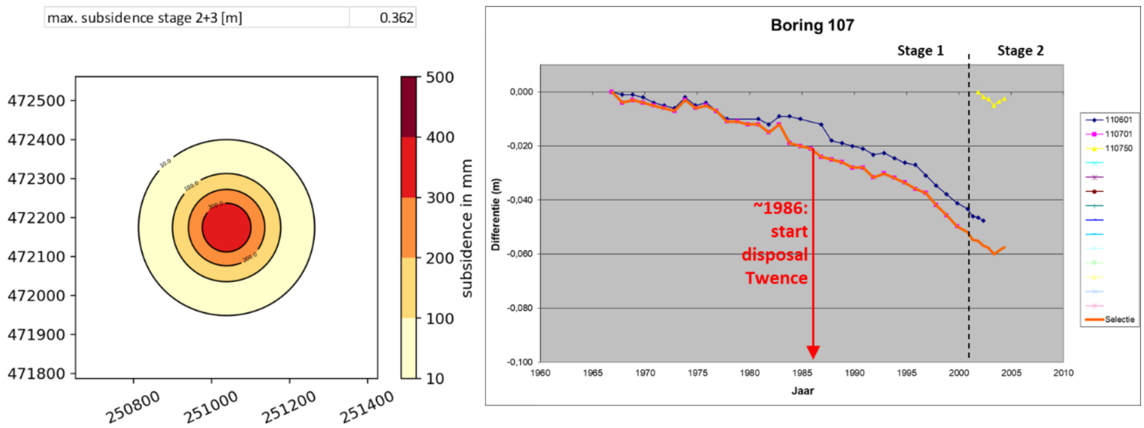

Figure 93 C106-17: Stage 2+3 subsidence contours as calculated by the BJP-Algorithm (l) and measured subsidence (r). Stage 2 subsidence started in 1996 with the start of cavern migration. Measured subsidence in 2005 in red (4 cm), corrected subsidence in 2005 in green (2,5 cm)

The measured subsidence only relates to Stage 1 subsidence. A comparison between calculated and measured subsidence due to migration cannot be made as the subsidence measurements stop in 2005 at the approximate moment that the cavern migration starts. The subsidence caused by migration of C106-107 is thus not captured by this figure. The wells of the cavern system are located on the outer edge of the landfill operated by Twence BV. The start of disposal on the landfill around 1986 leads to the rise in subsidence rate in the late 1990's. In conclusion, it is recommended that an assessment of the measured subsidence from 2005 onwards is performed to complete the shown comparison.

5. Reverse operation of the BJP-Algorithm

The cavern development and subsequent migration history of caverns C30-31 and C33-34-35-36 are not sufficiently documented to allow the reconstruction process applied to the caverns described prior. Despite the lack of information, these caverns were reconstructed using the BJP-algorithm by operating it in “reverse”. In other words, using the actual measured subsidence and the production history as the input parameters to, iteratively, determine the most likely migration column shape and extend, thus enabling the reconstruction of the original cavern volumes with confidence.

The reverse operation of the algorithm will play a crucial role during the future Phase III of the UMS-TWR in which the cavern volume developed from wells TWR-001 to TWR-050 will need to be reconstructed. Only salt production data and subsidence data is available for these caverns; sonar images are very rare and are only available for C15, C37 and C49-50 as discussed earlier in this report.

Testing the reverse operation of the algorithm for C30-31 also revealed a last shortcoming in the algorithm which prevented a smooth transition between the calculated Stage 4-Trough subsidence and Stage 4-Sinkhole subsidence. The algorithm was therefore adapted as a result to include a smooth non-linear transition of stage 4 subsidence with increasing cavern height at the Top Rock (i.e. bottom Tertiary) for different cavern radii. This adaption and the non-linear transition are detailed in Report 2, paragraph 3.4, pages 20 and 21.

The main complexity in the reconstruction of caverns C30-31 and C33-34-35-36 is the uncertainty in relation to the spatial distribution of cavern space in the salt layers. Very few sonar images are available. Furthermore, these caverns were part of a larger cavern system C29-30-31-33-34-35-36-42-43 for which the available production values per cavern were combined into a single value after each connection of individual cavern parts, i.e. C29, C30-31, C33-34, C35-36 and C42-43. This prevented a cavern volume reconstruction on a yearly basis per cavern as the configuration of water injection and brine production wells is not known. The final salt production for the individual cavern parts has been estimated in [23]. These estimates are stated in the Nobian digital production database (Nobian BPB) and are presented in Table 49.

Table 49: Salt production of caverns C29, C30-31, C33-34, C35-36 and C42-43 according to the digital production database (“Nobian BPB”)

Cavern	Salt Prod (t)
C29	331.373
C30-31	404.984
C33-34	410.783
C35-36	529.984
C42-43	343.731

To aid clarity on the location of the mentioned wells and caverns, an extract from the cavern map is presented in Figure 94, left picture in figure, showing all wells of the cavern system. The dates at which individual cavern parts were hydraulically connected are also included in this picture. Furthermore, Figure 94 presents a cut-out of the Depth Map of the Top RNSO (Solingen Formation), i.e. the Bottom of the Salt A member The identified offsets in the stratigraphy encountered in the wells are shown as red lines in this figure. Lastly, this figure presents the thickness of the RNRO1, i.e. Salt A to Anhydrite-E (Main Röt Evaporite Member). All pictures are at the same scale to ease direct comparison.

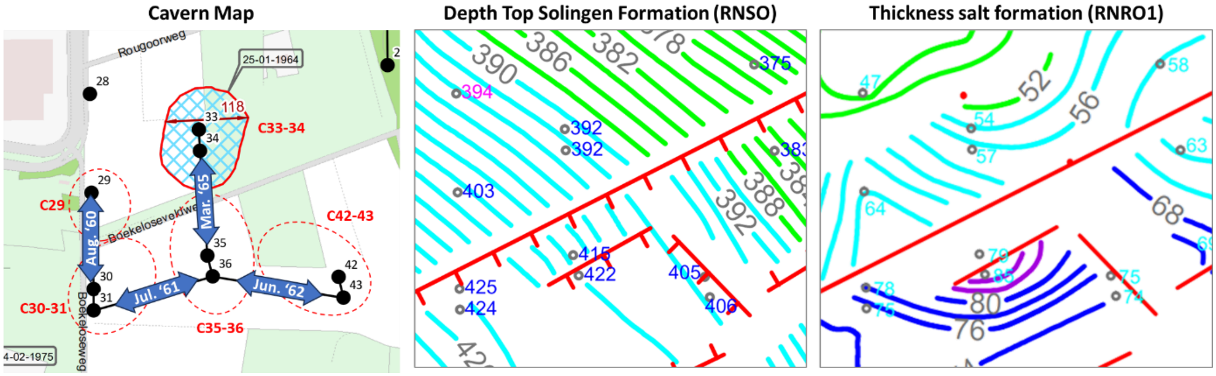

Figure 94: *Relative position of wells TWR-028, TWR-029, TWR-030, TWR-031, TWR-032, TWR-033, TWR-034, TWR-035, TWR-036, TWR-042 and TWR-043 on the cavern map [20] (left). Detailed view from Depth Top Solingen Formation Map with offsets indicated as red line, adapted from Attachment C to [13]*

A possible explanation for the extensive connections between caverns in this area can be found considering the presence of offsets in the stratigraphy, indicated by red lines in the middle picture of Figure 94. These offsets can be interpreted as faults in the Soling formation. These faults do not propagate through the salt members, but the offset in the base of the salt members will have caused salt flow due to salt creep on a geological timescale. As can be seen from this figure, more than 20 m offset has been identified between wells TWR-034 and TWR-035 for example. Smaller offsets are present between wells TWR-029 and TWR-030, as wells as between TWR-035 and TWR-036.

The salt has either thinned-out or thickened, as can be seen in the right picture in this figure. As an example, the total RNRO1 thickness at well TWR-034 is 57 m while at well TWR-036 this is 79 m, i.e. 22 m more. The difference in thickness of salt layers cause "misalignment" of the salt members and intermediate claystone benches. The depth differences cause an upward gradient in the Top Soling and intermediate claystone benches towards C29 and C33-34. This gradient forced injected water to flow preferably in this direction thereby leading to asymmetric cavern development. The asymmetric, northwards development of C30-31, C35-36 and C42-43 likely led to the formation of hydraulic connections as discussed prior.

In conclusion, the reconstruction of C30-31 and C33-34-35-36 cannot be performed in the manner as discussed in the previous chapters. Nonetheless, a plausible cavern geometry was derived from the total salt production figures presented in Table 49, two available sonar images in C33-34 and C35-36 and the subsidence caused by the migration of C30-31 and C33-34-35-36 by reverse operation of the BJP-Algorithm.

5.1. Measured subsidence

The reverse operation workflow starts with the result of cavern migration, i.e. the measured subsidence. Detailed subsidence measurements between the start of production and 2005 are available for C30-31 and C33-34-35-36 as shown in Figure 95.

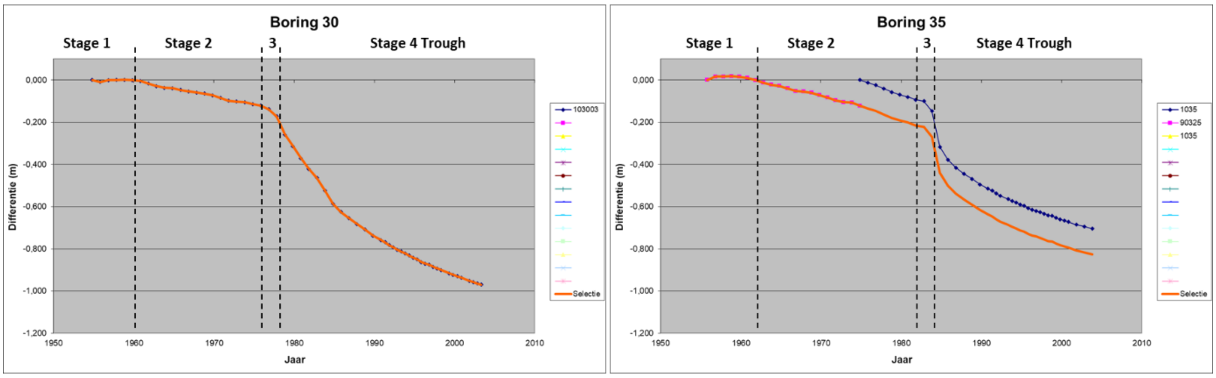

Figure 95: Measured subsidence from start production until 2005 for C30-31 (l) and C33-34-35-36 (r).

As can be seen from this figure, Stage 4 Trough subsidence developed due to the migration of both caverns. The subsidence stages 1 through 4 can be clearly distinguished from the orange curves and are marked for reference. In 2005 the Stage 4 subsidence at both caverns is still ongoing but the subsidence rate is decreasing signalling the transition to Stage 5 subsidence caused by consolidation of the bulked overburden under the load of the collapsed Tertiary, see Report 2, paragraph 3.5 for details.

The further subsidence development between approximately 2012 and 2022 can be estimated from the “Algemeen Hoogtebestand Nederland” database (AHN) accessible via [24]. Figure 96 presents a comparison of the AHN2 database values from 2012 with the AHN4 database values from 2022 for the two Stage 4 Troughs developed over C30-31 and C33-34-35-36.

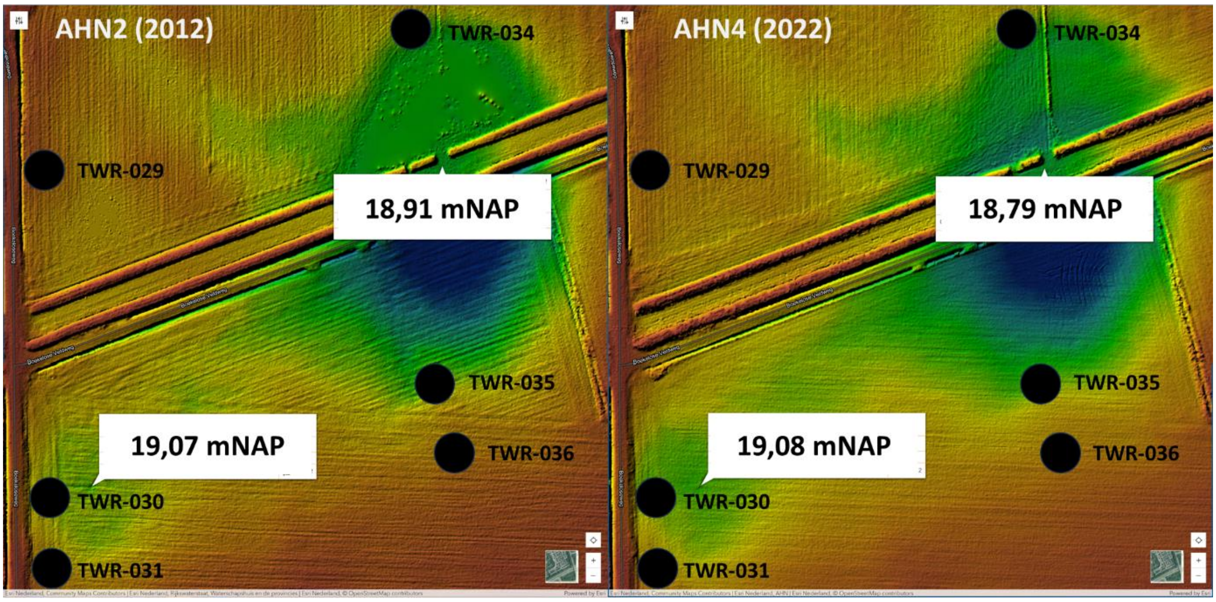

Figure 96: C30-31 & C33-34-35-36: Comparison of terrain models AHN2 model (2012, left) and AHN4 (2022, right) relative to position of relevant wells in the area. Stage 4 troughs visible as dark green / blue areas.

This figure shows that the Stage 4 Trough over C30-31 is located slightly east of well TWR-030. The trough has not deepened between 2012 and 2022, therefore Stage 5 subsidence appears to have been fully developed by 2012. Based on these values, further subsidence caused by cavern migration should thus not occur at this cavern.

The Stage 4 Trough over C33-34-35-36 is located in the middle between wells TWR-034 and TWR-035. This position is somewhat remarkable considering this cavern comprises two parts: C33-34 and C35-36 which have each developed around their respective wells. The location of the trough thus indicates “merging” of migration columns arising from the two individual caverns parts of C33-34-35-36. This will be further discussed in the next paragraph.

The comparison of the AHN2 and AHN4 database values presented in Figure 96 shows that the Stage 4 Trough over C33-34-35-36 has deepened by approximately 11-12 cm between 2012 and 2022. Further comparison of the AHN2 (2012) with AHN3 (2018, not shown in Figure 96) values reveals that 8 cm developed between 2012 and 2018 and 3 cm between 2018 and 2022. Based on these values, the development of Stage 5 subsidence seems to near completion in 2022.

The measured subsidence over the two caverns forms the data anchor to which the representative cavern volume is fitted during the reverse operation of the BJP-Algorithm. The following paragraphs describe these two examples of the reverse operation of the algorithm and demonstrate that a plausible cavern geometry can be fitted to the measured subsidence. Please note that the development of C33-34-35-36 is better documented than the development of C30-31 and, as such, it will be discussed first. The insights gained during the reconstruction of C33-34-35-36 enabled the later reconstruction of C30-31.

5.2. Reconstruction C33-34-35-36 (reverse operation)

Cavern 33-34-35-36 (C33-34-35-36) is a multi-completion cavern (MCC) comprising wells TWR-033, TWR-034, TWR-035 and TWR-036. No blanket medium was used during the cavern development. Backfill was not applied in this cavern either. The key data for this cavern are included in Table 50 and additional information can be found in APPENDIX I.

Table 50: Key data C33-34-35-36

Wells	X (WGS84)	Y (WGS84)	Z (mNAP)	Final depth (mbgl)	Final depth (mNAP)	Well ready	Start production	End production	Cemented
33	250879,7	473396,0	20,82	418,97	-398,15	3-6-1953	3-7-1953	30-4-1964	18-9-1974
34	250881,2	473366,0	20,5	416,55	-396,09	3-9-1954	17-9-1954	30-4-1964	8-2-1974
35	250891,7	473217,5	20,3	439,47	-419,14	6-12-1954	20-12-1954	1-11-1964	10-5-1974
36	250899,6	473188,7	20,3	446,03	-425,71	4-4-1955	22-4-1955	1-11-1964	12-2-1973

C33-34-35-36, comprising the wells included in Table 50, was initially developed as four independent SCC caverns between 1953 and 1955. Sump caverns SCC 33 and SCC 34 connected in November 1955, more than two years after the start of production. The time until connection is remarkable considering the distance between these wells is only 30 m. This can however be explained by the fact these wells were operated in bottom injection which promoted vertical development over lateral development of the sumps. Cavern C33-34 was operated as a MCC from 1956 onwards according to the production records. This continued until the end of production in April of 1964 as can be seen in Table 50.

Sump caverns SCC 35 and SCC 36 connected in October 1956, nearly two years after the start of production from well TWR-035 and 18 months after start of production from well TWR-036. The distance between these wells is again only 30 m and bottom injection explains the late connection of the two sumps. Cavern C35-36 was operated as a MCC from 1957 onwards according to the production records. This cavern connected to the surrounding caverns at the dates stated in Figure 94.

The initial reconstruction of cavern development of C33-34-35-36 will be presented in three snapshots of the cavern development. The first snapshot is the situation in 1955/1956 at the end of the sump phase. This situation is shown in Figure 97.

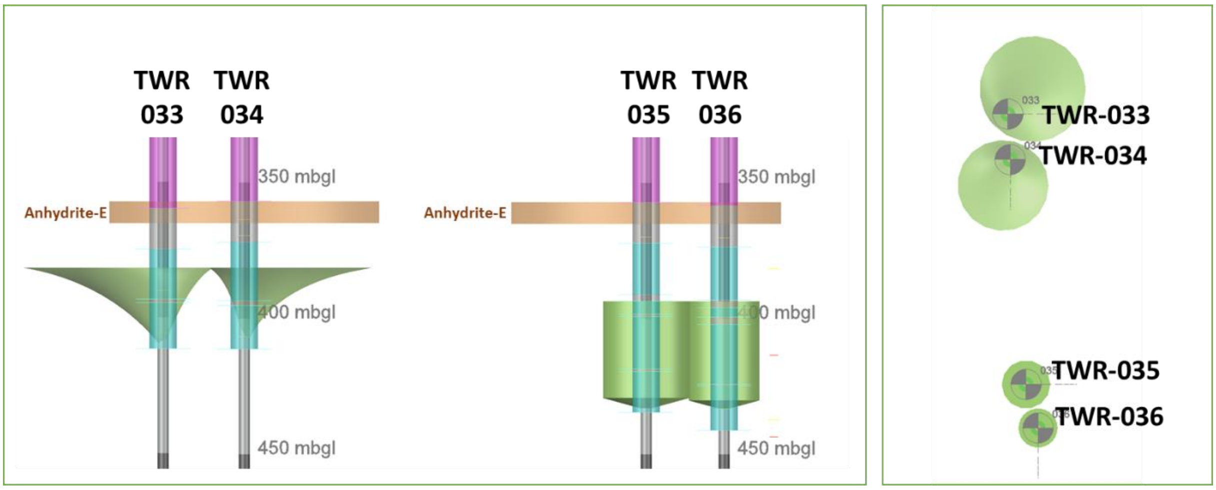

Figure 97: C33, C34, C35 and C36 sump phase development 1954 to 1956.

The sump shapes shown in this figure are approximations based on the salt geology and the later sonar images which will be discussed in the second snapshot. The total salt thickness at wells TWR-033 and TWR-034 is limited, and the sump development will primarily have taken place in Salt C as a result. The intermediate claystone benches did not act as a blanket medium and asymmetric Morning Glory sumps likely developed as is shown. Further cavern volume developed upwards and outwards from the maximum contour after connection of the two sumps in November 1955.

At wells TWR-035 and TWR-036, the salt layer is much thicker, and the sump development took place in Salt A and perhaps Salt B. As bottom injection was used, the two sumps extended vertically and remained isolated from another until reaching the intermediate claystone benches. As these benches acted as a roof protection, the contour of the sump extended laterally and caused their eventual collapse. The connection between the sumps was possibly formed during the lateral sump extension underneath the claystone or alternatively by its collapse. Further cavern volume developed upwards and outwards into Salt C towards C33-34 due to the gradient in the salt base. The volumes of the sump caverns are presented in Table 51.

Table 51: Reconstruction SCC Sumps 33, 34, 35 and 36

Cavern	Years	Production (t)	Sump volume (m³)
33	1954-55	40,780	22,913
34	1954-55	24,120	13,553
35	1955-56	53,150	29,864
36	1955-56	35,595	20,000

The second snapshot is the situation in 1964 at the end production of C33-34 as presented in Figure 98. A sonar image taken from well TWR-034 shows the final cavern directly underneath the inferred position of the Anhydrite-E. Gamma Ray logs confirming the position of this member are not available but information from adjacent wells was used to derive the position shown. Apart from this 1964 sonar image, Figure 98 also shows a reconstruction of a sonar image from well TWR-035 in 1963. A digital copy of this image was not available. Paper sections from a Prakla report were therefore used to prepare a reconstructed sonar volume in AutoCAD.

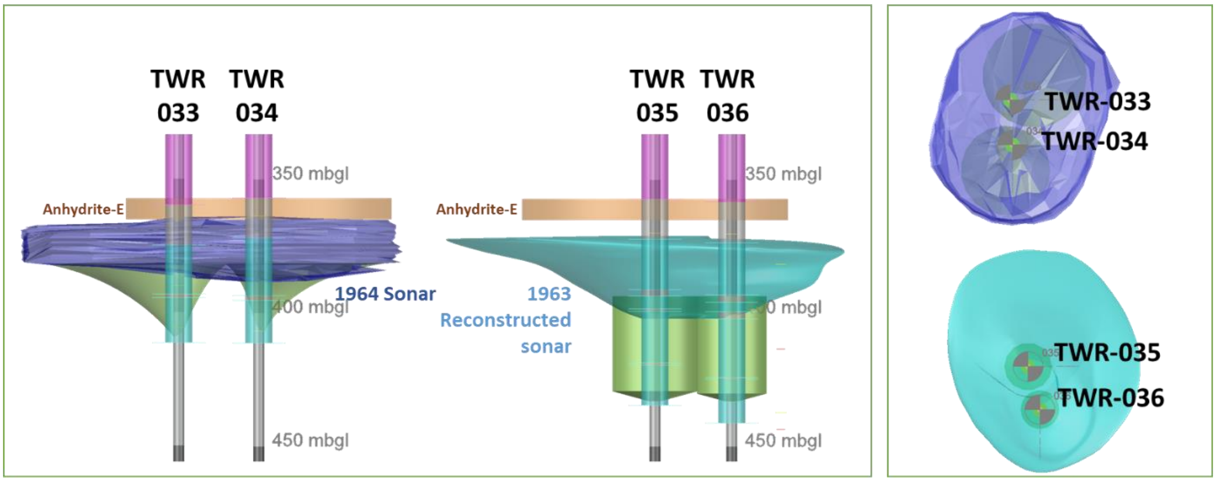

Figure 98: *C33-34 in 1964 (end of production) and C35-36 in 1963 according to sonar images from wells TWR-034 and TWR-035 respectively. Side view (l) and top view (r, not to scale).*

The sonar in C33-34 has a volume of 210.130 m³. The production from C33-34 until the end of production in 1964 is 410.783 t (see Table 49) which corresponds to 230.810 m³ production volume. After subtraction of bulked insolubles (10.305 m³), 220.505 m³ net cavern volume remains. This volume aligns very closely with the sonar image from 1964 in this cavern. The difference of approximately 10.000 m³ can be attributed to the conservative estimate of insolubles bulking and possibly some sonar shadow towards the sump at well TWR-033 especially since the sonar technology was still in an early stage of development.

The accuracy of the reconstructed sonar image from well TWR-035 in 1963 is not sufficient to estimate its volume. In 1962/1963 the cavern connects hydraulically to C30-31 and C42-43, which makes estimation of the production volume for C35-36 in 1963 ambiguous. As such, an estimate for the volume of C35-36 is not provided for this snapshot.

The third snapshot alleviates the ambiguity on the C35-36 volume as the final 1965 salt production value stated in Table 49 for this cavern enabled an approximate reconstruction. The 1965 final volumes of C33-34 and C35-36, as based on salt production values from Table 49, are presented in Table 52.

Table 52 *C33-34-35-36: Insoluble material fill until 1964 (end of production by leaching)*

Final cavern volume C33-34			**Final cavern volume C35-36**		
1964 cavern volume	230.810	m³	1965 cavern volume	297.787	m³
Insoluble fill volume	10.305	m³	Insoluble fill volume	13.295	m³
Final reconstructed volume	**220.505**	**m³**	**Final reconstructed volume**	**284.492**	**m³**

The approximate reconstruction of C33-34 based on the volume stated in this table is shown in Figure 99. The approximate reconstruction of C35-36 is based on the upward and outward development from the 1963 sonar in this cavern as shown in Figure 98. The top of Salt C was taken as an upper limit.

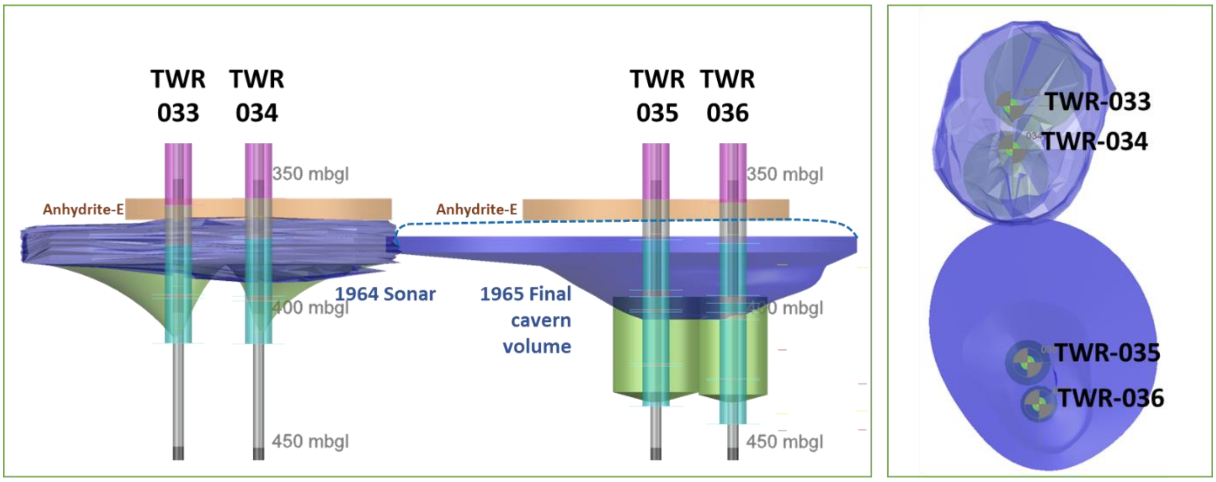

Figure 99: C33-34 in 1964 as per sonar image (end of production) and approximate reconstruction of C35-36 in 1965 (end of production). Side view (l) and top view (r, not to scale).

It is possible that the Claystone CD collapsed between 1963 and 1965 which would place the final cavern directly underneath the inferred Anhydrite-E layer. In this alternative scenario the C35-36 volume as shown is effectively shifted upwards by approximately 5 m.

The (likely) position of both C33-34 and C35-36 directly underneath the Anhydrite-E will have exposed it to water thus promoting its deterioration. This deterioration in combination with a laterally extended roof contour most likely caused initial migration of the cavern by collapse of the Anhydrite-E member. The presence of offsets in the salt base may have also played a role which will be further discussed in paragraph 6.3.

The position and extend of the measured Stage 4 subsidence indicates that the migration of the two individual cavern parts C33-34 and C35-36 merged into a single migration column. This has been established by repeated testing of representative cavern volume variations during the reverse operation of the BJP-Algorithm. Tests in which two representative volumes were used, i.e. representing C33-34 and C35-36 separately, did not lead to the observed subsidence trough. Even when using two cones with a steep cone angle as a cavern shape (to increase the migration height by the radius reduction mechanism) Stage 4 subsidence was not achieved by the calculation. The volumes of the individual cavern parts are simply too small to lead to a trough.

As such, the volumes of C33-34 and C35-35 were combined to increase the potential migration height. The combined volume was positioned directly underneath the deepest point of the trough shown in Figure 96. With the combined volume, a new series of representative volumes were tested from cylindrical to cone shaped. Examples of tests performed during the reverse operation of the algorithm are shown in Figure 100 for illustrative purposes.

The tests with a combined volume showed that the measured Stage 4 subsidence could be modelled. This enabled a more detailed fitting of the measured and calculated subsidence by variation of the representative cavern dimensions, i.e. radius, cone height and cylinder height. The sensitivity of these dimensions is high, making increments of 5 cm necessary to achieve optimal fitment between calculated and measured subsidence.

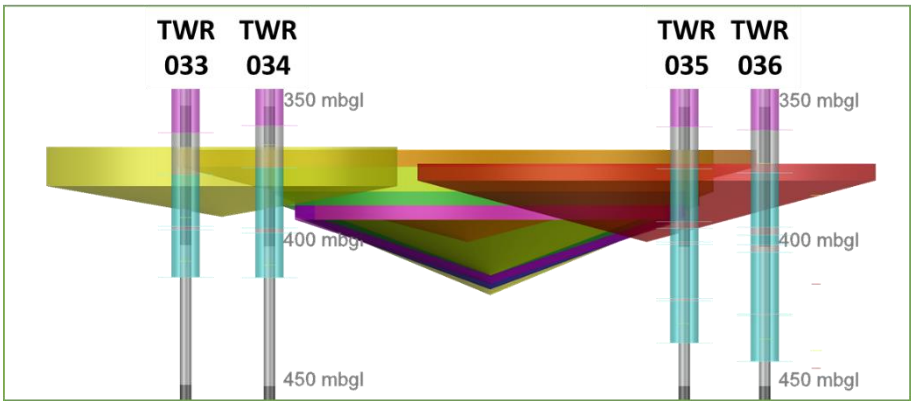

Figure 100: *C33-34-35-36: Examples of tested representative volumes, both as separate parts C33-34 and C35-36) and as a single volume (C33-34-35-36).*

After several iterations, and adaptation of the algorithm to include a smooth non-linear transition of Stage 4 trough to sinkhole subsidence , the final version of the BJP-Algorithm was used to derive input parameters as presented in Table 53 and depicted in Figure 101 below.

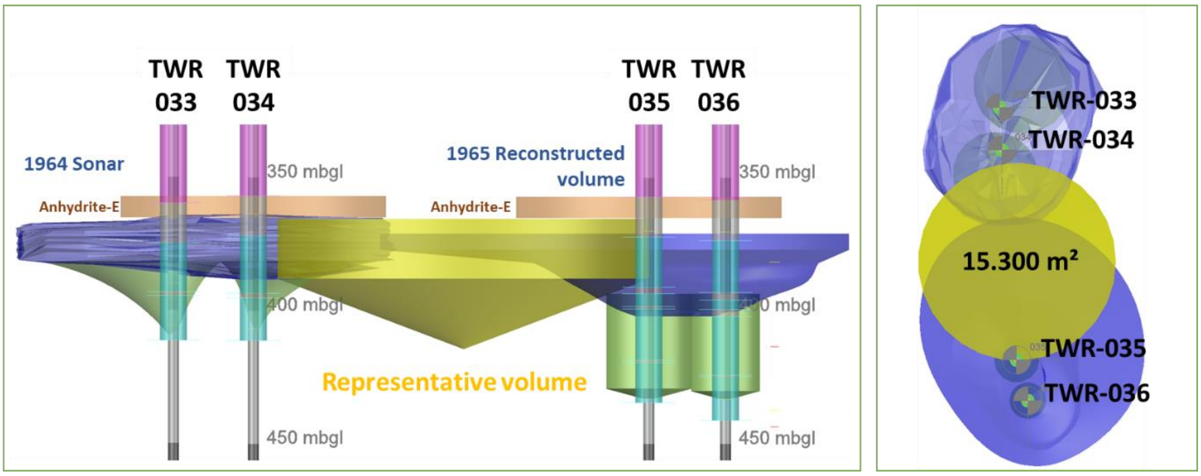

Figure 101: *C33-34-35-36: Final tested „Representative volume" (yellow). Original and reconstructed sonars volumes shown in blue.*

The representative volume of C33-34-35-36 leading to the measured subsidence comprises a cone-shaped bottom with a 70 m radius and 26,35 m height and a cylinder with 70 m radius and 22,55 m height. No backfill has been applied in this cavern.

Table 53 C33-34-35-36 cavern specific input parameters

Cavern	35
Relevant borehole	35
X coordinate	250891,7
Y coordinate	473217,5
Z coordinate GL (mNAP)	20,3
Depth of top rock [mbGL]	128,9
Depth of top salt [mbGL]	374,4
Base of actual cavern [mbGL]	414,23
Base of initial cavern [mbGL]	410,96
Top of actual cavern [mbGL]	365,33
Height of cavern (m)	48,9
X coordinate migration centre	250892,0
Y coordinate migration centre	473287,0
Volume fitting	
Maximum BPB Prod.(t)	940767
Cavern vol based on BPB (m³)	**528597**
Actual volume (recon./sonar)(m³)	482844
Insolubles (bulked) (m³)	23600
Part of BPB prod. Vol. not acc. (m³)	45753
Part of BPB prod. Vol. not acc. (%)	**9%**
Cavern geometry conversion	
Migration column Surface area (m²)	15300
Constructed cavern radius [m]	70,0
Hydraulic Radius constructed cav. [m]	35,0
Const. cavern height (cylindrical) [m]	22,55
Const. cavern height (conical) [m]	26,35
Constructed volume (cylindrical) [m³]	347130
Constructed volume (conical) [m³]	135209
Constructed volume total [m³]	482339
Part of BPB prod. Vol. not acc. (m³)	46258
Part of BPB prod. Vol. not acc. (%)	9%
Height correction backfill insitu [m]	0
Backfill insitu unconsolidated (m³)	0
Backfill consolidation (%)	0

The representative cavern shape as depicted in Figure 101 does not reflect the shape of the shown (reconstructed) sonar images. An illustration of a plausible situation after 50 m of migration above the Anhydrite-E is provided by Figure 102 which explains how the two individual migration contours of C33-34 and C35-36 merged into a single migration column.

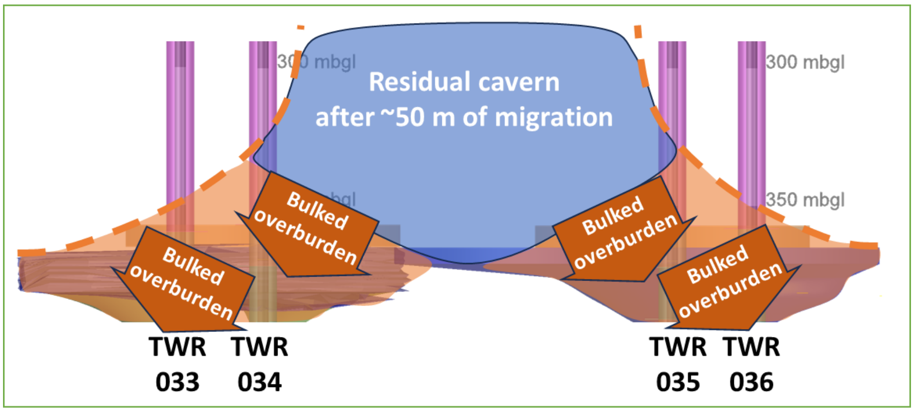

Figure 102: C33-34-35-36: Likely situation after 50 m of migration above the Anhydrite-E showing the "merging" of initial migration contours of C33-34 and C35-36 into a single migration column.

After initial collapse of the Anhydrite-E, the bulked overburden fills the two individual caverns. As the original caverns are filled, a single residual cavern develops between these two caverns as shown in Figure 102.

Using the input parameters stated in Table 53, the BJP-Algorithm produced the output for C33-34-35-36 as presented in Figure 103. As there are no GR-logs to compare to, the outcomes of the BJP-Algorithm cannot be confirmed by them.

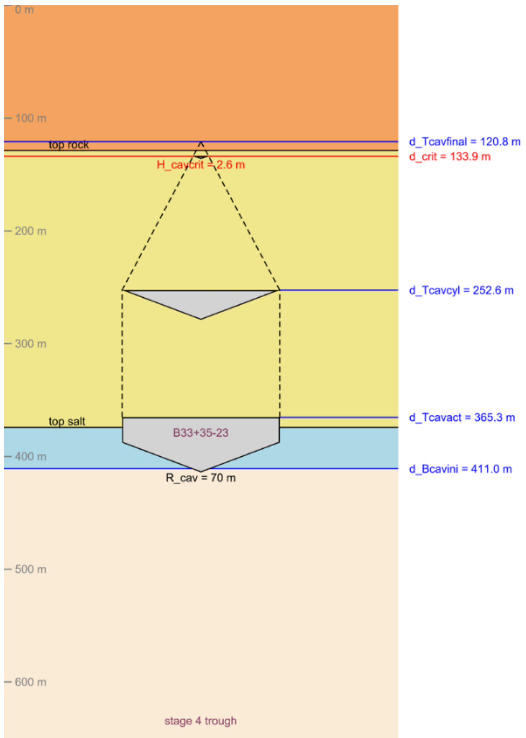

Figure 103: C33-34-35-36: BJP-Algorithm output for best fitting representative cavern volume

The calculated subsidence contours are shown in Figure 104. The actual measured subsidence at TWR-035 is also shown in this figure for comparison. The location of the levelling point was just south of the deepest point of the subsidence trough.

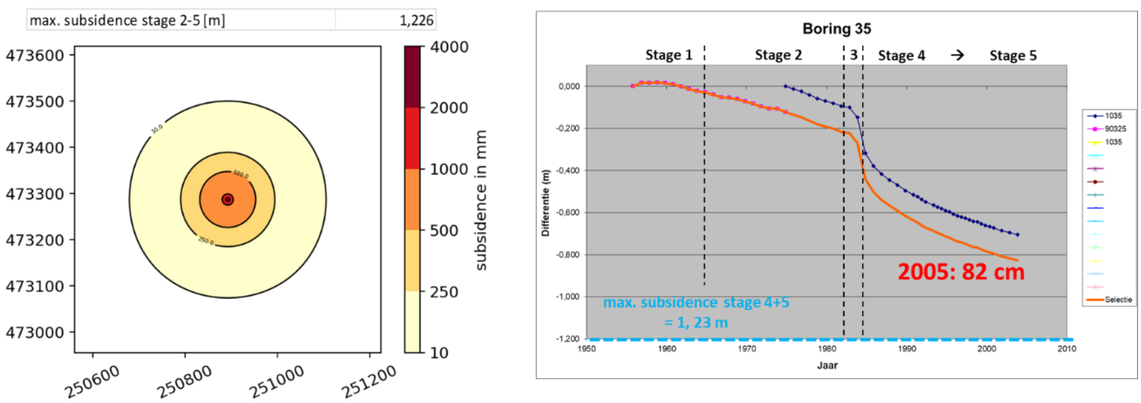

Figure 104: C33-34-35-36: subsidence contours as calculated by the BJP-Algorithm (l) and measured subsidence (r) at TWR-035.

As can be seen from this figure, the calculated subsidence fits well to the measured subsidence. The apparent overestimation by the algorithm (123 cm calculated versus 82 cm measured) is caused by the conservatism of the BJP-Algorithm and the still ongoing development subsidence in 2005 as explained at the start of this chapter. By 2022, the subsidence rate has significantly decreased according to Figure 96, signalling the end of Stage 5 subsidence.

In conclusion, the reverse operation of the BJP-Algorithm enabled a plausible reconstruction of cavern migration for C33-34-35-36 caverns and demonstrates the ability to reconstruct migration cases that are not well documented.

5.3. Reconstruction C30-31 (reverse operation)

Cavern 30-31 (C30-31) is a multi-completion cavern (MCC) comprising wells TWR-030 and TWR-031. No blanket medium was used during the cavern development and backfill was not applied. The key data for this cavern are included in Table 54 and additional information can be found in APPENDIX I.

Table 54: Key data C30-31

Wells	X (WGS84)	Y (WGS84)	Z (mNAP)	Final depth (mbgl)	Final depth (mNAP)	Well ready	Start production	End production	Cemented
30	250730,8	473170,3	20,82	431,29	-410,47	15-6-1953	8-7-1953	1-11-1964	23-7-1973
31	250731,2	473140,3	20,5	426,16	-405,70	16-10-1953	2-11-1953	1-11-1964	31-7-1979

C30-31 was initially developed as two independent SCC caverns. Sump caverns SCC 30 and SCC 31 connected in June 1957, more than four years after the start of production. The distance between these wells is again only 30 m. As described for C33-34-35-36, bottom injection was also used for these two SCCs and explains the late connection between TWR-030 and TWR-031. After their connection, C30-31 was operated as an MMC until August 1960 when a hydraulic connection to C29 was established. The cavern was further operated as MCC 29-30-31 with TWR-029 as the brine production well. Most volume development after 1960 will thus have taken place in C30-31. Further connections with the adjacent well have been presented in Figure 94.

As with C33-34-35-36, the salt production from C30-31 cannot be established on a year-by-year. As such, the total salt production from C30-31, as stated in Table 49 will be used for the cavern reconstruction. The only other available information on this cavern is the measured subsidence. Consequently, reverse operation of the BJP-Algorithm was used to reconstruct a plausible cavern shape and volume based on the salt production which achieves the measured subsidence after migration.

The tested representative volumes were all positioned directly underneath the deepest point of the trough shown in Figure 96 for C30-31. Examples of tests performed during the reverse operation of the algorithm for this cavern are shown in Figure 100 for illustrative purposes.

The tests with a combined volume showed that the measured Stage 4 subsidence could be modelled by the BJP-Algorithm. This enabled a more detailed fitting of the measured and calculated subsidence by variation of the representative cavern dimensions, i.e. radius, cone height and cylinder height. The sensitivity of these dimensions is high, making increments of 5 cm necessary to achieve optimal fitment between calculated and measured subsidence.

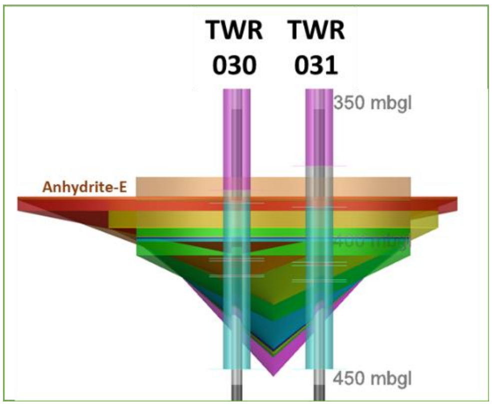

Figure 105: C30-31: Examples of tested representative volumes.

After several iterations, and adaptation of the algorithm to include a smooth non-linear transition of Stage 4 trough to sinkhole subsidence , the final version of the BJP-Algorithm was used to derive input parameters as presented in Table 55 and depicted in Figure 106 below.

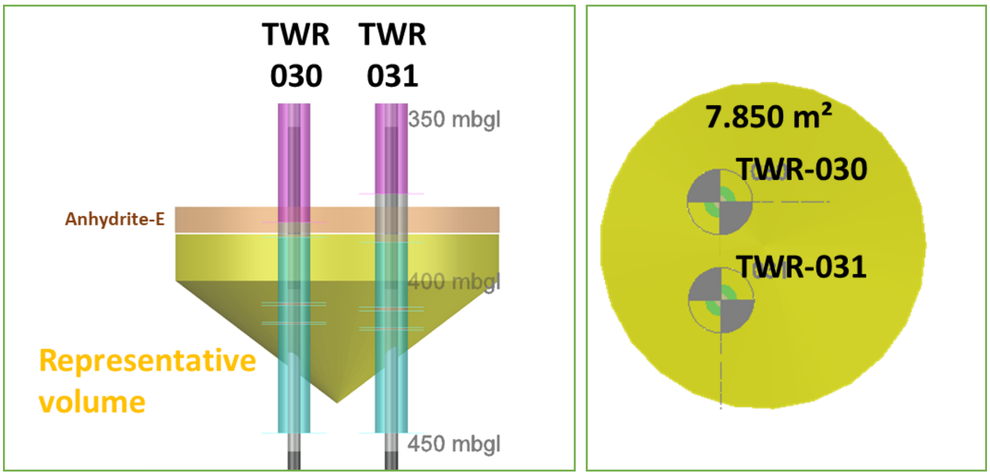

Figure 106: C30-31: Final tested „Representative volume" (yellow).

The representative volume of C30-31 leading to the measured subsidence comprises a cone-shaped sump with a 50 m radius and 37,23 m height and a cylinder with 50 m radius and 14,43 m height. No backfill has been applied in this cavern.

Using the input parameters stated in Table 55, the BJP-Algorithm produced the output for C30-31 as presented in Figure 107. A comparison of the results of the subsidence calculations and the observations from GR logs cannot be made due to the absence of the latter.

Table 55 C30-31 cavern specific input parameters

Cavern	30
Relevant borehole	30
X coordinate	250730,8
Y coordinate	473170,3
Z coordinate GL (mNAP)	20,6
Depth of top rock [mbGL]	130,1
Depth of top salt [mbGL]	384,0
Base of actual cavern [mbGL]	433,8
Base of initial cavern [mbGL]	444,3
Top of actual cavern [mbGL]	381,6
Height of cavern (m)	52,2
X coordinate migration centre	250744,0
Y coordinate migration centre	473157,0
Volume fitting	
Maximum BPB Prod.(t)	404984
Cavern vol based on BPB (m^3)	**227552**
Actual volume (recon./sonar)(m^3)	210584
Insolubles (bulked) (m^3)	10159
Part of BPB prod. Vol. not acc. (m^3)	16968
Part of BPB prod. Vol. not acc. (%)	**7%**
Cavern geometry conversion	
Migration column Surface area (m^2)	7850
Constructed cavern radius [m]	50,0
Hydraulic Radius constructed cav. [m]	25,0
Const. cavern height (cylindrical) [m]	14,425
Const. cavern height (conical) [m]	37,725
Constructed volume (cylindrical) [m^3]	113294
Constructed volume (conical) [m^3]	98764
Constructed volume total [m^3]	212058
Part of BPB prod. Vol. not acc. (m^3)	15494
Part of BPB prod. Vol. not acc. (%)	**7%**
Height correction backfill insitu [m]	0
Backfill insitu unconsolidated (m^3)	0
Backfill consolidation (%)	0

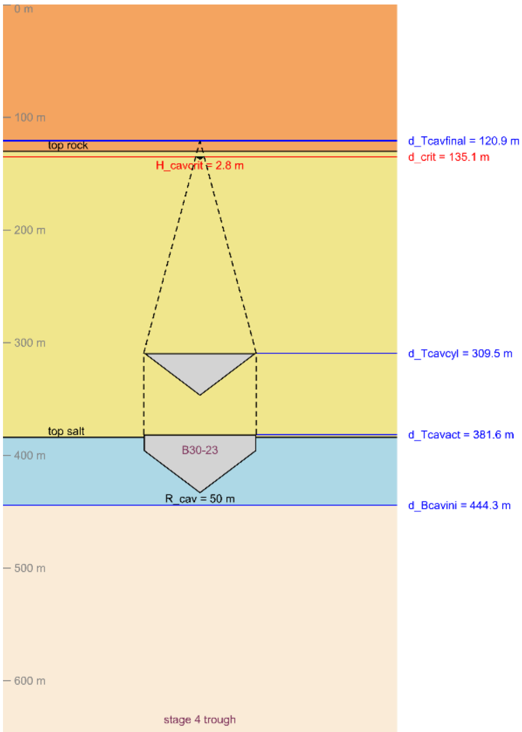

Figure 107: C30-31: BJP-Algorithm output for best fitting representative cavern volume

The calculated subsidence contours are shown in Figure 108. The actual measured subsidence at TWR-030 is also shown in this figure for comparison. The location of the levelling point was just west of the deepest point of the subsidence trough.

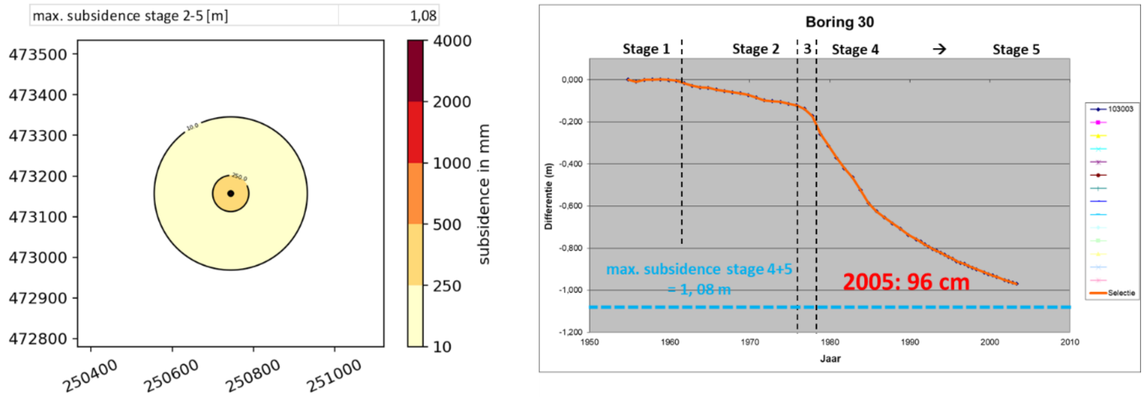

Figure 108: C33-34-35-36: subsidence contours as calculated by the BJP-Algorithm (l) and actual measured subsidence (r) at TWR-035.

As can be seen from this figure, the calculated subsidence fits well to the actual measured subsidence. The apparent overestimation by the algorithm (108 cm calculated versus 96 cm measured) is caused by the conservatism of the BJP-Algorithm and the still ongoing development of Stage 4 subsidence in 2005 as explained at the start of this chapter. Between 2012 and 2022, the subsidence rate has diminished according to Figure 96, signalling the completion of Stage 5 subsidence.

In conclusion, the reverse operation of the BJP-Algorithm enabled a plausible reconstruction of cavern migration for C30-31 in the absence of documentation. As such, the reverse operation of the algorithm is successfully demonstrated.

6. Likelihood of cavern migration

The previous chapters mainly discussed the result of cavern migration but have not elaborated on the causes of migration. To close this gap, this Chapter 6 investigates the potential causes for cavern migration by assessing the conditions under which migration at the previously discussed caverns initiated and propagated. The causes and rate of migration have historically been investigated by Bekendam in [25] and [26]. These reports mainly focus on the link between faults and migration and the rate of migration within the Anhydrite and the overlying Röt Claystone.

The work during the UMS-TWR allowed for a detailed assessment of the likelihood of migration for the well-documented cavern migration cases. This assessment was supported by recent scientific publications which were not available historically. The results of the literature research and the assessment have been collated into a new cavern migration likelihood scoring system. This scoring system will be validated by the cavern migration cases discussed in previous chapters.

The establishment of a unified cavern migration likelihood scoring system has now enabled Nobian to systematically determine the appropriate "Frequency (F)-class" for each studied cavern in their TWR cavern risk matrix. An impact assessment based on the output of the subsidence prognoses produced by the BJP-Algorithm, establishes the "Severity (S)-class" for each cavern. With a F and S classification, the position of each cavern in the TWR cavern risk matrix is determined and planning of appropriate mitigative measures by Nobian can be improved.

Chapter 6 will first discuss causes for migration initiation and the conditions under which migration can propagate. The second paragraph of this chapter discusses the term "caveability" and introduces the "hydraulic radius" as a criterion for cavern migration initiation and propagation. The influence of faults in the under- or overlying strata of the Röt Evaporite member on the initiation of migration will be elaborated in the third paragraph. Chapter 6 is concluded by the presentation of the newly developed migration likelihood scoring system and the resulting scores for the well-documented migration cases.

6.1. Migration initiation and propagation

The initiation of cavern migration has been a subject of research in the TWR area for decades, going back to the sinkhole event at C69-70-71 in 1991. Historic investigations concluded that the "Top Anhydrite" (Anhydrite-E in this report) can withstand collapse for decades and the migration rate through this layer is relatively slow. Once the Top Anhydrite fully collapsed, Bekendam estimated the migration rate through the Röt Claystone at 10,3 ± 2,6 m/year in [25]. The UMS-TWR did not focus on the rate of migration as this is extensively covered by the Bekendam investigations on this subject. These investigations did not focus extensively on the reasons for the collapse of the Top Anhydrite and the UMS-TWR aims to fill that gap in the next three sub-paragraphs. These will discuss hydraulic pressure-driven cavern roof collapse, hydration-driven deterioration of the Anhydrite-E and lastly "Cave back propagation", a critical factor in block cave mining operations, as an analogue for the situation in the TWR area.

6.1.1. Hydraulic pressure-driven cavern roof collapse

The hydraulic pressure-driven cavern roof collapse is introduced by Bekendam in [27] as criterion for cavern migration. He provides the following simplified explanation [25] (translated):

> "An individual roof layer directly above a cavern can collapse only if it separates from the layers above it through deflection ("bed separation"). When this is about to happen, however, the situation is such that the roof layer experiences hydrostatic brine pressure from below and hydrostatic water pressure at the top. Despite the weight of the roof layer, there will be a net upward pressure directed at the roof layer. Thus, a direct roof layer can only separate when a hydraulic connection exists between the cavern and the top of the roof layer, allowing brine to percolate to the top of the layer can percolate, and a downward directed vertical pressure on the layer is created."

A graphical explanation of this quote is provided by Figure 109 below in which three (progressive) situations for a cavern positioned directly underneath the Top Anhydrite.

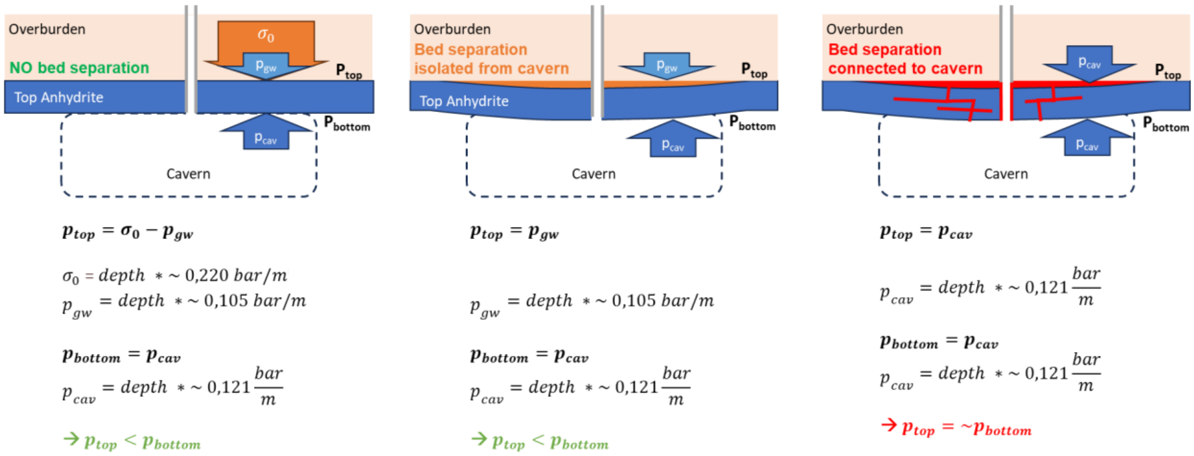

Figure 109: Graphical explanation of hydraulic pressure driven cavern roof collapse, after [27]

The first situation is shown in the left picture and represents a cavern that has reached the underside of Top Anhydrite by leaching. Initially, the Top Anhydrite will not have deflected which means that no "Bed separation" has developed between the Top Anhydrite and the Overburden. The effective pressure that acts on the Top Anhydrite is lower than the pressure in the cavern as is presented in the example calculation. The lithostatic gradient used in the example calculation is 0,22 bar/m based on [28]. The Top Anhydrite is thus supported by the cavern pressure and collapse is not likely to initiate.

The extension of the cavern contour directly underneath the Top Anhydrite will eventually lead to a deflection of the Top Anhydrite layer as shown in the middle picture of Figure 109. The deflection causes bed separation as is shown in orange. When the bed separation is isolated from the cavern, the cavern pressure will still support the Top Anhydrite in this situation assuming the density of the formation water in the overburden is lower than the density of the brine in the cavern. This is demonstrated in the example calculation under the middle picture.

This situation changes when the bed separation is hydraulically connected to the cavern as shown in the right picture of Figure 109. Mechanical deterioration of the cement around the Last Cemented Casing (LCC) may lead to a hydraulic connection and allow brine to percolate up into the bed separation. Alternatively, vertical tensile cracks may appear and form a connection, via bedding planes within the Top Anhydrite, to the bed separation. As the higher density brine replaces the lower density formation water in the bed separation, the pressure on both sides of the Top Anhydrite equalizes. An equal pressure on itself does not necessarily lead to a collapse when the overall strength of the Top Anhydrite layer is sufficient to overcome the stresses build-up within due to the deflection. However, when the strength of the Top Anhydrite alone is not sufficient, the formation of a hydraulic connection between the cavern and the top side could cause the Top Anhydrite to collapse as the supporting cavern pressure diminishes during pressure equalisation.

Although hydraulic pressure-driven roof collapse as just described is certainly a plausible mechanism for roof collapse, it cannot explain why the Anhydrite-E member has relatively quickly collapsed for several of the well-documented cavern migration cases, whilst remaining stable for decades in a multitude of other cases.

6.1.2. Hydration-driven deterioration of Anhydrite-E

Geohazards related to anhydrite and gypsum are well-known in the geotechnical and civil engineering industries. As soluble minerals, their presence in a water rich environment can cause dissolution and consequently the formation of karst structures and caverns. In addition, the hydration and recrystallisation of anhydrite to gypsum can cause considerable expansion and pressures capable of causing uplift and heave, i.e. the expansion of soils. [29]

The hydration and weakening of anhydrite under stress has been investigated during a recent study based on extensive experimental work. The findings of this study show mechanical-chemical weakening through hydration of anhydrite along stressed fractures. It also shows how rapidly mechanical weaknesses may form and threaten the stability of caverns in natural evaporite deposits [30]. In other words, when anhydrite is under stress and exposed to water, gypsum rapidly forms. As gypsum has a larger volume than the original anhydrite after exposure to water, heave or bed separation may develop. These findings are illustrated in Figure 110 below.

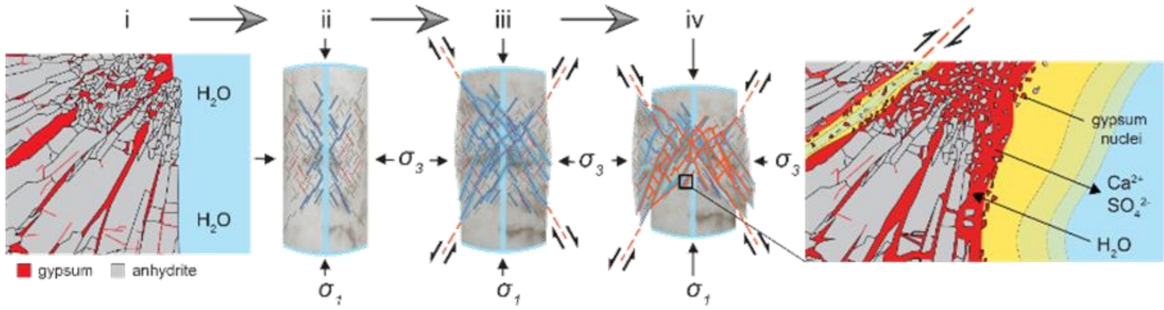

Figure 110: Schematic fracture formation and anhydrite hydration under increasing load steps, adapted from [30].

The findings of this study are found to be a potential analogue to the situation at migrated caverns in the TWR area. As the cavern develops upwards by leaching and reaches the Top Anhydrite, the vertical stress from the load of the overburden is deflected outwards arching over the cavern. This leads to an increase in stress in the Top Anhydrite towards the outer contour of the cavern while reducing the stress within the arch (where it can even become tensile) [27].

Application of these two principles leads to the hypothesis that the Top Anhydrite in the TWR can deteriorate under the influence of water and that the location of the highest hydration potential is unfavourable for cavern roof stability. This hypothesis is illustrated by Figure 111.

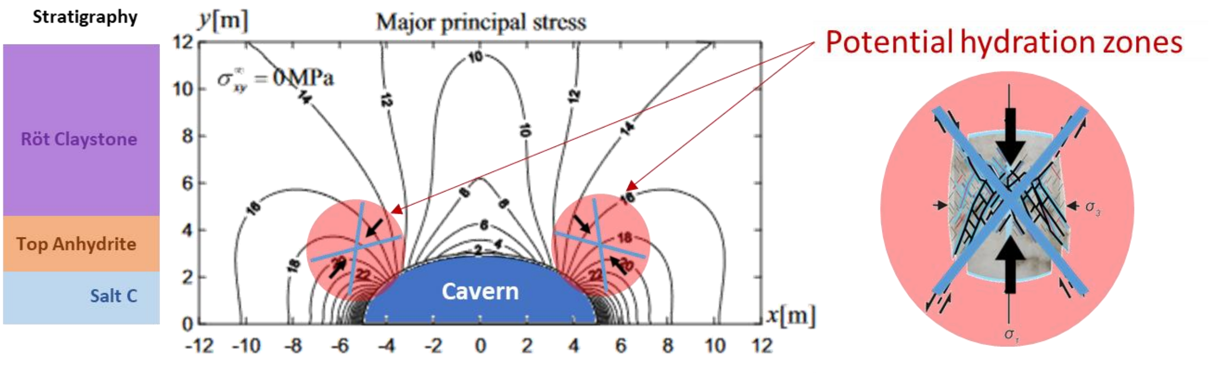

Figure 111: Unfavourable location of potential hydration zone of Top Anhydrite in cavern roof leading to collapse, adapted from [30] and [31].

Considering the stress contours around a cavern shown in Figure 111, the potential anhydrite hydration zone will be located around the outer contour of the cavern roof in case of water exposure. The weakness planes, as indicated by the blue lines in the detail view of the hydration zone, are unfavourably oriented for roof stability. The sub-horizontal plane causes gypsum formation between bedding layers within the Top Anhydrite thus causing their delamination. The sub-vertical plane on the other had will introduce weakness planes near perpendicular to the bedding. This can lead to the formation of a hydraulic connection between the cavern and the bed separation above the Top Anhydrite, which subsequently promotes pressure-driven collapse as discussed in the previous paragraph.

As during operation of all the well-documented migration cases, the Top Anhydrite was exposed to water for a prolonged period of time, the presented anhydrite hydration process is deemed a likely cause for deterioration of the Anhydrite-E member in these cases. This deterioration leads to pressure-driven collapse of the Anhydrite-E. Once the Anhydrite-E collapses, the migration has started and will continue until the residual cavern is fully filled with bulked overburden or reaches the surface causing a trough or sinkhole.

6.2. Caveability and the “Hydraulic Radius” principle

The migration propagation after the collapse of the Anhydrite-E member at the well-documented cases in the TWR area is not observed to stall until the residual cavern is fully filled with bulked overburden. The performance of the UMS-TWR also did not observe a permanent stalling of cavern migration due to “arching”[4]. A temporary pause in migration may be caused by relatively competent layers in the Röt Claystone as discussed for C69-70-71 in paragraph 4.2.

To understand the reasons behind this seemingly self-sustained migration potential, an industrial analogue was identified in block cave mining. This mining method relies on the undercutting of a large block of resource until the roof collapses thus liberating it. By continuously removing the collapsed material, the propagation of the cave is enabled as bulking of the collapsed material cannot stop the further collapse as in the case of a cavern migration in the TWR area.

[4] Arching in the meaning of the formation of a stable “arch-shaped” residual cavern roof under which a residual cavern can reside in the Röt Claystone.

The layout of a block cave mine and the main behavioural zones of a propagating cave are presented in Figure 112. A detailed explanation of the main zones in a propagating cave, i.e. a migration column, are discussed in paragraph 3.2.3 by Figure 14.

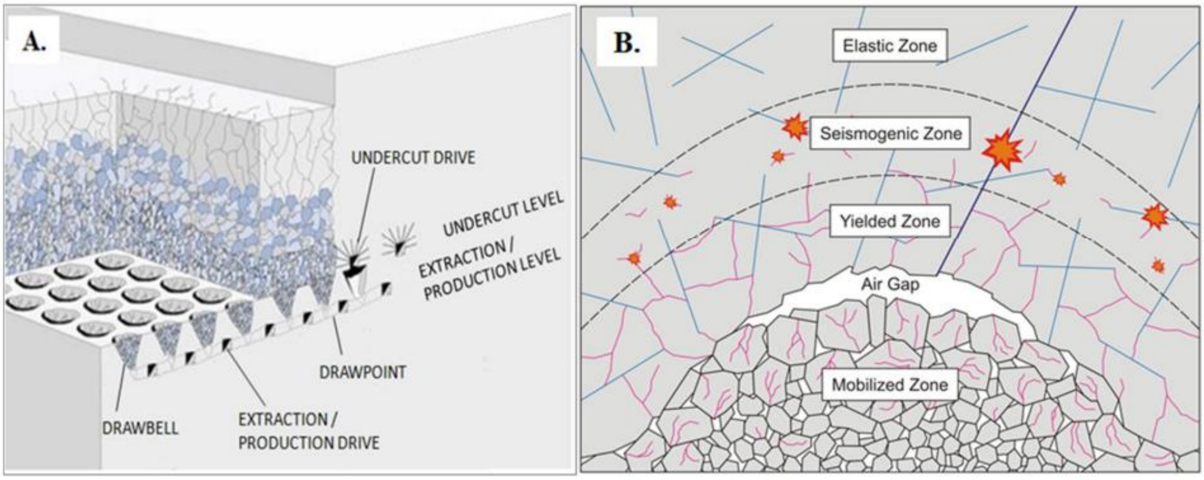

Figure 112: (A) Schematic representation of a typical block cave mine (B) Main behavioural regions of a propagating cave. (Figure 1 in [32]).

In the case of block cave mining, a self-sustaining propagation of the collapse front is an obvious design goal. A successful design of a block cave mine must therefore consider the geological/-structural-/mechanical conditions in the caving zone to enable self-sustaining propagation of the cave roof and consequently the continuous liberation of resources. Extensive work by Sainsbury on the numerical modelling of block caving propagation as reported in [1] has provided valuable insights into the possible reasons for the observed propagation of cavern migration in the TWR area. The first of these insights has been discussed in paragraph 3.2.3 and relates to the behavioural zones in the migration column as shown in Figure 112.

The second insight is the definition and use of the so-called Hydraulic Radius (HR) as a measure of caveability. The Hydraulic Radius (HR) is defined as:

HR = Undercut area (m²) / Undercut perimeter (m)

The critical HR will have been reached when the cave propagation is self-sustaining. The caveability for block cave mining has been historically estimated by empirical methods. The most commonly used one was developed by Laubscher and is based on a compilation of case histories, largely derived from, low, strength, kimberlitic deposits in South Africa [1]. Laubscher devised a chart ("Laubscher's chart") in which the HR is plotted against the Mining Rock Mass Rating (MRMR[5]).

The Laubscher's chart is presented in Figure 113 and defines three possible caving states, as indicated by this figure. The states are defined based on the MRMR and the HR of the cave's undercut. Although not the state-of-the-art, the Laubscher's chart is still a widely used empirical method to estimate caveability in block cave mines. It is particularly suited to MRMR values below 50 [33] which is the range applicable to the TWR area as will be explained next.

---

[5] MRMR is Laubscher's modification of the Rock Mass Rating (RMR) system of Z.T. Bieniawski in which the stability and support of a mined opening are considered in addition to the rock quality and strength. The combination of RMR and MRMR value therefore determines the reinforcement potential of a rock. [36]

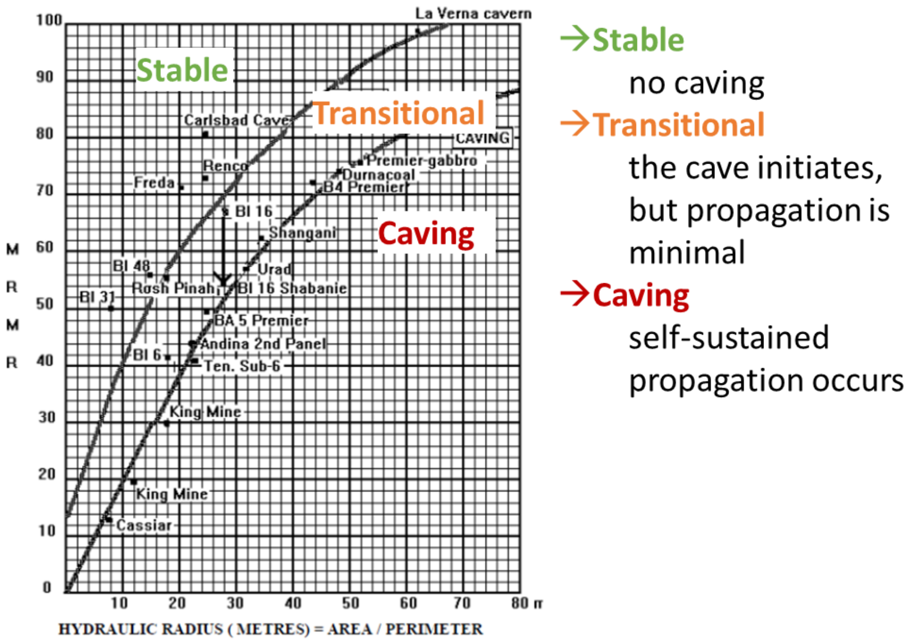

Figure 113: Laubscher's caveability chart for cave propagation [34], adapted from [1].

An assessment of the HR values for the studied migration cases shows that migrated caverns in the TWR area seem to have a HR of 20 m or higher, see Figure 114.

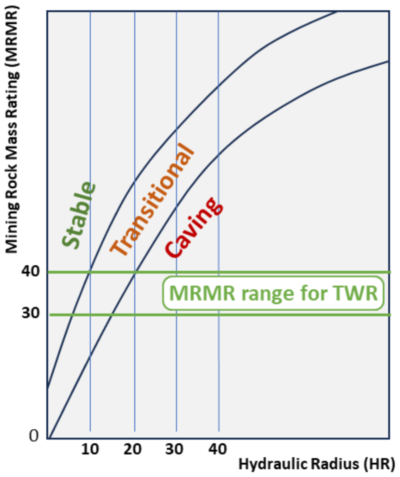

Cavern	Migrated?	Backfilled?	Salt C 5m Safety Roof intact?	Hydraulic Radius (m)
15	Yes	Yes	No	24,5
30	Yes	No	No	25
35	Yes	No	No	35
37	Yes	No	No	20
49	Yes	Yes	No	16,5
50	Yes	Yes	No	22
64	Yes	Yes	No	33,5
69	Yes	Partly	No	25
72	Yes	Yes	No	27,5
86	Yes	No	No	22
106	Yes	Yes	No	25

Hydraulic radius of 49+50 combined >20 m

Figure 114: Estimation of a conservative MRMR range for the TWR area (Röt Claystone) based on a HR > 15 of well-documented migration caverns.

To ensure a conservative approach in the determination of the likelihood of migration, a HR of 15 is selected as the boundary between Caving and Transitional, bringing the conservative MRMR value to 30 for the TWR area Röt Claystone.

The state-of-the-art numerical modelling work by Sainsbury on cave propagation also provided an insight into potential cavern migration behaviour for varying joint orientations. This is illustrated by Figure 115.

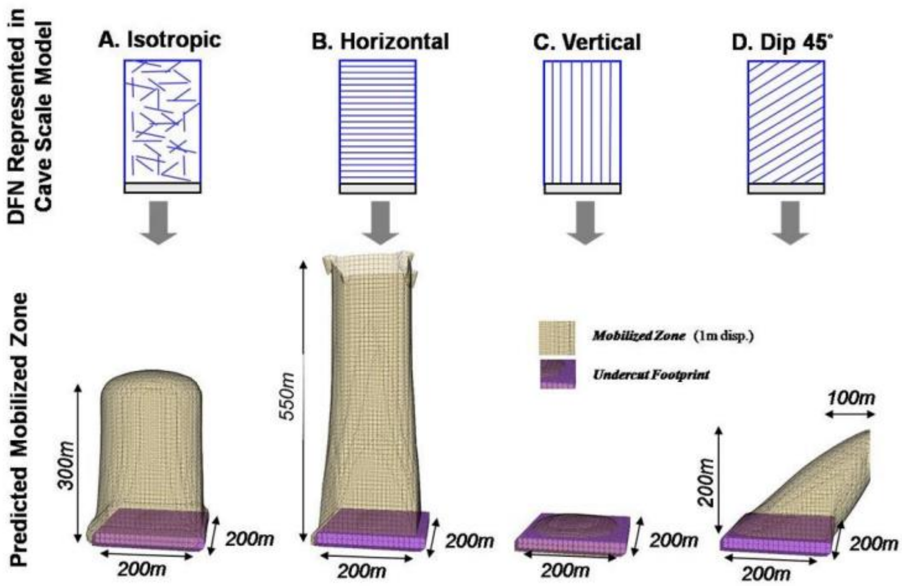

Figure 115: *Cave propagation behaviour for varying joint orientations simulated in the numerical demonstration model by Sainsbury (Figure 75 in [1]). DFN = Discrete Fracture Network. Case B closely resembles the situation in the TWR area.*

The shown variations in the joint orientation are represented by four cases of a Discrete Fracture Network (DFN): isotropic, horizontal, vertical and dip 45°. The situation in the TWR area is best represented by the horizontal model as the bedding planes are mostly (sub-) horizontal. The horizontal bedding planes act as the DFN and lead to a self-sustaining cave propagation as shown in Figure 115 and observed for the well-documented cavern migration cases discussed in this report. The figure above also shows that an inclined DFN, representing an inclined bedding plane for example, may lead to lateral deflection of a migration column. This effect may have influenced the migration of cavern C33-34-35-36 ("merging" migration column as discussed in paragraph 5.2) in addition to the presence of faults in under- and/or overlying strata.

In conclusion, the numerical modelling work by Sainsbury confirms that the conditions in the TWR area (Röt Claystone) are ideal for a self-sustaining cavern migration when the HR > 15 m. This value will be used in the likelihood scoring system as will be discussed in paragraph 6.4.

6.3. Presence of faults in under- and overlying strata of the Röt Evaporite

The influence of faults in the under- and overlying strata of the Röt Evaporite has been investigated by Bekendam in [25]. The UMS-TWR continued these efforts and plotted the well-documented cavern migration cases on the Depth maps prepared by GeoWulf Laboratories [13]. The depth maps of the bottom of the salt formation ("Top RNSO") and the bottom of the Röt Claystone ("Top RNRO1") are presented in Figure 116 and Figure 117 respectively.

The offsets in the stratigraphy are indicated in these figures by the red lines. These offsets can be interpreted as faults in the under- and overlying strata of the salt formation. Figure 116 and Figure 117 both show a clear correlation between cavern migration and the presence of faults in the under- and overlying strata. Except for C86-87 and C106-107, all studied migrated cases are located in the vicinity of observed faults. The presence of unobserved faults in the vicinity of C86-87 and C106-107 cannot be ruled out.

Although such faults are not observed to propagate into the salt, their presence in the under- and overlying strata appear to have an influence on the migration potential of a cavern. As such the presence of faults is also considered in the newly developed likelihood scoring system as presented in the next paragraph.

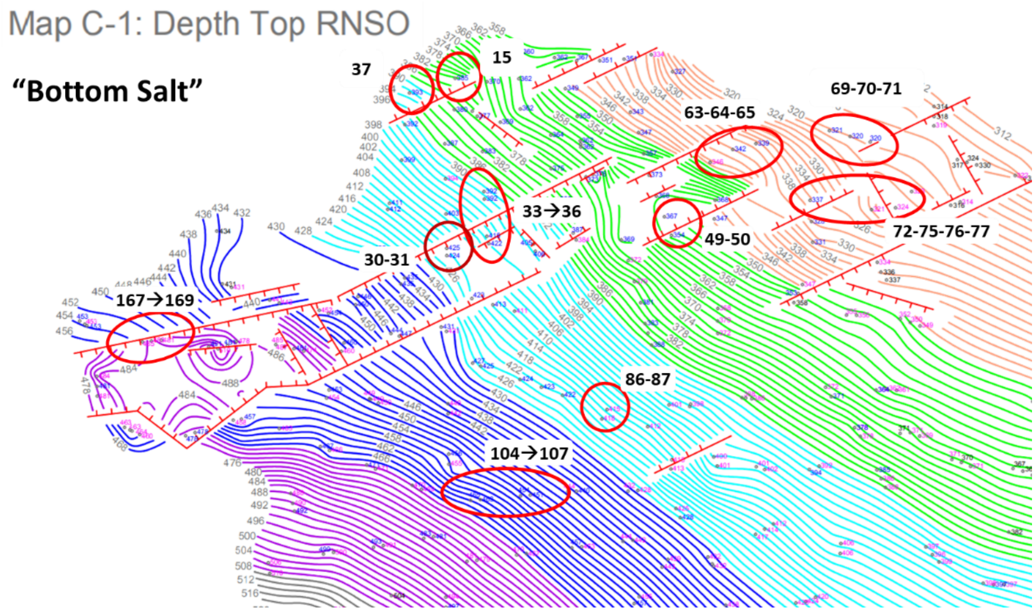

Figure 116: *Depth Top RNSO (Bottom Salt) with location of well-documented migration cases indicated by red ellipses. Adapted from Map C-1 in [13].*

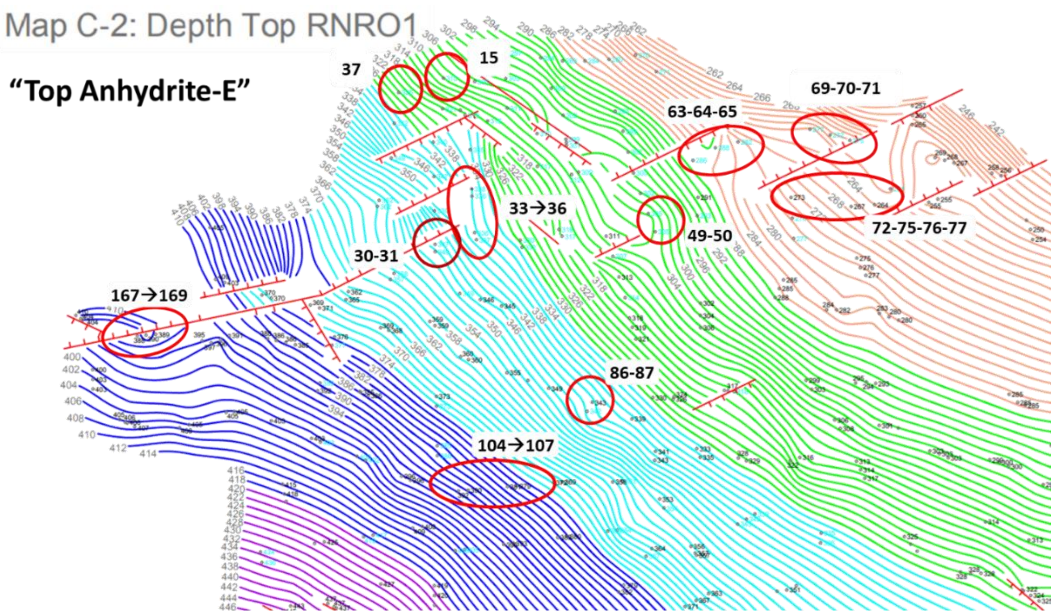

Figure 117: *Depth Top RNRO1 (Bottom Röt Claystone) with location of well-documented migration cases indicated by red ellipses. Adapted from Map C-2 in [13].*

6.4. Likelihood of migration for TWR caverns – a new scoring system

The detailed assessment of the likelihood of migration for the well-documented cavern migration cases has enabled the development of a "Cavern Migration Likelihood Scoring System" (CMLSS). The establishment of this unified CMLSS has now enabled Nobian to systematically determine the appropriate "Frequency (F)-class" for each studied cavern in their TWR cavern risk matrix. The CMLSS distinguishes the scoring criteria, categories and scores as defined by Table 56.

Table 56: Cavern Migration Likelihood Scoring System (CMLSS): criteria, categories and scores

Criterion	Catergories	Score
HR of intersection cavern with Salt C-5m contour measured in latest sonar. HR=0 refers to a fully intact Salt C- 5 m Safety Roof over the cavern.	HR = 0 : HR = 1 – 10 m: HR = 10 – 15 m: HR > 20 m:	0 1 2 3
Anhydrite-E exposed in the cavern roof by leaching and/or collapse of the Claystone CD bench?	No Likely Yes	0 1 2
Prolonged exposure of Anhydrite-E to water during cavern operation?	No: Likely or blanket medium: Yes	0 1 2
Faults in nearby (in under- / overlying strata)	No Yes	0 1

The scoring system collates the individual categories to a total likelihood score between 0 and 8. A score of 6 or higher is considered a high potential of migration initiation. Using the defined criteria, categories and scores as stated in this table, the CMLSS was populated for the well-documented migration cased based on the information gathered during the UMS-TWR. The results for the well-documented migration cases in presented in Table 57.

Table 57: Cavern Migration Likelihood Scoring System (CMLSS) applied to well-documented migration cases.

Cavern	Migrated?	Backfilled?	Salt C 5m Safety Roof intact?	Hydraulic Radius (m)	Score	Anh.-E exposed?	Score	Water exposure Anh.-E?	Score	Blanket used?	Faults nearby?	Score	Likelihood Score
15	Yes	Yes	No	24,5	3	Yes	2	Yes	2	No	Yes	1	8
30	Yes	No	No	25	3	Likely	1	Likely	1	No	Yes	1	6
35	Yes	No	No	35	3	Yes	2	Yes	2	No	Yes	1	8
37	Yes	No	No	20	3	Yes	2	Yes	2	No	Yes	1	8
49	Yes	Yes	No	16,5	3	Yes	2	Yes	2	No	Yes	1	8
50	Yes	Yes	No	22	3	Yes	2	Yes	2	No	Yes	1	8
64	Yes	Yes	No	33,5	3	Yes	2	Yes	2	No	Yes	1	8
69	Yes	Partly	No	25	3	Yes	2	Yes	2	No	Yes	1	8
72	Yes	Yes	No	27,5	3	Likely	1	Likely	1	No	Yes	1	6
86	Yes	No	No	22	3	Yes	2	Blanket	1	Yes	No	0	6
106	Yes	Yes	No	25	3	Yes	2	Blanket	1	Yes	No	0	6

In conclusion, the population of the CMLSS shows that the well-documented cavern migration cases all have a high to very high likelihood score which confirms the applicability of this scoring system. The CMLSS will be applied to the caverns for which an update of the subsidence prognosis is required in Report 4.

7. Conclusion and recommendations

The validation of the developed prognosis algorithm presented in Report 2, has been achieved by demonstrating that the derived relationships and selected input parameters are applicable to the well-documented cavern migration cases. Initial validation of the algorithm was achieved based on the reconstruction of 5 cavern migration cases. The validation was strengthened by the reconstruction of a further 4 complex migration cases The applicability to poorly documented migration cases was demonstrated by operating the algorithm in reverse for 2 caverns to reconstruct the migration column and the likely original cavern shape based on the measured subsidence and salt production figures. The final well-documented cavern migration case, i.e. C167-168-169, has a very complex development history for which the reconstruction proved to be of little value for the validation process due to the many uncertainties involved. The performed reconstruction work on this cavern will be delivered in an addendum to this Report: i.e. ADDENDUM I after finalisation. This addendum is expected to be delivered in Q1-2025.

The validation shows that the BJP-Algorithm is applicable to the entire TWR area. The validated applicability focused on the four main input parameters:

1. Effect of cavern shape on migration column shape.
2. Bulking Factor of insolubles, intermediate claystone benches and overburden.
3. Backfill volume balance: actual insitu backfill versus pumped slurry.
4. Backfill behaviour under load: consolidation by self-weight and under load of bulked overburden.

At each stage of the parameter selection process care was taken to maintain a conservative but realistic approach. The main conservatisms used in the reconstruction and the parameter selection process are:

- Introduction of the radius reduction mechanism based on a cone-shaped cavern (bottom) leading to higher migration column potential compared to purely cylindrical migration columns as historically used.
- Analysis of actual cavern shape, volume and position in the stratigraphy as the basis for a representative cavern volume compared to the use of only cavern height as a measure for migration potential as historically applied.
- Determination of representative cavern volume on salt production rather than sonar volume, consequently considering sonar shadow and other sources of sonar inaccuracy.
- Distinction between Bulking Factor for insolubles, intermediate claystone benches and overburden and selection of conservative values based on the validation of well-documented migration cases such as the C15 and C37 reconstructions.
- Backfill application based on the actual pumped slurry volume and with SWC, consolidation under load of bulked overburden and a lack of bearing capacity in the top layers considered in the volume balancing. Historically, backfill height was simply subtracted from cavern height to estimate the resulting migration column height, thus not accounting for realistic backfill behaviour.
- Use of the Hydraulic Radius and consideration of the exposure history of the Anhydrite-E as a measure of migration likelihood.

The result of this approach is an updated and validated prognosis method for potential subsidence caused by cavern migration in the TWR area, i.e. the BJP-Algorithm. The methodology and the results should be updated when new information arises from the operation of caverns in the Hengelo brinefield.

8. References

[1] B.-A. L. Sainsbury, “A MODEL FOR CAVE PROPAGATION AND SUBSIDENCE ASSESSMENT IN JOINTED ROCK MASSES,” The University of New South Wales, Sydney, 2012.

[2] REinvent GmbH, “Update Migration Study - Report 1 – Fundamental principles used in reconstruction,” REinvent GmbH, Sondershausen, 2023.

[3] REinvent gmbH / K-UTEC AG Salt Technologies, “Report 2 - The Bekendam-Jakob-Pinkse (BJP) subsidence prognosis algorithm for migrating salt caverns in a bedded stratigraphy,” REinvent GmbH, Sondershausen, 2024.

[4] REinvent GmbH, “Reconstruction of well documented cavern migration cases - Status and Outlook - Part B + C - Meeting SodM - 21-12-2023,” REinvent GmbH, Amersfoort/Sondershausen, 2023.

[5] REinvent GmbH, “Subsidence Prognosis Fase II caverns (1st Batch) - Prognosis algorithm and Input parameters - Meeting SodM, 04-04-2024,” REinvent GmbH, Amersfoort/Sondershausen, 2024.

[6] Oranjewoud, “Meetreeksen boringen Twenthe-Rijn - 15575-08773-33,” Oranjewoud, 2006.

[7] Oranjewoud, “Zakkingsgebied westzijde Boekeloseweg, Hengelo - 15575-08773-35,” Oranjewoud, 2006.

[8] GEOWULF Laboraties, “TWR North identification of delamination based on GR logs,” GEOWULF Laboraties, 2019.

[9] Akzo Nobel, “Eindrapport putreparatie boring 37 - 0307302,” Akzo Nobel, Hengelo, 2003.

[10] AKZO, “Slurry hoeveelheden in cavernes 1966-1991 (handwritten list),” AKZO, Hengelo, 1992.

[11] Nobian - Mining, Development & Compliance, “Twence cavernes - Stabiliteit cavernes 60 en 86 na aanboren in 2022,” NOBIAN, Hengelo, 2022.

[12] Staatstoezicht op de Mijnen - Geo&M - Duquesnoy, “Rapport van bevindingen en aanbevelingen - Instortingskrater rond boring 70 TWR,” SodM, Den Haag, 1991.

[13] GEOWULF Laboratories, “Detailed Geology of the Hengelo Solution Mining Area Part 2 - GL.901,” GEOWULF Laboratories, 2011.

[14] Prakla GmbH, “Ergebnisse der echometrische Hohlraummessungen in den Bohrungen HENGELO 15, 72, 75, 76, 77, 120, 121, 122, 123 - 068078,” Prakla GmbH, Hannover, 1968.

[15] Nobian, “Data Slurry hoeveelheden - extract from BPB,” Nobian, Hengelo, 2023.

[16] AKZO, “Slurryberging Stromingtstabel 1975-1998,” AKZO, Hengelo, 1998.

[17] AKZO, “Slurry in cavernes 55, 72 en 78 1973-1990,” AKZO, Hengelo, 1991.

[18] Nobian, “Memorandum Migratie caverne 72 - aanvullingen 2024,” Nobian, Hengelo, 2024.

[19] GEOWULF Laboratories, “TWR-072 delamination from Gamma Ray history - GL22.1203,” GEOWULF Laboratories, 2022.

[20] antea group, “Basisgegevens holruimtemetingen Boorterrein Hengelo - P55.20.01/926,” antea group, 2024.

[21] GEOWULF Laboratories, “TWR North identification of delamination based on GRlogs: B106 & B107,” GEOWULF Laboratories, 2020.

[22] Nobian, “Memorandum Migratie caverne 106-107 - NH20241022,” Nobian, Hengelo, 2024.

[23] R. Calis, “Reconstruction and safety assessment of the Hengelo Brinefield phase 1 area - Master Thesis,” TU Delft, Delft, 2018.

[24] esri Nederland, AHN, “esri Nederland Hoogteviewer,” esri Nederland, 2024. [Online]. Available: https://apps.arcgisonline.nl/hoogteviewer/. [Accessed 17 12 2024].

[25] GeoControl, “Invloed van tektonische breuken en cavernedimensies op cavernemigratie voor het Twenthe-Rijn zoutwinningsgebied - S01017,” GeoControl, Maastricht, 2014.

[26] GeoControl, “Migratiesnelheden cavernes boven de Top Anhydriet - M01634_V3,” GeoControl, Maastricht, 2017.

[27] GeoControl, “Induction of subsidence by brine removal 51/062726,” GeoControl, Maastricht, 2002.

[28] Well Engineering Partners B.V, “Abandonment study Nedmag caverns - Cavern squeeze modeling and geophysical analysis of brine permeation and containment,” Well Engineering Partners B.V, Hoogeveen, 2015.

[29] A. H. Cooper, “Geohazards caused by gypsum and anhydrite in the UK: including dissolution, subsidence, sinkholes and heave,” in *Geological Hazards in the UK: Their Occurrence, Monitoring and Mitigation – Engineering Group Working Party Report.*, London, Geological Society, 2020, p. 403–423.

[30] J. Heeb, D. Healy, N. Timms and E. Gomez-Rivas, “Rapid hydration and weakening of anhydrite under stress: implications for natural hydration in the Earth’s crust and mantle,” *Solid Earth,* vol. 14, pp. 985-1003, 2023.

[31] H. Wang , M. Jiang, T. Zhao and G. Zeng, “Viscoelastic solutions for stresses and displacements around non-circular tunnels sequentially excavated at great depths,” *Acta Geotechnica,* 2019.

[32] B.-A. L. Sainsbury, “A historical review of the development of numerical cave,” in *Proceedings of the 2nd International FLAC/DEM Symposium on Numerical Modelling*, Melbourne, 2011.

[33] R. Trueman and Mawdesley, C. , "Predicting cave initiation and propagation," *CIM Bulletin,* vol. 96, no. 1071, p. 54, 2003.

[34] D. Laubscher, "Cave mining – the state of the art," *Journal of the South African Institute of Mining and Metallurgy,* pp. 279-293, 1994.

[35] REinvent GmbH, "Reconstruction of well documented cavern migration cases - Status and Outlook - Part A + B - Meeting SodM 17-10-2023," REinvent GmbH, Amersfoort/Sondershausen, 2023.

[36] D. Laubscher, "A geomechanical classification system for the rating of rock mass in mine design.," *Journal of the South African Institute of Mining and Metallurgy,* vol. 90, no. 10, pp. 257-273, 1990.

APPENDIX I – Detailed information per cavern

See attachment:

241230 Update Migration Study TWR – Report 3 – Validation of BJP Algorithm APPENDIX I.pdf

Caverns included in APPENDIX I:

C15

C30-31

C33-34-35-36

C37

C49-50

C63-64-65

C69-70-71

C72-75-76-77

C86-87

C104-105-106-107

APPENDIX II – Detailed input-output chart for C72-75-76-77

(Extracted from [16])